CIVIL ENGINEERING STUDY
STRUCTURAL SERIES 85-10

OPTIMUM DESIGN OF BRACED AND UNBRACED FRAMES FOR STATIC, SEISMIC, AND WIND FORCES WITH UBC, ATC-3, AND TJ-11

by
Franklin Y. Cheng
Professor

Der-Shin Juang
Graduate Assistant

Department of Civil Engineering
University of Missouri-Rolla
Rolla, Missouri
1985

Report Series
Prepared for the National Science Foundation Under Grant No.
NSF CEE 8213477

CIVIL ENGINEERING STUDY

STRUCTURAL SERIES 85-10

OPTIMUM DESIGN OF BRACED AND UNBRACED FRAMES FOR STATIC, SEISMIC, AND WIND FORCES WITH UBC, ATC-3, AND TJ-11

by

Franklin Y. Cheng

Professor

Der-Shin Juang

Graduate Assistant

Department of Civil Engineering

University of Missouri-Rolla

Rolla, Missouri

1985

Report Series

Prepared for the National Science Foundation Under Grant No.

NSF CEE 8213477

ABSTRACT

An automatic design method based on an optimality criterion and constraint gradients is presented for designing various two-dimensional steel structures subjected to the multicomponent input of static, dynamic, earthquake, and wind forces. The structural systems can be trusses, unbraced and braced frameworks. The seismic input can be one-dimensional and two-dimensional; one-dimension is horizontal, two-dimension is horizontal coupled with vertical. The dynamic forces may be seismic excitations at the base, applied forces at the structural nodes, and wind forces acting on the structural surfaces. The seismic excitations include actual earthquake records, response spectra, and seismic building design provisions. The code provisions include Uniform Building Code, Chinese Seismic Design Code, and ATC-3-06.

The structural formulation is derived on the basis of the matrix displacement method and the consistent mass method with consideration of the second-order P-Δ forces. The constituent members of a system are made of either built-up sections or AISC WF sections. The constraints include stresses, displacements, story drifts, natural frequencies, maximum differences between relative stiffnesses, and lower bound of cross sections. The objective function can be either minimum weight or minimum cost. A sophisticated computer program, ODSEWS-2D-II (Optimum Design of 2-Dimensional Steel Structures for Static, Earthquake, and Wind Forces - Version II), was developed for both analysis and design of structural systems.

Seventy-seven numerical examples are provided to illustrate the

advantages of using the proposed design method, the assessment of the ATC-3-06 parameters, the effect of soil-structure interaction of the ATC-3-06 provisions, the effectiveness of various bracing systems in designing aseismic structures, the effect of the P-Δ forces and the vertical ground excitations on the optimum design, the stiffness distribution of highrise buildings, the comparision of various seismic code provisions, the comparison of minimum weight and minimum cost design, and the influence of story drift constraint and displacement constraint on optimum design. The notable observations are: 1) the fundamental period calculated on the basis of mechanics is much higher than the upper bound of the fundamental period, $1.2T_a$, recommended in ATC-3-06, 2) the stability coefficients are much less than the upper bound, 0.1, required in the ATC-3-06 provisions, 3) ATC-3-06 equivalent lateral force method and the modal analysis method produce similar optimal stiffness distributions for a structural system regardless the irregularity of the structural configuration, however, the equivalent lateral force method requires a heavior design, 4) soil-structure interaction within the ATC-3-06 provisions reduces the design base shear, 5) the Uniform Building Code produces the lightest weight among the three seismic structural design provisions, 6) the K-braced system provides better seismic resistance than the single, double, eccentric double, and eccentric-K bracing systems, 7) the combined ground motions of vertical and horizontal associated with the P-Δ forces increases the optimal design weight, 8) the dynamic story drift based on the root-mean-square superposition of modal drifts

provides more conservative design than that based on the total dynamic displacements.

ACKNOWLEDGMENTS

This report is one of a series of reports on optimum design of structural systems with parametric multicomponent earthquake motion and code provisions supported by the National Science Foundation under the grant CEE 8213477. Supports for this study are gratefully acknowledged. The authors also wish to thank the Civil Engineering Department for providing facilities and a substantial amount of computer time for this work.

TABLE OF CONTENTS

LIST OF ILLUSTRATIONS

List of Illustrations (continued)

List of Illustrations (continued)

Figures page

List of Illustrations (continued)

Figures page

List of Illustrations (continued)

Figures page

List of Illustrations (continued)

Figures page

List of Illustrations (continued)

Figures page

List of Illustrations (continued)

Figures page

List of Illustrations (continued)

Figures page

List of Illustrations (continued)

Figures page

List of Illustrations (continued)

Figures page

List of Illustrations (continued)

List of Illustrations (continued)

Figures page

List of Illustrations (continued)

Figures page

List of Illustrations (continued)

Figures page

List of Illustrations (continued)

Figures page

List of Illustrations (continued)

Figures page

LIST OF TABLES

List of tables (continued)

List of tables (continued)

LIST OF SYMBOLS

A_a = coefficient of effective ground acceleration

A_i = cross-sectional area of member i

A_v = coefficient of effective ground velocity

A' = required sectional area of the plate at beam-column connections

a = ground acceleration normalized by g

a_{max} = maximum expected normalized ground acceleration in the lifetime of the building

a^* = the design normalized ground acceleration

B = width of the building in the direction orthogonal to the direction of analysis; or the distribution parameter that describes seismic severity

b = width of wide flange section

b_j = limitation imposed on the j^{th} behavior constraint

C = seismic coefficient of UBC; or the structural influence coefficient of Chinese Seismic Design Code

C_{con} = total connection costs

C_{cl} = total construction costs of a building

C_D = total nonstructural damage repair costs in the lifetime of a structure

C_d = deflection amplification factor of ATC-3-06

C_{EX} = total extra charge of structural members

C_e = the combined height, exposure and gust factor coefficient

$(C_{nc})_i$ = construction cost of damage items on story i

C_p = total painting cost; or wind pressure coefficient

$(C_{pc})_i$ = cost of the steel plates at connections of beam i

C_{pl} = unit price of the plate at connections

C_{pt} = unit price of painting

C_q = pressure coefficient for the structure or portion of the structure under consideration

$(C_r)_i$ = nonstructural damage repair cost of story i

C_s = seismic design coefficient of ATC-3-06; or unit price of structural members

$\widetilde{C}_s$, $\widetilde{C}_{s1}$ = seismic design coefficient corresponding to the effective fundamental period $\widetilde{T}$ or $\widetilde{T}_1$

C_{sm} = the modal seismic design coefficient corresponding to the m^{th} mode

C_T = framing coefficient of ATC-3-06

C_{TB} = total basic charge of structural members

C_{vx} = vertical distribution factor of ATC-3-06 in equivalent lateral force method

C_{vxm} = vertical distribution factor of ATC-3-06 in modal analysis method

C_w = unit price of welding

$(C_{wc})_i$ = welding cost of each beam i

$[M_s]_i$ = mass matrix of member i in global coordinates

d = depth of wide flange section

E = modulus of elasticity

F_t = UBC design seismic force at the top floor level

F_x = equivalent lateral force induced at level x

F_{xm} = modal seismic base shear induced at level x

G = gust factor

g = gravity acceleration

$\bar{h}$ = effective height of a building

h_g = gradient height

h_i, h_x = the height of floor levels i and x above the base

h_n = height of the heighest level above the base

h_{sx} = story height below level x

I = importance factor of structural system of UBC

I_i = moment of inertia of member i

J = set of design variables that is not constrained by the lower bound

J_o = set of design variables constrained by the lower bound

K = a factor depending on the type of structural system of UBC

$[K]$ = stiffness matrix of the structure in global coordinates

$[K]_i$ = stiffness matrix of the member i in global coordinates

$[K_g]_i$ = geometric matrix of member i in global coordinates

K_y = lateral stiffness of a foundation

K_θ = rocking stiffness of a foundation

k = distribution coefficient of seismic forces of ATC-3-06

$\bar{k}$ = effective stiffness of a building when fixed at the base

k' = initial stiffness of a connection

L = overall length of a building at base in the direction of analysis

M_o, M_{ol} = the overturning moment at the foundation-soil interface

M_p = plastic moment of a beam

M_p' = plastic moment capacity induced by the plates at beam-column connections

M_x = overturning design moment at level x

n_s = total number of floor level

P_i' = derivative of P-Δ forces acting on the member i

P_x = total unfactored vertical design load at and above level x

p = forcing frequency based on Rayleigh quotient

p_{dh} = dynamic wind pressure at height h

p_h = wind pressure at height h

$\{Q_j\}$ = vector of virtual load in the j^{th} direction and zero values for others

$\{\bar{Q}_j\}_{ei}$ = nodal forces of member i in local coordinates due to the virtual load vector $\{Q_j\}$

$\{\bar{Q}_j\}_{gi}$ = nodal forces of member i in global coordinates due to the virtual load vector $\{Q_j\}$

$\{\bar{Q}_{gj}\}_{ei}$ = geometric forces vector of member i in local coordinates due to the virtual displacement resulting from the virtual load vector $\{Q_j\}$

$\{q_j\}$ = vector of virtual displacements resulting from the virtual load vector $\{Q_j\}$

q_s = the wind stagnation pressure coefficient at the standard height of 30 feet

R = response modification factor of ATC-3-06

$\{R\}$ = load vector

r = the power law coefficient

$\{r\}$ = displacement vector

$\{\bar{r}\}_{ei}$ = static displacement vector corresponding to the local coordinate of member i

$\{\bar{r}\}_{gi}$ = static displacement vector in global coordinates corresponding to the degrees of freedom of member i

$\{r(x,t)\}$ = dynamic displacement vector

$\{r(x,t)\}_{ei}$ = dynamic displacement vector corresponding to the local coordinates of member i

r_x = radius of gyration of wide flange sections

$\{dr\}_i$ = the change in displacement vector, $\{r\}$, due to the change in design variable x_i

Δr_j = total influence on the displacement of j^{th} degree of freedom due to the change of design variables x

dr_{ji} = the change of displacement in j^{th} degree of freedom due to the change in design variable x_i

S = site coefficient of ATC-3-06 or the site resonance factor factor of UBC

S_1, S_2, S_3 = the Soil Profile Types of ATC-3-06

S_a = spectral acceleration

S_d = spectral displacement

S_v = spectral velocity

s = step size for the contribution based on constraint gradients

[T] = transformation matrix

$\tilde{T}$, $\tilde{T}_1$ = effective fundamental period of a building

T_a = approximate fundamental period of ATC-3-06

T_i, T_m = modal period of i^{th} and m^{th} mode

T_s = site period of UBC

t = time

U = strain energy of a system

u_i = strain energy of member i

$u_j(x)$ = static constraint function for the j^{th} direction

V = seismic design base shear

V_m = seismic design base shear of mode m

V_x = seismic shear forces at any level x

$(V_{TW})_i$ = volume of welding metal of each connection

v_h = mean wind velocity at height h

v_g = gradient wind velocity

ΔV = the reduction in base shear, V, due to the effect of soil-structure interaction

W = total gravity load applied on a building

$\overline{W}$ = the effective gravity load of a building

$\overline{W}_m$ = the effective modal gravity load of m^{th} mode

$W(x)$ = objective function

w_i, w_x = portion of W which is located at or assigned to level i or x

x_i = i^{th} design variable

x_i^o = lower bound of j^{th} design variable

dx_i = the change of design variable x_i

$y_j(x)$ = j^{th} behavior constraint

Z = a zone coefficient of UBC

Z_x = plastic modulus of wide flange sections

α = seismic influence coefficient of Chinese Seismic Design Code

α_a = amplification factor of spectral acceleration of Newmark's spectra

α_d = amplification factor of spectral displacement of Newmark's spectra

α_i = i^{th} relative design variable

α_v = amplification factor of spectral velocity of Newmark's spectra

$\delta\alpha_i$ = departure of new relative design variable from present design for member i

β = the friction of critical damping for the coupled structure-foundation system; or damping ratio of a structure

β_o = the foundation damping factor

Δ_a = allowable story drift of ATC-3-06

Δ_i = story drift between level i and level i-1

Λ = scaling factor

Ω, Ω_1 = constant proportionalities of the constraint gradient method for displacement constraint and stress constraint respectively

$\Delta\sigma_j$ = total influence on the stress of member j due to the change of design variables x

$d\sigma_{ji}$ = the influence on the stress of member j due to the change of design variable x_i

σ_y = yielding stress of beam

σ_y' = yielding stress of the plate at beam-column connection

$\{\phi_j\}$ = eigenvector of j^{th} mode

ϕ_{im} = displacement amplitude of m^{th} mode at i^{th} level

ℓ_i = length of member i

ℓ'_{bw} = welded length of the bottom plate at beam-column connections

ℓ'_{tw} = welded length of the top plate at beam-column connections

ℓ'_{uw} = unwelded length of the plate at beam-column connections

ℓ'_w = welded length of the plate at beam-column connections

ρ = mass density of air

ρ_i = mass density of member i

η_i = ratio of the cross-sectional area, A_i, to the design variable, x_i, for i^{th} member

λ_j = j^{th} Lagrange multiplier

κ = overturning moment reduction factor in ATC-3-06

δ' = deflection at unwelded part of the plate at beam-column connections

δ_x = deflection at floor level x

δ_{xe} = deflection at floor level x determined by an elastic analysis

$\tilde{\delta}_x$, $\tilde{\delta}_{x1}$ = deflection at level x by considering the effect of soil-structure interaction

δ_{xem} = modal deflection at level x as determined by an elastic analysis

δ_{xm}, δ_{xm} = modal deflection at level x

θ = stability coefficient for P-Δ effect considered in ATC-3-06

ε_y = yielding strain of the plate at beam-column connections

ξ = damage ratio

χ = ratio of the construction cost of damage items to the construction of a structure

ω_j = undamped natural frequency of j^{th} mode

I. INTRODUCTION

A. OBJECTIVE

A considerable amount of research has been expended in the study of seismic building code provisions of various countries.[70,71] For instance, extensive investigation of ATC-3-06[3,4] provisions has been performed around the world since it was published. The studies in the U.S. on ATC-3-06 have principally emphasized the logic of the provisions,[29] comparatively analyzed the structural system of the various codes provisions,[46] reviewed the conventional designs of typical systems, and improved the tentative provisions.[72] It has long been practiced that conventional structural designs are based on repeated analyses with assumed stiffnesses of the constituent members of a given structure. If the preliminary stiffnesses are not correctly ascertained, a poor design will be the result in spite of the number of analysis cycles and the sophistication of the analysis computer programs. Consequently, various response behaviors can be obtained with different sets of given stiffnesses for a structural system. Apparently, conventional design processes cannot guarantee an efficient design. This is particularly true in the case of an aseismic design. Therefore, if a design is to be reliable, it should be based on optimum design procedures from which an economic and serviceable structure can be obtained. The results of an optimum design should satisfy a set of constraints, such as stresses, displacements, frequencies, buckling loads, member sizes, and dynamic forces, as well as the story drifts. Therefore, the redistribution of the stiffnesses in a system can be

mathematically determined according to the constraint and loading requirements. Furthermore, it is worth noting that with the use of an optimum design computer program, the design process can be accelerated and the time needed to produce the design can be reduced considerably.

The primary objectives of this study are to develop an optimization technique and an associated computer program for structural design with various building codes including, UBC, Chinese-TJ-11-78, ATC-3-06 Tentative Provisions, and others. Specifically, the studies are 1) to derive a primary recursion formula that is based on optimality criteria, 2) to derive a secondary recursion formula that is based on constraint gradients from which the local optimal design resulting from the primary recursion formula can be reduced further, 3) to develop a mathematical model for minimum cost design, 4) to study the parameters of ATC-3-06 provisions, 5) to compare the optimum solutions of various seismic-resistant design code provisions, 6) to study the effect of different bracing systems on the optimum design of seismic structures, 7) to study the influence of different support conditions on the stiffness distribution of structures, 8) to study the effect of soil-structure interaction, 9) to compare the differences between optimum solutions based on drift constraints and displacement constraints, 10) to study the effect of multi-component ground motions and the second order P-Δ effect on relative stiffness requirements and overall stiffness distributions, and 11) to illustrate the design procedures by using an optimum design computer program and to show the benefit of using the optimum design computer program in engineering practice and academic usage.

B. LITERATURE REVIEW

The automatic design of structural systems for which optimization techniques are used has developed rapidly in the past two decades because of the availability of high speed digital computers and the growing knowledge developed in optimization theory. Typically, two distinct approaches to optimal structural design have been used in recent research programs. The first is based on standard mathematical programming methods.[5,12,14,35,40,48,49] A comprehensive review of these techniques was provided by Pope and Schmit.[45] The second is based on optimality criteria. In the early 1970's, Gellatly, Berke, Venkayya and others made extensive contributions to this area.[28,37,60,62] These two approaches are mostly used in the area of structural optimization. The other approaches are optimal control theory[67] and special optimization techniques such as dynamic programming method.[21]

Because of the complexity of the problem and insufficient knowledge of the dynamic behavior of complex structures, most of the earlier investigators restricted their designs to structures that were subjected to static loadings and constraints. A few researchers confined their designs for structures subjected to static equivalent seismic forces for simple structures and shear buildings.[52,64] However, with the growth in knowledge about the dynamic analysis of complex structures, a considerable number of investigators have shown an interest in developing optimization algorithms for structures subjected to dynamic loadings and constraints.[14,16,17,27,47,48,63,69] Kato et al.[35] and Solnes and Holst[52] applied structural optimization techniques to buildings subjected to earthquake loads by using a sequential linear

programming technique. Cheng and Botkin[14,15] used a feasible direction technique for the design of tall buildings and large frameworks and included the effect of second-order P-Δ forces in their design. Similar methods were also used by Ray et al.,[48] and Walker and Pister.[66] Recently, Venkayya and Cheng[63] and Cheng and Srifuengfung[16,17] extended the use of an optimization algorithm based on optimality criteria to structures subjected to multicomponent ground motions. Balling, Pister, etc.[6] used an analysis technique based on nonlinear step-by-step integration to design a four-story, three-bay, moment-resisting, planar steel frame.

The method that is used in this study is based on the work of Cheng et al.[18] The primary algorithm, which they use, is derived based on an optimality criterion technique. The method is very attractive for designing structures with a large number of design variables. To improve the previous work, a secondary recursion formula based on constraint gradients has been introduced. It is believed that in some cases the use of this formula coupling with the first recursion can improve the optimal solution.

The work related to ATC-3-06 may be briefly cited in References. Tso and Dempsey[56] compared the torsional provisions of various codes with the torsional moment that had been obtained by using a response spectrum technique. Sveinsson et al.[53] studied the provisions for masonry structures. Zagajeski and Bertero[68] briefly compared ATC-3-06 and UBC provisions for reinforced concrete buildings. Comparative studies of optimal solutions by Cheng and his associates. BSSC and others also performed some comparative studies based on conventional

analysis and design.

C. SCOPE OF THE REPORT

A computer program designated as ODSEWS-2D-II (Optimum Design of 2-Dimensional Steel Structures for Static, Earthquake, and Wind Forces-Version II) was developed for the purpose of analyzing and designing two-dimensional structures. The formulation is based on the displacement method, and consistent mass method and includes second-order P-Δ forces. The structural systems to which it can be applied are trusses, and unbraced and braced frames. The seismic information can be one-dimensional or two-dimensional; one-dimension is horizontal, two-dimensions is horizontal coupled with vertical. The dynamic forces may be 1) seismic excitations at the base, 2) dynamic forces applied at the structural nodes, and 3) wind forces acting on the structural surfaces. The seismic excitations include 1) the records of actual earthquakes, 2) response spectra of Newmark, Seed, and Housner, and those available in the Chinese Seismic Building Code and ATC-3-06, 3) the Uniform Building Code, 4) the Chinese Seismic Building Code, and 5) the ATC-3-06 provisions including the equivalent lateral forces with or without soil-structure interaction and the modal analysis with or without soil-structure interaction. The constituent members of a system are made of either built-up sections or hot-rolled wide flange sections. The constraints considered are stresses, displacements, story drifts, natural frequencies, maximum differences between relative stiffnesses, and upper and lower bounds of cross sections. The objective is to obtain the minimum weight or minimum cost of a structural system.

A brief discussion of the contents of each chapter of this report is given below.

In Chapter II, the derivation of the recursion formulas, which are based on optimality criteria and constraint gradients, is given, and the determination of the Lagrange multiplier for multiple constraints and loadings in the numerical procedures is also discussed in detail.

In Chapter III, the mathematical modeling of the structural costs, which include the basic charges for material, extra size, painting, connections, and repair of lifetime damage is discussed.

In Chapter IV, the response spectra, which are generated in the computer program, are introduced.

In Chapter V, the seismic design codes are briefly reviewed. The provisions include 1) the ATC-3-06 equivalent lateral force method with or without soil-structure interaction, 2) the ATC-3-06 modal analysis method with or without soil-structure interaction, 3) the Uniform Building Code, and 4) the Chinese Seismic Building Code equivalent lateral force method.

In Chapter VI, numerical design results and observations are given.

In Chapter VII, the complete design procedure in which the ODSEWS-2D-II computer program is used is illustrated.

In Chapter VIII, the work is reviewed, and the conclusions based on the optimum design results are listed.

II. OPTIMALITY ALGORITHM

A. MODIFICATION OF KUHN-TUCKER CONDITIONS

Let us assume the objective function is W(x's). This represents either the structural weight or the structural cost, and the x's are the primary variables. In optimization, the objective is to minimize the weight or costs of the structural system so that they satisfy the behavior constraint requirements, y_j(x's), such as allowable stresses, allowable deflections, and lower bounds of natural frequency of any particular mode. In the mathematical expressions, we will minimize

$$W(x_1,x_2,\ldots,x_m) \tag{2.1}$$

subject to

$$y_i(x_1,x_2,\ldots,x_m) \leq b_i, \quad i = 1,2,\ldots,n, \tag{2.2a}$$

$$y_{n+j}(x_1,x_2,\ldots,x_m) \leq -x_j^o, \quad j = 1,2,\ldots,m. \tag{2.2b}$$

in which b's are the behavior constraints, x^o's are the side constraints for lower limits of the member sizes, and $y_{n+j}(x_1,x_2,..,x_m)$ is equal to $-x_j$.

The necessary requirement for a local minimum is to satisfy the Kuhn-Tucker condition

$$\frac{\partial}{\partial x_i}(W(x_1,x_2,\ldots,x_m)) + \sum_{j=1}^{n+m} \lambda_j \frac{\partial}{\partial x_i}(y_j(x_1,x_2,\ldots,x_m)) = 0,$$

$$i = 1,2,\ldots,m \tag{2.3}$$

with

$$\lambda_i(y_i(x_1,x_2,\ldots,x_m)-b_i) = 0, \quad i = 1,2,..,n, \tag{2.4a}$$

$$\lambda_{n+j}(y_{n+j}(x_1,x_2,\ldots,x_m)+x_j^o) = 0, \quad j = 1,2,..,m, \tag{2.4b}$$

$$\lambda_i \geq 0, \quad i = 1,2,..,n, \tag{2.4c}$$

$$\lambda_{n+j} \geq 0, \quad j = 1,2,..,m. \tag{2.4d}$$

By substituting Eq.(2.4b) into Eq.(2.3), one obtains

$$\frac{\partial}{\partial x_i}(W(x_1,x_2,\ldots,x_m)) + \sum_{j=1}^{n} \lambda_j \frac{\partial}{\partial x_i}(y_j(x_1,x_2,\ldots,x_m)) - \lambda_{n+i} = 0,$$

$$i = 1,2,\ldots,m. \tag{2.5}$$

Let us consider two sets of design variables in Eq. (2.2b) as J, a set of $\{x_i\}$ satisfying inequality, and J_o, a set of $\{x_i\}$ satisfying equality. Then, for x_i in J, λ_{n+i} is equal to zero in Eq. (2.5). Therefore, for such i, Eq. (2.5) becomes

$$\frac{\partial}{\partial x_i}(W(x_1,x_2,\ldots,x_m)) + \sum_{j=1}^{n} \lambda_j \frac{\partial}{\partial x_i}(y_j(x_1,x_2,\ldots,x_m)) = 0. \tag{2.6}$$

For x_i in J_o, Eq.(2.5) becomes

$$\frac{\partial}{\partial x_i}(W(x_1,x_2,\ldots,x_m)) + \sum_{j=1}^{n} \lambda_j \frac{\partial}{\partial x_i}(y_j(x_1,x_2,\ldots,x_m)) - \lambda_{n+i} = 0. \tag{2.7}$$

Equations (2.6) and (2.7) are the modified Kuhn-Tucker conditions. From these two equations, one obtains

$$\frac{-\sum_{j=1}^{n} \lambda_j \frac{\partial}{\partial x_i}(y_j(x_1,x_2,\ldots,x_m))}{\frac{\partial}{\partial x_i}(W(x_1,x_2,\ldots,x_m))} = 1, \quad \text{for } x_i \in J, \tag{2.8}$$

and

$$\frac{-\sum_{j=1}^{n} \lambda_j \frac{\partial}{\partial x_i}(y_j(x_1,x_2,\ldots,x_m))}{\frac{\partial}{\partial x_i}(W(x_1,x_2,\ldots,x_m))} \leq 1, \quad \text{for } x_i \in J_o. \tag{2.9}$$

If any behavior constraint, y_t, is not active, then from Eq. (2.2a),

$$y_t(x_1,x_2,\ldots,x_m) - b_t < 0, \tag{2.10}$$

and from Eq. (2.4a),

$$\lambda_t = 0. \tag{2.11}$$

Let the number of active constraints be N, then the number of non-active constraints can be given by n-N. In Eqs. (2.8) and (2.9), we may pick up the potentially nonzero λ_j's, which correspond to active behavior constraints, and rearrange these λ_j's in Eqs. (2.8) and (2.9), which may now be expressed as

$$\frac{-\sum_{j=1}^{N} \lambda_j \frac{\partial}{\partial x_i}(y_j(x_1,x_2,\ldots,x_m))}{\frac{\partial}{\partial x_i}(W(x_1,x_2,\ldots,x_m))} = 1, \quad \text{for } x_i \in J, \tag{2.12}$$

and

$$\frac{-\sum_{j=1}^{N} \lambda_j \frac{\partial}{\partial x_i}(y_j(x_1,x_2,\ldots,x_m))}{\frac{\partial}{\partial x_i}(W(x_1,x_2,\ldots,x_m))} \leq 1, \quad \text{for } x_i \in J_o. \tag{2.13}$$

We now consider all x_i's belong to set J. By multiplying x_i^2 on both sides of Eq. (2.12), and then taking the square root as follows:

$$x_i = \left(\frac{-\sum_{j=1}^{N} \lambda_j \frac{\partial}{\partial x_i}(y_j(x_1,x_2,\ldots,x_m))}{\frac{\partial}{\partial x_i}(W(x_1,x_2,\ldots,x_m))} \right)^{1/2} x_i, \quad \text{for } x_i \in J. \tag{2.14}$$

According to Eq. (2.14), a recurrence relation on the basis of Kuhn-Tucker conditions can be obtained,

$$x_i^{v+1} = \left(\frac{-\sum_{j=1}^{N} \lambda_j \frac{\partial}{\partial x_i}(y_j(x_1,x_2,\ldots,x_m))}{\frac{\partial}{\partial x_i}(W(x_1,x_2,\ldots,x_m))} \right)^{1/2} x_i^{v}, \tag{2.15}$$

where v is the cycle number. If x_i^{v+1} converges to x_i^v, then x_i, which is a solution of Eq. (2.14), also satisfies Eq. (2.12).

B. OPTIMUM CRITERION BASED ON STATIC STIFFNESS

According to Clapeyron's theorem, the strain energy of a structure is expressed by

$$U = \frac{1}{2}\{R\}^T\{r\} \tag{2.16}$$

in which $\{R\}$ and $\{r\}$ represent load and displacement vectors respectively. The total strain energy, however, should have some limited value

$$\frac{1}{2}\{R\}^T\{r\} \leq \text{given value}, \tag{2.17}$$

which is a measurement of structural stiffness. According to Eqs. (2.6) and (2.7), one of the Kuhn-Tucker conditions may be expressed as

$$\frac{\partial W}{\partial x_i} + \lambda \frac{\partial}{\partial x_i}\left(\frac{1}{2}\{R\}^T\{r\}\right) = 0, \quad i = 1,2,\ldots,m. \tag{2.18}$$

The force-displacement relationship can be expressed in terms of structural stiffness matrix, $[K]$,as

$$\{R\} = [K]\{r\} = \sum_{i=1}^{m} [K]_i\{r\} \tag{2.19}$$

in which $[K]_i$ is the element stiffness matrix in global coordinates. In Eq. (2.18),

$$\frac{\partial}{\partial x_i}\left(\frac{1}{2}\{R\}^T\{r\}\right) = \frac{1}{2}\{R\}^T\frac{\partial\{r\}}{\partial x_i}. \tag{2.20}$$

By differentiating Eq. (2.19) with respect to x_i, one obtains

$$\begin{aligned} 0 &= \left([K]_1\frac{\partial\{r\}}{\partial x_i} + \ldots + [K]_m\frac{\partial\{r\}}{\partial x_i} \right) + \frac{\partial[K]_i}{\partial x_i}\{r\} \\ &= [K]\frac{\partial\{r\}}{\partial x_i} + \frac{\partial[K]_i}{\partial x_i}\{r\}. \end{aligned} \tag{2.21}$$

For a truss element, the design variable is the cross-sectional area, therefore

$$[K]_i = A_i \begin{bmatrix} E/\ell_i & -E/\ell_i \\ -E/\ell_i & E/\ell_i \end{bmatrix} = A_i [K]_i' \tag{2.22}$$

in which $[K]_i' = [K]_i / A_i$. For a column element of bending deformation combined with axial deformation, or a beam element with bending deformation only, the design variable is the moment of inertia of the cross section, I_i. For simplicity, the ratio of the cross-sectional area to the moment of inertia is assumed to be constant, η_i. Thus

$$[K]_i = \begin{bmatrix} EA_i/\ell_i & 0 & 0 & -EA_i/\ell_i & 0 & 0 \\ & 12EI_i/\ell_i^3 & 6EI_i/\ell_i^2 & 0 & -12EI_i/\ell_i^3 & 6EI_i/\ell_i^2 \\ & & 4EI_i/\ell_i & 0 & -6EI_i/\ell_i^2 & 2EI_i/\ell_i \\ & & & EA_i/\ell_i & 0 & 0 \\ & \text{sym.} & & & 12EI_i/\ell_i^3 & -6EI_i/\ell_i^2 \\ & & & & & 4EI_i/\ell_i \end{bmatrix}$$

$$= I_i \begin{bmatrix} E\eta_i/\ell_i & 0 & 0 & -E\eta_i/\ell_i & 0 & 0 \\ & 12E/\ell_i^3 & 6E/\ell_i^2 & 0 & -12E/\ell_i^3 & 6E/\ell_i^2 \\ & & 4E/\ell_i & 0 & -6E/\ell_i^2 & 2E/\ell_i \\ & & & E\eta_i/\ell_i & 0 & 0 \\ & \text{sym.} & & & 12E/\ell_i^3 & -6E/\ell_i^2 \\ & & & & & 4E/\ell_i \end{bmatrix}$$

$$= I_i [K]_i' \tag{2.23}$$

By combining Eqs. (2.22) and (2.23), one obtains

$$[K]_i = x_i [K]_i' \tag{2.24}$$

from which

$$[K]_i' = \frac{\partial [K]_i}{\partial x_i} \tag{2.25}$$

By substituting Eq. (2.25) into Eq. (2.21), one finds that

$$0 = [K]\frac{\partial \{r\}}{\partial x_i} + \frac{1}{x_i} [K]_i \{r\}. \tag{2.26}$$

from which

$$\frac{\partial \{r\}}{\partial x_i} = -\frac{1}{x_i} [K]^{-1}[K]_i \{r\}. \tag{2.27}$$

By combining Eqs. (2.19), (2.20) and (2.27), one obtains

$$\frac{\partial}{\partial x_i}\left(\frac{1}{2}\{R\}^T\{r\}\right) = -\frac{1}{2x_i}\{r\}^T[K]_i\{r\}. \tag{2.28}$$

The symbolic form of objective function is

$$W = \sum_{i=1}^{m} \rho_i A_i \ell_i = \sum_{i=1}^{m} \rho_i \eta_i x_i \ell_i \tag{2.29}$$

in which ℓ_i is the length of an element, i, ρ_i the unit weight of an element, i, and η_i the ratio of the cross-sectional area, A_i, to the

design variable, x_i. Then by substituting Eqs. (2.28) and (2.29) into Eq. (2.18), one obtains

$$\rho_i \eta_i \ell_i - \frac{\lambda}{2x_i} \{r\}^T [K]_i \{r\} = 0 \tag{2.30}$$

from which

$$1 = \frac{\lambda \{r\}^T [K]_i \{r\}}{2\rho_i \eta_i \ell_i x_i}. \tag{2.31}$$

The strain energy stored in an element, i, is

$$u_i = \frac{1}{2} \{r\}^T [K]_i \{r\}, \tag{2.32}$$

therefore,

$$\sum_{i=1}^{m} u_i = \sum_{i=1}^{m} \frac{1}{2} \{r\}^T [K]_i \{r\} = \frac{1}{2} \{r\}^T [K] \{r\}, \tag{2.33}$$

which may also be expressed as

$$\sum_{i=1}^{m} u_i = \frac{1}{2} \{r\}^T \{R\} = U. \tag{2.34}$$

From Eq. (2.31).

$$\frac{1}{\lambda} \sum_{i=1}^{m} \rho_i \eta_i x_i \ell_i = \sum_{i=1}^{m} \frac{1}{2} \{r\}^T [K]_i \{r\} = U \tag{2.35}$$

we have

$$\lambda = \frac{W}{U} \tag{2.36}$$

By multiplying x_i^2 on both sides of Eq. (2.31) and then taking the square root, one obtains

$$x_i = (\lambda)^{\frac{1}{2}} \left(\frac{\frac{1}{2}\{r\}^T [K]_i \{r\}}{\rho_i \eta_i \ell_i} \right)^{\frac{1}{2}} (x_i)^{\frac{1}{2}} \tag{2.37}$$

By substituting Eqs. (2.35) and (2.36) into the above equation, yields

$$x_i = \left(\frac{W}{U}\right)^{1/2} \left(\frac{u_i}{\rho_i \eta_i \ell_i}\right)^{1/2} (x_i)^{1/2} \tag{2.38}$$

in which x_i must satisfy at the optimum state. Let us now consider the following recursion relationship at v and v+1 cycles,

$$x_i^{(v+1)} = \left(\left(\frac{W}{U}\right)^{1/2} \left(\frac{u_i}{\rho_i \eta_i \ell_i}\right)^{1/2}\right)^{(v)} (x_i^{(v)})^{1/2} \tag{2.39}$$

when $\lim_{v\to\infty} x_i^{(v)} = x_i$, $\lim_{v\to\infty} U^{(v)} = U$, $\lim_{v\to\infty} W^{(v)} = W$, $\lim_{v\to\infty} u_i^{(v)} = u_i$, then Eq. (2.39) converges to Eq. (2.38), which indicates that $\lim_{v\to\infty} x_i^{(v)} = x_i$ satisfies both the recursion relationship and the necessary conditions of optimality. By introducing $x_i = \Lambda \alpha_i$ into Eq. (2.39) one obtains

$$(\Lambda\alpha_i)^{(v+1)} = \left(\left(\frac{W}{U}\right)^{1/2} \left(\frac{u_i \Lambda}{\alpha_i \eta_i \rho_i \ell_i}\right)^{1/2} \alpha_i\right)^{(v)}. \tag{2.40}$$

in which α_i is the relative design variable, and Λ the scaling factor whose value is equal to the maximum moment of inertia among all members of a framework or the maximum cross-sectional area among all members of a truss. If $u_i' = u_i \Lambda$, and $\zeta_i' = \alpha_i \eta_i \rho_i \ell_i$, Eq. (2.40) becomes

$$(\Lambda\alpha_i)^{(v+1)} = \left(\left(\frac{W}{U}\right)^{1/2} \left(\frac{u_i'}{\zeta_i'}\right)^{1/2} \alpha_i\right)^{(v)}. \tag{2.41}$$

If one considers the P-Δ effect resulting from the axial force on a member, Eq. (2.35) may be rewritten as

$$\frac{1}{\lambda} \sum_{i=1}^{m} \rho_i \eta_i x_i \ell_i = \sum_{i=1}^{m} \frac{1}{2} \left(\{r\}^T [K]_i \{r\} - P_i' \{r\}^T [K_g]_i \{r\}\right) \tag{2.42}$$

in which P_i' is equal to $\rho_i \eta_i \ell_i / 2$ which is half weight of the member differentiate with respect to the design variable, x_i, and $[K_g]_i$ is the geometric stiffness matrix in global coordinates associated with the P-Δ effect.

Because the structural weight is to be minimized however, sufficient strain energy is required to bring the structure stay in the feasible region. For this purpose, u_i'/ζ_i' in Eq. (2.41) is necessary to be selected as large as possible, that is, λ should be selected as small as possible. For programming convenience, the Lagrange multiplier in Eq. (2.41) associated with W/U may be replaced by

$$\lambda_{min} = \min\left(\left(\frac{\zeta_i'}{u_i'}\Lambda^2\right)\left(\frac{R_{x_j}}{R_{x_{max}}}\right)^2\right)$$

$$= \min\left(\left(\frac{\eta_i x_i \rho_i \ell_i}{\frac{1}{2}(\{r\}^T[K]_i\{r\} - P_i'\{r\}^T[K_g]_i\{r\})}\right)\left(\frac{R_{x_j}}{R_{x_{max}}}\right)^2\right) \qquad (2.43)$$

This means that λ_{min} is the minimum value chosen from all the members under each loading condition. R_{x_j} is the maximum ratio of the actual stress to the allowable stress among all members at the loading condition j, and $R_{x_{max}}$ is the maximum value of all the ratios based on the constraints of stresses, displacements, and frequencies. $R_{x_j}/R_{x_{max}}$ is used as an approximate approach to adjust the original scaling factor, Λ, which is based on the maximum ratio for all constraints. Note that the stiffness constraint is now treated as stress constraint. For NLC loading conditions, one should obtain NLC λ_{min}. One may use either Eq. (2.36) or (2.43) to evaluate the Lagrange multiplier.

C. OPTIMUM CRITERION BASED ON STATIC DISPLACEMENT CONSTRAINTS

For convenience of formulation and calculation, let us consider one of several displacement constraints. If the j^{th} degree of freedom is active, one may express this displacement as

$$u_j(x_1, x_2, \ldots, x_m) \leq \text{given value} \qquad (2.44)$$

in which x's are primary design variables. One of the Kuhn-Tucker conditions of Eqs. (2.3) and (2.4) is

$$\frac{\partial W}{\partial x_i} + \lambda \frac{\partial u_j}{\partial x_i} = 0, \quad i = 1,2,\ldots,m. \tag{2.45}$$

The term u_j can be expresses as

$$u_j = \{Q_j\}^T\{r\} \tag{2.46}$$

in which $\{r\}$ is the actual displacement vector, and $\{Q_j\}$ the virtual load vector in the following form

$$\{Q_j\} = [0\ 0\ldots 0\ \underset{j^{th}\text{ column}}{\overset{\uparrow}{1}}\ 0\ldots 0\ 0]^T. \tag{2.47}$$

In Eq. (2.45),

$$\frac{\partial u_j}{\partial x_i} = \{Q_j\}^T \frac{\partial\{r\}}{\partial x_i}. \tag{2.48}$$

If one uses the same process of derivation for the energy constraints of Eq. (2.27), then

$$\frac{\partial\{r\}}{\partial x_i} = -\frac{1}{x_i}[K]^{-1}[K]_i\{r\}. \tag{2.49}$$

If we consider $\{Q_j\}$ of Eq. (2.47) as load vector that is virtually applied to the structure, the force-displacement relationship can be expressed as

$$\{Q_j\} = [K]\{q_j\}. \tag{2.50}$$

in which $\{q_j\}$ is the displacement resulting from virtual load vector $\{Q_j\}$. By substituting Eqs. (2.49) and (2.50) into Eq.(2.48), one then obtains

$$\frac{\partial u_j}{\partial x_i} = -\frac{1}{x_i}\{q_j\}^T[K]_i\{r\}. \tag{2.51}$$

If we introduce

$$\{\bar{Q}_j\}_{gi} = [K]_i\{q_j\}, \tag{2.52}$$

then $\{\bar{Q}_j\}_{gi}$ becomes the nodal forces of element i in global coordinates due to the virtual load, $\{Q_j\}$. From Eqs. (2.51) and (2.52),

$$\frac{\partial u_j}{\partial x_i} = -\frac{1}{x_i}\{\bar{Q}_j\}_{gi}^T\{r\}. \tag{2.53}$$

Remove those degrees of freedom that are not related to the element i in $\{q_j\}$, which is modified as $\{\bar{q}_j\}$. Then Eq. (2.52) becomes

$$\{\bar{Q}_j\}_{gi} = [K]_i\{\bar{q}_j\}. \tag{2.54}$$

Let $\{\bar{r}\}_{gi}$ be the actual displacements at the nodes of element i in the global coordinates; then Eq. (2.53) yields

$$\frac{\partial u_j}{\partial x_i} = -\frac{1}{x_i}\{\bar{Q}_j\}_{gi}^T\{\bar{r}\}_{gi}. \tag{2.55}$$

By using the transformation matrix, [T], from the local coordinates to

the global coordinates, we have

$$\{\bar{Q}_j\}_{gi} = [T]\{\bar{Q}_j\}_{ei}, \tag{2.56}$$

and

$$\{\bar{r}\}_{gi} = [T]\{\bar{r}\}_{ei} \tag{2.57}$$

in which the subscript ei represents the element i in local coordinates. Substituting Eqs. (2.56) and (2.57) into Eq.(2.55), yields

$$\frac{\partial u_j}{\partial x_i} = -\frac{1}{x_i}\{\bar{Q}_j\}^T_{ei}\{\bar{r}\}_{ei}. \tag{2.58}$$

Consider the objective function

$$W = \sum_{i=1}^{m} \rho_i \eta_i x_i \ell_i. \tag{2.59}$$

Then substituting Eqs. (2.58) and (2.59) into Eq. (2.45) gives

$$\eta_i \rho_i \ell_i = \frac{\lambda}{x_i}\{\bar{Q}_j\}^T_{ei}\{\bar{r}\}_{ei} \tag{2.60}$$

or

$$\lambda = \frac{\eta_i \rho_i \ell_i x_i}{\{Q_j\}^T_{ei}\{r\}_{ei}}. \tag{2.61}$$

By multiplying both sides by x_i^2 and then taking the square root,

$$x_i = (\lambda)^{\frac{1}{2}} \left(\frac{\{\bar{Q}_j\}^T_{ei}\{\bar{r}\}_{ei}}{\eta_i \rho_i \ell_i} \right)^{\frac{1}{2}} (x_i)^{\frac{1}{2}}. \tag{2.62}$$

By using $x_i = \Lambda\alpha_i$, and then considering the recursion relationship, we will have

$$(\Lambda\alpha_i)^{(v+1)} = (\lambda_{min})^{\frac{1}{2}} \left(\frac{\{Q_j\}^T_{ei}\{r\}_{ei}\Lambda}{\eta_i \alpha_i \rho_i \ell_i} \right)^{\frac{1}{2}} \alpha_i^{(v)} \tag{2.63}$$

In the computer analysis, λ_{min} is obtained as follows:

$$\lambda_{min} = \min \left(\left(\frac{\zeta_i'}{u_i'} \Lambda^2 \right) \left(\frac{R_{x_j}}{R_{x_{max}}} \right)^2 \right)$$

$$= \min \left(\left(\frac{\eta_i x_i \rho_i \ell_i}{\{\bar{Q}_j\}^T_{ei}\{\bar{r}\}_{ei}} \right) \left(\frac{R_{x_j}}{R_{x_{max}}} \right)^2 \right) \tag{2.64}$$

in which ζ_i' is equal to $\eta_i \alpha_i \rho_i \ell_i$, u_i' is equal to $\{\bar{Q}_j\}^T_{ei}\{\bar{r}\}_{ei}\Lambda$, and R_{x_j} is the ratio of the actual displacements (i.e., only those displacements associated with the j active displacement constraints) to the allowable displacement for each loading condition. $R_{x_{max}}$ is the maximum value of all the ratios for all the constraints and loading conditions considered. Thus, λ_{min} is sorted out as the minimum value for all members under each active displacement due to each loading condition. For NLC loading conditions with total nJ active displacements, we can have nJ λ_{min}. $R_{x_j}/R_{x_{max}}$ is used to adjust the original scaling factor, Λ, which is based on the maximum value of the ratios.

By considering the P-Δ effect on the stiffness, one may write Eq. (2.63) as

$$(\Delta\alpha_i)^{(v+1)} = \left((\lambda_{min})^{\frac{1}{2}} \left(\frac{(\{\bar{Q}_j\}^T_{ei}\{\bar{r}\}_{ei} - P_i'\{\bar{Q}_{gj}\}^T_{ei}\{\bar{r}\}_{ei})\Delta}{\eta_i\alpha_i\rho_i\ell_i} \right)^{\frac{1}{2}} \alpha_i \right)^{(v)} \tag{2.65}$$

in which $\{\bar{Q}_{gj}\}_{ei}$ is the geometric force vector of the element i occasioned by the displacement resulting from the load vector $\{Q_j\}$, and λ_{min} should be obtained in a similar manner as shown in Eq. (2.64) with the inclusion of the P-Δ effect.

D. OPTIMALITY CRITERION BASED ON THE CONSTRAINTS OF DYNAMIC ENERGY, DISPLACEMENT AND NATURAL FREQUENCIES[18]

1. Dynamic Stiffness Constraints. The derivation of the dynamic constraints is similar to that of static stiffness, which is also treated as the dynamic stress constraints. The recursion equation may be expressed as

$$\begin{aligned}(\Delta\alpha_i)^{(v+1)} = ((\frac{W}{U})^{1/2}(&(\{r(x,t)\}^T[K]_i\{r(x,t)\} \\ &- P_i'\{r(x,t)\}^T[K_g]_i\{r(x,t)\} \\ &- p^2\{r(x,t)\}^T[M_s]_i\{r(x,t)\})\Delta/2\eta_i\alpha_i\rho_i\ell_i)^{1/2}\ \alpha_i)^{(v)}\end{aligned} \tag{2.66}$$

in which p is the frequency obtained on the basis of Rayleigh quotient,

$[M_s]_i$ is the structural mass matrix of member i in global coordinates, and the variables, x and t, represent the design variable and time respectively.

$$U = \sum_{i=1}^{m} u_i = \sum_{i=1}^{m} \frac{1}{2}(\{r(x,t)\}^T[K]_i\{r(x,t)\} - P_i'\{r(x,t)\}^T[K_g]_i\{r(x,t)\} - p^2\{r(x,t)\}^T[M_s]_i\{r(x,t)\}) \tag{2.67}$$

and

$$W = \sum_{i=1}^{m} w_i = \sum_{i=1}^{m} \eta_i x_i \rho_i \ell_i \tag{2.68}$$

However, W/U may be replaced by λ_{min} as in

$$\lambda_{min} = \min\left(\left(\frac{\zeta_i'}{u_i'} \Lambda^2 \right) \left(\frac{R_{x_i}}{R_{x_{max}}} \right)^2 \right)$$

$$= \min\left(\left(\frac{w_i}{u_i} \right) \left(\frac{R_{x_i}}{R_{x_{max}}} \right)^2 \right) \tag{2.69}$$

in which u_i and w_i are expressed in Eqs. (2.67) and (2.68) respectively, ζ_i' is equal to w_i/Λ, u_i' is equal to $u_i\Lambda$ and the other terms have already been explained in Eq. (2.43).

2. Dynamic Displacement Constraints. Similiar to the derivation of the recursion for static displacement constraints, the recursion expression for the dynamic case can be expressed as

$$(\Delta\alpha_i)^{(v+1)} = ((\lambda_{min})^{1/2}\ \alpha_i((\{\bar{Q}_j\}^T_{ei}\{r(x,t)\}_{ei} - P_i'\{\bar{Q}_{gj}\}^T_{ei}\{r(x,t)\}_{ei}$$

$$- p^2\{\bar{\bar{Q}}_j\}^T_{ei}\{r(x,t)\}_{ei})\Delta/\eta_i\alpha_i\rho_i\ell_i)^{1/2})^{(v)} \qquad (2.70)$$

in which $\{\bar{\bar{Q}}_j\}_{ei}$ is the inertia force vector of the element i due to displacement resulting from the load vector, $\{Q_j\}$, and

$$\lambda_{min} = \min\left((\frac{\zeta_i'}{u_i'}\Lambda^2)(\frac{R_{x_j}}{R_{x_{max}}})^2\right)$$

$$= \min\ ((\eta_i x_i\rho_i\ell_i/(\{\bar{Q}_j\}^T_{ei}\{r(x,t)\}_{ei} - P_i'\{\bar{Q}_{gj}\}^T_{ei}\{r(x,t)\}_{ei}$$

$$- p^2\{\bar{\bar{Q}}_j\}^T_{ei}\{r(x,t)\}_{ei}))(\frac{R_{x_j}}{R_{x_{max}}})^2) \qquad (2.71)$$

in which R_{x_j} and $R_{x_{max}}$ are for the dynamic case, that are similarly defined in Eq. (2.64), ζ_i' is equal to $\eta_i\alpha_i\rho_i\ell_i$, and u_i' is equal to $\Lambda(\{\bar{Q}_j\}^T_{ei}\{r(x,t)\}_{ei} - P_i'\{\bar{Q}_{gj}\}^T_{ei}\{r(x,t)\}_{ei} - p^2\{\bar{\bar{Q}}_j\}^T_{ei}\{r(x,t)\}_{ei})$.

3. Dynamic Frequency Constraint. For the constraint on any natural frequency, ω_j, the recursion equation may be written as

$$(\Delta\alpha_i)^{(v+1)} = ((\lambda_{min})^{1/2}\ \alpha_i\ (\{\phi_j\}^T[K]_i\{\phi_j\} - P_i'\{\phi_j\}^T[K_g]_i\{\phi_j\}$$

$$- \omega_j^2\{\phi_j\}^T[M_s]_i\{\phi_j\})\Delta/\eta_i\alpha_i\rho_i\ell_i)^{1/2})^{(v)} \qquad (2.72)$$

in which $\{\phi_j\}$ is the normal mode and

$$\lambda_{min} = \min \left(\left(\frac{\zeta_i'}{u_i'} \Lambda^2 \right) \left(\frac{R_{x_j}}{R_{x_{max}}} \right)^2 \right)$$

$$= \min \left(\left(\eta_i x_i \rho_i \ell_i / \left(\{\phi_j\}^T [K]_i \{\phi_j\} - P_i' \{\phi_j\}^T [K_g]_i \{\phi_j\} \right. \right. \right.$$

$$\left. \left. \left. - \omega_j^2 \{\phi_j\}^T [M_s]_i \{\phi_j\} \right) \right) \left(\frac{R_{x_j}}{R_{x_{max}}} \right)^2 \right) \qquad (2.73)$$

where R_{x_j} is the ratio of the allowable frequency to the actual frequency of the j^{th} mode and $R_{x_{max}}$ is the maximum value of all the ratios for various constraints and loading conditions including static and dynamic loadings, if any. It is apparent that the maximum is searched for in each member i corresponding to the particular mode being investigated. ζ_i' is equal to $\eta_i \alpha_i \rho_i \ell_i$, and u_i' is equal to $\Lambda(\{\phi_j\}^T [K]_i \{\phi_j\} - P_i' \{\phi_j\}^T [K_g]_i \{\phi_j\} - \omega_j^2 \{\phi_j\}^T [M_s]_i \{\phi_j\})$.

4. Determination of Energy Density for Dynamic Design. As discussed in Sections D.1, D.2, and D.3, the strain energy, virtual strain energy, and kinetic energy are included in the calculation of energy density for each individual member i. However, in designing high-rise buildings or buildings with a low value of the fundamental natural frequency, the negative value of energy density may be obtained for the members on the upper stories. According to the numerical procedures, all members with negative values of energy density should be redesigned as passive elements. The weight of a structure would not be further reduced and sometimes could be increased in the next cycle of iteration because of the enormous

increment in structural flexibility; the excessive deflection would cause a larger scaling factor. To prevent an incorrect redistribution in the sizes of the members, the kinetic energy should be taken as zero when the energy desity of the member is negative. Therefore, if the energy density of the member i is negative, then Eqs. (2.66), (2.70), and (2.72) can be rewritten as Eqs. (2.74), (2.75), and (2.76) respectively.

$$(\Lambda\alpha_i)^{(v+1)} = \left(\left(\frac{W}{U}\right)^{1/2} \left(\left(\{r(x,t)\}^T[K]_i\{r(x,t)\}\right.\right.\right.$$
$$\left.\left.\left. - P_i'\{r(x,t)\}^T[K_g]_i\{r(x,t)\}\right)\Lambda/2\eta_i\alpha_i\rho_i\ell_i\right)^{1/2} \alpha_i\right)^{(v)} \tag{2.74}$$

$$(\Lambda\alpha_i)^{(v+1)} = \left(\left(\frac{W}{U}\right)^{1/2} \left(\left(\{\bar{Q}_j\}^T_{ei}\{r(x,t)\}_{ei}\right.\right.\right.$$
$$\left.\left.\left. - P_i'\{\bar{Q}_{gj}\}^T_{ei}\{r(x,t)\}_{ei}\right)\Lambda/\eta_i\alpha_i\rho_i\ell_i\right)^{1/2} \alpha_i\right)^{(v)} \tag{2.75}$$

$$(\Lambda\alpha_i)^{(v+1)} = \left(\left(\frac{W}{U}\right)^{1/2} \left(\left(\{\phi_j\}^T[K]_i\{\phi_j\}\right.\right.\right.$$
$$\left.\left.\left. - P_i'\{\phi_j\}^T[K_g]_i\{\phi_j\}\right)\Lambda/\eta_i\alpha_i\rho_i\ell_i\right)^{1/2} \alpha_i\right)^{(v)} \tag{2.76}$$

in which the total energy, U, should not include the kinetic energy term.

E. RECURSION RELATION BASED ON MULTIPLE ACTIVE CONSTRAINTS

In any design, it is possible to have more than one active

constraint when the restraints on displacements, stresses, and frequencies are imposed simultaneously. Therefore, it is necessary to find the Lagrange multipliers corresponding to the active constraints of current design variables. However, because of the difficulty in making a numerical calculation, the minimum value of λ for all active constraints of member i is adopted in the recursion relation, which is given as

$$(\alpha_i)^{(v+1)} = (\alpha_i)^{(v)}\left(\frac{\max(u'_{ij}\lambda_J)}{\zeta'_{ij}}\right)^{1/2} \tag{2.77}$$

in which λ_J is the minimum value of λ determined from all active constraints for an individual member i and expressed as $\min(\lambda_{ij})$. The maximum value of u'_{ij} is also obtained from all active constraints of member i. Thus $\max(u'_{ij}\lambda_J)$ is the upper bound of the member size requirement for all active constraints for all loading conditions. Note that the static displacements are combined with dynamic displacements from which the stresses are calculated.

F. CALCULATION OF CONSTRAINT GRADIENTS

The recursion relation based on strain energy criterion in conjunction with the scaling procedure presented in the previous sections is sufficient for designing optimum structures with various constraints. The design , however, can be further improved by using an iterative algorithm based on constraint gradients for which the algorithm is of the following form

$$\alpha_i^{(v+1)} = \alpha_i^{(v)} + s(\Delta\alpha_i) \tag{2.78}$$

in which v and v+1 refer to the cycle of iteration, α_i is the relative design variable of member i, and s is the step size determining the rate of approach to the algorithm. The value $\Delta\alpha_i$ is determined by the influence of the design variable of member i on the active constraints. The procedures for determining $\Delta\alpha_i$, which is based on the active displacement constraint and active stress constraint, are presented below.

1. Determination of $\Delta\alpha_i$ Based on Displacement Constraints. Let us consider a structure has been optimized to a local minimum. If we increase a member size and reanalyze it, two possibilities can be found in the behavior of the structure: a) the displacements in active degrees of freedom are increased, and b) the displacements in active degrees of freedom are decreased. The former is called negative influence because the structure is less stiff when the member size is increased, and the latter is called positive influence. If the procedure is repeated by changing member size one by one, one can discover which member can be reduced in size. However, this information does not provide the magnitude of change. An overshooting problem could occur in the optimal process if the magnitude of change in the member size is not suitably chosen. To overcome this problem, the following procedures are derived.

Let us reduce size of all the members in a structure by a certain

percentage. This change will reduce the structural stiffness, and consequently, the active displacement, r_j, is increased beyond the constrained surface by Δr_j. In order to bring it back to the constrained surface, one can increase the size of members which have positive influence. The magnitude of the increment of member size, Δx_i, is determined on the basis of the assumptions that the change in displacement is directly proportional to the change of member size, and the change of member size is inversely proportional to the member length because an increase in size of a member with a larger length causes a larger increase in weight. Thus, the increment in member size, Δx_i, can be expressed as follows:

$$\Delta x_i = \Omega \frac{dr_{ji}}{\ell_i} \tag{2.79}$$

in which dr_{ji} is the change of displacement in the active degree of freedom j due to the unit change in the size of member i, and Ω is a constant proportionality, which is determined by evaluating the average influence on the change of the displacement in the active degree of freedom occasioned by the unit change in the size of members those have positive influence. In order to determine Ω, let us assume that dr_{ji} is directly proportional to the member size, x_i, and the change in r_j due to Δx_i is Δr_{ji}, then

$$\frac{\Delta r_{ji}}{\Delta x_i} = \frac{dr_{ji}}{x_i} \tag{2.80}$$

from which

$$\Delta r_{ji} = \frac{dr_{ji}}{x_i} \Delta x_i \tag{2.81}$$

By introducing $x_i = A\alpha_i$ into the above equation, one has

$$\Delta r_{ji} = \frac{dr_{ji}}{\alpha_i} \Delta \alpha_i \tag{2.82}$$

Thus, the total change in r_j due to the change in member size, Δx_i, is

$$\Delta r_j = \sum_{i=1}^{m} \Delta r_{ji} = \sum_{i=1}^{m} \frac{dr_{ji}}{\alpha_i} \Delta \alpha_i \tag{2.83}$$

in which m is the number of members that have postive influence on r_j. By substituting Eq. (2.79) into Eq. (2.83), one has

$$\Delta r_j = \bar{\Omega} \sum_{i=1}^{m} \frac{1}{\alpha_i \ell_i} (dr_{ji})^2 \tag{2.84}$$

in which $\bar{\Omega} = \Omega / A$. From Eq.(2.84), one finds that

$$\bar{\Omega} = \frac{\Delta r_j}{\sum_{k=1}^{m} \frac{1}{\alpha_k \ell_k} (dr_{jk})^2} \tag{2.85}$$

Substitution of Eq. (2.85) into Eq. (2.79) gives

$$\Delta \alpha_i = \frac{\Delta r_j}{\sum_{k=1}^{m} \frac{1}{\alpha_k \ell_k} (dr_{jk})^2} \left(\frac{dr_{ji}}{\ell_i} \right). \tag{2.86}$$

$\Delta\alpha_i$ is assumed to be zero if the value computed from Eq. (2.85) is negative.

It is possible that more than one displacement exceeds the limit. Under these circumstances then, it is necessary to determine the change in each element size separately for each constraint. The largest value of $\Delta\alpha_i$ shall be used for the actual change in the size of the i^{th} element.

2. Determination of $\Delta\alpha_i$ Based on Stress Constraints. The determination of $\Delta\alpha_i$ based on stress constraints is similar to that discussed in Sec. F.1. If "j" is the member at which the stress constraint is active, and $d\sigma_{ji}$ is the change in σ_j occasioned by a unit change in the size of element i, then the required change in the size of i^{th} element is determined by the following expression:

$$\Delta\alpha_i = \overline{\Omega}_1 \frac{d\sigma_{ji}}{\ell_i} \tag{2.87}$$

in which $d\sigma_{ji}$ is calculated on the basis of dr_{ji}, and the constant of proportionality is

$$\overline{\Omega}_1 = \frac{\Delta\sigma_j}{\sum_{k=1}^{m} \frac{1}{\alpha_k \ell_k} (d\sigma_{jk})^2} \tag{2.88}$$

in which $\Delta\sigma_j = \sum_{i=1}^{m} \Delta\sigma_{ji}$, which is determined from the summation of the differential stress (the difference between the actual stress and the allowable stress) associated with the active stress constraint of

member j, occasioned by the size changes of member i. The required change in relative design variable for Eq. (2.78) is then given as

$$\Delta\alpha_i = \frac{\Delta\sigma_j}{\sum_{k=1}^{m} \frac{1}{\alpha_k \ell_k} (d\sigma_{jk})^2} \left(\frac{d\sigma_{ji}}{\ell_i}\right). \tag{2.89}$$

3. Numerical Procedures for Calculating the Constraint Gradients. The detailed numerical procedures for calculating the constraint gradients are given below.

Step 1. Determine the most active constraint based on the design variables that satisfies the optimum criterion. At this step, the system stiffness matrix, [K], and the displacement vector, {r}, are stored as well.

Step 2. Calculate the stiffness matrices, $[K]_i$ and $[K']_i$, of each individual element i. Here, $[K]_i$ is the element stiffness matrix in the global coordinate corresponds to the design variable x_i determined in Step 1, and $[K']_i$ is the element stiffness matrix in the global coordinate and corresponds to the design variable with the unit change x_i+1.

Step 3. Calculate $\{dr\}_i$ according to Eq. (2.78). If the displacement constraint is the most active constraint, then proceed to Step 5.

Step 4. Calculate $\{d\sigma\}_i$ by using the result of Step 3.

Step 5. Reduce the design variable x_i of each element i by a reduction factor β. (Assume that β is 10~20%). Then check the reduced

design variable, $x_i' = (1-\beta)x_i$, with the size constraint. If x_i' is less than the lower bound of member size, x_{min}, then assume that x_i' is equal to x_{min}.

Step 6. Analyze the structure by using the reduced design variable to obtain the new displacement vector {r}. If the displacement constraint is the most active constraint, which is determined in Step 1, then proceed to Step 8.

Step 7. Calculate the new stress vector, {σ}, by using the displacement vector, {r}.

Step 8. Compute Δr_j or $\Delta\sigma_j$ by using the result of either Step 6 or 7: a) if the displacement constraint control, then $\Delta r_j = |r_j| - r_{ja}$ in which r_j is the displacement of {r} in the active constraint direction j, and r_{ja} is the allowable displacement, and if b) the stress constraint is the most active constraint, then $\Delta\sigma_j$ is determined according to $\Delta\sigma_j = |\sigma_j| - \sigma_{ja}$ in which σ_j is the active stress of member j in {σ}, and σ_{ja} is the allowable value of the stress.

Step 9. Calculate the required change in the size of each element i, α_i by using either Eq. (2.86) or (2.89). If a displacement constraint is active, Eq. (2.86) is used. For the value of dr_{ji} in Eq.(2.86), when $r_j < 0$ and $dr_{ji} > 0$ or when $r_j > 0$ and $dr_{ji} < 0$, then let dr_{ji} be equal to zero. If the stress constraint is active, then Eq. (2.89) is used. For the value of $d\sigma_{ji}$ in Eq. (2.88), when $\sigma_j < 0$ and $d\sigma_{ji} > 0$ or $\sigma_j > 0$ and $d\sigma_{ji} < 0$, then let $d\sigma_{ji}$ be equal to zero.

Step 10. Redistribute the member sizes according to Eq. (2.78).

III. OBJECTIVE COST FUNCTION

The recursion formulas for the design of a minimum weight structure that are based on energy and constraint gradients have been discussed in Chapter II. In this chapter, the discussion will be centered on the objective function for the design of a structure that has a minimum cost. The objective function of such a minimum cost design includes the costs of the structural members, painting, connections, and damage. These are discussed individually in the following sections.

A. STRUCTURAL MEMBER COSTS

The discussion of steel costs may be divided into two parts: one the basic charge, which is estimated on the basis of the weight of the purchased steel members, and the other the extra size charge, which is appraised on the basis of the shapes of the members.[65]

An evaluation of the basic charge can be easily calculated in accordance with the following equation:

$$C_{TB} = C_s \sum_{i=1}^{m} \rho_i A_i \ell_i \tag{3.1}$$

in which C_{TB} is the total basic charge of the structural members ($), C_s the unit price of steel ($/lb), m the total number of members of the structure, ρ_i the mass density of a steel member, i (lb/in^3), A_i the cross sectional area of a member, i (in^2), and ℓ_i the length of a member, i (in.). The design variable of the girders and columns, as

mentioned in Chapter II, is the moment of inertia, I. By replacing A_i in Eq. (3.1) with $A_i I_i / I_i$ for the girders and columns and assuming that the mass density of all the members is the same, Eq. (3.1) may be changed to the following form:

$$C_{TB} = C_s \rho \left(\sum_{i=1}^{m_g} \frac{A_i}{I_i} I_i \ell_i + \sum_{i=1}^{m_c} \frac{A_i}{I_i} I_i \ell_i + \sum_{i=1}^{m_b} A_i \ell_i \right)$$

$$= C_s \rho \left(\sum_{i=1}^{m_g} \eta_i I_i \ell_i + \sum_{i=1}^{m_c} \eta_i I_i \ell_i + \sum_{i=1}^{m_b} A_i \ell_i \right) \qquad (3.2)$$

in which η_i is equal to A_i/I_i, m_g is the total number of girders, m_c the total number of columns, and m_b the total number of bracings.

An appraisal of the extra size charge is based on the shape of the steel members. According to the industrial practice, a higher extra cost per pound for smaller shapes than that for larger ones as indicated in Figure 1 which may be represented by

$$C_{ex} = 0.00916 \, A^{-0.21} \qquad (3.3)$$

in which C_{ex} is quoted in dollars per pound. The extra size charge of each individual member, $(C_{EX})_i$, is then obtained as

$$(C_{EX})_i = 0.00916 \, \rho_i A_i^{0.79} \, \ell_i . \qquad (3.4)$$

By assuming that the extra size charges of bracings have a similar model as that of the members with wide flange sections, one can obtain the total extra size charge of the system with the following

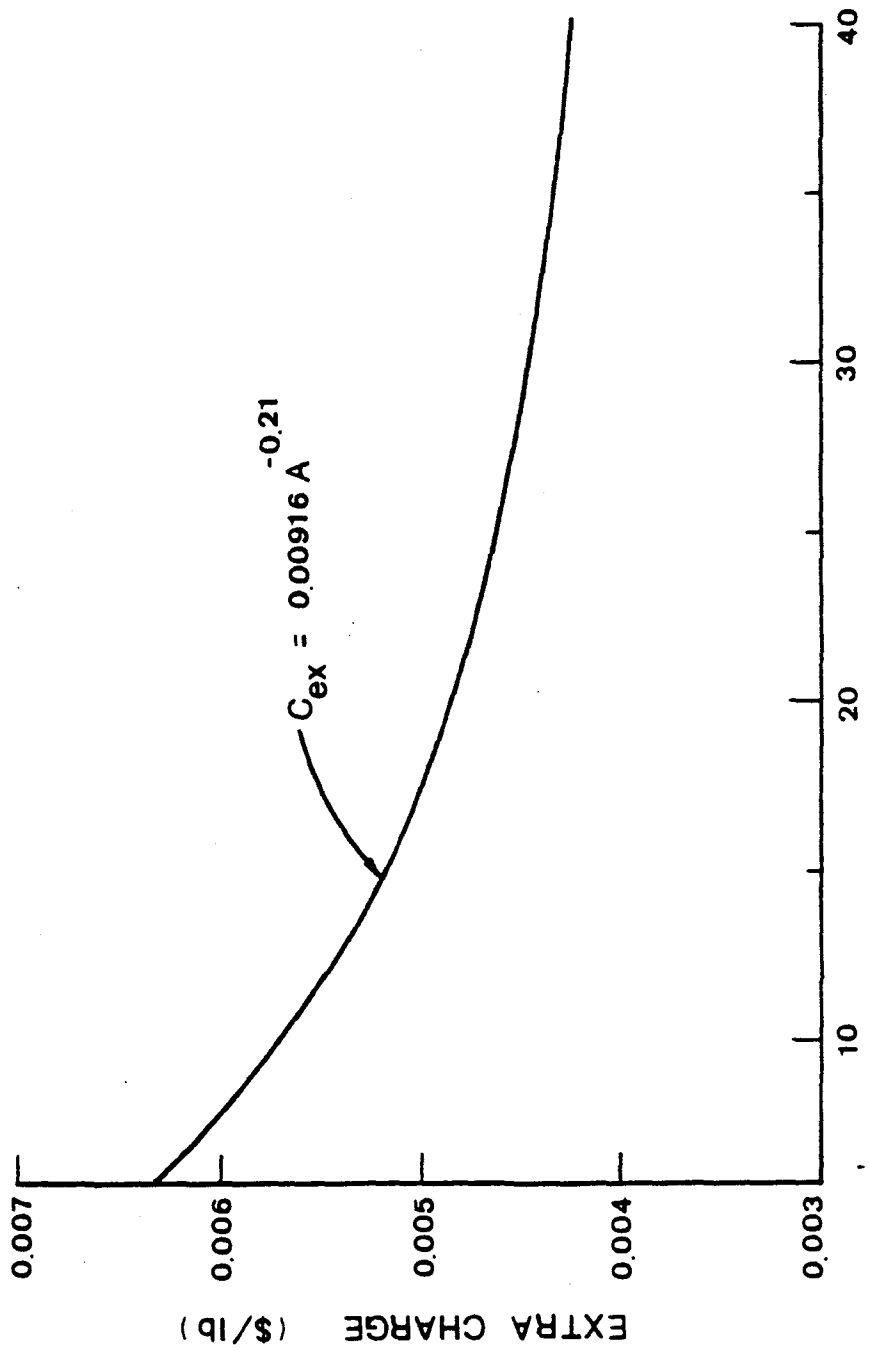

Figure 1. Extra Charge v.s. Sectional Area

formula:

$$C_{EX} = 0.00916 \sum_{i=1}^{m} \rho_i A_i^{0.79} \ell_i$$

$$= 0.00916\ \rho\ \Big(\sum_{i=1}^{m_g} \eta_i^{0.79}\ I_i^{0.79}\ \ell_i + \sum_{i=1}^{m_c} \eta_i^{0.79}\ I_i^{0.79}\ \ell_i$$

$$+ \sum_{i=1}^{m_b} A_i^{0.79}\ \ell_i \Big). \qquad (3.5)$$

B. PAINTING COSTS

The amount of painting is measured according to the surface area of the members. For simplicity, the cross section of a bracing member is assumed to be square. Thus, the surface area of each individual bracing member, i, is $4\sqrt{A_i}\ell_i$. For wide flange sections, the surface area is $(4b+2d)\ell$ for which b and d are the flange width and the depth of the section respectively. In order to model the cost of painting the wide flange sections, the relationship between the flange width and the design variable, I, and the relationship between the depth of the section and I must be developed. Unfortunately, there is no direct relationship that can be used for this development. For the selected economic sections from AISC Manual, the relationship developed between radius of the gyration, r_x, and depth, d, is

$$r_x \simeq 0.52\ d^{0.92} \qquad \text{(for beams)} \qquad (3.6)$$

in which the appropriate moment of inertia is between 180 in^4 and 2500

in^4, and

$$r_x \simeq 0.39\ d^{1.04} \qquad \text{(for columns)}. \tag{3.7}$$

where the appropriate moment of inertia is between 200 in^4 and 1500 in^4. Because $I = Ar_x^2$, Eqs. (3.6) and (3.7) become

$$d = \left(\frac{I}{0.2704\ A}\right)^{1/1.84} \qquad \text{(for beams)} \tag{3.8}$$

and

$$d = \left(\frac{I}{0.1521\ A}\right)^{1/2.08} \qquad \text{(for columns)} \tag{3.9}$$

The development of the relationship between flange width and moment of inertia is based on the assumption that the web thickness, t_w, and the flange thickness, t_f, can be expressed as $t_w \simeq t_f$ for most compact sections. By using this relationship and the cross-sectional depth, the approximate equations for moment of inertia and cross-sectional area can be established from which the flange width can be roughly expressed by

$$b = \frac{2.35\ (I/Z_x)}{2.09 - 0.812\ (Z_x^4/I^3)} \tag{3.10}$$

in which Z_x is the plastic modulus of the section that is expressed as $Z_x = 0.953\sqrt{AI}$. The mean value computation of Z_x for the selected sections results in

$$Z_x \simeq 2.25 \frac{I}{d} . \tag{3.11}$$

By substituting Eq. (3.11) into (3.10), one obtains

$$b = \frac{2.35\ d/2.25}{2.09 - 0.812\ (2.25\ I/d)^4/I^3} . \tag{3.12}$$

By using Eqs. (3.8), (3.9), and (3.12), the surface area of wide flange sections is obtained with the following formula:

$$(4b_i+2d_i)\ell_i = \eta_i^{-0.54328} \left(\frac{8.5043}{2.09 - 1.212\ \eta_i^{2.17391}\ I_i} + 4.0712 \right) \ell_i$$

(for beams) (3.13)

and

$$(4b_i+2d_i)\ell_i = \eta_i^{-0.4808} \left(\frac{10.3312}{2.09 - 0.5565\ \eta_i^{1.9231}\ I_i} + 4.946 \right) \ell_i$$

(for columns). (3.14)

Let us suppose that the unit price of painting is C_{pt}, then total painting cost of the structure, C_p, is

$$C_p = C_{pt} \left(\sum_{i=1}^{m_g} \eta_i^{-0.54328} \left(\frac{8.5043}{2.09 - 1.212\ \eta_i^{2.17391}\ I_i} + 4.0712 \right) \ell_i \right.$$

$$+ \sum_{i=1}^{m_c} \eta_i^{-0.4808} \left(\frac{10.3312}{2.09 - 0.5565\ \eta_i^{1.9231}\ I_i} + 4.946 \right) \ell_i$$

$$\left. + 4 \sum_{i=1}^{m_b} A_i^{0.5}\ \ell_i \right). \tag{3.15}$$

C. CONNECTION COSTS

The discussion of connection costs is primarily concerned with welded plate beam-column connections, which include the costs of steel plate and welding. Figure 2 shows a typical model of a steel plate, which is to be welded to the top and bottom flanges of beams at each beam-column connection. The connections are required to be able to develop the full moment capacity of beams. That is, the plastic moment of the connection, M_p', must be larger than the plastic moment of the beam, M_p. For simplicity, M_p' is taken to be equal to M_p. The plastic moment of the connections is given as

$$M_p' = \sigma_y' \, d \, A' \tag{3.16}$$

in which σ_y' is the yielding stress of the plate (psi), A' the cross sectional area of the plate (in^2), and d the depth of the beam (in.). By rearranging Eq. (3.16) and assuming that the plates are A514 steel and the beams are A36 steel, it can be said that the cross-sectional area of the plate is

$$A' = \frac{M_p'}{\sigma_y' \, d} = \frac{M_p}{\sigma_y' \, d} = 0.36 \, \frac{Z_x}{d} \, . \tag{3.17}$$

Equation (3.16) can be also rearranged as follows:

$$\sigma_y' = \frac{M_p'}{A' d} \, . \tag{3.18}$$

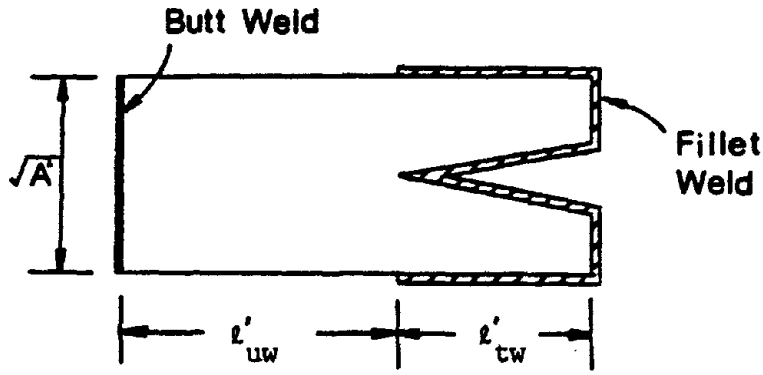

(a) Plate on the Top Flange of Beam

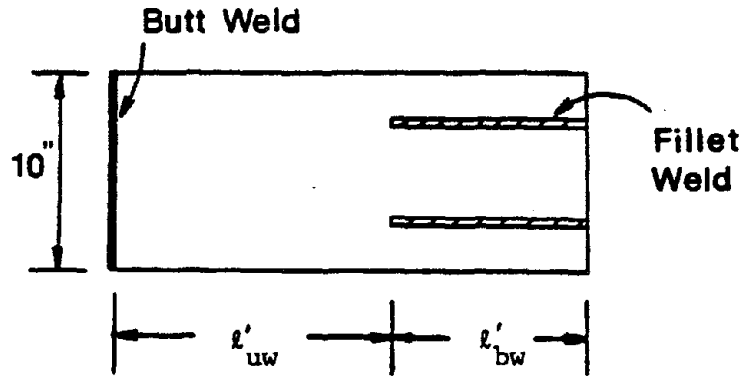

(b) Plate on the Bottom Flange of Beam

Figure 2. Typical Model of Plates at Beam-Column Connections

Then, from the stress-strain relation,

$$\sigma_y' = E\varepsilon_y'. \tag{3.19}$$

Let δ' be the deformation of the plate at the unwelded part, then the strain becomes

$$\varepsilon_y' = \frac{\delta'}{\ell_{uw}'}. \tag{3.20}$$

From Eqs. (3.18) through (3.20)

$$\delta' = \frac{M_p'}{A'dE}\ell_{uw}'. \tag{3.21}$$

Thus, the rotation, θ, at the connection is found to be

$$\theta = \delta' \frac{2}{d} = \frac{2 M_p' \ell_{uw}'}{A'd^2E}. \tag{3.22}$$

Let us suppose that k' is the initial stiffness of the connection, which is defined as the ratio of the plastic moment to the rotation of the connection, then

$$k' = \frac{M_p'}{\theta} = \frac{A'd^2E}{2\ell_{uw}'}. \tag{3.23}$$

The unwelded length of the plate, ℓ_{uw}', is then given as

$$\ell'_{uw} = \frac{A'd^2E}{2k'} . \tag{3.24}$$

By substituting Eq. (3.17) into Eq. (3.24), we will then get

$$\ell'_{uw} = \frac{0.36Z_xEd}{2k'} . \tag{3.25}$$

If the modulus of elasticity, E, is 30×10^6 psi, then

$$\ell'_{uw} = \frac{54 \times 10^5 Z_x d}{k'} . \tag{3.26}$$

The welding length of the plate is necessarily designed to develop a plastic moment of the section. Because the plate is A514 steel, the luxury of an E110 electrode with a 3/8 in. fillet weld is assumed, and a strength of 8900 lb/in. is obtained. Suppose that the total length of the fillet weld is ℓ'_w, then the moment capacity developed by the weld is $8900\ell'_w d$ in.-lbs which must be larger than the plastic moment of the beam, i.e.,

$$8900\ell'_w d \geq M_p . \tag{3.27}$$

Thus, the minimum welding length is given as

$$\ell'_w = \frac{\sigma_y Z_x}{8900\ d} = 4.04\frac{Z_x}{d} . \tag{3.28}$$

If the length of the butt weld in Figure 2 is neglected, and the four primary legs of the fillet weld on the top plate are equal in length, then ℓ'_{tw} would be equal to $\ell'_w/4$. The bottom plate in Figure 2 is welded only along the outside edges of the bottom flange, thus ℓ'_{bw} is equal to $\ell'_w/2$. The lengths of the plates are then found to be $\ell'_{uw} + \ell'_{tw}$ for the top plate and $\ell'_{uw} + \ell'_{bw}$ for the bottom plate. Because there are two beam-column connections on each beam, combining the previous equations with Eq. (3.11) yields the cost of the steel plates for each beam as

$$(C_{pc})_i = 2\, C_{pl}\, \rho A' \,(\, 2\,\ell'_{uw} + \ell'_{tw} + \ell'_{bw}\,)$$
$$= 0.72\, C_{pl}\, \rho Z_x^2 \,(\, \frac{10800000}{k'} + 0.6\,(\frac{Z_x}{I})^2\,) \qquad (3.29)$$

in which C_{pl} is the unit price, $\$/in^3$, of the steel plate. By substituting Eqs. (3.19) and (3.11) into Eq. (3.29), one obtains

$$(C_{pc})_i = 0.8796\, C_{pl}\, \rho \eta_i^{1.087}\, I_i^2 \,(\, \frac{10800000}{k'_i} + 0.73301\, \eta_i^{1.087}\,). \qquad (3.30)$$

In order to determine the cost of the welding, the total amount of metal contained in the weld should be estimated. First it is assumed that the cross section of the top plate is square, that the root gap between the ends of the plates and the column is 3/16 in. wide, and that the plates have been beveled to 45°. Then the metal volume in the butt weld for the top plate is $A'(\sqrt{A'}/2 + 3/16)$ in^3. If the width of bottom plate is assumed to be 10 in., then the volume

of the metal in the butt weld is $A'(A'/20 + 3/16)$ in^3.

The metal volume of a 3/8 in. fillet weld for a beam is $0.3403\ell_w'$ in^3. This is 10% over the specification to provide an additional factor of safety.

The total volume of metal used for the welding of each beam is then found by summing up the metal volume of the butt weld and of fillet weld as follows:

$$(V_{TW})_i = 2A_i' \left(\frac{\sqrt{A_i'}}{2} + \frac{3}{16}\right) + 2A_i' \left(\frac{A_i'}{20} + \frac{3}{16}\right) + 0.3403\ (\ell_w')_i$$

$$= A_i' \left(0.75 + 0.1\ A_i' + \sqrt{A_i'}\right) + 0.3403\ (\ell_w')_i. \qquad (3.31)$$

By substituting Eqs. (3.11), (3.17), and (3.28) into Eq. (3.31) and assuming that the unit price of welding is C_w, then the welding cost of each individual beam, i, is

$$(C_{wc})_i = C_w \rho \left(0.8919\ \eta_i^{1.087}\ I_i + 3.881 \times 10^{-3}\ \eta_i^{2.174}\ I_i^2 + 0.08643\ \eta_i^{1.6304}\ I_i^{1.5}\right). \qquad (3.32)$$

Then by adding the steel plate cost obtained with Eq. (3.30) and the welding cost obtained with Eq.(3.32) for all the beams, one obtains the connection cost, which is given as

$$C_{con} = \sum_{i=1}^{m} g\left((C_{pc})_i + (C_{wc})_i\right). \qquad (3.33)$$

D. DAMAGE COSTS

Several factors influence the appraisal of damage costs. Some of these are magnitude of seismic excitations, site condition, properties of construction materials, and others. The difficulty in damage modeling is that two seismic excitations of equal magnitude will yield totally different damage results. The absence of data, which could be used to develop models of damage costs, causes further difficulties in modeling. Consequently, the development of damage models in this study is limited to the costs of repairing non-structural damage. This type of damage can be simply modeled by using a function of story drift, which according to most investigators is the best indicator for damage.[25,65]

Let the damage ratio, ξ, be the ratio of nonstructural damage repair cost per story to the construction cost of the damaged items on that story. The damaged items indicated here are partitions and glasses. The relationship between the damage ratio and the story drift, Δ, can therefore be obtained on the basis of the previous research data and is given by

$$\xi = 8.52\ \Delta. \tag{3.34}$$

If the construction costs of the damaged items on i^{th} story is $(C_{nc})_i$, then the repair costs on that story will be

$$\begin{aligned}(C_r)_i &= (C_{nc})_i(\xi)_i \\ &= 8.52(C_{nc})_i\Delta_i\end{aligned} \tag{3.35}$$

The story drift is a function of ground acceleration and member properties; however, as soon as the size of members is determined, the story drift may be simply expressed as a function of ground acceleration such that

$$\Delta_i = c_i a \tag{3.36}$$

where the subscript i represents i^{th} story. According to Eq. (3.36), if the structure is designed on the basis of ground acceleration, a^*, and the resulting story drift on i^{th} story is Δ_i^*, then c_i is given as

$$c_i = \Delta_i^*/a^* \tag{3.37}$$

By substituting Eq. (3.36) into Eq. (3.35) one obtains

$$(C_r)_i = 8.52(C_{nc})_i c_i a. \tag{3.38}$$

Equation (3.38) represents the relationship between damage repair costs and ground acceleration.

In its lifetime, a structure may be subjected to earthquake excitations of different magnitudes. To estimate the nonstructural damage repair costs in the lifetime of the structure, the repair costs for all expected earthquake damage must be evaluated. The number of seismic shocks may be reasonably estimated by using n_o to designate earthquake frequency. This term is defined as

$$n_o = -\frac{dN}{dM} = \frac{1}{B} AN_o e^{-M/B} \tag{3.39}$$

in which N is the annual number of shallow earthquakes having magnitudes equal to or greater than M, in area A, M the Richter magnitude, A the amount of area, B the distribution parameter that describes seismic severity, and N_o the annual number of seismic shocks per unit area. The value of n_o then represents the number of shocks having magnitudes between M and M+dM in area A.

To develop a similar formula in terms of ground acceleration, an idealized relation between area, ground acceleration and magnitude shown in Figure 3[33,34] is used. According to this figure, the area over which a certain range of ground acceleration will exist for a given magnitude earthquake can be obtained. For an example, let us assume that the parameters N_o and B are known, then if we substitute each individual covered area listed in Table I, which is estabilished on the basis of Figure 3, into Eq. (3.39), we can estimate the annual number of seismic shocks within the specified range of ground acceleration for a given seismic intensity. Because the influenced area in Figure 3 decreases when the ground acceleration increases for any given magnitude. If we assume that the influenced area is linearly decreased, then it is clear that the average number of shocks for any given magnitude within the specified range of ground acceleration could be obtained by dividing by a factor of 2. The results of an estimation of the number of shocks are given in Table II for southern California, where N_o was 1.7/mile^2 and B was 0.48.

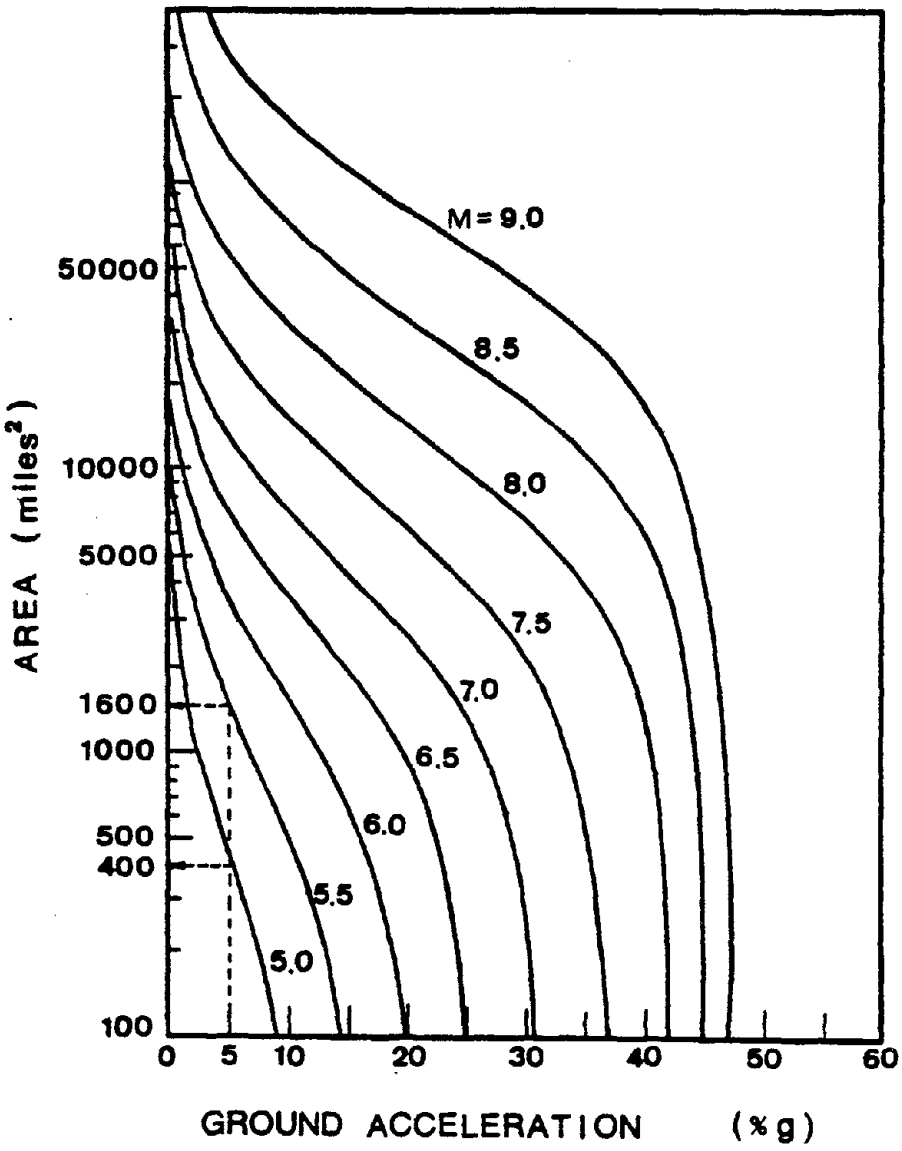

Figure 3. Affected Area Curves

TABLE I. COVERED AREA IN 1000 miles^2

Acceleration (%g)	M 5.0	5.5	6.0	6.5	7.0	7.5	8.0	8.5
≥ 5	0.4	1.6	3.6	6.8	13.0	28.0	56.0	130.0
≥ 10		0.6	1.6	3.6	7.6	14.0	32.0	72.0
≥ 15			0.6	2.0	4.4	9.6	21.0	47.0
≥ 20				0.9	2.5	6.0	14.0	33.0
≥ 25					1.3	4.0	10.0	24.0
≥ 30					0.25	2.0	6.4	17.0
≥ 35						0.6	4.0	12.0
≥ 40							1.2	5.8
≥ 45								0.2

TABLE II. CALCULATIONS OF EARTHQUAKE FREQUENCIES

Acceleration (g)	M 5.0	5.5	6.0	6.5	7.0	7.5	8.0	8.5	Total = Σ of Row	Mean = Total/0.05
0.05 - 0.10	2.12×10^{-2}	1.87×10^{-2}	1.32×10^{-2}	7.45×10^{-3}	4.44×10^{-3}	4.06×10^{-3}	2.45×10^{-3}	2.09×10^{-3}	7.36×10^{-2}	1.47
0.10 - 0.15		1.12×10^{-2}	6.60×10^{-3}	3.72×10^{-3}	2.63×10^{-3}	1.28×10^{-3}	1.12×10^{-3}	9.02×10^{-4}	2.75×10^{-2}	0.55
0.15 - 0.20			3.96×10^{-3}	2.56×10^{-3}	1.56×10^{-3}	1.04×10^{-3}	7.16×10^{-4}	5.05×10^{-4}	1.03×10^{-2}	0.206
0.20 - 0.25				2.09×10^{-3}	9.86×10^{-4}	5.80×10^{-4}	4.09×10^{-4}	3.25×10^{-4}	4.39×10^{-3}	0.0878
0.25 - 0.30					8.62×10^{-4}	5.80×10^{-4}	3.68×10^{-4}	2.53×10^{-4}	2.06×10^{-3}	0.0412
0.30 - 0.35					2.05×10^{-4}	4.06×10^{-4}	2.45×10^{-4}	1.80×10^{-4}	1.04×10^{-3}	0.0208
0.35 - 0.40						1.74×10^{-4}	2.86×10^{-4}	2.24×10^{-4}	6.84×10^{-4}	0.0137
0.40 - 0.45							1.23×10^{-4}	2.02×10^{-4}	3.25×10^{-6}	0.0065
0.45 - 0.50								7.22×10^{-6}	7.22×10^{-6}	0.000144

To estimate the number of shocks for any given ground acceleration, the mean values in Table II were obtained by dividing the total number of shocks by the increment of ground acceleration of each specified range of acceleration, 0.05. These mean values are plotted in Figure 4. A least square curve fitted function is obtained by using

$$n_o = 2.9335\ e^{-14.6118a} \tag{3.40}$$

in which a is the ground acceleration normalized by gravity acceleration, g, and $n_o da$ represents the annual number of shocks having a normalized ground acceleration between a and a+da. As indicated in Figure 4, the number of shocks is dropped off at a ground acceleration 0.45g. Equation (3.40) may be modified to the following general form as

$$n_o = \gamma\ e^{-\vartheta a}. \tag{3.41}$$

Let us suppose that the lifetime of the structure is N_ℓ years, then the number of shocks with ground accelerations between a and a+da in the lifetime will be $N_\ell n_o da$. Then by using Eqs. (3.38) and (3.41), we can determine that the damage repair costs on i^{th} story is

$$\begin{aligned}(C_D)_i &= 8.52\ N_\ell\ (C_{nc})_i\ c_i \gamma \int_o^{a_{max}} a e^{-\vartheta a}\ da \\ &= 8.52\ N_\ell\ (C_{nc})_i\ c_i\ \gamma\ \mathcal{L}\end{aligned} \tag{3.42}$$

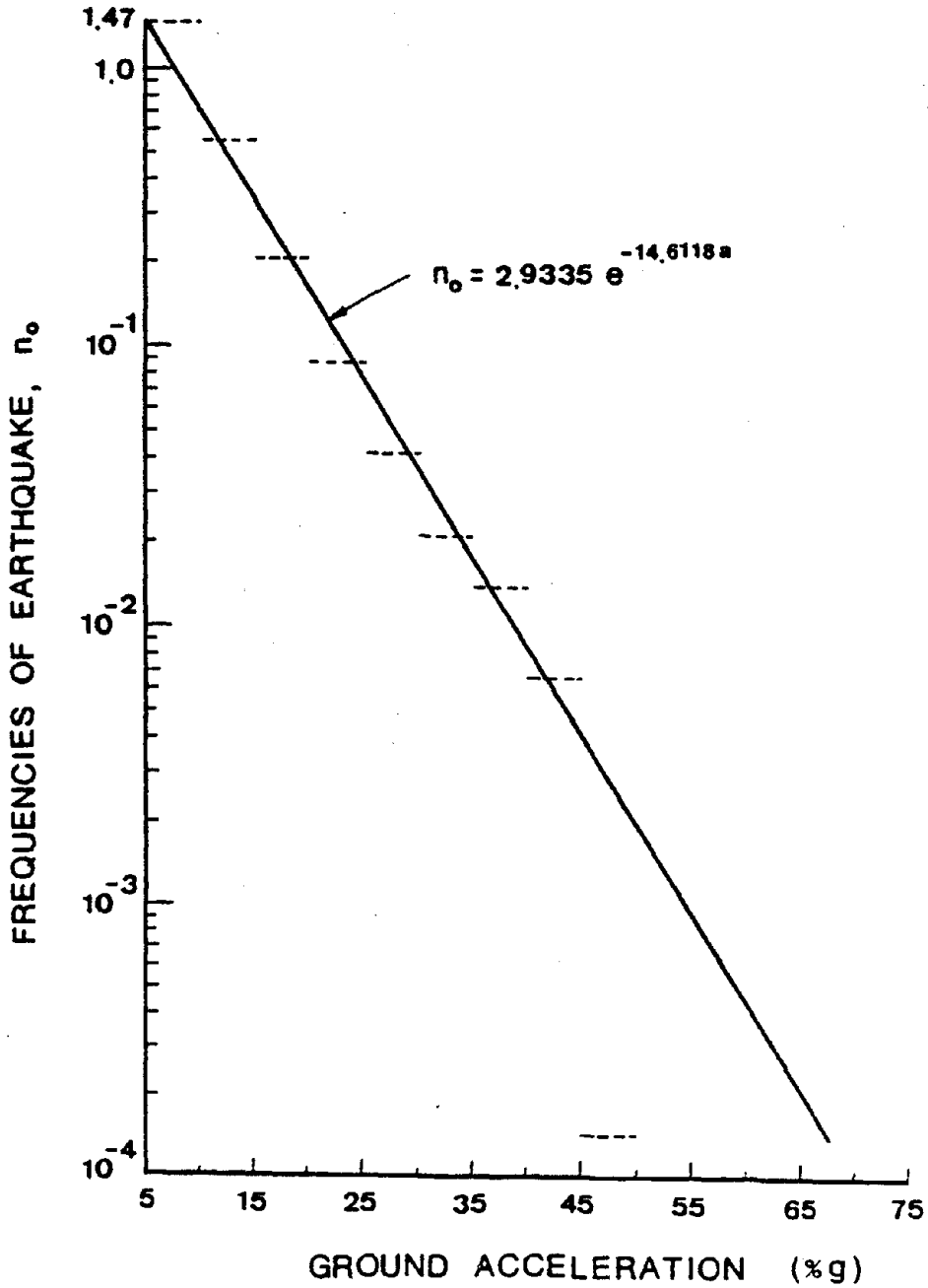

Figure 4. Annual Number of Earthquake Shocks for the Specified Ground Accelerations

in which a_{max} is the maximum expected normalized ground acceleration in the lifetime of the structure, and

$$f = -\frac{1}{\vartheta}\left(a_{max}\exp(-\vartheta a_{max}) + \frac{1}{\vartheta}\exp(-\vartheta a_{max}) - \frac{1}{\vartheta}\right). \tag{3.43}$$

The total nonstructural damage repair costs is then levied by summing up the damage repair costs of all floor levels. If the construction cost of the nonstructural items is the the same for every story, and the ratio of the nonstructural construction costs to the construction costs of the structure is χ, then the construction costs of the nonstructural items per story is

$$(C_{nc})_i = \frac{\chi C_{c1}}{n_s} \tag{3.44}$$

in which the construction cost of the structure, C_{c1}, is the summation of the steel costs, connection costs, and painting costs of the structural members. By substituting Eq. (3.44) into Eq. (3.42), one obtains the total nonstructural damage repair cost in the lifetime of the structure with the following formula:

$$C_D = 8.52\, N_\ell\, \chi\, C_{c1}\, \gamma\, f\left(\sum_{i=1}^{n_s} c_i\right)\frac{1}{n_s}. \tag{3.45}$$

IV. VARIOUS RESPONSE SPECTRA

It is well known that the spectral analysis has been widely accepted in structral dynamic practice for aseismic design in recent years. The main advantage of the spectral analysis is that the time dependency can be avoided from the solution of motion equation. Based on the Duhamel's integration, the spectral displacement, S_d, which is the maximum displacement related to the ground, is defined as

$$S_d = \left| \frac{1}{\omega_d} \int_0^t a_g(\tau)\, e^{-\beta\omega(t-\tau)} \sin\omega_d(t-\tau)\, d\tau \right|_{max} \tag{4.1}$$

in which $a_g(\tau)$ is the ground acceleration, ω the natural frequency, ω_d the frequency including damping, and β the damping ratio. In practice, the damping effect is permissible to be neglected in the ω_d, thus Eq. (4.1) can be rewritten as

$$S_d = \left| \frac{1}{\omega} \int_0^t a_g(\tau)\, e^{-\beta\omega(t-\tau)} \sin\omega(t-\tau)\, d\tau \right|_{max} \tag{4.2}$$

The spectral pseudo-velocity, S_v, and spectral acceleration, S_a, are given as

$$S_v = \omega\, S_d \tag{4.3}$$

and

$$S_a = \omega^2\, S_d \tag{4.4}$$

Several earthquake response spectra are available in practical

engineering and research fields as will be discussed in this chapter. For automatic search of spectral accelerations in the computer program, most spectra were generated as polynomial functions in terms of natural period based on the least-square curve fitting technique. For those spectra plotted on a logarithmic tripartite charts, the spectral accelerations can be obtained on the basis of the relationships of Eqs. (4.3) and (4.4). This interpolating technique was used in Newmark's spectra as given in the Section A of this chapter.

A. NEWMARK'S SPECTRA

On a logarithmic tripartite chart, the relationships between coordinates of displacement, velocity, and acceleration are given in Eqs. (4.3) and (4.4). As shown in Figure 5, when the frequency $f \leq f_1$, or the period $T \geq T_1$, the spectral curve is perpendicular to the displacement-axis, which means it corresponds to a constant displacement value, d_1. Therefore, the spectral acceleration can be obtained by using Eq. (4.4), that is, when $T \geq T_1$

$$S_a = \omega^2 d_1 = \left(\frac{2\pi}{T}\right)^2 d_1. \tag{4.5}$$

When $f_1 < f \leq f_2$, that is, $T_1 > T \geq T_2$, the spectral curve is corresponding to a constant velocity, v_1, therefore, S_a can be obtained by using

$$S_a = \omega v_1 = \left(\frac{2\pi}{T}\right) v_1. \tag{4.6}$$

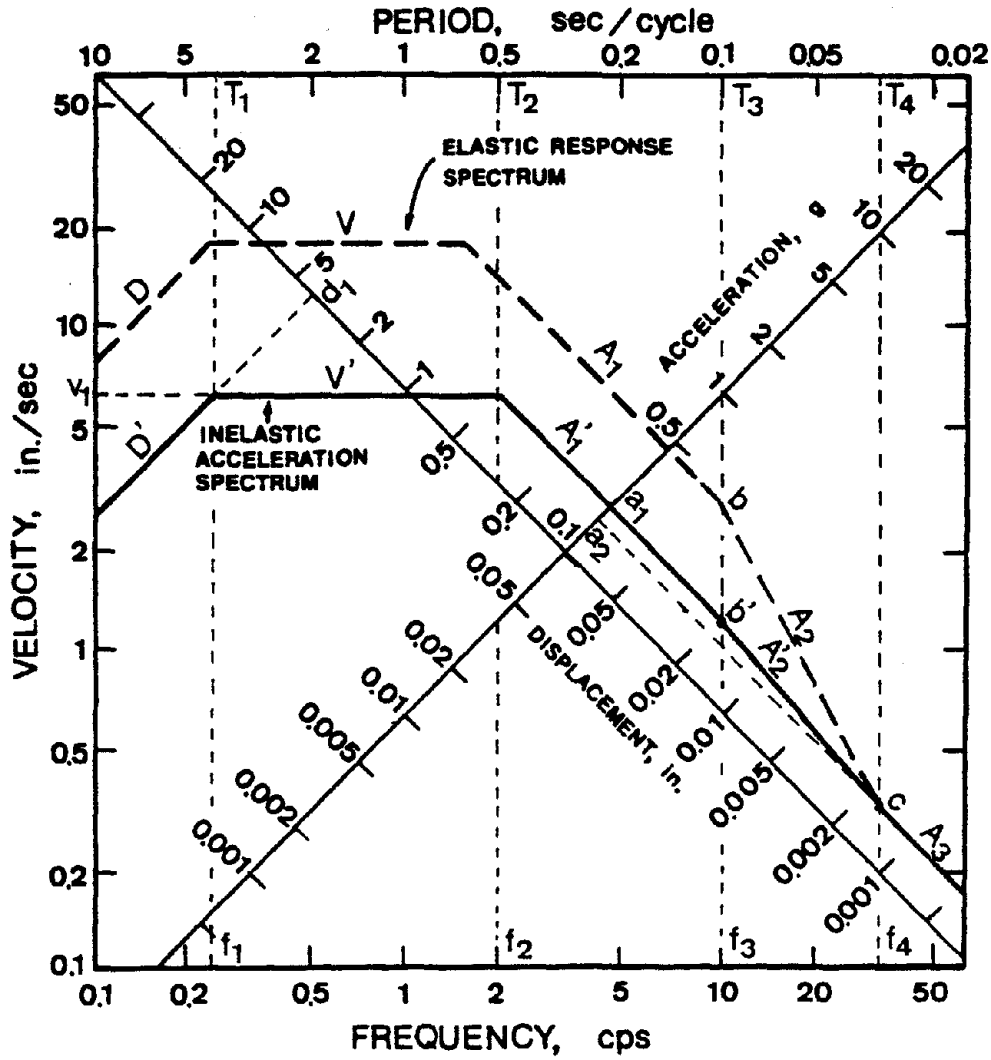

Figure 5. Inelastic Design Spectrum with 5% Critical Damping and a Ductility Factor of 3. (1 in. = 2.54 cm)

When $f_2 < f \leq f_3$ or $f > f_4$, that is, $T_2 > T \geq T_3$ or $T < T_4$, the spectral curve corresponds to a constant acceleration, a_1 or a_2, therefore

$$S_a = a_1, \qquad \text{for } T_2 > T \geq T_3 \tag{4.7}$$

or

$$S_a = a_2, \qquad \text{for } T < T_4. \tag{4.8}$$

When $T_3 > T \geq T_4$, that is, $f_3 < f \leq f_4$, one may generate a curve-fitted polynomial function or use linearized relationship of natural logarithm to interpolate the spectral acceleration. For the latter method, any spectral acceleration, S_a, corresponds to a natural frequency, f, in the range is given as

$$\frac{\ln(S_a)-\ln(a_2)}{\ln(f)-\ln(f_4)} = \frac{\ln(a_2)-\ln(a_1)}{\ln(f_4)-\ln(f_3)} \tag{4.9}$$

from which, one obtains

$$S_a = \exp\left(\frac{\ln(a_1/a_2)\ \ln(f_4/f)}{\ln(f_4/f_3)}\right) a_2 \tag{4.10}$$

1. Inelastic Design Spectrum with 5% Critical Damping and a Ductility Factor of 3. The elastic response spectrum is reasonable to be used to design structures subjected to earthquake excitations with moderate intensity. However, for severe earthquakes, it is not economical to design the structures for elastic behavior. In order to design structures for elasto-plastic behavior, the elastic response

spectrum has been extended by Newmark and Hall[41] to include the inelastic range. In general, the inelastic acceleration spectra have similar appearance to the elastic response spectra, but the curves are moved downward by an amount related to the ductility factor, μ, which is defined as the ratio of the maximum permissible displacement, r_m, to the yield displacement, r_y.

The elastic response spectrum shown in Figure 5 is constructed on the basis of the maximum ground acceleration of 0.16 g, the damping ratio (β) of 0.05, and 84.1 percentile. A percentile of 84.1 means the spectrum amplication factors, those are used to construct the elastic design spectrum, is obtained on the basis of cumulative probability of 84.1%. That is, 84.1 percent of the actual spectral values corresponding to the specified damping ratio can be expected to fall at or below the smoothed maximum ground motion values mutiplied by these particular spectrum amplification factors. A ductility factor of 3 is introduced into the elastic design spectrum to construct inelastic acceleration spectrum. According to Newmark's procedure, the maximum spectral displacement approaches the maximum ground displacement in the low frequency region. Because the force in the inelastic range does not increase, the spectral acceleration is reduced by dividing ordinate values of the regions D and V by μ. In very high frequency region A_3, the maximum spectral acceleration approaches the maximum ground acceleration, therefore A_3 was not reduced. For region between these two extremes, the energy is preserved. Recent research[41] indicated that a reduction factor of $1/\sqrt{2\mu-1}$, which was derived on the basis of an equivalence of energy between the elasto-plastic system

and an elastic system having the same frequency, provides better agreement with the actual earthquake response spectra. By dividing ordinate values of region A_1 by $\sqrt{2\mu-1}$, the inelastic spectral acceleration is located. For region A_2, the inelastic acceleration spectrum is simply obtained by connecting points b' and c together. Following this procedure, the inelastic acceleration spectrum, $D'V'A'_1A'_2A_3$, is constructed.

Although the inelastic acceleration spectrum is different from the elastic response spectrum, the mathematical relationships between the coordinates of displacement, velocity, and acceleration are not changed, which means Eqs. (4.5) through (4.10) can be used to generate spectral acceleration for both elastic and inelastic spectra in a computer program.

With a computer program, the inelastic spectral accelerations in Figure 5 correspond to the natural period of mode i, T_i, can be founded by using the following equations:

$$(S_a)_i = 0.16\ g, \qquad \text{for } T_i \leq 0.03 \text{ sec}, \tag{4.11}$$

$$(S_a)_i = (0.142857 + 0.5714286\ T_i)\ g, \qquad \text{for } 0.03 \text{ sec} < T_i \leq 0.1 \text{ sec}, \tag{4.12}$$

$$(S_a)_i = 0.2\ g, \qquad \text{for } 0.1 \text{ sec} < T_i \leq 0.5 \text{ sec}, \tag{4.13}$$

$$(S_a)_i = 6.15\ \left(\frac{2\pi}{gT_i}\right)\ g, \qquad \text{for } 0.5 \text{ sec} < T_i \leq 4.0 \text{ sec}, \tag{4.14}$$

$$(S_a)_i = 3.92 \frac{1}{g} \left(\frac{2\pi}{T_i} \right)^2 g,$$

$$\text{for } 4.0 \text{ sec} < T_i \leq 10.0 \text{ sec}, \qquad (4.15)$$

and when $T_i > 10.0$ sec, Eq. (4.15) is used by assuming T_i is equal to 10.0 sec.

2. Inelastic Design Spectrum with 10% Critical Damping and a Ductility Factor of 4. The design spectrum of Figure 6 was constructed on the basis of an elastic design spectrum that is normalized to 1.0 g. By introducing a damping ratio of 10% and a ductility factor of 4, the design spectrum was generated by using curve fitting polynomial function for the period between 0.1 and 0.22 sec. in a computer program. The spectral accelerations can be found by using the following equations:

$$(S_a)_i = 1.0 \text{ g}, \qquad \text{for } T_i \leq 0.1 \text{ sec}, \qquad (4.16)$$

$$(S_a)_i = (1.333333 - 3.333333\ T_i)\ g,$$

$$\text{for } 0.1 \text{ sec} < T_i \leq 0.22 \text{ sec}, \qquad (4.17)$$

$$(S_a)_i = 0.6 \text{ g}, \qquad \text{for } 0.22 \text{ sec} < T_i \leq 0.4 \text{ sec}, \qquad (4.18)$$

$$(S_a)_i = 14.76 \left(\frac{2\pi}{gT_i} \right) g,$$

$$\text{for } 0.4 \text{ sec} < T_i \leq 3.5 \text{ sec}, \qquad (4.19)$$

and

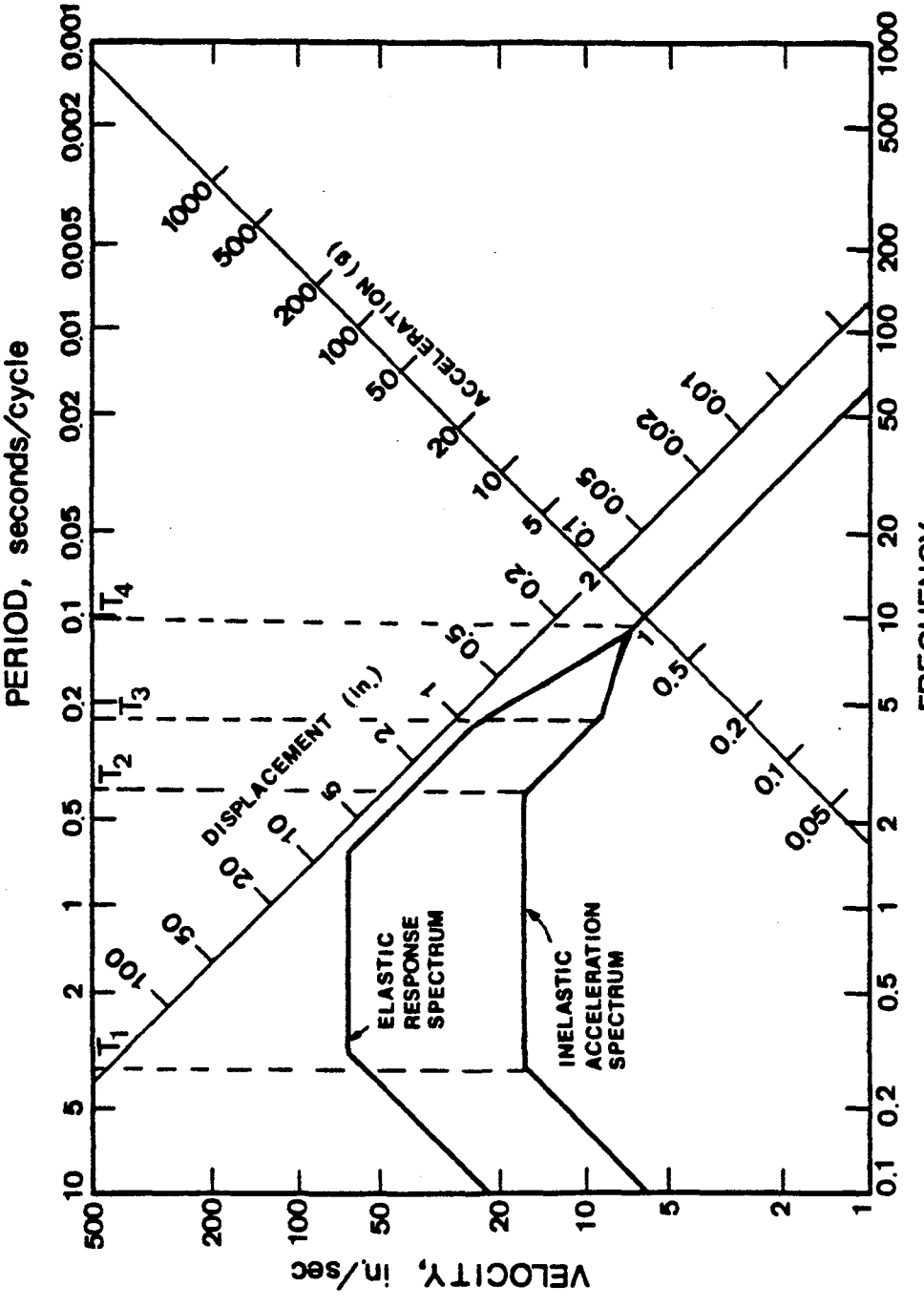

Figure 6. Inelastic Design Spectrum with 10% Critical Damping and a Ductility Factor of 4. (1 in. = 2.54 cm)

$$(S_a)_i = 8.22 \frac{1}{g} \left(\frac{2\pi}{T_i} \right)^2 g,$$

$$\text{for } T_i > 3.5 \text{ sec.} \qquad (4.20)$$

3. 50 Percentile and 90 Percentile Design Spectra with 5% Critical Damping for Alluvium.[77] Figures 7, 8, 9, and 10 show the design spectra for the horizontal and vertical directions of 50 percentile and 90 percentile respectively. All spectra are normalized to 1.0 g. These spectra are developed with regard to the soil effect. The soil type considered in these spectra is alluvium. To find the normalized spectra accelerations, one can use the following equations that correspond to different frequency regions:

$$(S_a)_i = \alpha_d \frac{ad}{v^2} \left(\frac{v}{a} \right)^2 \omega_i^2 a, \qquad \text{for } \frac{\omega_i}{2\pi} \leq f_1, \qquad (4.21)$$

$$(S_a)_i = \alpha_v \left(\frac{v}{a} \right) \omega_i a, \qquad \text{for } f_1 < \frac{\omega_i}{2\pi} \leq f_2, \qquad (4.22)$$

$$(S_a)_i = \alpha_a a, \qquad \text{for } f_2 < \frac{\omega_i}{2\pi} \leq f_3, \qquad (4.23)$$

$$(S_a)_i = \exp\left(\frac{\ln(\alpha_a) \ln(2\pi f_4/\omega_i)}{\ln(f_4/f_3)} \right) a,$$

$$\text{for } f_3 < \frac{\omega_i}{2\pi} \leq f_4, \qquad (4.24)$$

and

$$(S_a)_i = a, \qquad \text{for } \frac{\omega_i}{2\pi} \geq f_4, \qquad (4.25)$$

in which ω_i is the circular frequency, and α_a, α_v and α_d are the

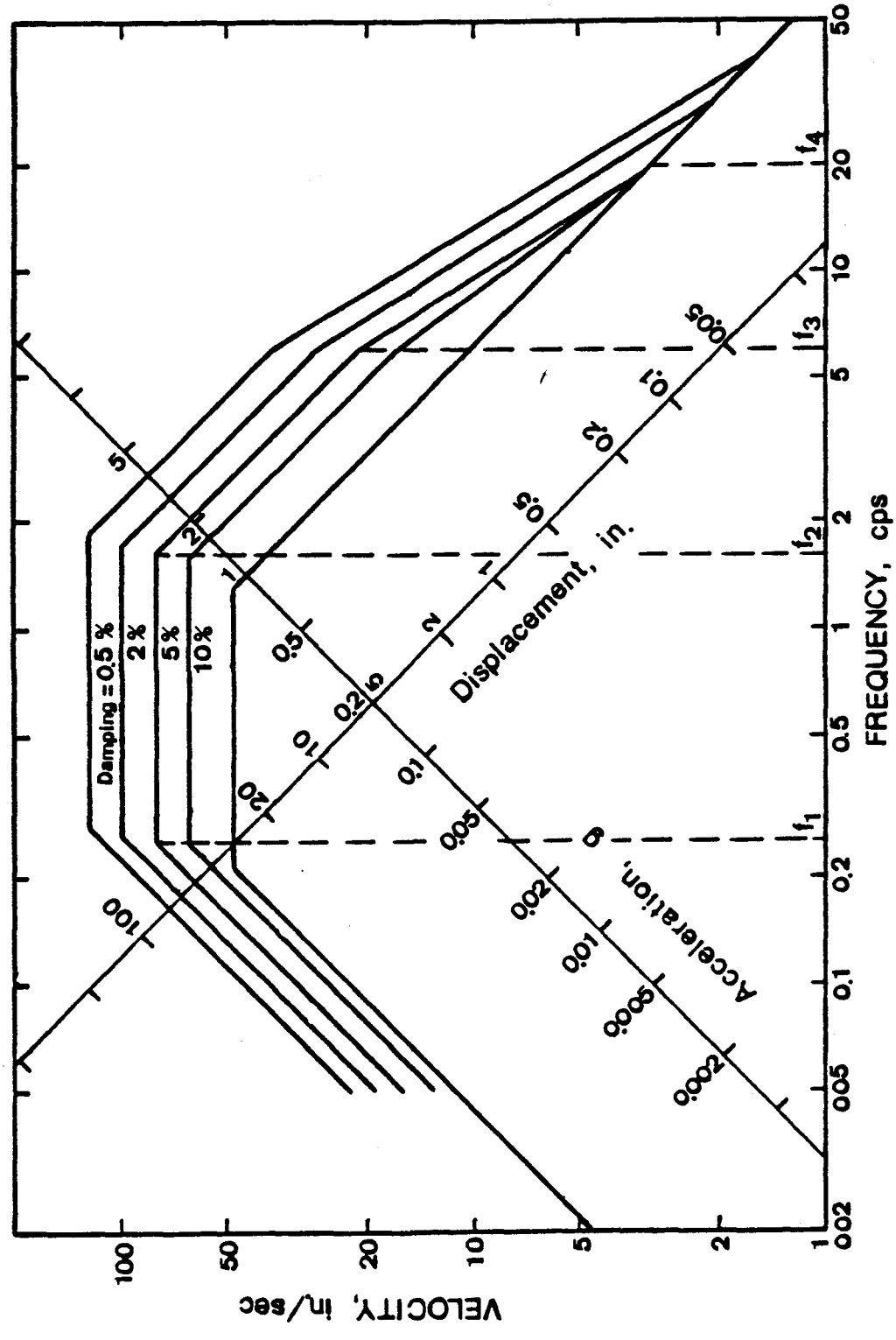

Figure 7. Design Spectra for Horizontal Motion, Alluvium, and 50 Percentile. (1 in. = 2.54 cm)

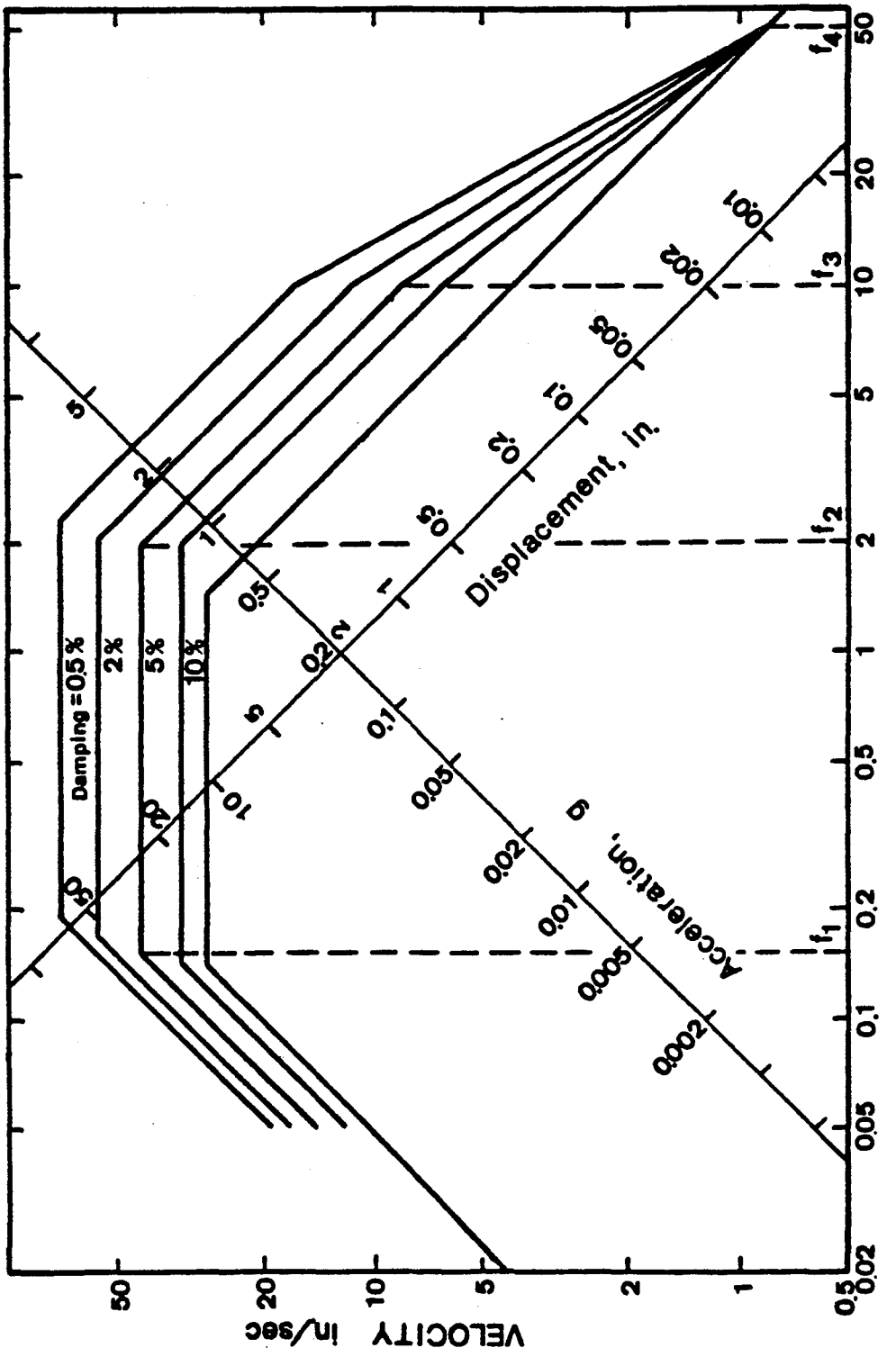

Figure 8. Design Spectra for Vertical Motion, Alluvium, and 50 Percentile. (1 in. = 2.54 cm)

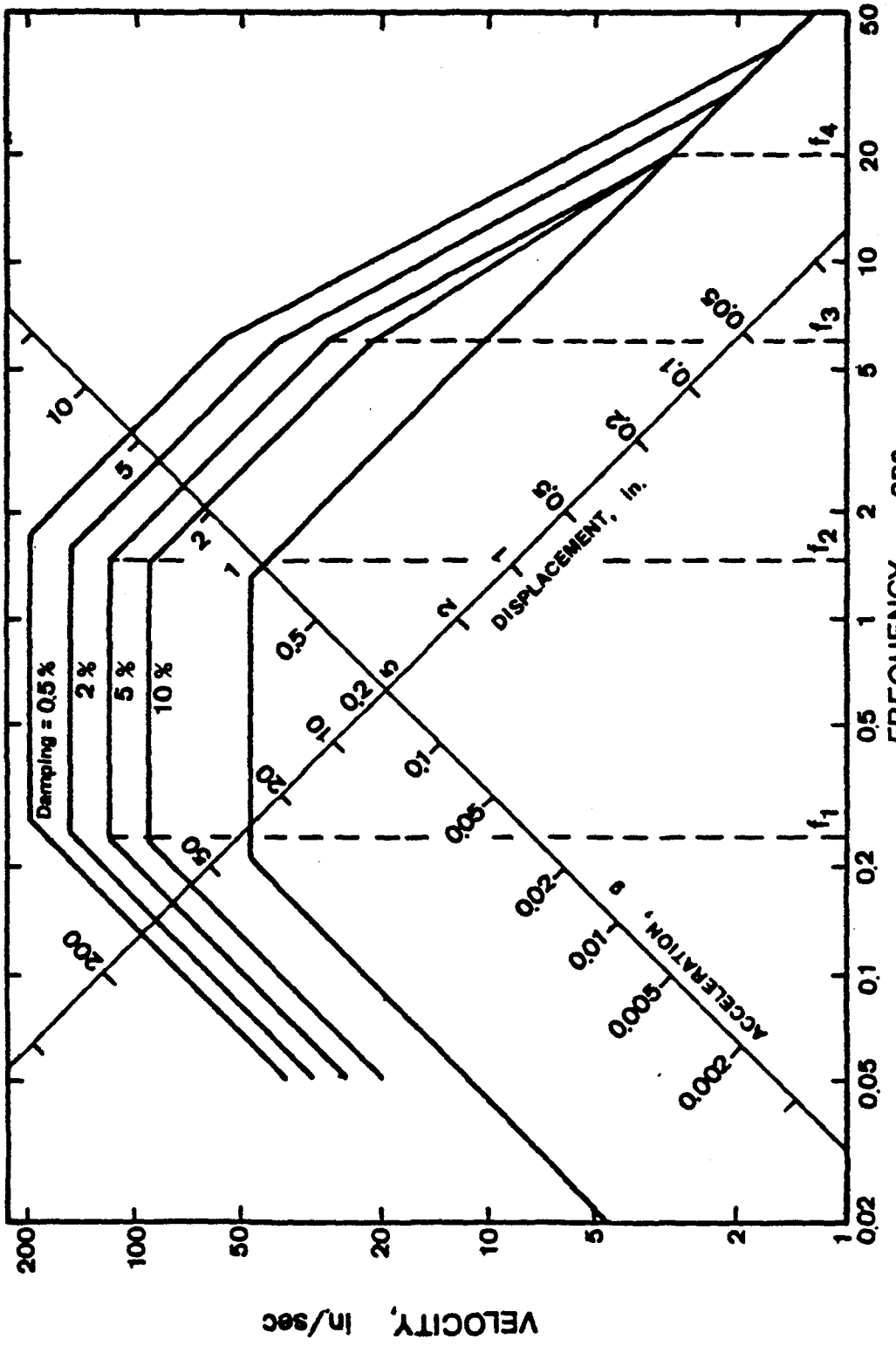

Figure 9. Design Spectra for Horizontal Motion, Alluvium, and 90 Percentile. (1 in. = 2.54 cm)

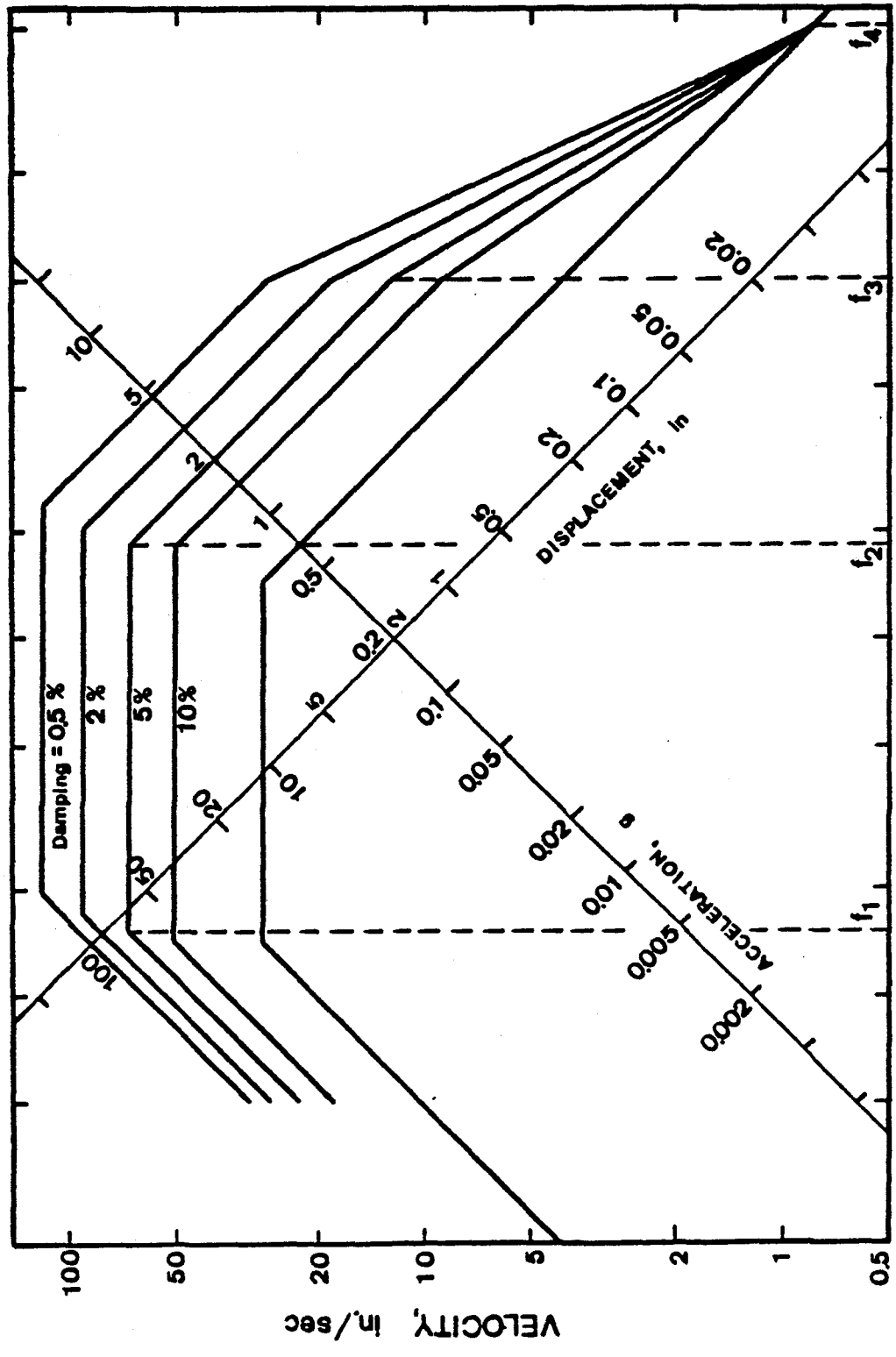

Figure 10. Design Spectra for Vertical Motion, Alluvium, and 90 Percentile. (1 in. = 2.54 cm)

amplification factors of the spectral acceleration, velocity, and displacement respectively. The values of α_a, α_v, and α_d are listed in Table III. For horizontal ground motions, the acceleration, a, velocity, v, and displacement, d, are 1.0 g, 48 in./sec, and 36 in. respectively. For vertical ground motions, a, v, and d are respectively given as 2/3 g, 29 in./sec, and 33 in.

B. HOUSNER'S AVERAGE RESPONSE SPECTRUM WITH 5% DAMPING

The average response spectra shown in Figure 11 were proposed by Housner in 1959.[31] The spectral shapes were obtained by averaging the normalized response spectra for the eight strong motion records obtained in four earthquakes (El Centro 1934, El Centro 1940, Olympia 1949 and Tehachapi 1952). The ordinates of Figure 11 should be multiplied by factors representative of the spectrum intensities to bring them into agreement with the different recorded ground motions. The scale factor of each different recorded ground motion is presented in Table IV.

In a computer program, the spectral shape corresponding to 5% damping is generated by using least-square, curve fitting polynomial expressions:

$$(S_a)_i = 0.12250006 + 0.23919934\ T_i, \quad \text{for } T_i \leq 0.3 \text{ sec}, \tag{4.26}$$

and

$$(S_a)_i = 0.25845146 - 0.22122407\ T_i + 0.08188504\ T_i^2 - 0.0108108\ T_i^3, \quad \text{for } 0.3 \text{ sec} < T_i \leq 3.0 \text{ sec}, \tag{4.27}$$

TABLE III. THE AMPLIFICATION FACTORS OF NEWMARK'S DESIGN SPECTRA FOR ALLUVIUM

Direction	Percentile	Amplification Factor		
		α_a	α_v	α_d
Horizontal	50	2.11	1.66	1.40
	90	2.82	2.51	2.21
Vertical	50	2.05	1.51	1.40
	90	3.04	2.37	2.18

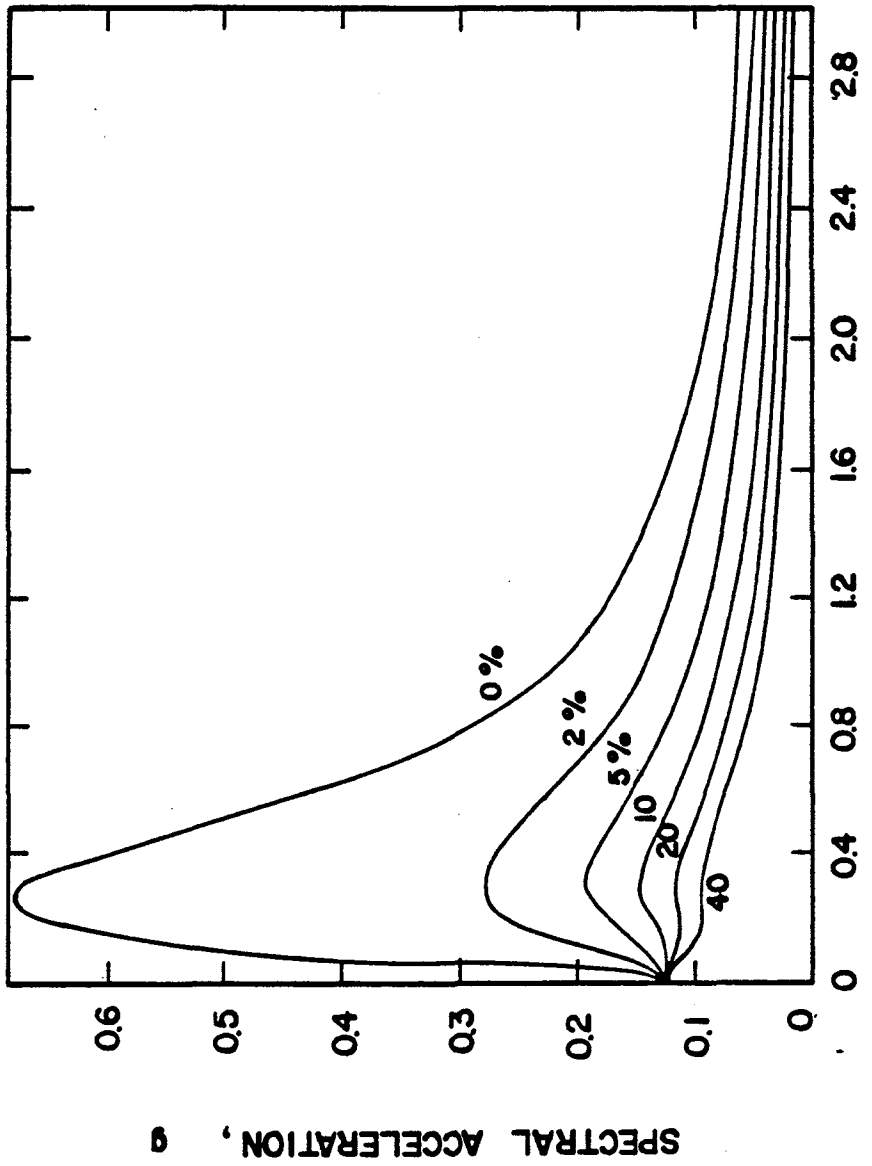

Figure 11. Housner's Average Response Spectra. (1 in. = 2.54 cm)

TABLE IV. THE SCALING FACTORS OF DIFFERENT EARTHQUAKE RECORDS USED IN HOUSNER'S AVERAGE RESPONSE SPECTRA

Earthquake	Factor
El Centro, 18 May 1940	2.7
El Centro, 30 December 1949	1.9
Olympia, 13 April 1949	1.9
Taft, 21 July 1952	1.6

in which T_i is the natural period of mode i, and $(S_a)_i$ is the normalized spectral acceleration corresponding to period, T_i.

C. THE AVERAGE ACCELERATION SPECTRA FOR DIFFERENT SITE CONDITIONS

The average acceleration spectra of Figure 12 were presented in a study of Seed et al. for which 104 ground motion records obtained from 23 earthquakes were studied and analyzed for different soil and geological conditions.

To find the normalized spectral accelerations, one can generate the following curve fitting polynomial functions in a computer program.

1. Soil Type 1 (Rock). The following equations are used to find the spectral acceleration in a computer program:

$$(S_a)_i = 1.0349855 + 17.000336\ T_i - 45.001083\ T_i^2, \quad \text{for } T_i \leq 0.3 \text{ sec}, \tag{4.28}$$

$$(S_a)_i = 2.0243101 - 3.9684248\ (T_i - 0.3) + 3.6514969\ (T_i - 0.3)^2 - 1.525775\ (T_i - 0.3)^3 + 0.2316342\ (T_i - 0.3)^4, \quad \text{for } 0.3 \text{ sec} < T_i \leq 3.0 \text{ sec}, \tag{4.29}$$

and when $T_i > 3.0$ sec, Eq. (4.29) is used by assuming that T_i is equal to 3.0 sec.

2. Soil Type 2 (Stiff Site Condition). The following equations were generated to compute the spectral acceleration:

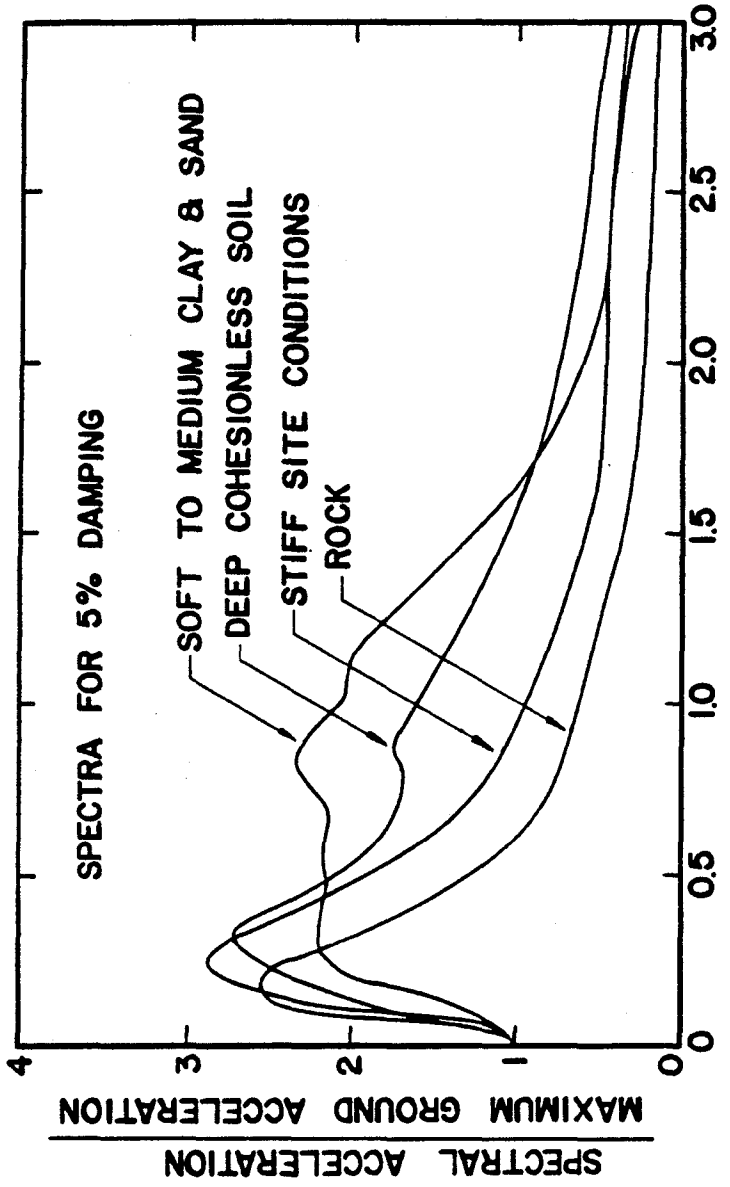

Figure 12. Seed's Average Acceleration Spectra for Different Site Conditions.

$$(S_a)_i = 0.93516338 + 13.936761\ T_i - 26.141937\ T_i^2,$$

$$\text{for } T_i \leq 0.4 \text{ sec}, \qquad (4.30)$$

$$(S_a)_i = 2.229723 - 3.6186724\ (T_i - 0.4) + 2.9960575\ (T_i - 0.4)^2 - 1.1409359\ (T_i - 0.4)^3 + 0.16060048\ (T_i - 0.4)^4,$$

$$\text{for } 0.4 \text{ sec} < T_i \leq 3.0 \text{ sec}, \qquad (4.31)$$

and when $T_i > 3.0$ sec, use the upper bound, 3.0 sec, in Eq. (4.31).

3. Soil Type 3 (Deep Cohesionless Soil). The generated equations are:

$$(S_a)_i = 0.964302 + 10.203987\ T_i - 15.784999\ T_i^2,$$

$$\text{for } T_i \leq 0.4 \text{ sec}, \qquad (4.32)$$

$$(S_a)_i = 2.4632187 - 4.2025547\ (T_i - 0.4) + 5.5536652\ (T_i - 0.4)^2,$$

$$\text{for } 0.4 \text{ sec} < T_i \leq 0.9 \text{ sec}, \qquad (4.33)$$

$$(S_a)_i = 1.736083 - 1.3109751\ (T_i - 0.9) + 0.27382255\ (T_i - 0.9)^2 + 0.15717566\ (T_i - 0.9)^3 - 0.062189575\ (T_i - 0.9)^4,$$

$$\text{for } 0.9 \text{ sec} < T_i \leq 3.0 \text{ sec}, \qquad (4.34)$$

and if $T_i > 3.0$ sec, use the upper bound of 3.0 sec for period, T_i, in Eq. (4.34).

4. Soil Type 4 (Soft to Medium Clay and Sand). The following

equations are used to find spectral acceleration:

$$(S_a)_i = 0.95149982 + 4.9650021\ T_i - 2.2500134\ T_i^2,$$
$$\text{for } T_i \leq 0.3 \text{ sec}, \qquad (4.35)$$

$$(S_a)_i = 2.1899109 + 0.16158056\ (T_i - 0.3) - 6.1221199\ (T_i - 0.3)^2 + 29.51915\ (T_i - 0.3)^3 - 40.011734\ (T_i - 0.3)^4,$$
$$\text{for } 0.3 \text{ sec} < T_i \leq 0.7 \text{ sec}, \qquad (4.36)$$

$$(S_a)_i = 2.1389999 + 2.589987\ (T_i - 0.7) - 9.4999676\ (T_i - 0.7)^2,$$
$$\text{for } 0.7 \text{ sec} < T_i \leq 1.0 \text{ sec}, \qquad (4.37)$$

$$(S_a)_i = 2.0599957 + 0.0002992556\ (T_i - 1.0) - 4.0015287\ (T_i - 1.0)^2,$$
$$\text{for } 1.0 \text{ sec} < T_i \leq 1.2 \text{ sec}, \qquad (4.38)$$

$$(S_a)_i = 1.9126568 - 2.5098505\ (T_i - 1.2) + 0.96162301\ (T_i - 1.2)^2 + 0.32339907\ (T_i - 1.2)^3 - 0.20329118\ (T_i - 1.2)^4,$$
$$\text{for } 1.2 \text{ sec} < T_i \leq 3.0 \text{ sec}, \qquad (4.39)$$

and if $T_i > 3.0$ sec, use the upper bound $T_i = 3.0$ sec.

D. THE ATC-3-06 NORMALIZED RESPONSE SPECTRA

The normalized response spectra of Figure 13 are recommended by ATC-3-06 for designing buildings. The spectral shapes are

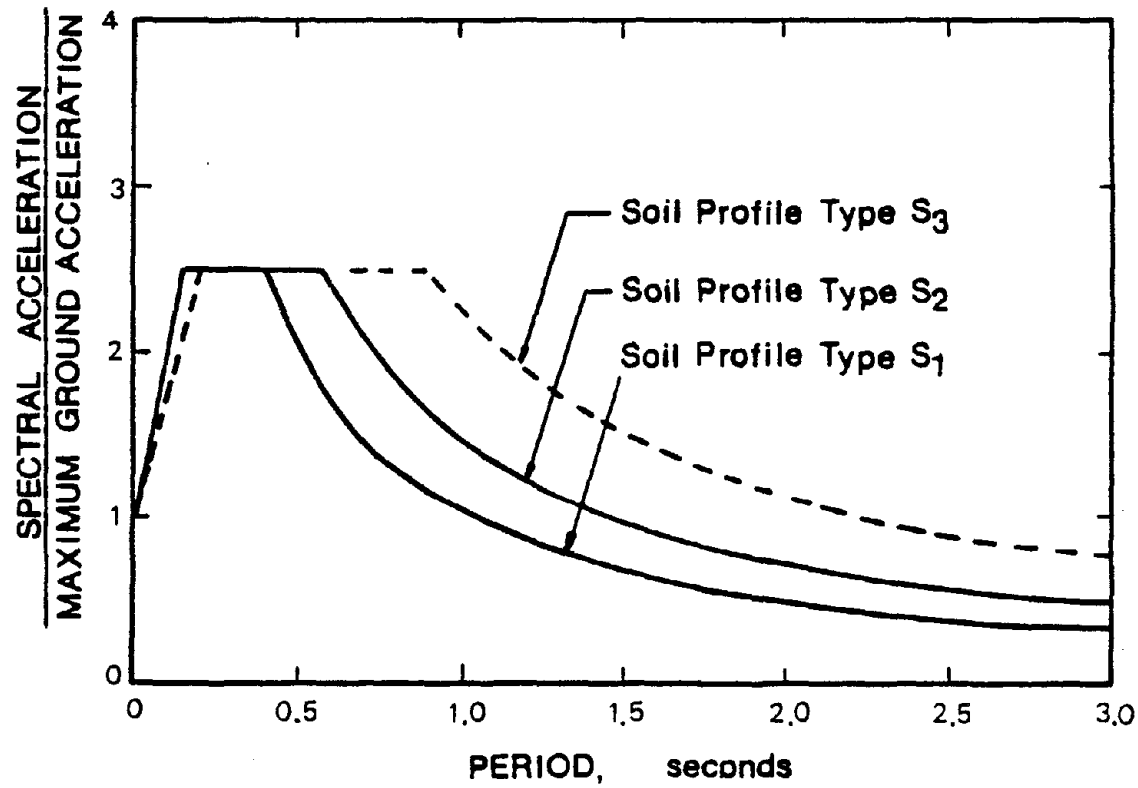

Figure 13. Normalized Design Spectra Recommended by the ATC-3-06.

determined on the basis of those proposed by Seed et al. (Fig. 12). By comparing spectral shapes of Seed's with those others (Newmark et al., Blume et al., and Mohraz) and studied their use in building regulations, the spectral curves in Figure 12 were simplified to a family of three by combining the spectra for rock and stiff soil conditions.

The recommended design spectra of Figure 13 is constructed on the basis of 5% damping. To obtain the acceleration, one must multiply the ordinates by the value of the effective peak ground accelerations and a correction factor of 0.8 if the soil profile type is S_3.

For vertical motions, the spectral value may be determined by multiplying the spectral acceleration of the horizontal motions by 0.67.

1. Soil Profile Type S_1. The curve fitting polynomial functions of the spectral curve are coded in a computer program as follows:

$$(S_a)_i = 1 + 10\ T_i, \qquad \text{for } T_i \leq 0.15 \text{ sec}, \tag{4.40}$$

$$(S_a)_i = 2.5, \qquad \text{for } 0.15 < T_i \leq 0.4 \text{ sec}, \tag{4.41}$$

$$(S_a)_i = 2.4291344 - 3.9693136\ (T_i - 0.4) + 3.4752331\ (T_i - 0.4)^2 - 1.4541187\ (T_i - 0.4)^3 + 0.22523707\ (T_i - 0.4)^4, \qquad \text{for } 0.4 < T_i \leq 3.0 \text{ sec}. \tag{4.42}$$

2. Soil Profile Type S_2. The curve fitting polynomial functions

are generated as follows:

$$(S_a)_i = 1 + 10\ T_i, \qquad \text{for } T_i \leq 0.15 \text{ sec}, \tag{4.43}$$

$$(S_a)_i = 2.5, \qquad \text{for } 0.15 < T_i \leq 0.57 \text{ sec}, \tag{4.44}$$

and

$$(S_a)_i = 2.5844088 - 2.9449358\ (T_i - 0.5) + 1.8397913\ (T_i - 0.5)^2 - 0.58476114\ (T_i - 0.5)^3 + 0.073747039\ (T_i - 0.5)^4, \quad \text{for } 0.57 < T_i \leq 3.0 \text{ sec}. \tag{4.45}$$

3. Soil Profile Type S_3 and Effective Peak Ground Acceleration, $A_a < 0.3$. The following equations are used to find spectral acceleration in a computer program:

$$(S_a)_i = 1 + 10\ T_i, \qquad \text{for } T_i \leq 0.15 \text{ sec}, \tag{4.46}$$

$$(S_a)_i = 2.5, \qquad \text{for } 0.15 \text{ sec} < T_i \leq 0.7 \text{ sec}, \tag{4.47}$$

and

$$(S_a)_i = 0.8\ (2.4989138 - 2.4919176\ (T_i - 0.9) + 1.8436747\ (T_i - 0.9)^2 - 0.80172771\ (T_i - 0.9)^3 + 0.14353234\ (T_i - 0.9)^4), \quad \text{for } 0.7 \text{ sec} < T_i \leq 3.0 \text{ sec}. \tag{4.48}$$

4. Soil Profile Type S_3 and Effective Peak Ground Acceleration, $A_a \geq 0.3$. The following equations are used in a computer program

to find the spectral acceleration:

$$(S_a)_i = 0.8\ (1 + 7.5\ T_i), \qquad \text{for } T_i \leq 0.2 \text{ sec}, \tag{4.49}$$

$$(S_a)_i = 2.0, \qquad \text{for } 0.2 \text{ sec} < T_i \leq 0.9 \text{ sec}, \tag{4.50}$$

$$(S_a)_i = 0.8\ (2.4989138 - 2.4919176\ (T_i - 0.9) + 1.8436747\ (T_i - 0.9)^2 - 0.80172771\ (T_i - 0.9)^3 + 0.14353234\ (T_i - 0.9)^4),$$
$$\text{for } 0.9 \text{ sec} < T_i \leq 3.0 \text{ sec}. \tag{4.51}$$

All spectral shapes presented in this section have the upper bound of 3.0 sec for the corresponding natural period. It is assumed that for any period longer than 3.0 sec the spectral acceleration corresponding to a period of 3.0 sec can be used.

In the ATC-3-06, the simplified equations were derived by considering more conservative criteria than the spectra discussed above for larger and longer period buildings. It has been pointed out in the ATC-3-06 commentary that there is an approximate 50 percent increment in the seismic forces at a period of 2.0 seconds for a stiff soil condition beyond the value obtained directly from the response spectrum .

E. CHINESE DESIGN SPECTRA

The horizontal design spectra of Figure 14 are recommended by

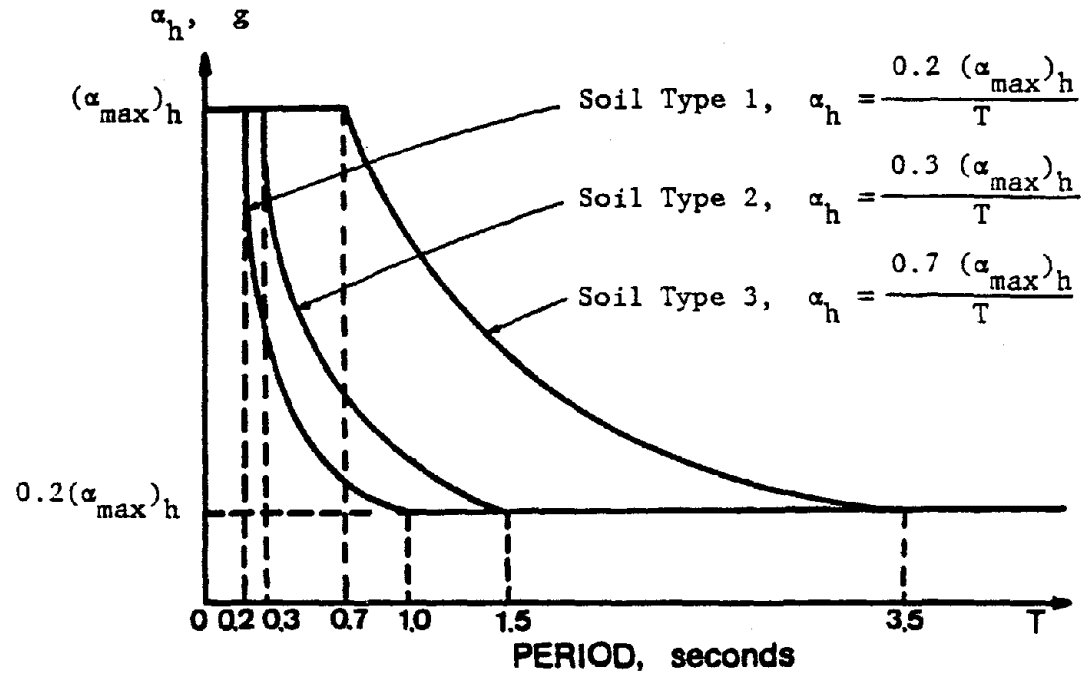

Figure 14. Chinese Design Spectra for Horizontal Motion.

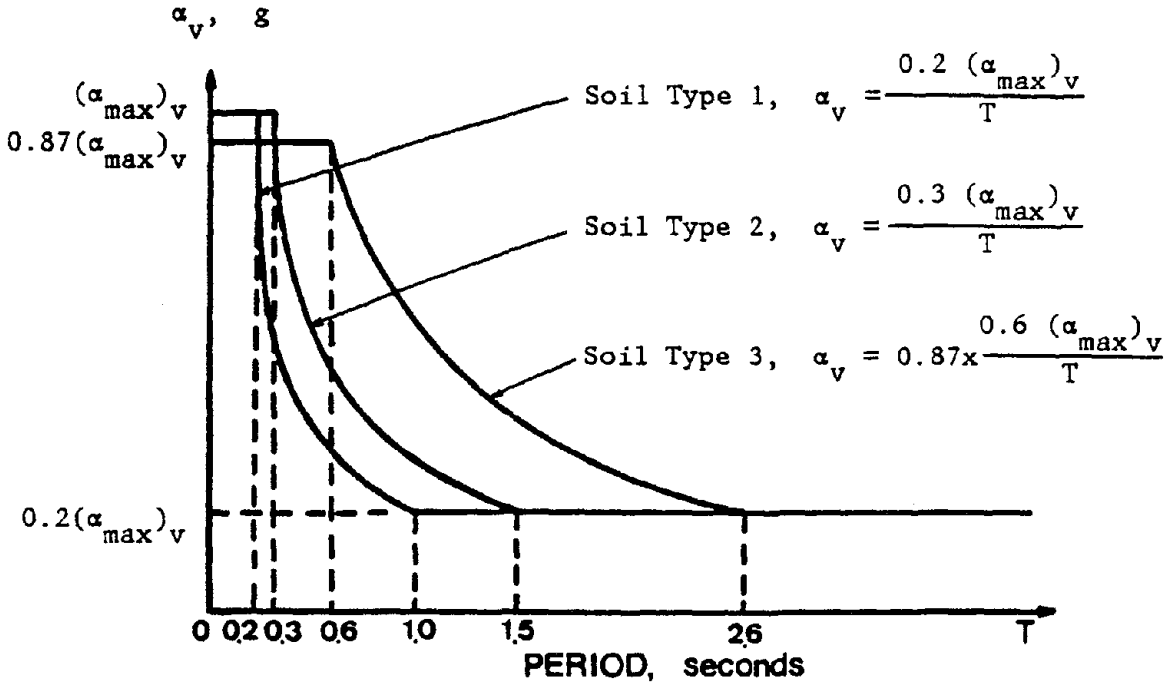

Figure 15. Chinese Design Spectra for Vertical Motion.

the Chinese Seismic Code Provisions[22] for the design of industrial and civic buildings. The spectral shapes were determined by simplifying the normalized acceleration spectra from the studies of the Institute of Engineering Mechanics of China. These studies were based on 68 ground motion records obtained in China and 115 ground motion records obtained from other countries. The different soil conditions were taken into consideration. The three different site conditions accounted for in Figure 14 are defined as follows: a) soil type 1 is rock or any stable rock-like condition, b) soil type 2 is all other types of soil that are not defined in soil types 1 and 3, and c) soil type 3 is saturated soft sand, soft to medium-stiff clays, silt, silty soil, alluvial soil or any other kind of backfill with a soft characteristic.

The maximum spectral acceleration for the horizontal motion, $(\alpha_{max})_h$, in Figure 14 was determined according to earthquake magnitude and is given in Table V.

Figure 15 shows the design spectra, which were recommended by She in 1982[51] for the vertical ground motions. He analyzed 203 earthquake recordes in the United States, 14 in Japan, and 40 in China then recommended that the maximum design ground accelerations of the various earthquake magnitudes for the vertical motions be determined by multiplying the ground acceleration for horizontal motions by a factor of 0.5.

The values of $(\alpha_{max})_v$ for different earthquake magnitudes are given in Table V.

TABLE V. THE MAXIMUM SPECTRAL ACCELERATION OF VARIOUS EARTHQUAKE MAGNITUDES USED IN CHINESE DESIGN SPECTRA FOR HORIZONTAL AND VERTICAL MOTIONS

Magnitude	7	8	9
$(\alpha_{max})_h$	0.23	0.45	0.90
$(\alpha_{max})_v$	0.115	0.230	0.460

F. COMPARISON OF DUCTILITY EFFECT CONSIDERED IN VARIOUS CODE PROVISIONS BASED ON THE CONCEPT OF SPECTRAL ANALYSIS

In the spectral analysis, the design base shear can be measured via the spectral acceleration, S_a, obtained from elastic response spectrum, that is,

$$V = S_a M = \frac{S_a}{g} W \tag{4.52}$$

in which V, M, and W are design base shear, mass of the system, and weight of the system respectively. In Eq. (4.52), S_a/g may be interpreted as design base shear coefficient in seismic design codes.

The design base shear for inelastic systems can be obtained by modifying Eq. (4.52) as follows:

$$V = \frac{S_a'}{g} W \tag{4.53}$$

in which S_a' is the spectral acceleration corresponding to the inelastic acceleration spectrum. The displacement of the inelastic system, r, is then determined by multiplying displacement, r_e, which is calculated on the basis of elastic analysis, by the ductility factor, μ, that is

$$r = \mu r_e \tag{4.54}$$

In recent seismic design codes, using either the equivalent

lateral force method or the modal analysis method, the significance of inelastic behavior is recognized. The more ductile structure, the less design base shear is used. This reduction is mainly dependent on the ductility of the structural system.

In the ATC-3-06[4], the design base shear coefficient is reduced by dividing the response modification factor, R, to account for the inelastic behavior. The factor R is determined on the basis of the energy dissipation capacity in the inelastic deformation, damping, and observed the performance of various types of structural system in the past.

To determine total displacements, ATC-3-06 uses the deflection amplification factor, C_d, to partially offset the factor R so that the reduced strength requirement does not carry with it an equal reduced stiffness requirement. Essentially, C_d is the same as the ductility factor.

Although UBC[57] is based on the working stress level, the effect of inelastic behavior is also considered in UBC for which the design base shear is reduced by factor K for those types of structure having high ductility and damping. The K factor is determined largely based on the actual observed performance of buildings in past earthquakes, and its value reflects the ductilities of different types of structure. For stiffness requirement, UBC specifies that the displacements calculated from the design seismic forces are required to be divided by K factor for those structures having K smaller than 1.0. Thus, 1/K is essentially similar to C_d of the ATC-3-06.

Similar concept has been used in Chinese Seismic Design Code.[22] The factor C, which reflects the ductility of the structural system, is used to account for inelastic behavior. The design base shear coefficient is reduced by the C factor so that the strength requirement is reduced. However, the stiffness requirement is not mentioned in the code, so no discussion can be made in this part.

Although different design strength levels are based in different codes, the importance of inelastic behavior has been considered in all the codes, The R factor of the ATC-3-06, the K factor of the UBC, and C factor of the Chinese Seismic Design Code are similar in their meaning. The curves of elastic design spectra are moved downward by these factors. Therefore, the design base shear coefficients are reduced to account for the capacity of the structure to dissipate energy in inelastic deformation. The C_d factor of ATC-3-06 and 1/K of the UBC are essentially similar to the ductility factor to amplify the deformation to account for the inelastic behavior.

V. LATERAL FORCES OF WIND AND SEISMIC EXCITATIONS

A. THE ATC-3-06 PROVISIONS[4]

1. Equivalent Lateral Force Method. The equivalent lateral force method is for all buildings in Seismic Performance Category B and for buildings classified as regular in Categories C and D as prescribed in Sections 3.5.2 and 3.5.3 of the ATC-3-06. With this analysis procedure, one can view the effect of earthquake excitations as static lateral forces. The design base shear, V, is defined as

$$V = C_s W \tag{5.1}$$

in which C_s is the seismic design coefficient, W the total gravity load of the building including the structural weight and the weight of partitions, permanent equipment, and the effective snow load. For storage and warehouse structures, at least 25 percent of the live load on the floor should be included as well.

The seismic coefficient, C_s, is the lower value computed from the following formulas:

$$C_s = \frac{1.2A_v S}{RT^{2/3}} \tag{5.2}$$

and

$$C_s = \frac{2.5A_a}{R} \tag{5.3a}$$

or

$$C_s = \frac{2.0A_a}{R} \tag{5.3b}$$

for soil profile type S_3 and $A_a \geq 3$, in which A_a and A_v is the effective peak acceleration coefficient and effective peak velocity coefficient respectively (both values are determined from Table VI.), S the site coefficient, which is a value that represents the effect of site conditions on building response and is given in Table VII, R the response modification factor with various values for different structural systems to account for the ductility of the system, and T the fundamental period of the building.

The fundamental period, T, may be taken as the approximate fundamental period of the building, T_a, and is determined by either of the following formulas.

a. For moment-resisting frame structures without rigid components to resist seismic forces,

$$T_a = C_T(h_n)^{3/4} \qquad (5.4a)$$

in which C_T is equal to 0.025 for concrete frames, C_T is equal to 0.035 for steel frames, and h_n is the height of the highest level above the base, feet.

b. For all other buildings,

$$T_a = \frac{0.05h_n}{\sqrt{L}} \qquad (5.4b)$$

TABLE VI. COEFFICIENTS A_a AND A_v OF THE ATC-3-06[4]

Map Area Number	Coeff. A_a	Coeff. A_v
1	0.05	0.05
2	0.05	0.05
3	0.10	0.10
4	0.15	0.15
5	0.20	0.20
6	0.30	0.30
7	0.40	0.40

TABLE VII. SITE COEFFICIENT, S, OF THE ATC-3-06[4]

Soil Profile Type	Site Coeff., S
1	1.0
2	1.2
3	1.5

in which L is the overall length of the building at the base in the direction being considered, feet. Alternatively, the fundamental period of the building, T, may be determined by using the established methods of mechanics and assuming that the base of the building is fixed with $1.2T_a$ as the upper bound.

The distribution of lateral forces on each floor level, F_x, is determined in accordance with the formula

$$F_x = C_{vx}V \tag{5.5a}$$

in which

$$C_{vx} = \frac{w_x h_x^k}{\sum_{i=1}^{n} w_i h_i^k} \tag{5.5b}$$

and w_i, w_x are weights at level i and x, h_i, h_x are the height of levels i and x above the base, k is equal to 1 for $T \leq 0.5$ sec, k is equal to 2 for $T \geq 2.5$ sec, and k is equal to $0.75 + T/2$ for $0.5 \text{ sec} < T < 2.5$ sec.

At any level, the story shear, V_x, is related to the lateral forces by equation of statics,

$$V_x = \sum_{i=1}^{n} F_i. \tag{5.6}$$

The overturning moment, M_x, at level x is determined by the following formula:

$$M_x = \kappa \sum_{i=1}^{n_s} F_i (h_i - h_x) \qquad (5.7)$$

in which κ is equal to 1.0 for the top ten stories, to 0.8 for the 20th story from the top and below, and is a value determined by linear interpolation between 1.0 and 0.8 for stories between the 20th and 10th stories below the top. Except for inverted pendulum structures, the foundation overturning design moment, M_f, at the foundation-soil interface may be determined by using Eq. (5.7) with κ equal to 0.75 for all building heights.

The deflection at any level, δ_x, should be determined according to the formula

$$\delta_x = C_d \delta_{xe} \qquad (5.8)$$

in which C_d is the deflection amplification factor, and δ_{xe} the building's elastic displacement, which is occasioned by the seismic design forces, ,F_x. The base of the building should be considered as fixed.

The story drift, Δ, is the difference between deflection, δ_x, at the top and the bottom of the story under consideration and the maximum story drift of the building is limited to the allowable drift given in Table VIII.

TABLE VIII. ALLOWABLE STORY DRIFT OF THE ATC-3-06[4]

Seismic Harzard Exposure Group		
I*	II	III
$0.015\ h_{sx}$	$0.015\ h_{sx}$	$0.010\ h_{sx}$

* If there is no brittle-type finishes in buildings three stories or less in height, these limits may be increased one-third.

The P-Δ effects, which are also considered in ATC-3-06, define the stability coefficient, θ, as follows:

$$\theta = \frac{P_x \Delta}{V_x h_{sx} C_d} \tag{5.9}$$

in which Δ is the design story drift, V_x the seismic shear force at level x, which is determined from Eq. (5.6), h_{sx} the story height below level x, and P_x the total unfactored vertical design load at and above level x. The stability coefficient at any level can not exceed 0.10. If it is greater than 0.10, then the design story drift must be adjusted by a multiplying factor of 0.9/(1-θ), which must be equal to or greater than 1.0 to account for the P-Δ effect. The effect of P-Δ forces on story shears should be adjusted on the same rational analysis procedure.

If the effect of the soil-structure interaction is to be considered, several modifications should be made to obtain the design seismic forces.

The base shear determined from Eq. (5.1) may be reduced to

$$\tilde{V} = V - \Delta V \tag{5.10}$$

in which the reduction, ΔV, is determined from

$$\Delta V = (C_s - \tilde{C}_s \left(\frac{0.05}{\tilde{\beta}}\right)^{0.4}) \bar{W}. \tag{5.11}$$

In Eq. (5.11), C_s and C_s are the seismic design coefficients computed from either Eq. (5.2) or Eq. (5.3). However, C_s is computed by using the effective period of flexible supported structure, T, and is defined as

$$T = T\sqrt{1 + \frac{\bar{k}}{K_y}\left(1 + \frac{K_y \bar{h}^2}{K_\theta}\right)} \tag{5.12}$$

in which k is the effective stiffness of the building with a fixed base and is defined as

$$\bar{k} = 4\pi^2 \frac{\bar{W}}{gT^2}\,, \tag{5.13}$$

h is the effective height of the building (For buildings with the gravity load effectively concentrated at a single level, $\bar{h}$ should be taken as the height to that level. Otherwise, $\bar{h}$ should be taken as 0.7 h_n.), K_y is the lateral stiffness of the foundation, which is defined as the static horizontal force at the level of foundation necessary to produce a unit deflection at that level, K_θ is the rocking stiffness of the foundation and is defined as the static moment at the level of foundation necessary to produce a unit rotation at that level, and g is the gravity acceleration. The effective gravity load weight, $\bar{W}$, in Eqs. (5.11) and (5.13) should be equal to W for buildings with their gravity loads effectively concentrated at a single level, otherwise 0.7W should be used.

The effective damping factor, β, in Eq. (5.11) should be determined as follows

$$\tilde{\beta} = \beta_o + \frac{0.05}{(\tilde{T}/T)^3} \tag{5.14}$$

in which β_o is the foundation damping factor taken from Figure 16. The value of effective damping factor should in no case be less than 0.05.

The distribution of static lateral force should be computed according to Eq. (5.5), except that V is to be replaced by $\tilde{V}$. The deflection of the building should be modified as

$$\tilde{\delta}_x = \frac{\tilde{V}}{V} \left(\frac{M_o h_x}{k_\theta} + \delta_x \right) \tag{5.15}$$

in which M_o is the overturning moment at the base that is computed from unmodified forces and without a reduction factor.

2. Modal Analysis Method In a manner similar to that of the equivalent lateral force method, the modal analysis method can be used with the same simplified approaches to determine horizontal, vertical and torsional motions. However, the distribution of the seismic forces in the modal analysis method is based on the properties of natural vibration modes, consequently a more rigorous and accurate result can be obtained.

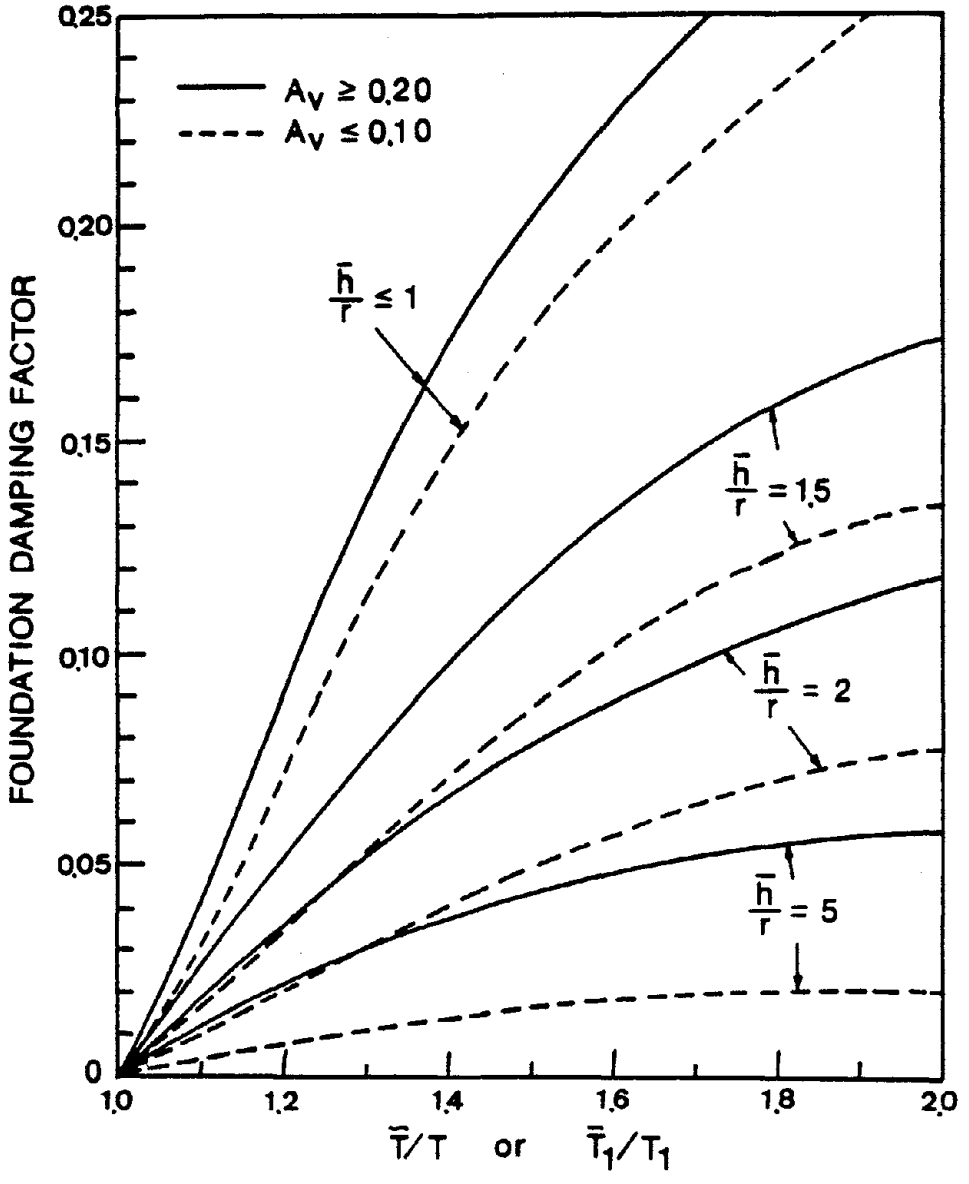

Figure 16. Foundation Damping Factor of the ATC-3-06

The modal base shear of the m^{th} mode, V_m, is computed by having

$$V_m = C_{sm}\overline{W}_m \tag{5.16}$$

in which C_{sm} is the modal seismic design coefficient, and $\overline{W}_m$ the effective modal gravity load, which is determined by using

$$\overline{W}_m = \frac{\left(\sum_{i=1}^{n_s} w_i \phi_{im}\right)^2}{\sum_{i=1}^{n_s} w_i \phi_{im}^2} \tag{5.17}$$

in which ϕ_{im} is the displacement amplitude at the i^{th} level and with the m^{th} mode vibration of the building.

The modal seismic design coefficient, C_{sm}, can be determined in accordance with Eqs. (5.2) and (5.3) by changing the fundamental period, T, in Eq. (5.2) to the modal period of mode m, T_m. However, if any T_m exceeds 4.0 seconds, C_{sm} can be computed by using

$$C_{sm} = \frac{3A_vS}{RT_m^{4/3}} . \tag{5.18a}$$

For soil profile type S_3, if the T_m of modes other than the fundamental mode is less than 0.3 seconds, C_{sm} is computed by using

$$C_{sm} = \frac{A_a}{R}(0.8 + 0.4T_m). \tag{5.18b}$$

The distribution of seismic forces of mode m, F_{xm}, at level x is determined according to the formula

$$F_{xm} = C_{vxm}V_m \tag{5.19a}$$

where

$$C_{vxm} = \frac{w_x \phi_{xm}}{\sum_{i=1}^{n_s} w_i \phi_{im}}. \tag{5.19b}$$

The deflection of mode m, δ_{xm}, at level x is determined as

$$\delta_{xm} = C_d \delta_{xem} \tag{5.20a}$$

in which

$$\delta_{xem} = \frac{g}{4\pi^2}\frac{T_m F_{xm}}{w_x}. \tag{5.20b}$$

The story drifts, shears, and overturning moments of each mode at each level should be computed in accordance with equations used in Section V.A.1. Then the design values should be obtained by taking the square root of the sum of squares of each of the modal values. The design base shear, V_t, should be compared with the base shear, $\overline{V}$, which is calculated according to Eq. (5.2) by using the

period equal to $1.4T_a$. Whenever V_t is less than $\overline{V}$, the design story drifts, shears, moments and deflections should be multiplied by $\overline{V}/V_t$. However, the base shear cannot exceed the value that is determined in accordance with the procedures of the equivalent lateral force method.

The overturning moment at the foundation-soil interface may be reduced by 10 percent of the design value. The P-Δ effects on story drifts and shears should be determined similar to the equations used in Section V.A.1.

The design values of the first mode of the modal analysis method should be modified to account for the effect of soil-structure interaction. The modification of the base shear corresponding to the fundamental mode by

$$\tilde{V}_1 = V_1 - \Delta V_1 \tag{5.21}$$

in which ΔV_1 is computed in accordance with the Eq. (5.11); however, the effective weight, $\overline{W}$, should be replaced by the the effective weight of the first mode, $\overline{W}_1$, and C_s is computed by using the period of the first mode, T_1. The value of $\tilde{C}_s$ is computed by using $\tilde{T}_1$, which is determined according to Eq. (5.12) with $\overline{W}$ equal to $\overline{W}_1$ and T equal to T_1, and the effective height, $\overline{h}$, is computed by using

$$\overline{h} = \frac{\sum_{i=1}^{n_s} w_i \phi_{i1} h_i}{\sum_{i=1}^{n_s} w_i \phi_{i1}}. \tag{5.22}$$

The value $\tilde{V}_1$, which is determined from Eq. (5.21) should not be taken less than $0.7V_1$.

The modal deflection of the fundamental mode should be modified in accordance with

$$\delta_{x1} = \frac{\tilde{V}_1}{V_1} \left(\frac{M_{o1} h_x}{K_\theta} + \delta_{x1} \right) \tag{5.23}$$

in which M_{o1} is the overturning moment of the fundamental mode of the building determined by using the unmodified base shear, V_1, and δ_{x1} is the unmodified deflection of the fundamental mode at level x.

By using the modified values, the design values of the seismic forces, the story shears, overturning moments, story drifts, and deflections should be determined by taking the square root of the sum of squares of each of the modal values.

B. THE UNIFORM BUILDING CODE[57]

The design base shear, V, of the Uniform Building Code, which governs earthquake resistant design in the United States, is computed in accordance with

$$V = ZIKCSW \tag{5.24}$$

in which Z is a zone coefficient determined from the earthquake zone map with values of 3/16, 3/8, 3/4, and 1 for earthquake zone 1, 2, 3, and 4 respectively, I an occupancy importance factor depending on the importance of the structure and having values ranging from 1.0 for

ordinary buildings to 1.5 for essential buildings, K a factor having values range from 0.67 to 1.33 depending on the type of structural system, C the seismic coefficient defined as $1/15\sqrt{T}$ but in no case greater than 0.12, T the fundamental period of the building, S the site-structure resonance factor which is determined based on the ratio of the building's fundamental period, T, to the site period, T_s, and W the total dead load and appropriate portions of live load, and snow load.

The fundamental period of the building, T, may be determined by using either the Rayleigh quotient formula,

$$T = 2\pi \sqrt{\frac{\sum_{i=1}^{n_s} w_i \delta_i^2}{g \sum_{i=1}^{n_s} F_i \delta_i}}, \qquad (5.25)$$

or the eigenvalue subroutine in the computer program to find the exact period. The value of T should not be less than 0.3 sec when it is used to determine the value of S.

The site period, T_s, must be determined by making a geotechnical investigation of the site. However, the value of T_s used to determine the site-structure resonance factor, S, should not be less than 0.5 sec nor greater than 2.5 sec.

The site-structure resonance factor, S, is determined by using the following formulas:

$$S = 1 + \frac{T}{T_s} - 0.5\left(\frac{T}{T_s}\right)^2 \qquad (5.26a)$$

for $T/T_s \leq 1$, and

$$S = 1.2 + 0.6\left(\frac{T}{T_s}\right) - 0.3\left(\frac{T}{T_s}\right)^2 \qquad (5.26b)$$

for $T/T_s > 1$.

The value of S should in no case be less than 1.0 nor greater than 1.5, and the product of C and S should not be greater than 0.14.

Because of the fact that the responses of higher modes will significantly affect the total responses in long period buildings, UBC introduced the following formulas to determine the force, F_t, on the top story where the higher modes have the greatest effect.

$$F_t = 0, \qquad \text{for } T \leq 0.7 \text{ sec} \qquad (5.27a)$$

$$F_t = 0.07TV, \qquad \text{for } T > 0.7 \text{ sec} \qquad (5.27b)$$

but in any case, F_t must be less than 0.25V. The remainder of the base shear is distributed to each floor level in accordance with the formula

$$F_x = \frac{(V - F_t)\, w_x\, h_x}{\sum_{i=1}^{n_s} w_i\, h_i}. \qquad (5.28)$$

in which F_x is the lateral force at floor level x, w_x and w_i are the weight at levels x and i, and h_x and h_i are the height above the ground surface to levels x and i.

C. THE EQUIVALENT LATERAL FORCE METHOD OF CHINESE PROVISIONS FOR INDUSTRIAL AND CIVIC STRUCTRUES[22]

The Chinese Seismic Code provides for the design of buildings subject to earthquake magnitudes of 7, 8, and 9 as based on the judgement of the Chinese regulations. Both the equivalent lateral force method and the modal analysis method are taken into consideration by the Code and are used according to the types and configurations of the structures. In this report, the equivalent static lateral force method is introduced. The method is applicable to a structure having the following properties: 1) the structural height is not higher than 50 meters, 2) the mass and stiffness are uniformly distributed along the height of the structure, 3) the deformations of the member are mainly due to the story shears, and 4) the structure can be modeled as a simple shear building whose masses are lumped on each floor level.

Basically, this method is similar in principle to the procedures of ATC-3-06 and UBC in which the design base shear is given by the formula

$$V = C \alpha W \tag{5.29}$$

in which C is the influence coefficient of the structure with a value ranging from 0.25 to 0.5 depending on the ductility and the type of the structure, α is the seismic influence coefficient which represents a spectral acceleration corresponding to the fundamental period of the structure divided by the gravity acceleration and is determined from Figure 14, and W is the total gravity load that includes the dead load, the live load, and 50 percent of the snow load.

There are several formulas available in the Chinese Building Design Code that can be used to calculate the approximate fundamental periods of different types of structures; however, in the computer program, the exact fundamental period can be calculated by using an eigenvalue subroutine.

The distribution of the equivalent lateral forces on each story, F_x, can be obtained by using the formula

$$F_x = \frac{w_x h_x}{\sum_{i=1}^{n_s} w_i h_i} V, \qquad i = 1,2,\ldots,n_s \tag{5.30}$$

in which w_x and w_i are the weight at level x and i, and h_x and h_i are the height above the ground surface to level x and i.

D. WIND FORCES

1. The Determination of Wind Velocity and Wind Forces Based on the Power Law. The basic equation that is used to determine the mean wind velocity, v_h, at a height h above the ground is given by

$$v_h = \left(\frac{h}{h_g}\right)^r v_g \tag{5.31}$$

in which h_g is the gradient height, which is a height measured from the ground surface (At this height, the influence of surface roughness may be neglected.), v_g is the gradient wind velocity, which is the wind velocity at the gradient height, and r is the power law coefficient.

The gradient height, h_g, and the power law coefficient, r, should be determined from Table IX in which the values of h_g and r versus the corresponding ground roughness are listed. To determine the gradient wind velocity, Eq. (5.31) and the annual fastest-mile wind speed at the reference height is used. The annual fastest-mile wind speed at the reference height is obtained from the wind-speed zoning map, which has been constructed through the use of statistical analysis. Figure 17 is an example of a wind-speed zoning map, which has been constructed on the basis of a 50-year return period. From Figure 17, one can obtain the annual fastest-mile wind speed at the height of 30 feet in the open country of various areas. By using the wind velocity, v_{30}, acquired from the map and the power law coefficient obtained from Table IX, one can compute the gradient wind velocity by using

$$v_g = v_{30} \left(\frac{900}{30}\right)^{1/7}. \tag{5.32}$$

The dynamic wind pressure at the height h, p_{dh}, is determined as

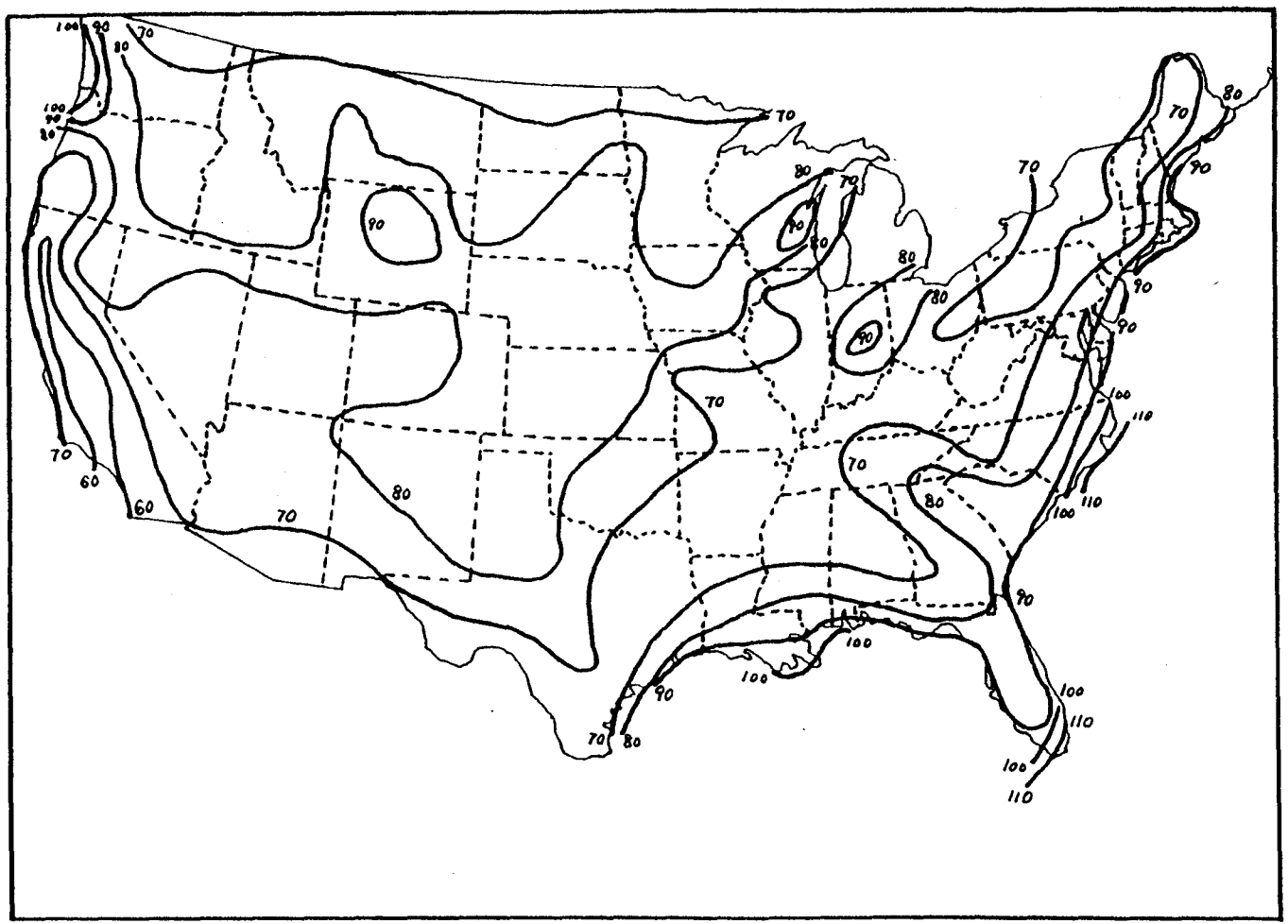

Figure 17. Wind-Speed Zoning Map, Annual Fastest-mile Wind Speed, miles/hr., for Open Country and at a Height of 30 ft. Based on 50-year Return Period. (1 mile = 1.609 km).

TABLE IX. MEAN-WIND SPEED POWER LAW COEFFICIENTS[2]

Surface Roughness	Gradient Height, h_g	Power Law Coeff., r
Central Area of Large Cities	1500 ft.	1/3
Wooded Areas, Small Towns, or Suburbs	1200 ft.	2/9
Open Country	900 ft.	1/7

$$p_{dh} = \frac{\rho v_h^2}{2} \tag{5.33}$$

in which ρ is the mass density of air, and v_h is the mean wind velocity at the height, h, which is determined in accordance with Eq. (5.31) for the actual surface roughness of the structural site.

The wind pressure per unit area, p_h, is then determined according to the following formula:

$$p_h = G\ C_p\ p_{dh} \tag{5.34}$$

in which G is the gust factor, and C_p the pressure coefficient.

There are two types of pressure coefficient. One is the external pressure coefficient, which is a function of building geometry and the direction of the wind; the other is the internal pressure coefficient, which is a function of the number of openings in the structure. A tabulated pressure coefficient for different structural configurations are given in Ref. 1. The dynamic wind pressure must be multiplied by the sum of the external and internal pressure coefficients.

The total lateral wind shear forces at floor level x, V_x, is determined in accordance with the formula:

$$V_x = \int_{h_x}^{h_n} (p_h B)\ dh \tag{5.35}$$

in which h_n is total height of the structure measured from the ground surface, h_x the height of level x above the ground surface, and B the width of the structure in the orthogonal direction of analysis.

The design wind force at floor level x, F_x, should be determined by

$$F_x = V_x - V_{x+1}. \tag{5.36}$$

In a computer program, the wind forces are computed by simply assuming that the wind pressure is trapezoidally distributed along the height of the structure between levels x and x+1 as shown in Figure 18. The lateral wind force at level x is then determined by using

$$F_x = \left(\frac{P_x + P_{x+1}}{2}\right)\left(\frac{h_{x+1} - h_{x-1}}{2}\right) \tag{5.37}$$

in which $P_x = p_{h1}B$, $P_{x+1} = p_{h2}B$, $h_1 = (h_x+h_{x-1})/2$, $h_2 = (h_{x+1}+h_x)/2$, and h_{x+1}, h_x, h_{x-1} is the height of floor levels x+1, x and x-1 above the ground surface respectively.

2. The Wind Design Provisions of UBC.[57] The UBC provisions are used to determine the design wind pressure, p, in accordance with the following formula:

$$p = C_e\, C_q\, I\, q_s \tag{5.38}$$

in which C_e is the combined height exposure, and gust factor coefficient, C_q the pressure coefficient for the structure or portion of

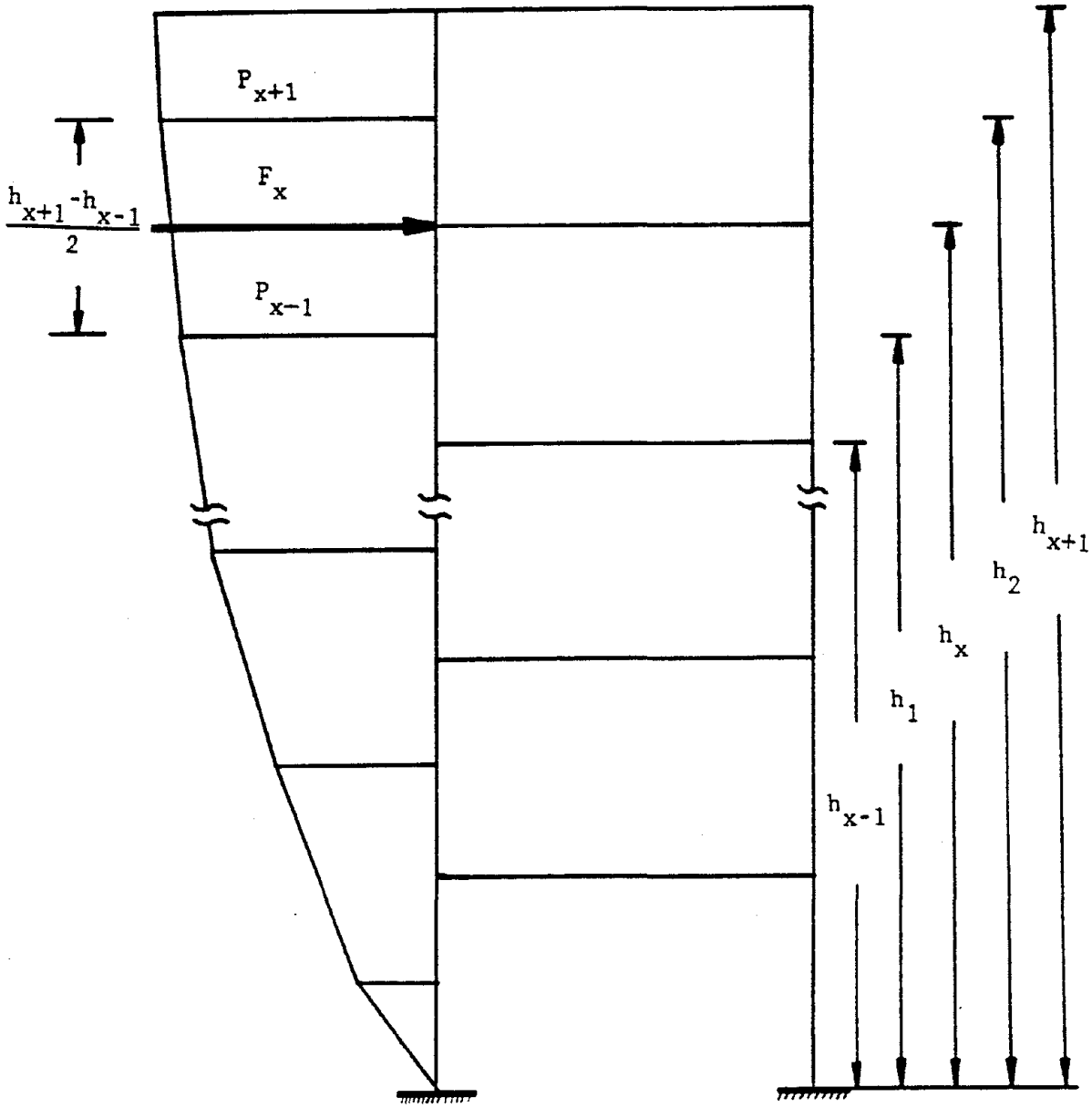

Figure 18. The Wind Pressure Distribution Model for Wind Design Based on Power Law.

the structure under consideration, q_s the wind stagnation pressure at the standard height of 30 feet, and I the importance factor of the structure.

The coefficient C_e is increased when the height is increased, whose value ranging from 1.2 to 2.2 for exposure C and 0.7 to 1.8 for exposure B. The pressure coefficient, C_q, depends on the configuration of the structure. Two methods are considered in the UBC to determine the wind forces. One is the normal force method, which is used for gabled rigid frames and may be used for any structure. The other is the projected area method, which is used for any structure less than 200 feet in height except those using gabled frames. Tabulated values of C_e are given in UBC. For the normal force method, the value of C_e on the leeward walls are evaluated at mean roof height. The determination of wind stagnation pressure is based on the basic wind speed, which is determined from the wind speed zoning map. The importance factor, I, has a value of 1.15 for essential buildings and 1.0 for all other buildings.

VI. PARAMETER STUDIES OF OPTIMAL DESIGN RESULTS

A. THE EFFECT ON THE OPTIMUM SOLUTION OF CONSTRAINT GRADIENTS

The cantilevered 10-bar truss shown in Figure 19 with its ten design variables and eight degrees of freedom was designed specially for the present study. Loads of 100 kips (444.8 kN) static were applied at nodes 2 and 4. The truss' modulus of elasticity was $E=10x10^6$ psi (6895 kN/cm^2), its mass density, $\rho=0.10$ lb/in^3 (0.0271 N/cm^2), and allowable stress, $\sigma_{all} = \pm 25{,}000$ psi (17.236 kN/cm^2). Its allowable displacements were ± 2.0 in. (5.08 cm) in both the x and y directions at nodes 1, 2, 3, and 4. The truss was designed for four different cases: Case (1) Stress constraint without using the constraint gradients; Case (2) Stress constraint and the constraint gradients; Case (3) Both stress and displacement constraints without constraint gradients; Case (4) Both stress and displacement constraints and the constraint gradients.

The optimum solutions, which include the sectional areas, stresses, and optimum weight, are shown in Table X. The plot of weight versus cycles of iteration is shown in Figure 20. The optimum weight of Case (3), as shown in Figure 20, can be reduced by applying the constraint gradient at the 10th cycle; as shown in Table X, the stresses of the passive elements are increased. However, the result of Case (1) is not improved significantly by applying the constraint gradient method. These design results indicate that the contribution method, which is based on the constraint gradient, can improve the optimum solution, but is time consuming to calculate constraint

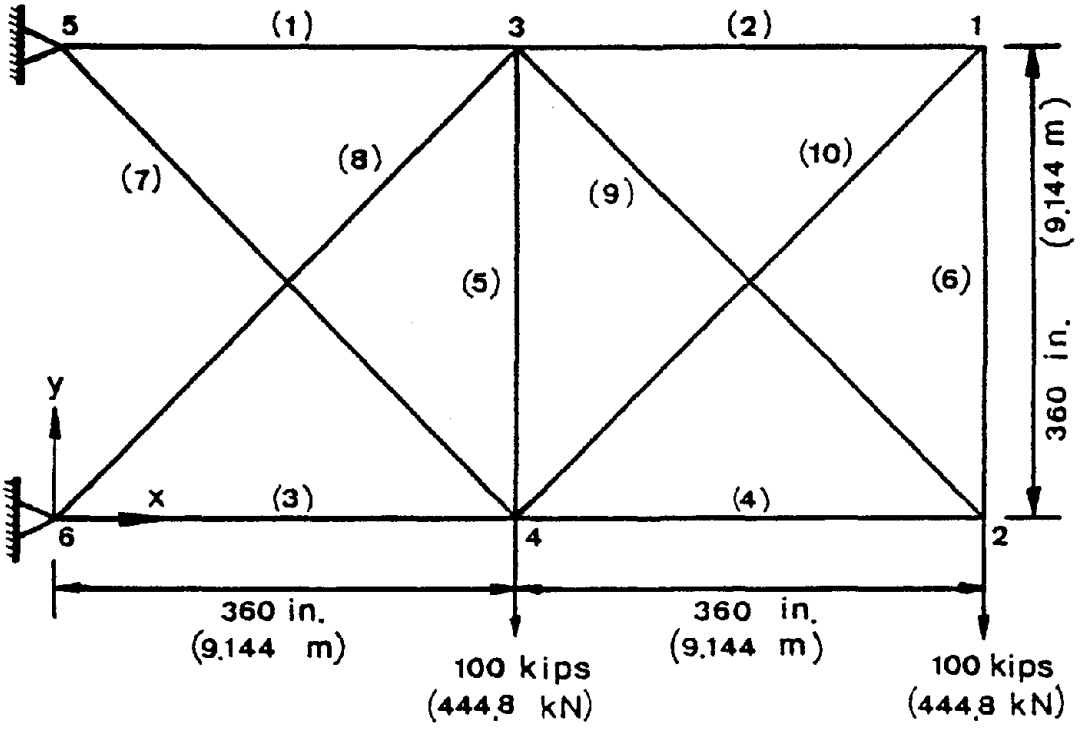

Figure 19. Ten-Bar Truss for Constraint Gradient Study

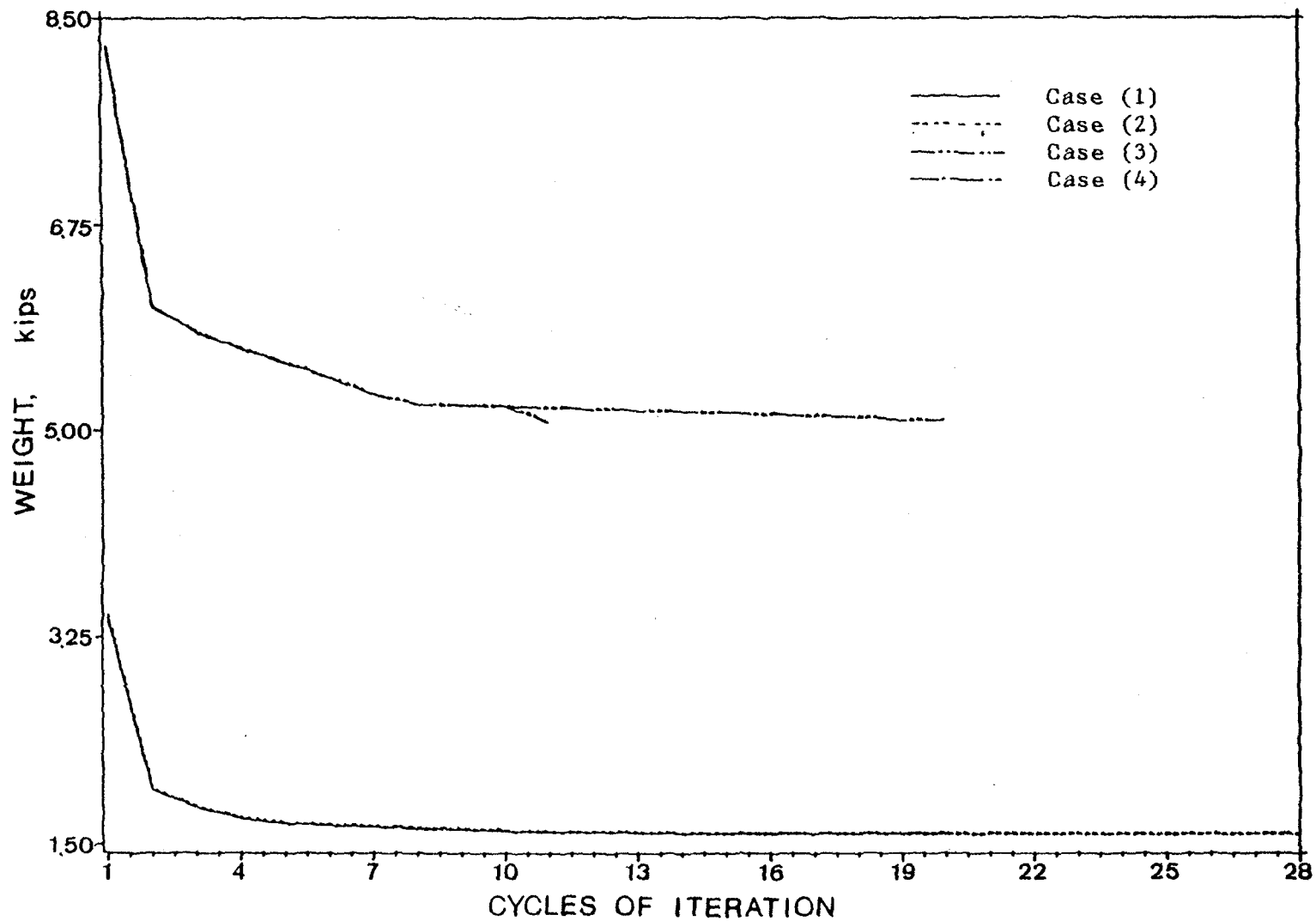

Figure 20. Weight v.s. Cycles of Iteration Plot of the Ten-Bar Truss for the Study of Constraint Gradient Method. (1 kip = 4.448 kN)

TABLE X. THE FINAL DESIGN RESULTS OF THE TEN-BAR TRUSS FOR CONSTRAINT GRADIENT STUDIES (1 in. = 2.54 cm, 1 lb = 4.448 N).

Member No.	Case (1)		Case (2)		Case (3)		Case (4)	
	Area (in^2)	Stress (lbs/in^2)	Area (in^2)	Stress (lbs/in^2)	Area (in^2)	Stress (lbs/in^2)	Area (in^2)	Stress (lbs/in^2)
1	7.9379	24999.9	7.9379	25000.0	30.512	6621.0	30.720	6598.0
2	0.1000	15533.0	0.1000	15533.0	0.100	52.0	0.100	1198.0
3	8.0622	24999.9	8.0622	25000.0	21.901	9040.0	22.390	8814.0
4	3.9379	25000.0	3.9379	25000.0	15.154	6599.0	15.140	6612.0
5	0.1000	0.078	0.1000	0.039	0.101	20047.0	0.100	24645.0
6	0.1000	15533.1	0.1000	15533.1	0.100	52.0	0.530	223.0
7	5.7447	25000.0	5.7447	25000.0	8.924	15526.0	7.660	17959.0
8	5.5690	24999.9	5.5690	25000.0	21.496	6712.0	21.530	6744.0
9	5.5690	25000.0	5.5690	25000.0	21.431	6599.0	21.420	6612.0
10	0.1000	21966.9	0.1000	21966.9	0.100	73.0	0.100	1695.0
Final Wt. (lbs)	1593.18		1593.18		5088.2		5065.0	
No. of Iterations	19		19		20		11	

gradients.

The ten-bar cantilevered truss has been studied by many researchers. Comparison of final results with previous results is made in Table XI.

B. PARAMETER STUDIES OF THE NATURAL PERIOD AND SEISMIC COEFFICIENT IN THE ATC ELF PROCEDURES

The 15-story, one-bay, unbraced frame shown in Figure 21 was designed according to the ATC-3-06, equivalent lateral force procedures. The design was based on a response modification factor of R=8, a deflection amplification factor of C_d=5.5, and an allowable story drift of Δ_a=0.015h_{sx}/C_d in which h_{sx} is the story height below level x. The stress constraint was not taken into consideration, and the nonstructural dead load on each floor level was set at 50,000 lbs (222.4 kN). The AISC wide-flange sections and both the energy distribution and constraint gradients discussed in Chapter II were used in the design.

Thirty-six cases were designed on the basis of different combinations of the effective peak ground acceleration, A_a, the effective peak ground velocity, A_v, and the soil profile type. The coefficients of A_a were changed to 1, 3, 5, and 7, and those of A_v to 3, 5, and 7 for three soil profile types S_1, S_2, and S_3. The plots of the fundamental periods, the seismic design coefficients, C_s, and the optimum weights of the 36 design cases are shown in Figures 22, 23, and 24 respectively. It is worth noting that all the fundamental periods are larger than the approximate fundamental period, T_a, as

TABLE XI. COMPARISON OF FINAL WEIGHTS FOR THE TEN-BAR CANTILEVERED TRUSS.

(1 lb = 4.448 N).

	Schmit and Miura[80]	Schmit and Farshi[49]	Kan, Willmart and Thornton[81]	Dobbs and Nelson[82]	Rizzi[83]	Present
(1)*, lbs	5076.85 (13)	5089.0 (23)	5066.98 (16)	5080.0 (15)	5076.66 (12)	5065.0 (11)
(2)**, lbs	1593.23 (15)	1593.2 (20)		1622.11 (11)	1593.18 (15)	1593.18 (19)

* Stress and displacement constraints.

** Stress constraints only.

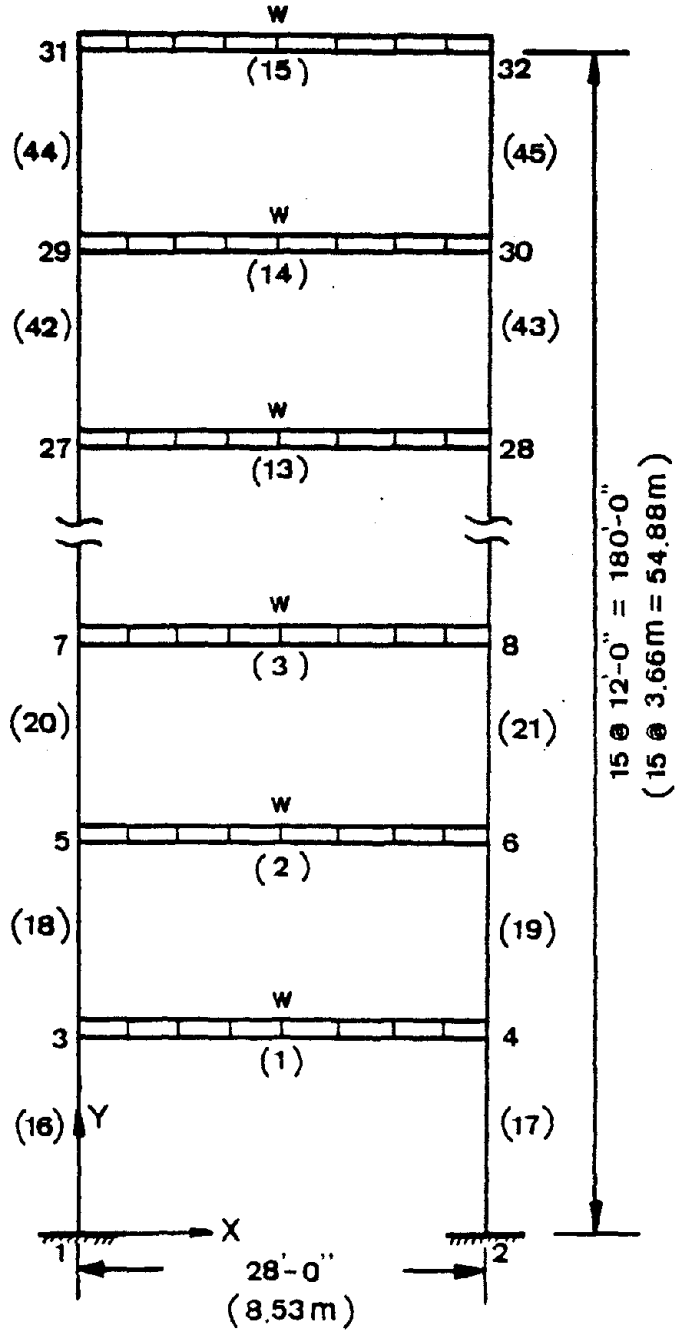

Figure 21. 15-Story, One-Bay, Unbraced Frame for the ATC-3-06 Parameters Studies.

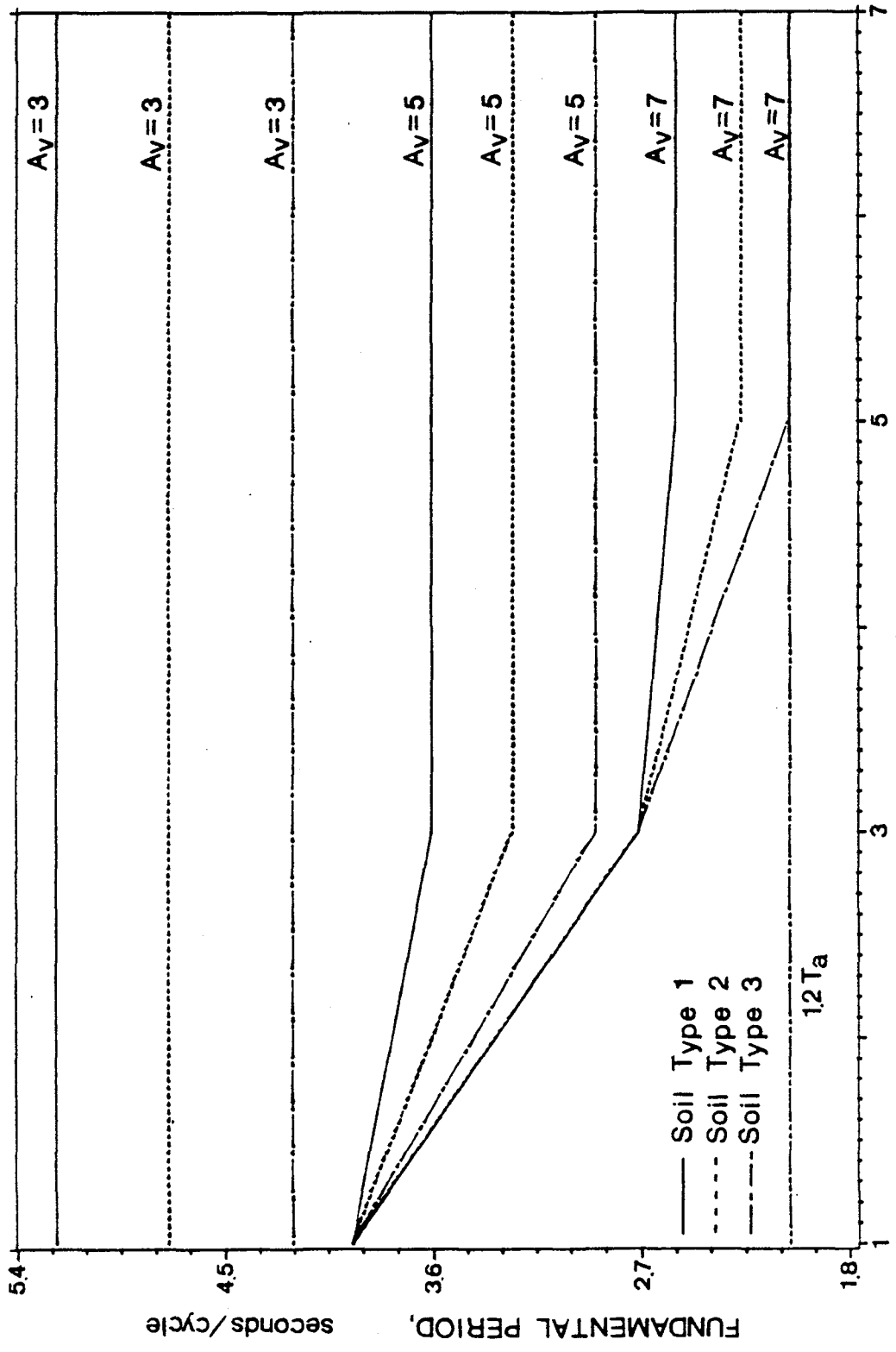

Figure 22. Fundamental Periods of the 15-Story, One-Bay, Unbraced Frame for the Study of ATC-3-06 Parameters.

well as $1.2T_a$. The seismic design coefficients of Figure 23 were varied only when A_a and the soil profile type were changed, because $1.2T_a$ controlled the design. In Figure 23, points marked by an asterisk were computed in accordance with the formula $C_s=2.5A_a/R$ in which the natural period is not needed. Based on the optimum design results, it was not necessary to use mechanical methods to determine the natural period, especially for those areas having low values of A_a and A_v.

Because $1.2T_a$ controls all the design results, some of the 36 design cases have identical optimal weight. The optimum solutions may be classified into 11 groups. In Figure 24, the number in parentheses indicates which group that the design case belongs to. The plot of weights versus cycles of iteration for these 11 groups is shown in Figure 25. All of the design results were improved by using the constraint gradients. The stability coefficients, that are determined according to Eq. (5.9), are shown in Figure 26 in which all of the values are less than the upper bound 0.1 except for the case corresponding to $A_a=1$, $A_v=3$, and soil profile type S_1. This case has a maximum value of 0.117 at the bottom story. Among these 36 design cases, the case corresponding to $A_a=7$, $A_v=7$ and soil profile type S_3 has a maximum eccentricity of 5.66 ft. (1.73 m) as measured from the center of the bay to the outside of the bay and induced by the resultant of the seismic forces as well as the vertical loads at the foundation-soil interface.

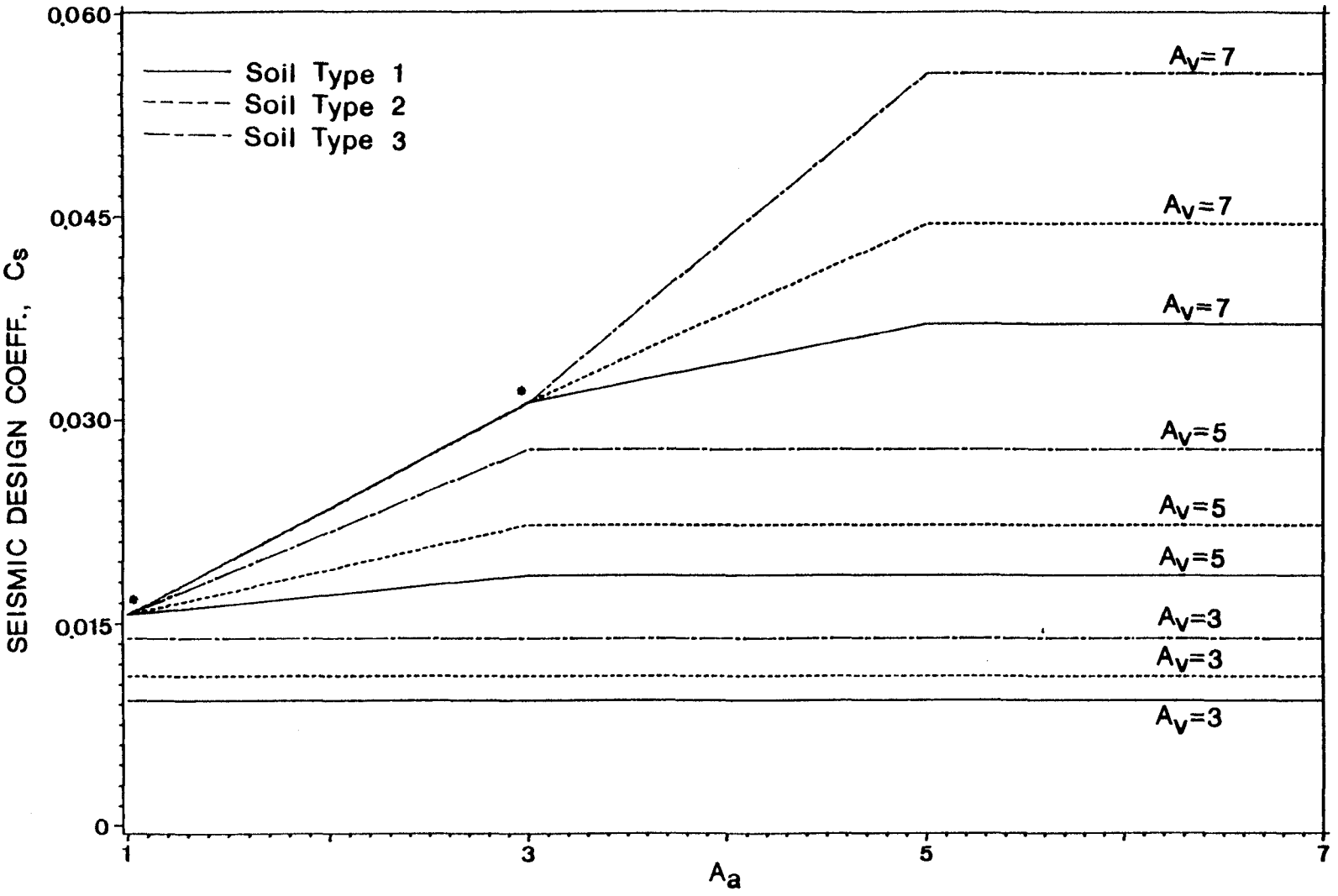

Figure 23. Seismic Design Coefficients, C_s, of the 15-Story, One-Bay, Unbraced Frame for the Study of ATC-3-06 Parameters.

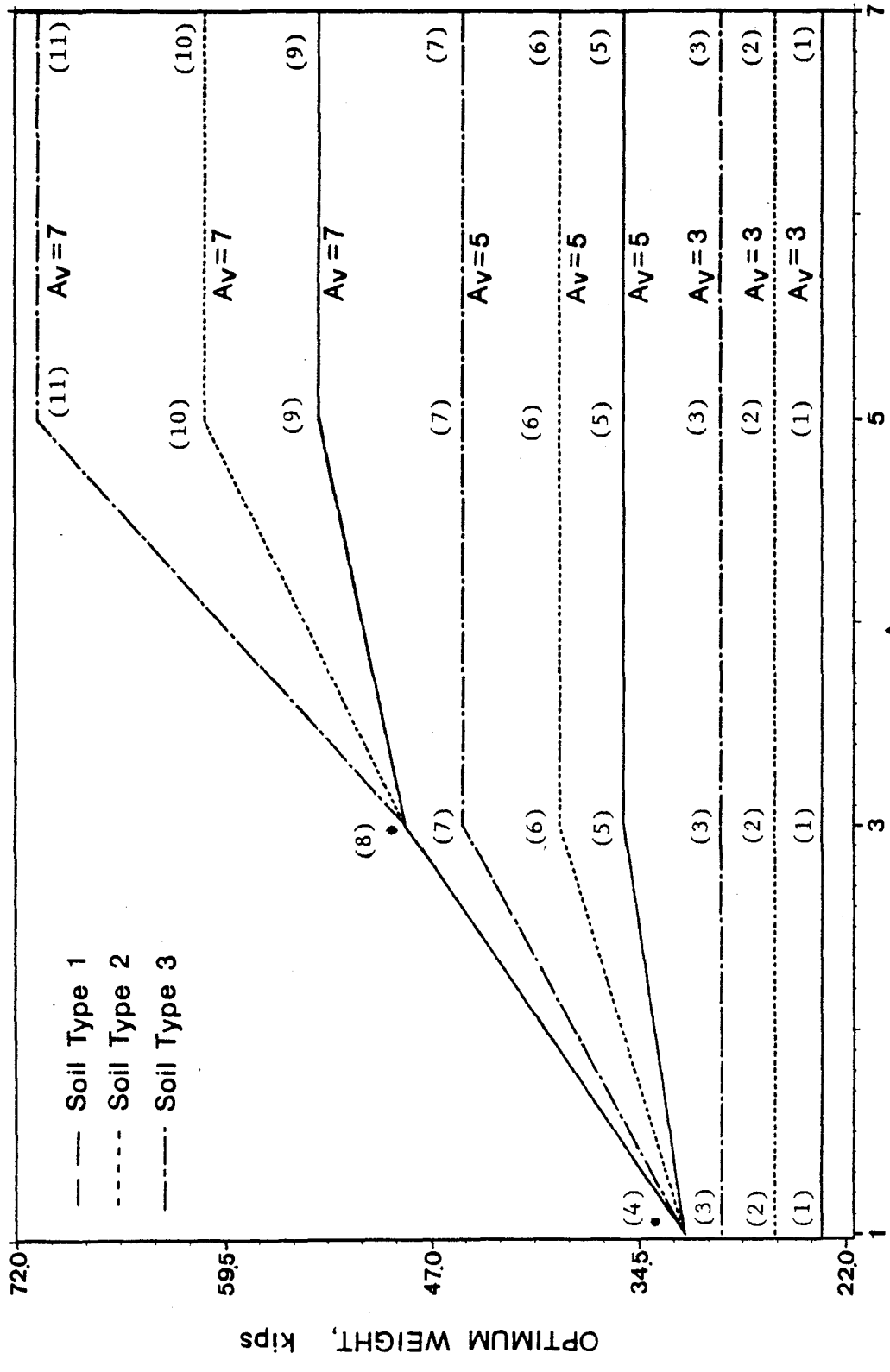

Figure 24. Optimum Weights of the 15-Story, One-Bay, Unbraced Frame for the Study of ATC-3-06 Parameters. (1 kip = 4.448 kN)

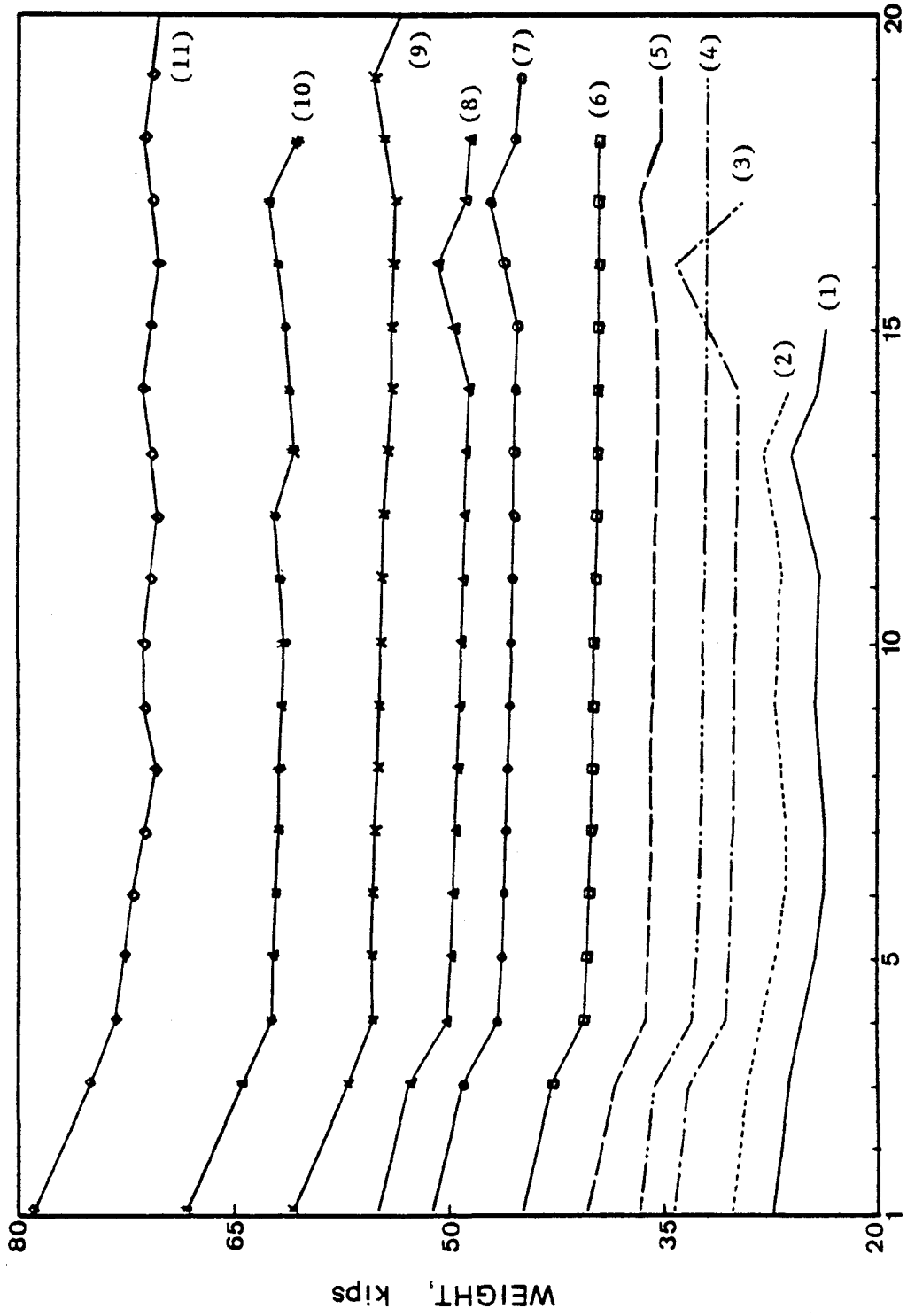

Figure 25. Weight v.s. Cycles of Iteration Plot of the 15-Story, One-Bay, Unbraced Frame for the Study of ATC-3-06 Parameters. (1 kip = 4.448 kN)

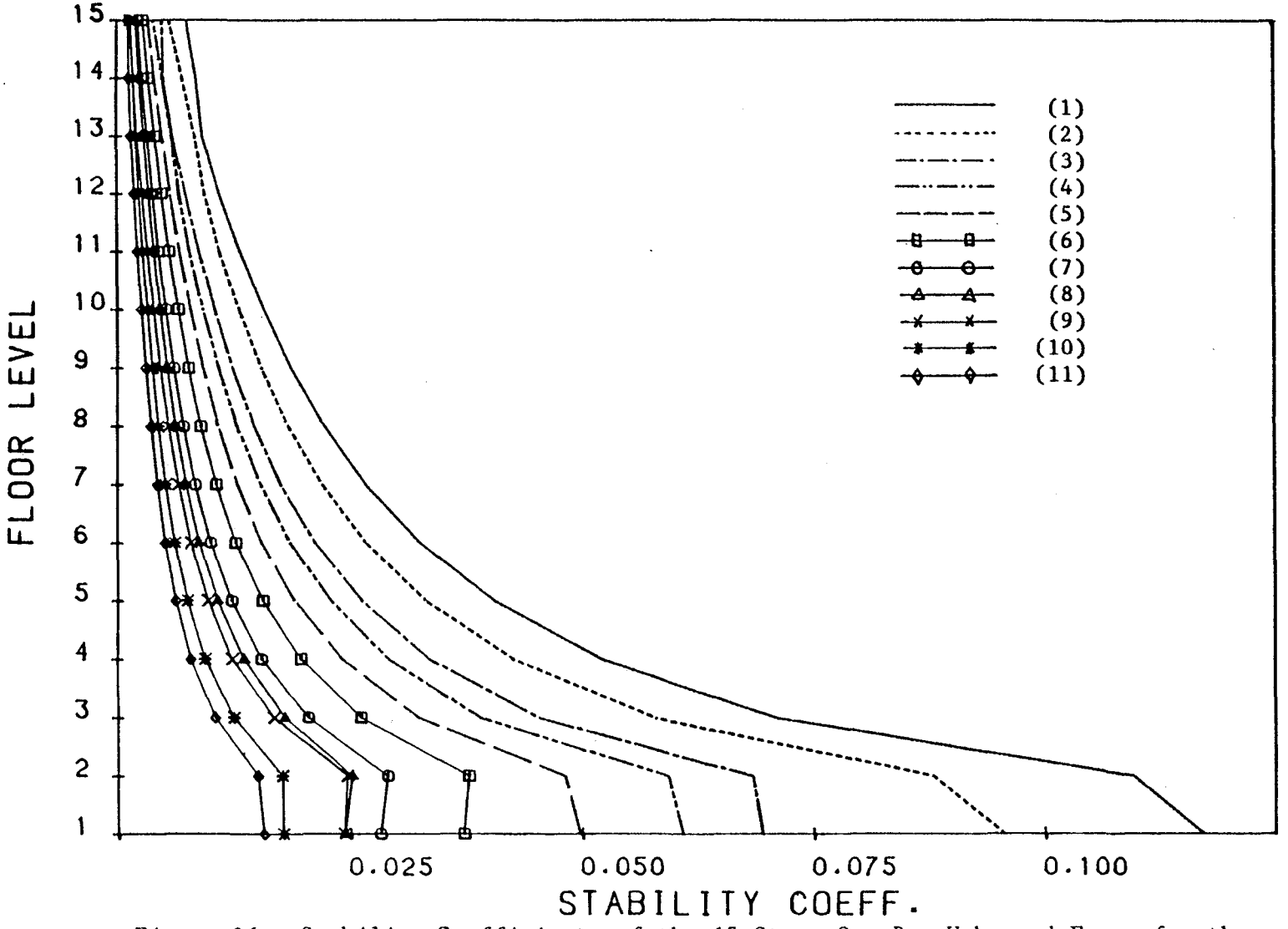

Figure 26. Stability Coefficients of the 15-Story, One-Bay, Unbraced Frame for the Study of ATC-3-06 Parameters.

Figure 27 shows the shear envelopes. The story shears become larger when the seismic excitations become more sensitive.

The moment of inertia of the girder on the first floor for all 11 groups, as shown in Figure 28, is much less than that of a girder on the second and third floors. The moment of inertia of the girder on either the second or third floor is the largest. The decrement of the moment of inertia decreases gradually from either the second or the third floor to the 15th floor.

As illustrated in Figure 30, in decending order, the moment of inertia of a column on the top story is the smallest but increases suddenly at the 14th story. The distribution from the 14th story to the second story is almost linearly increased, and at the first story, it abruptly increases again.

Because the story drifts are constrained, the story numbers of 9, 13, 10, 13, 10, 11, 11, 11, 10, 11, and 10 correspond to the curves 1 through 11 in Figure 32 respectively and have a maximum drift, which is equal to the maximum allowance of 0.393 in. (0.998 cm). However, the shape of lateral displacement of each floor is very different from that determined on the basis of allowable drift.

C. COMPARISON OF THE EQUIVALENT LATERAL FORCE METHOD AND THE MODAL ANALYSIS METHOD OF ATC-3-06

The ATC-3-06 provisions suggest two methods for seismic-resistant design: a) the equivalent lateral force method, which is based on simplified formulas and may be adequate for most regular buildings, and b) the modal analysis method, which is based on the modes of

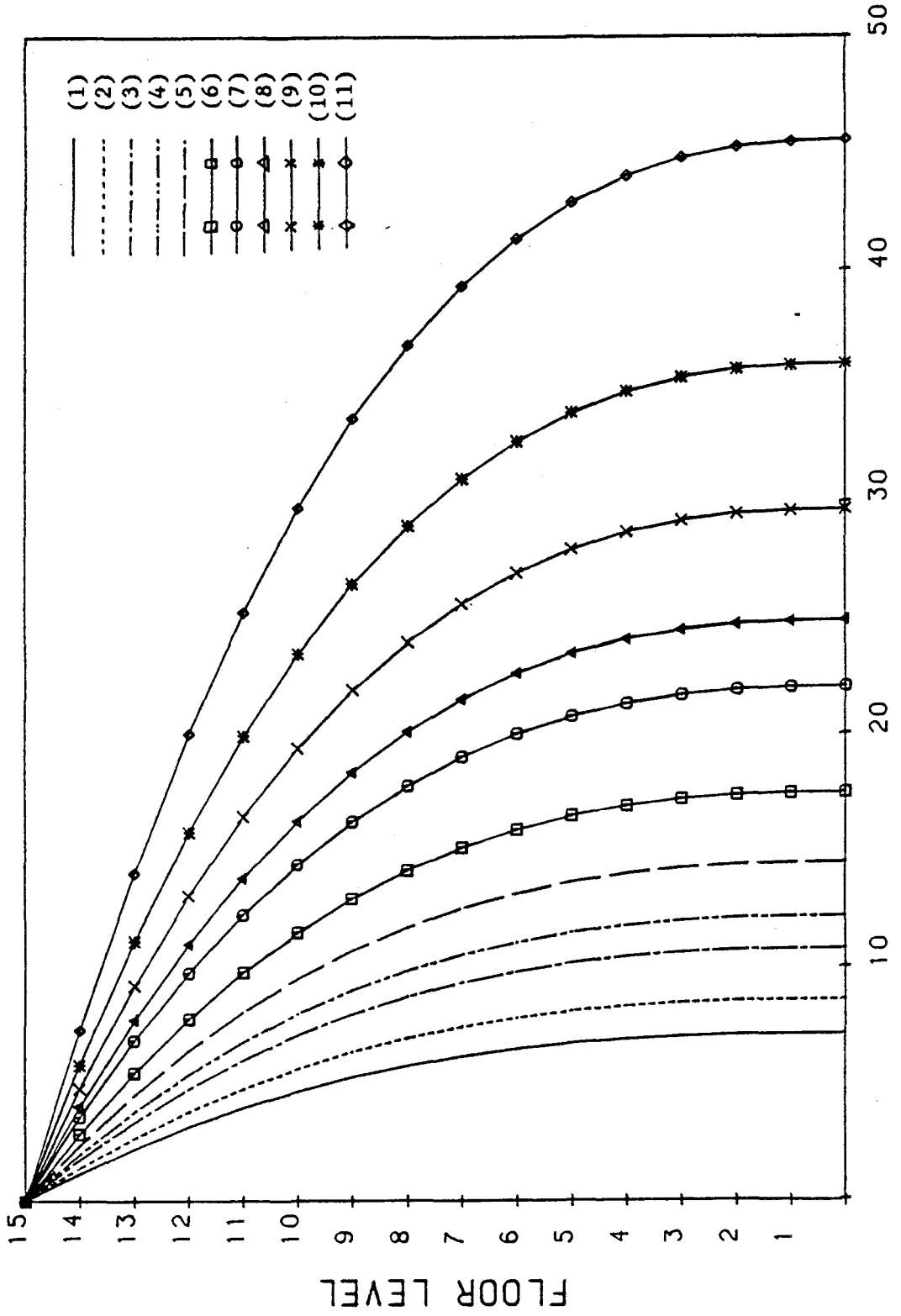

Figure 27. Shear Envelopes of the 15-Story, One-Bay, Unbraced Frame for the Study of ATC-3-06 Parameters. (1 kip = 4.448 kN)

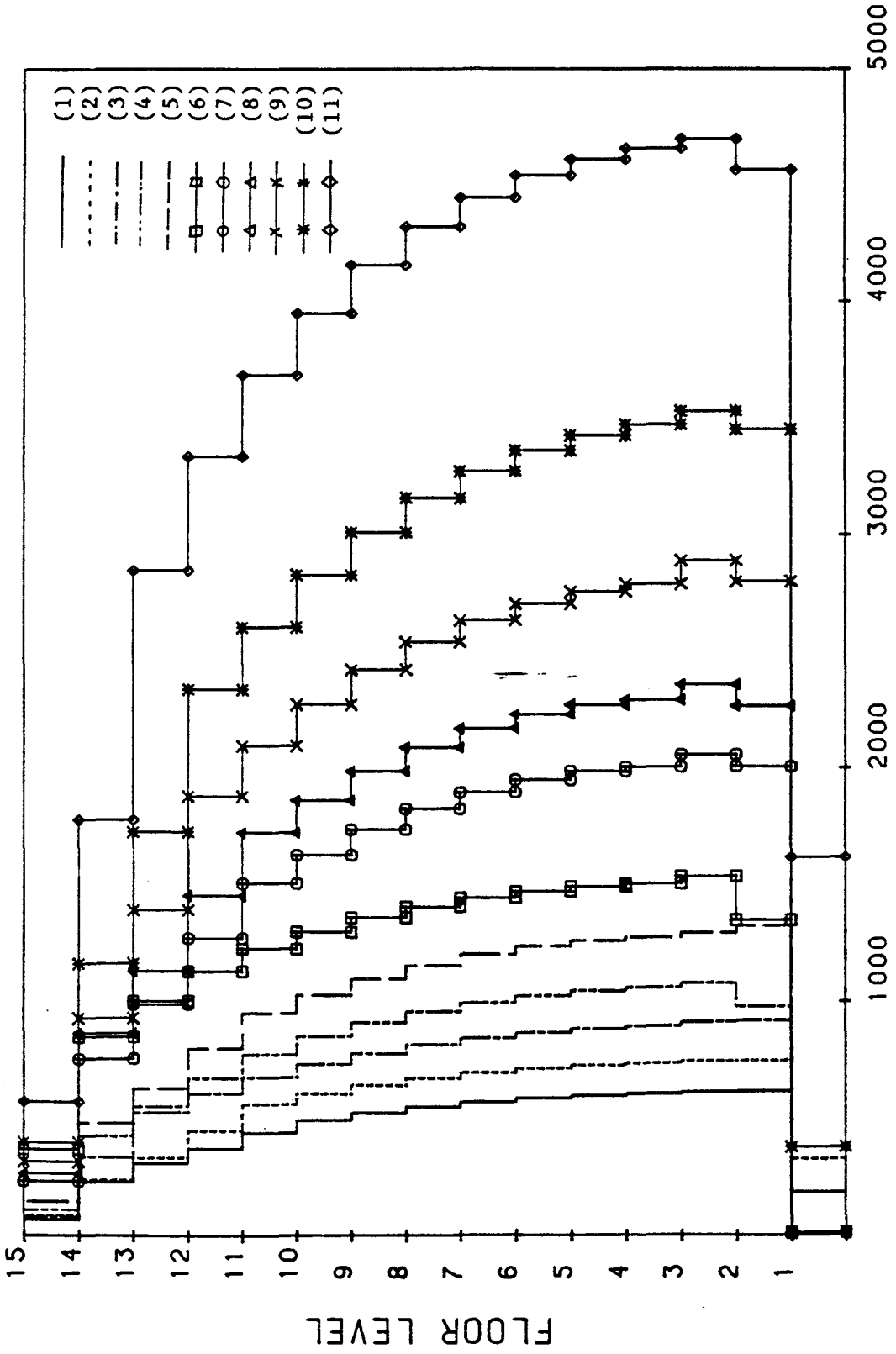

Figure 28. Distributions of the Moment of Inertia of the Girders of the 15-Story, One-Bay, Unbraced Frame for the Study of ATC-3-06 Parameters. (1 in. = 2.54 cm)

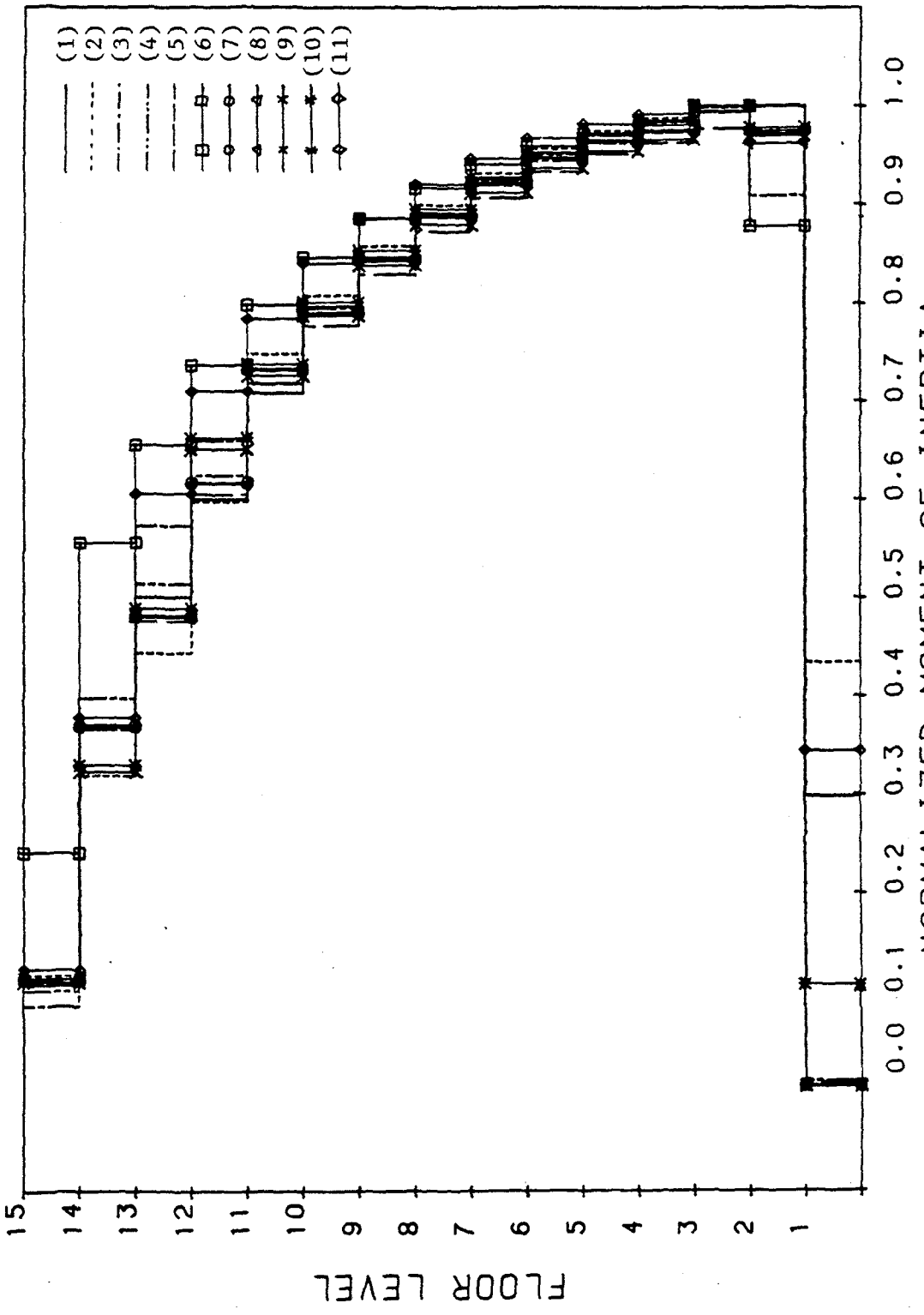

Figure 29. Distributions of the Normalized Moment of Inertia of the Girders of the 15-Story, One-Bay, Unbraced Frame for the Study of ATC-3-06 Parameters.

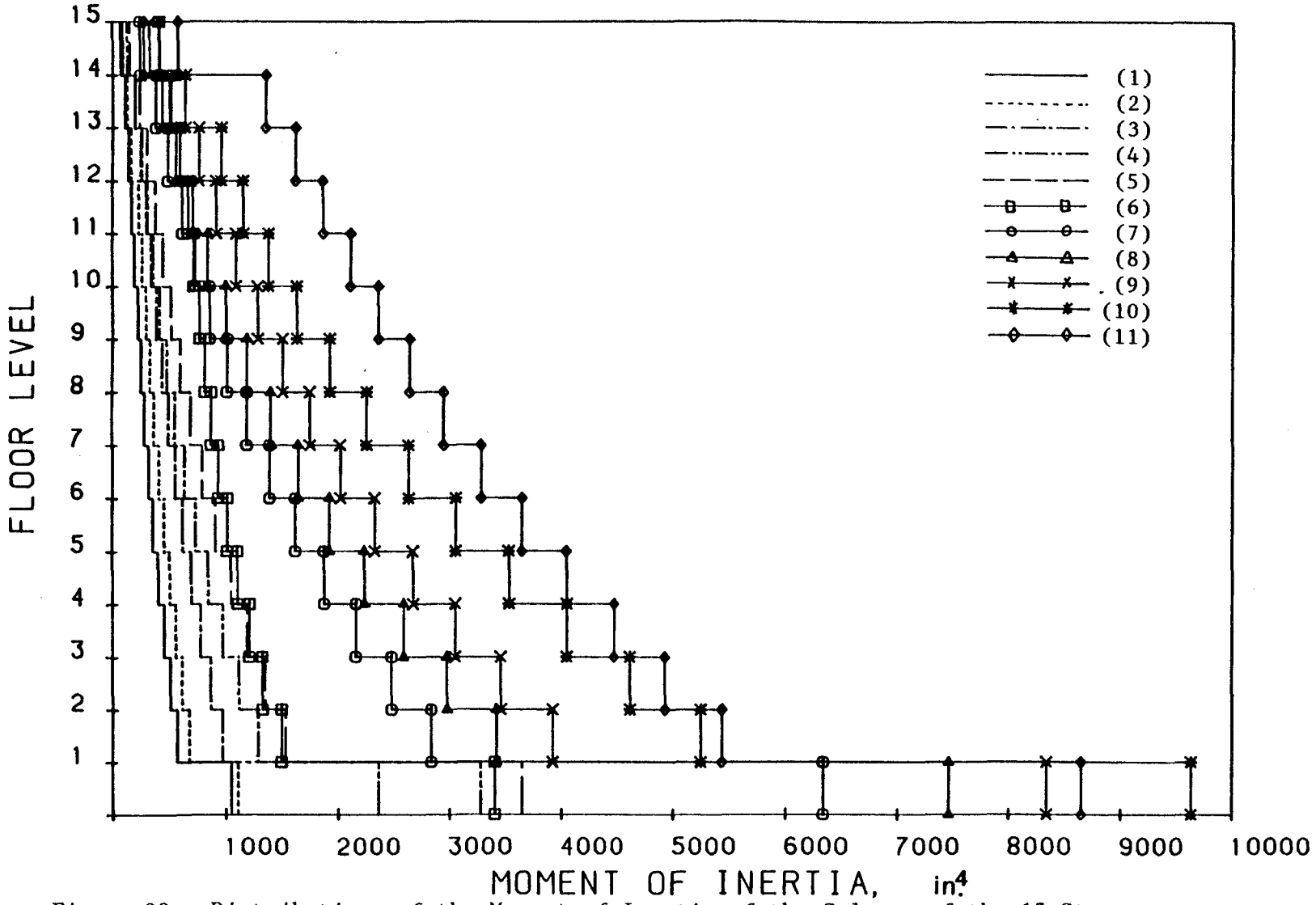

Figure 30. Distributions of the Moment of Inertia of the Columns of the 15-Story, One-Bay, Unbraced Frame for the Study of ATC-3-06 Parameters. (1 in. = 2.54 cm)

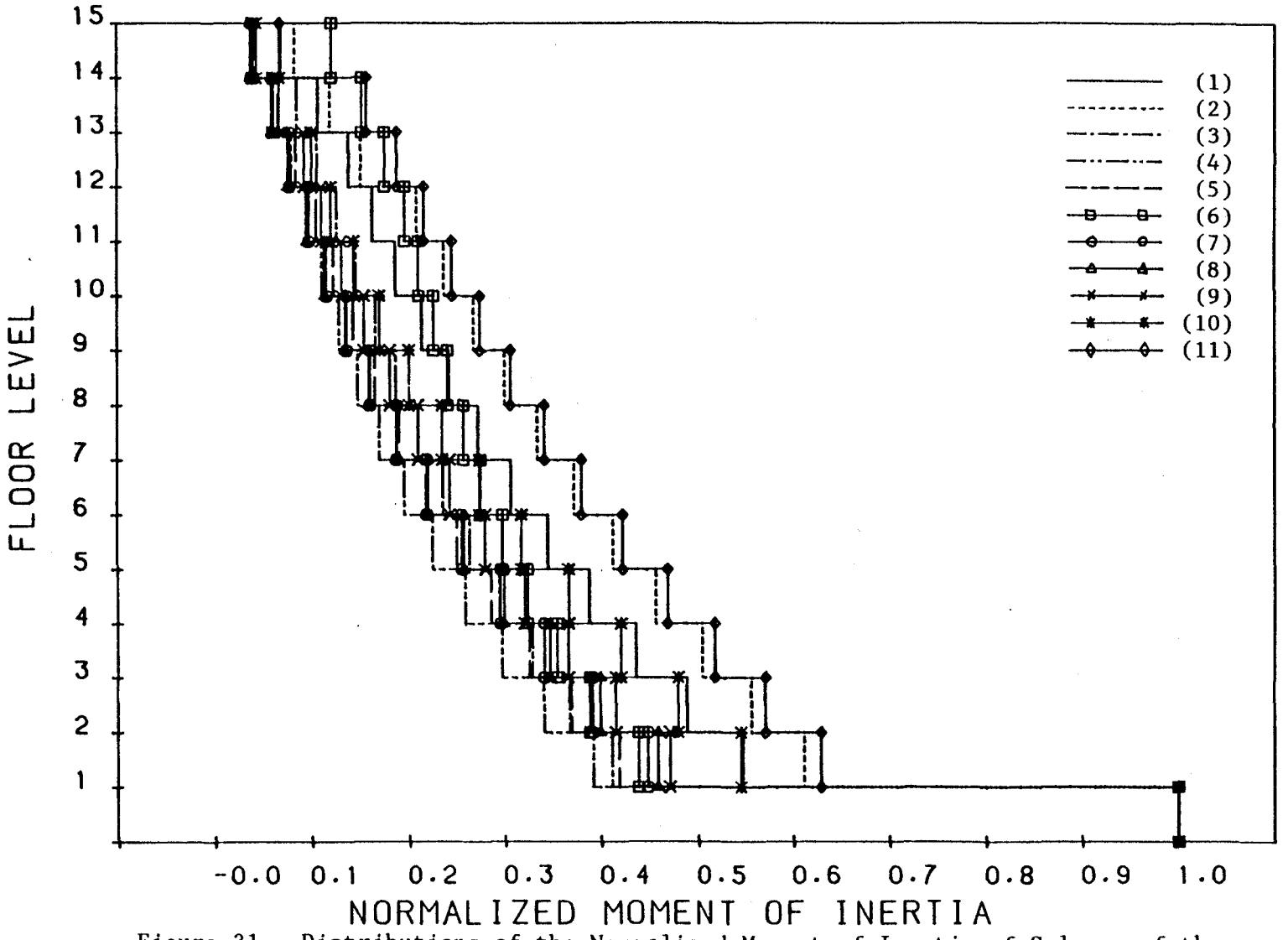

Figure 31. Distributions of the Normalized Moment of Inertia of Columns of the 15-Story, One-Bay, Unbraced Frame for the Study of ATC-3-06 Parameters.

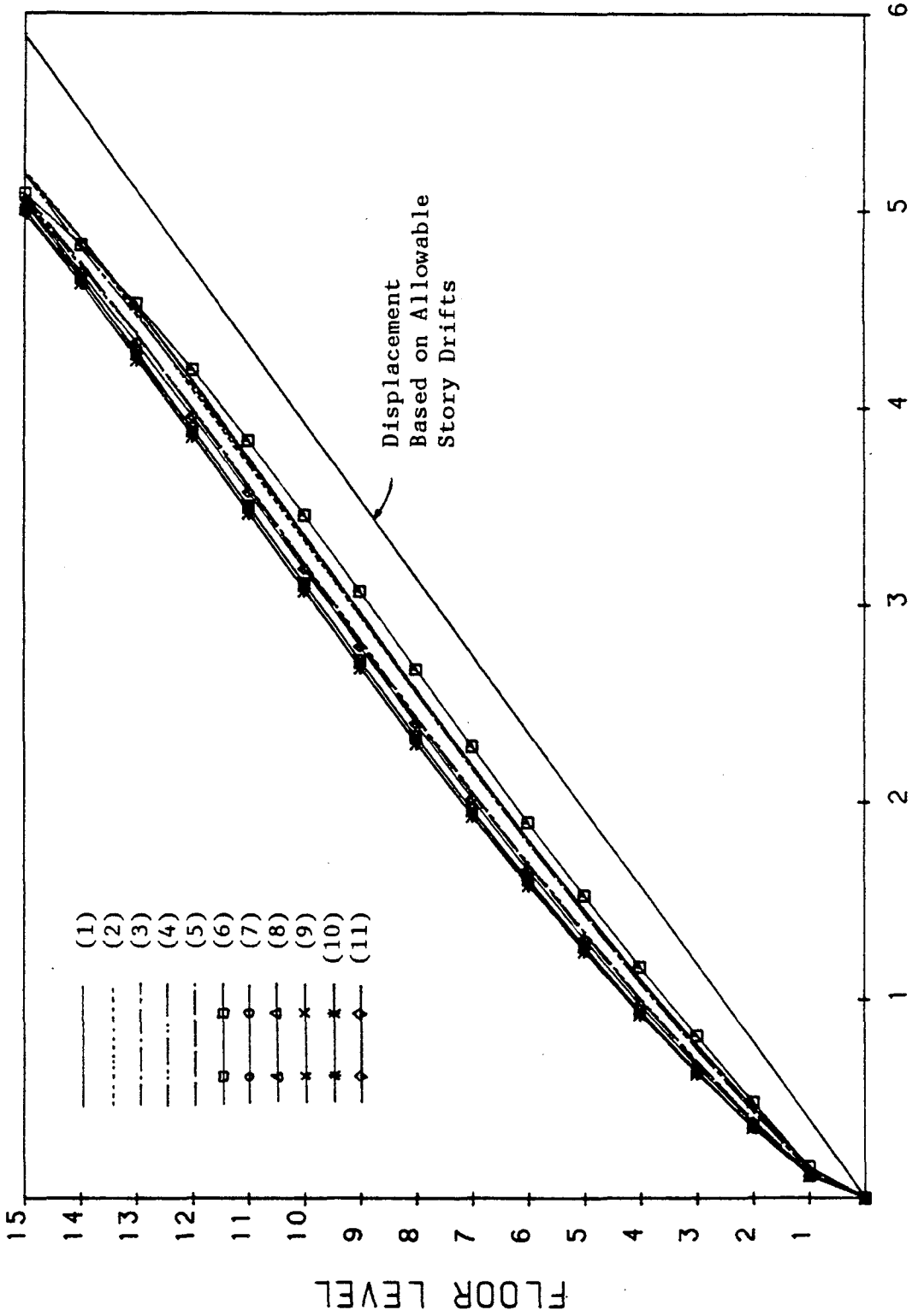

Figure 32. Displacements of the 15-Story, One-Bay, Unbraced Frame for the Study of ATC-3-06 Parameters. (1 in. = 2.54 cm)

natural vibration. A more rigorous and accurate result may be expected from use of the latter. The structures of regular and irregular configurations were designed for a comparison of the two methods. All of them were designed for areas of A_a=7, A_v=7, soil type 3, a response modification factor of R=8, an amplification factor of C_d=5.5, and an allowable story drift of $\Delta_a=0.015h_{sx}/C_d$. The effect of soil-structure interaction and the stress constraint were not considered in the design. The design results of the three types of structure are discussed separately in the following paragraphs of this section. Cases (a) and (b) are referred to whether the design is based on the equivalent lateral force method or the modal analysis method respectively. The constraint gradients were also considered in the designs.

1. Fifteen-story, One-bay, Unbraced Frame. The fifteen-story, one-bay frame shown in Figure 21 was redesigned by using the procedures of the modal analysis method. The plots of weight versus cycles of iteration, stability coefficients, shear envelopes, the moments of inertia and their normalized values for the girders as well as the columns are represented in Figures 33 through 39. The optimum weight for Case (b) is 61.28 kips (272.57 kN), which is less than the optimum weight of 70.07 kips (311.67 kN) for Case (a). The stability coefficients of Figure 34 have the maximum values of 0.0156 and 0.0186 at the bottom story for Cases (a) and (b) respectively. These values are much less than the upper bound, 0.1.

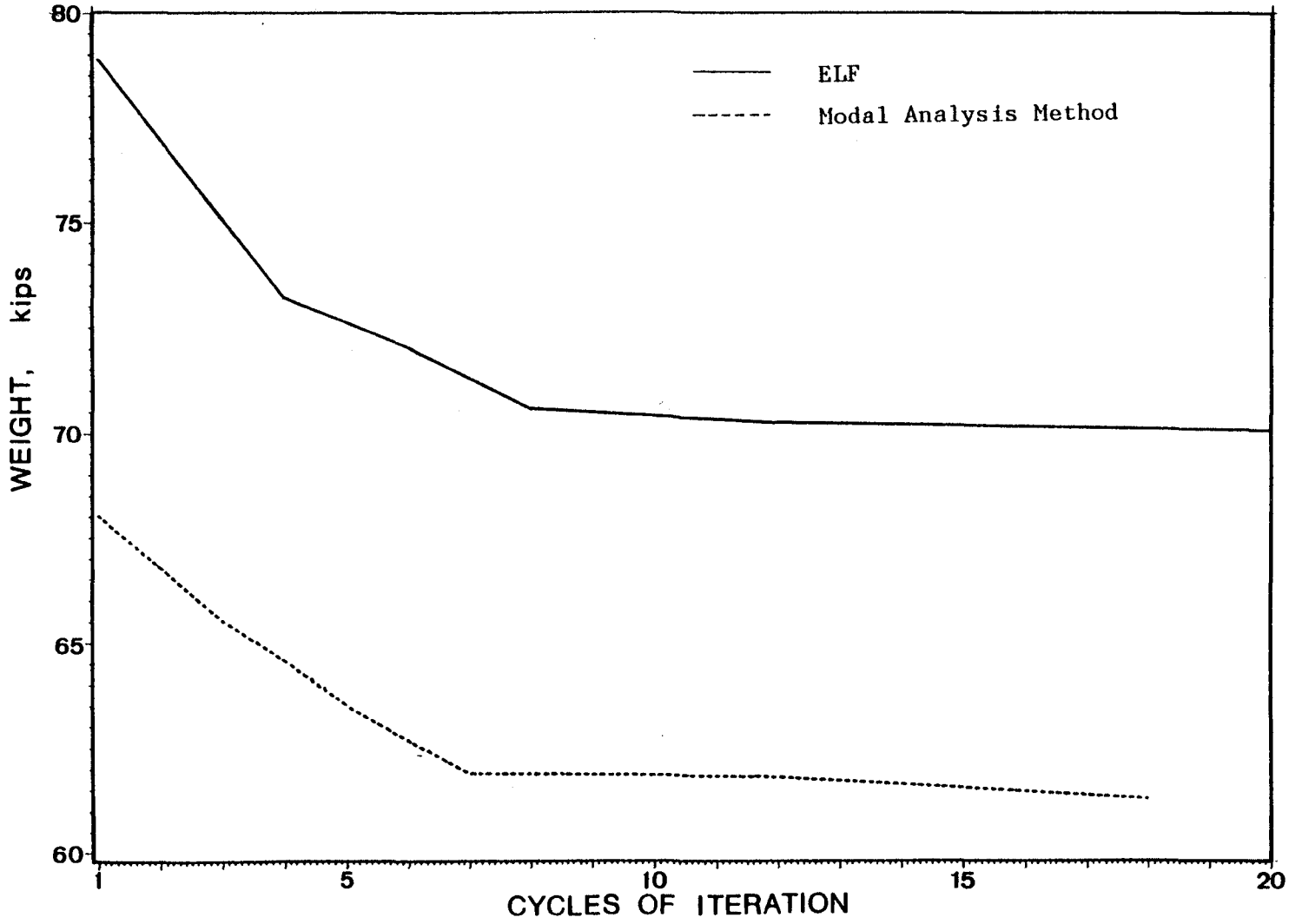

Figure 33. Weight v.s. Cycles of Iteration Plot of the 15-Story, One-Bay, Unbraced Frame for the Comparison of the ATC-3-06 ELF and Modal Analysis Methods. (1 kip = 4.448 kN)

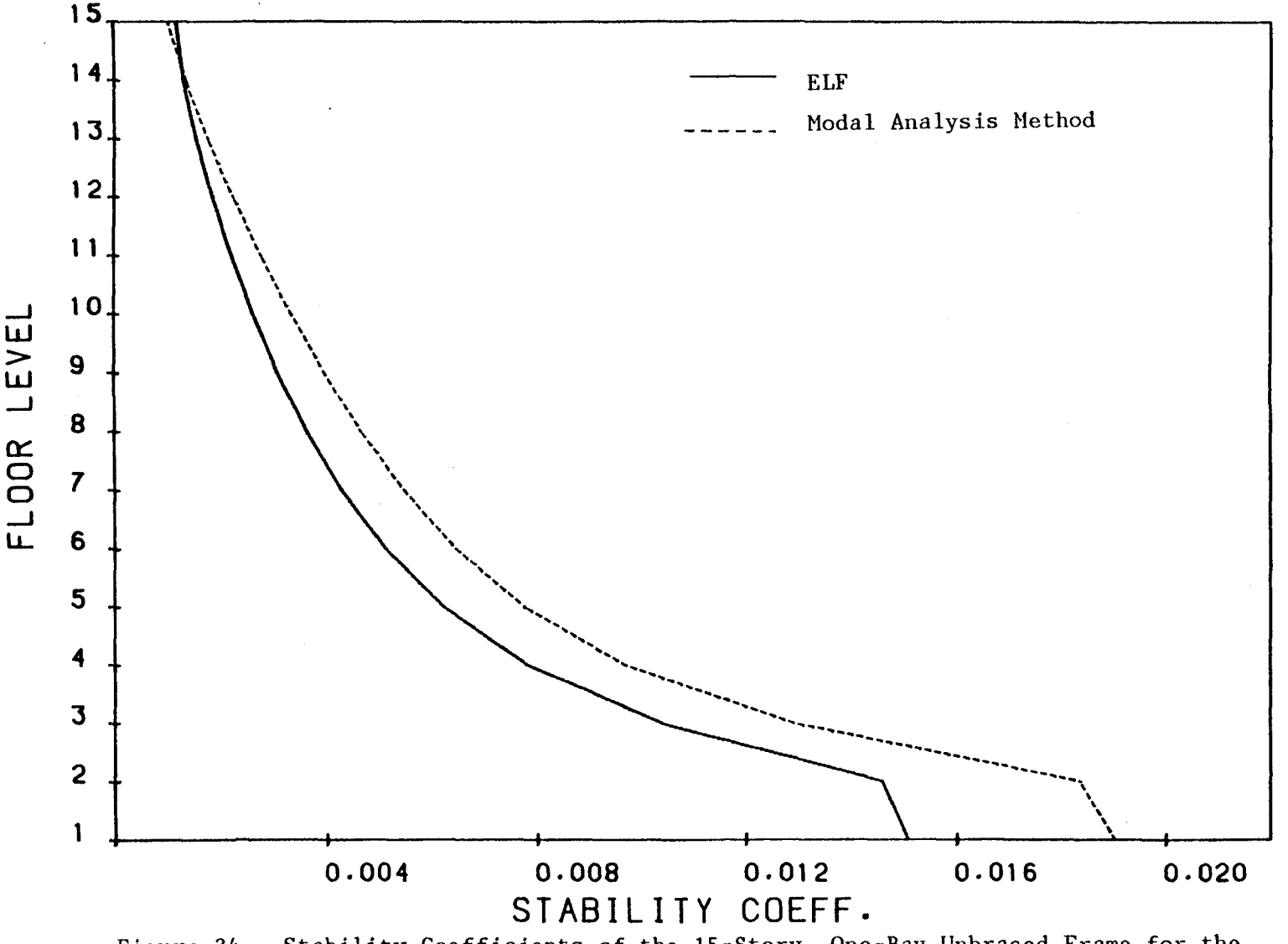

Figure 34. Stability Coefficients of the 15-Story, One-Bay, Unbraced Frame for the Comparison of the ATC-3-06 ELF and Modal Analysis Methods.

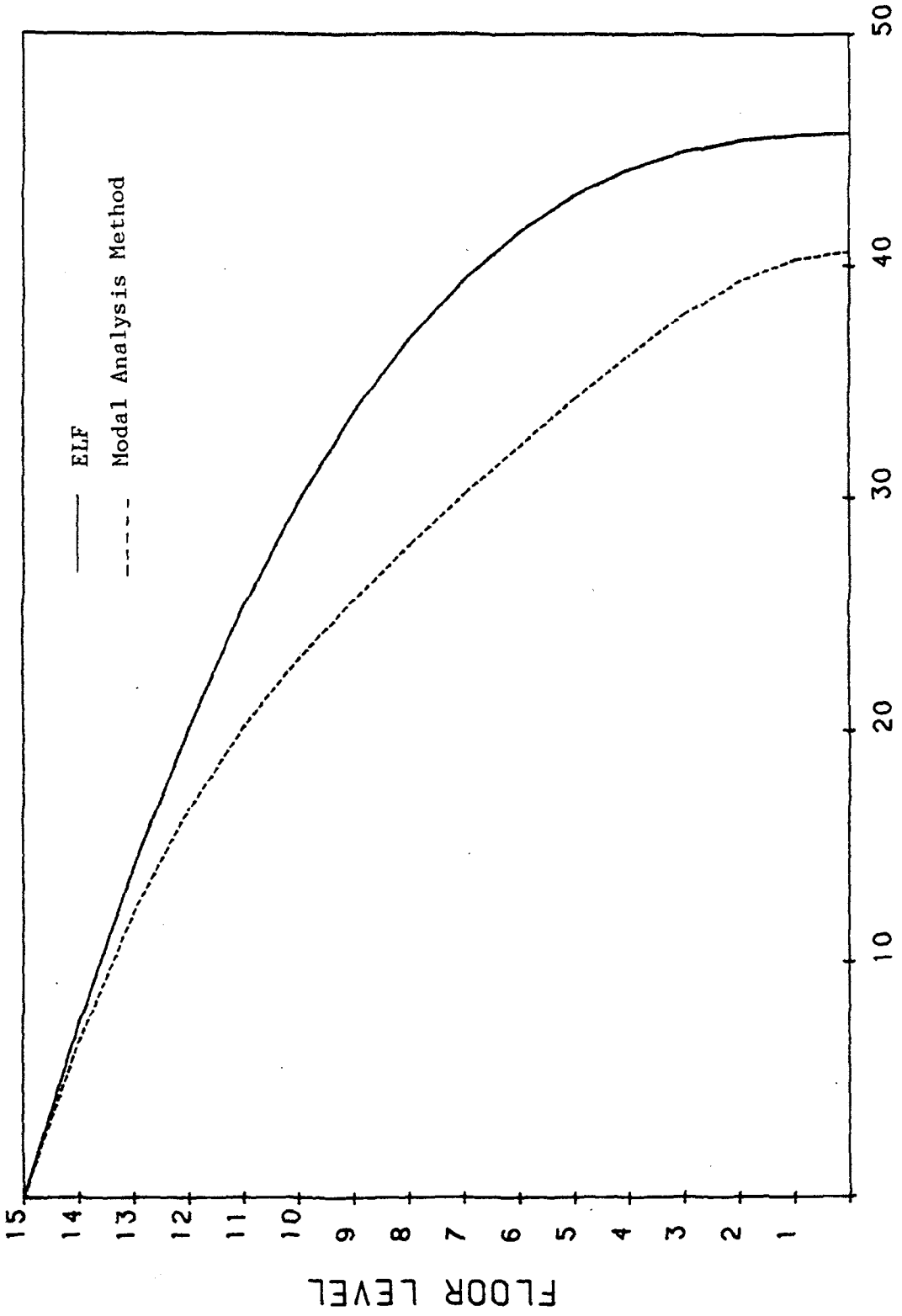

Figure 35. Shear Envelopes of the 15-Story, One-Bay, Unbraced Frame for the Comparison of the ATC-3-06 ELF and Modal Analysis Methods. (1 kip = 4.448 kN).

As shown in Figures 36 and 38, for almost all the members, the moments of inertia of the members for Case (b) are less than those of the corresponding members for Case (a); however, the distributions of the moments of inertia of the girders and columns of Case (a) are similar to those of Case (b).

In Figure 40, the curves indicate the lateral displacements at the different floor levels. As expected, because the story drifts are restrained, the lateral displacements are much less than the allowable displacements cumulated by using the allowable drifts, Δ_a, but the drift of the 10th story is violated.

2. Fifteen-story, Two-bay, Unbraced Frame. The structure shown in Figure 41 was designed to resist a nonstructural weight of 100,000 lbs (444.8 kN) per floor and seismic design forces. The constraints are the same as those for the one-bay frame. The structure was also used for other design cases which will be discussed in Sections VI.E and VI.F.

Figure 42 illustrates the plots of the weight versus cycles of iteration. Note that the modal analysis method requires less weight than the equivalent lateral force method.

In Figure 44, the stability coefficients are plotted. The stability cofficient of the bottom story is 0.0194 for Case (a) and 0.023 for Case (b).

As shown in Figures 45 through 49, the moments of inertia of the girders and exterior columns from the bottom to the top of the building have a distribution that is similar to that of the one-bay frame. The distribution of the moments of inertia of the interior columns,

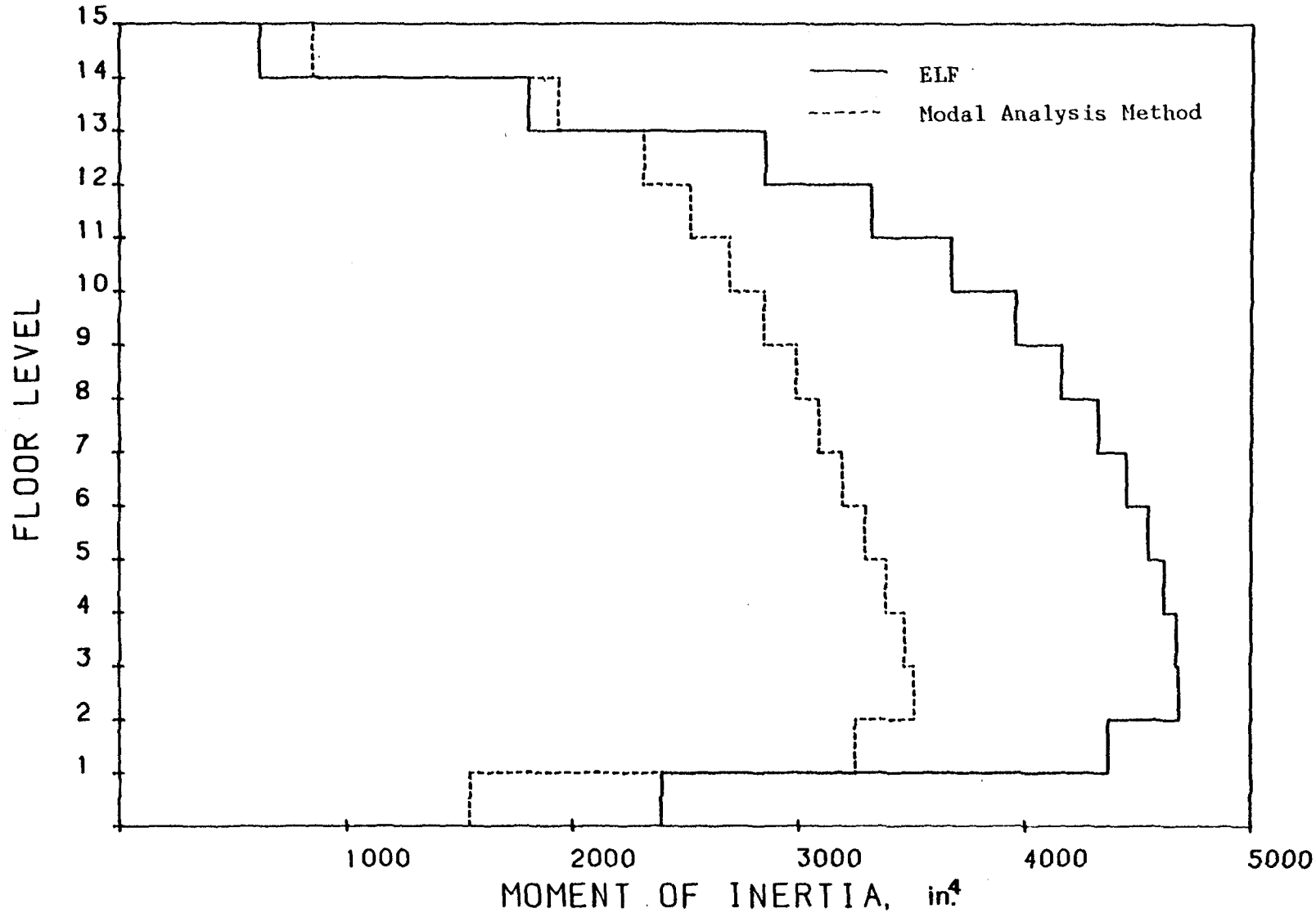

Figure 36. Moments of Inertia of the Girders of the 15-Story, One-Bay, Unbraced Frame for the Comparison of the ATC-3-06 ELF and Modal Analysis Methods. (1 in. = 2.54 cm)

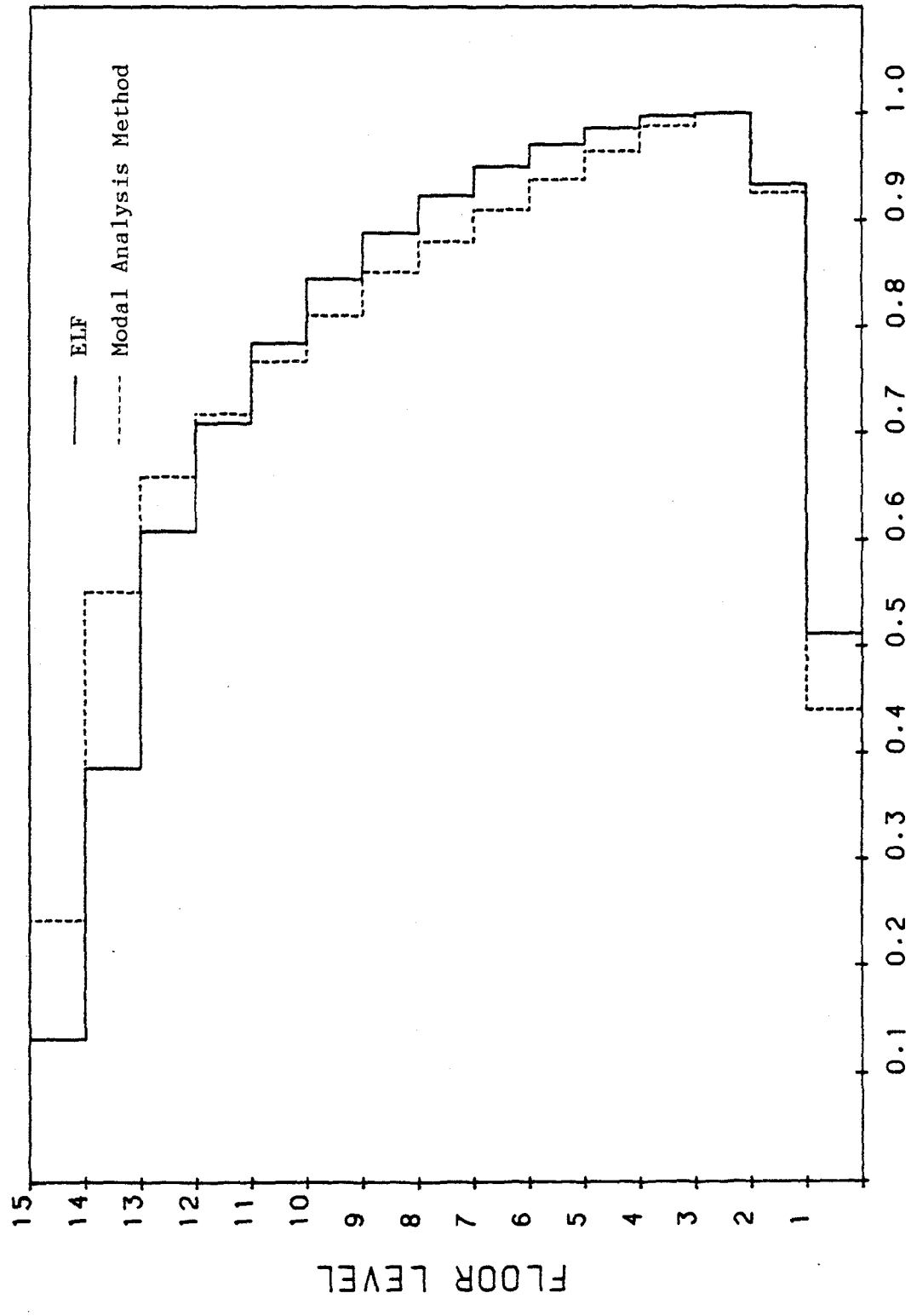

Figure 37. Normalized Moments of Inertia of the Girders of the 15-Story, One-Bay, Unbraced Frame for the Comparison of the ATC-3-06 ELF and Modal Analysis Methods.

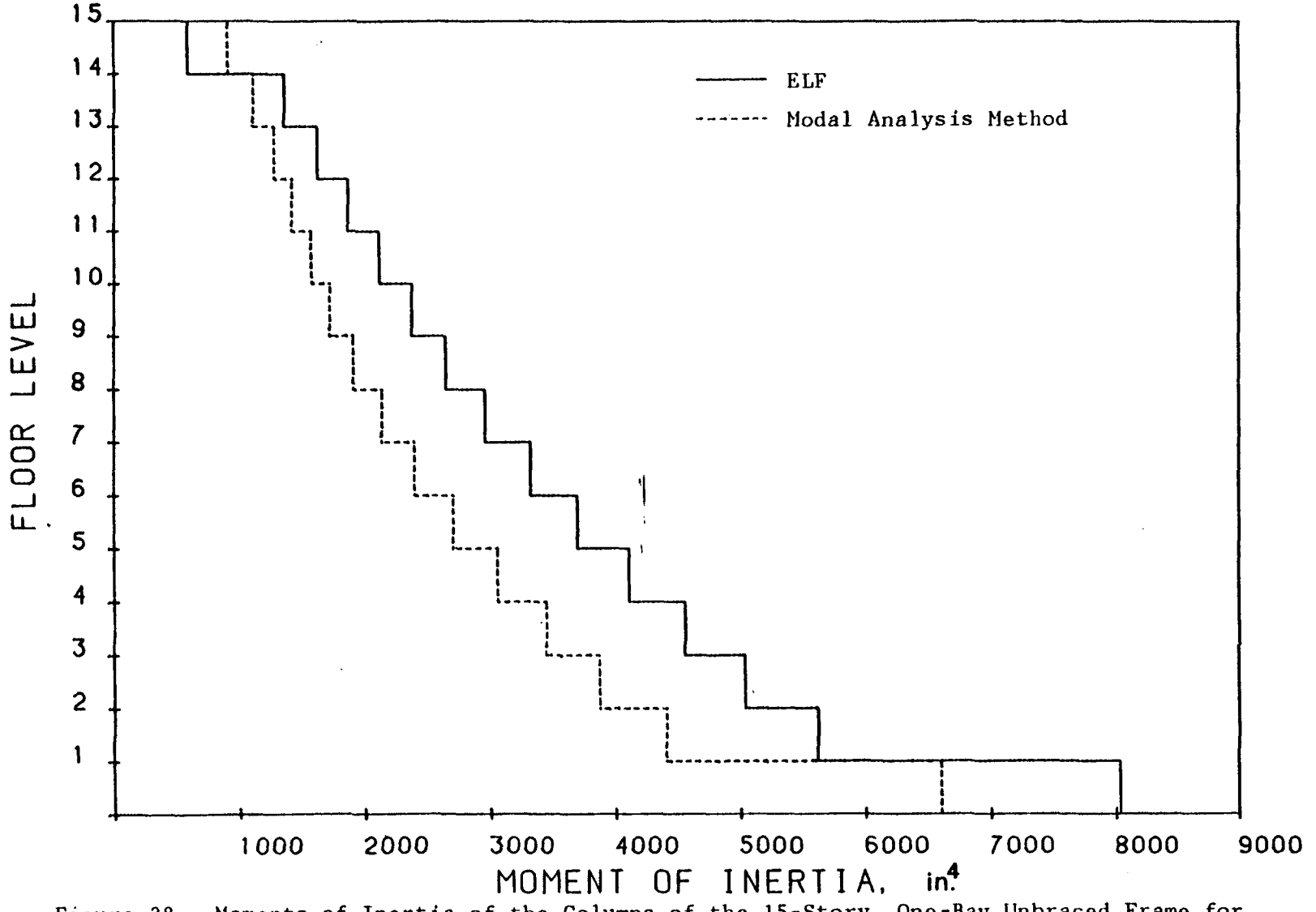

Figure 38. Moments of Inertia of the Columns of the 15-Story, One-Bay, Unbraced Frame for the Comparison of the ATC-3-06 ELF and Modal Analysis Methods. (1 in. = 2.54 cm)

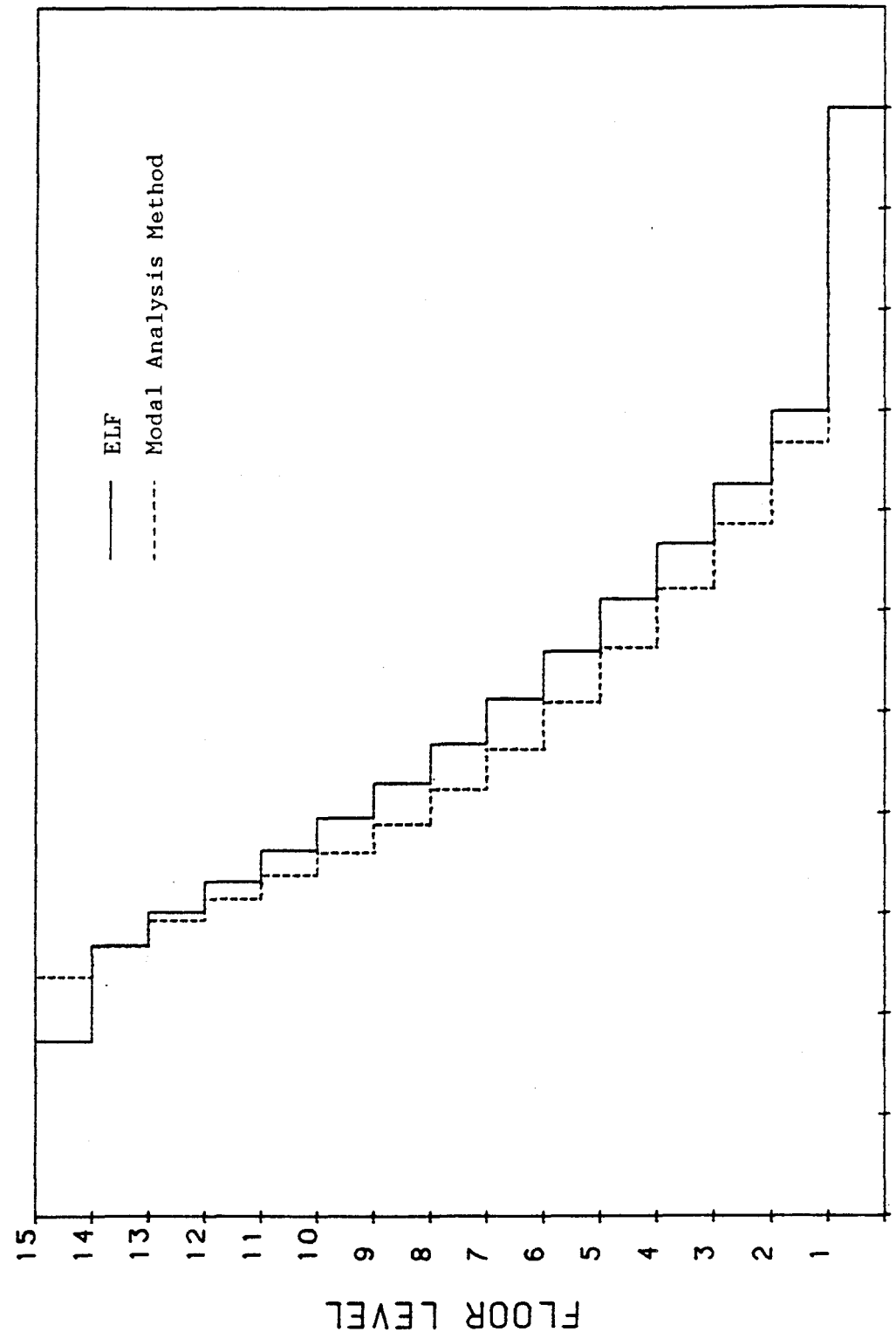

Figure 39. Normalized Moments of Inertia of the Columns of the 15-Story, One-Bay, Unbraced Frame for the Comparison of the ATC-3-06 ELF and Modal Analysis Methods.

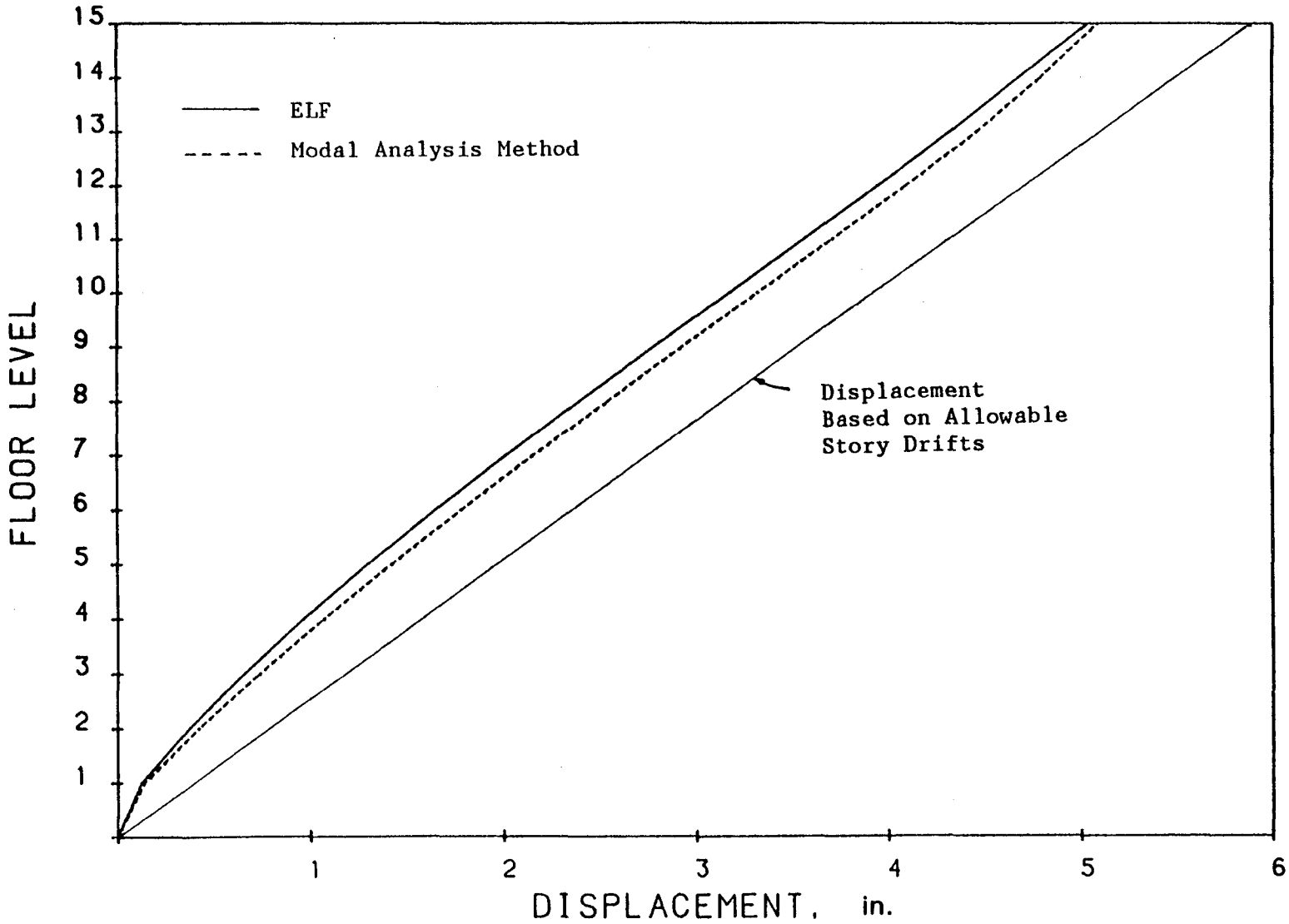

Figure 40. Displacements of the 15-Story, One-Bay, Unbraced Frame for the Comparison of the ATC-3-06 ELF and Modal Analysis Methods. (1 in. = 2.54 cm)

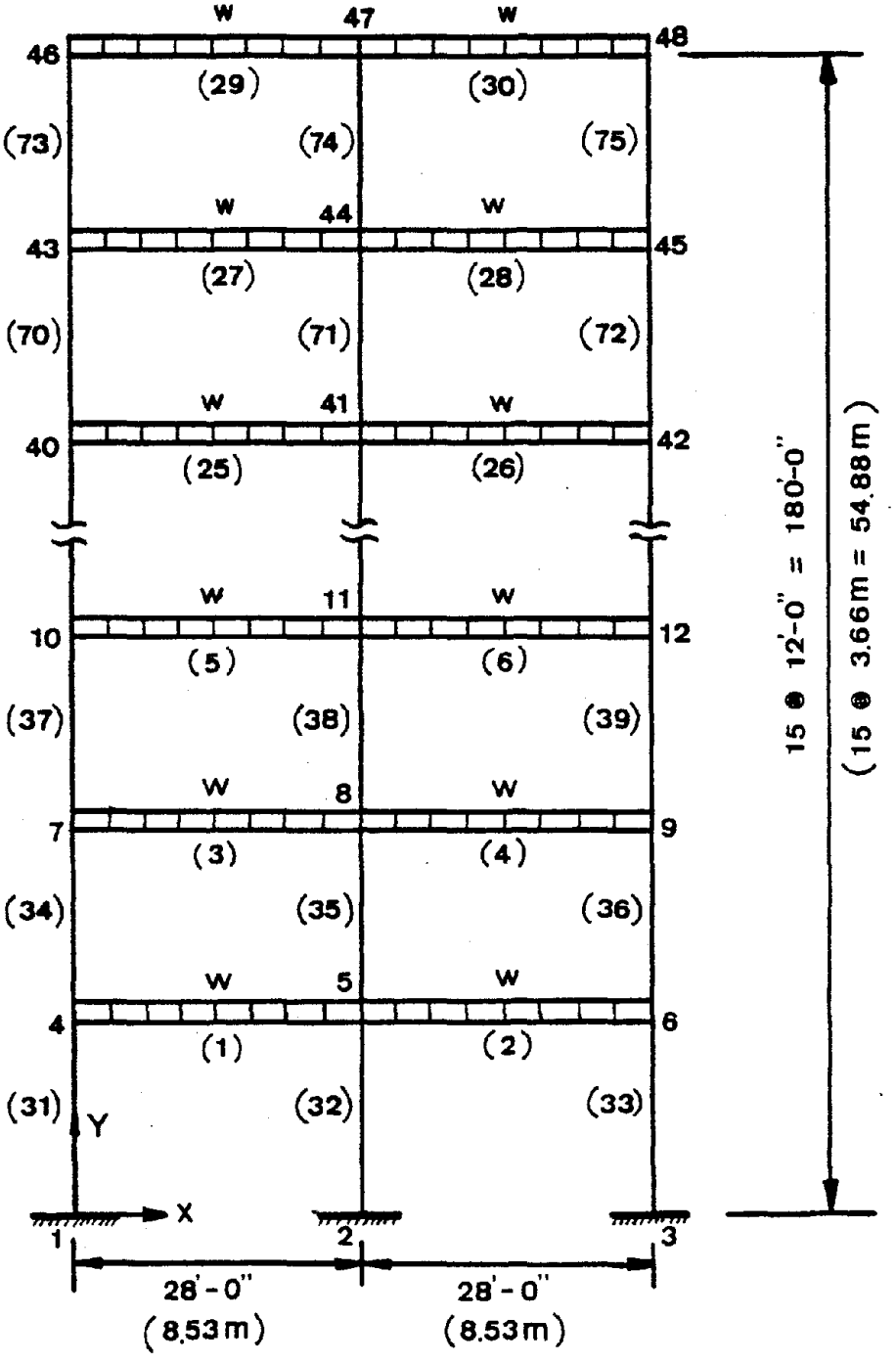

Figure 41. 15-Story, Two-Bay, Unbraced Frame for the Comparison of Various Earthquake Code Provisions, Minimum Weight and Minimum Cost, and Wind Designs.

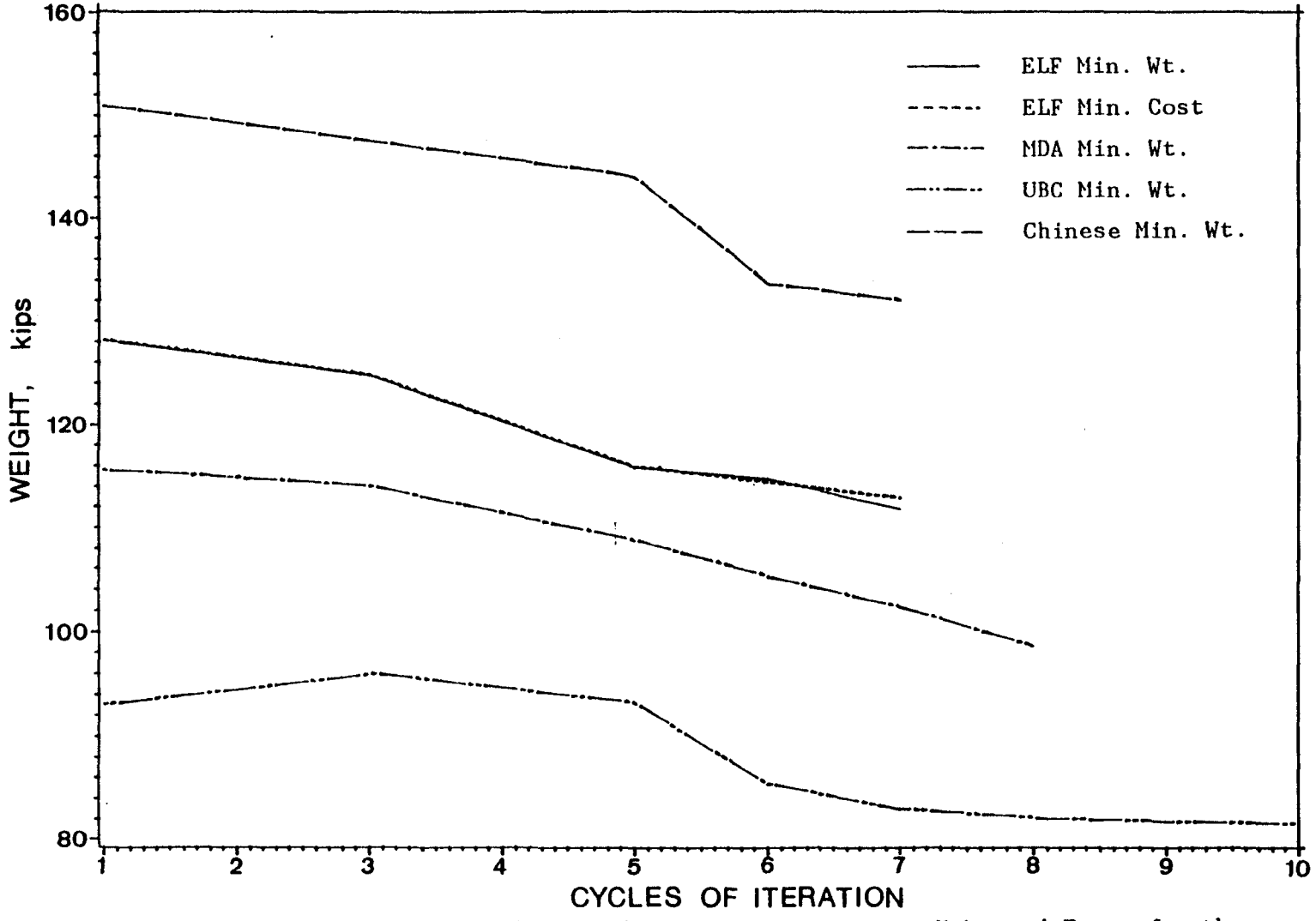

Figure 42. Weight v.s. Cycles of Iteration Plot of the 15-Story, Two-Bay, Unbraced Frame for the Comparison of Various Code Provisions, Min. Weight, and Min. Cost Designs. (1 kip = 4.448 kN).

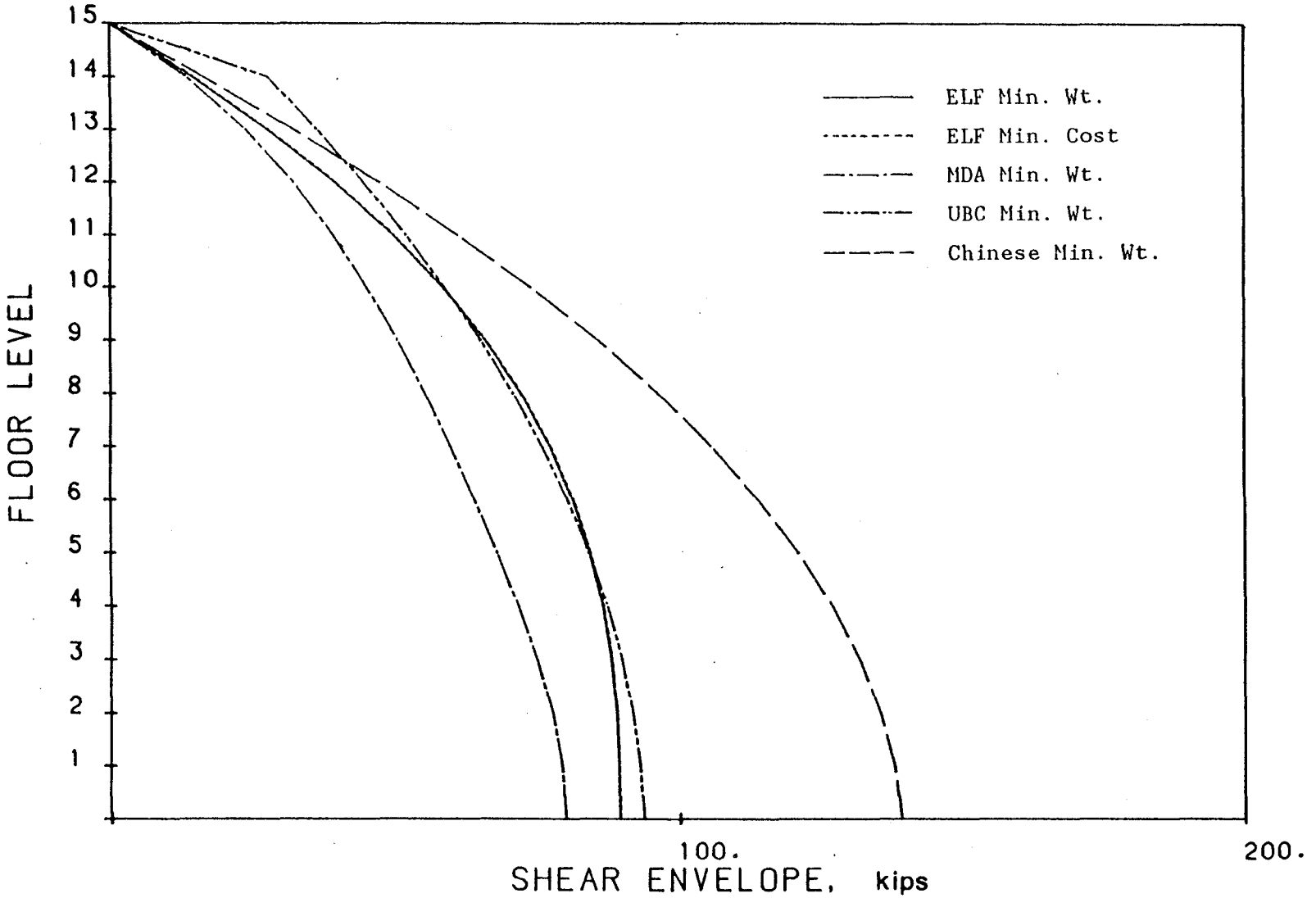

Figure 43. Shear Envelopes of the 15-Story, Two-Bay, Unbraced Frame for the Comparison of Various Code Provisions, Min. Weight, and Min. Cost Designs. (1 kip = 4.448 kN).

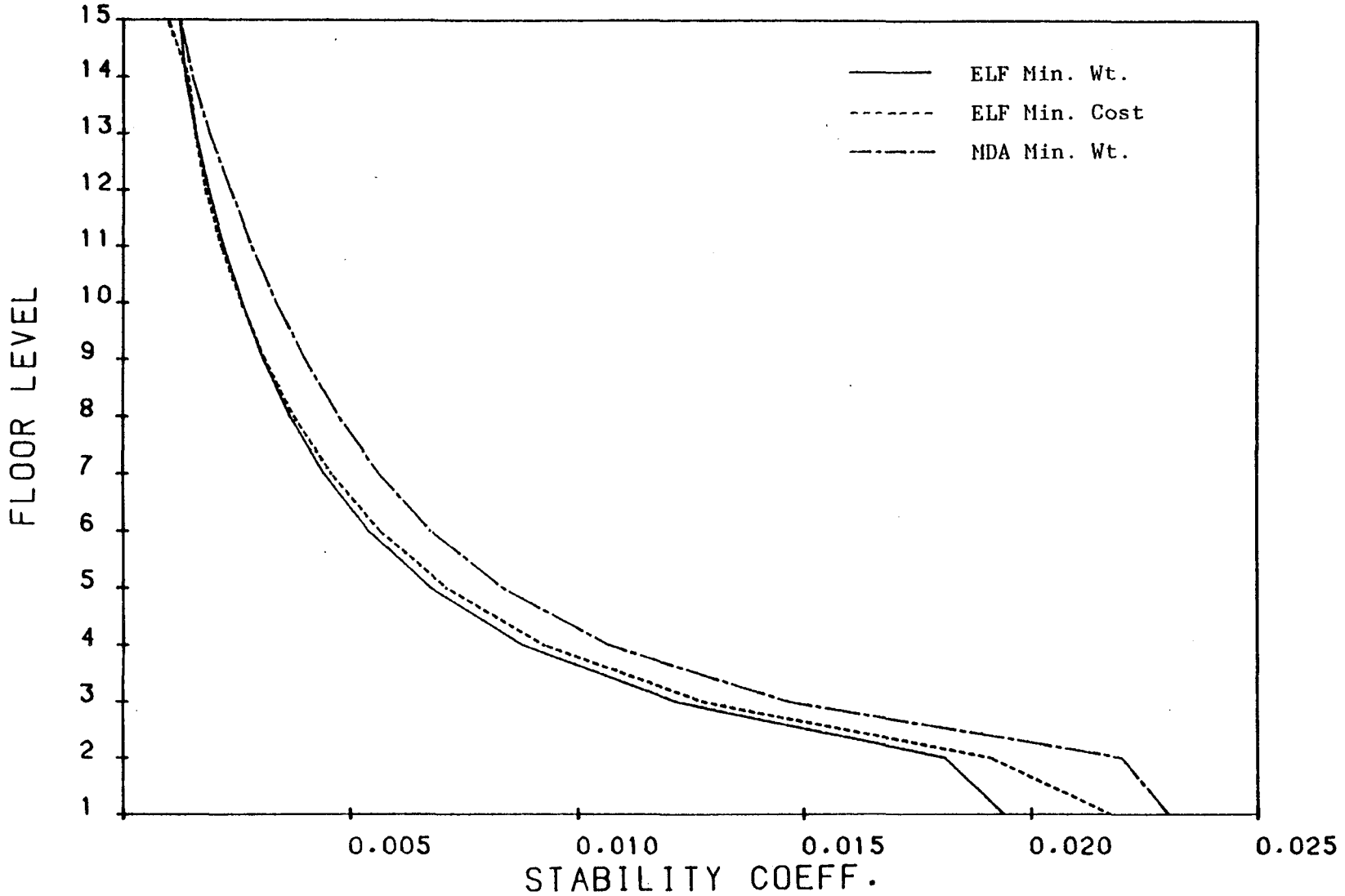

Figure 44. Stability Coefficients of the 15-Story, Two-Bay, Unbraced Frame for the Comparison of Various Code Provisions, Min. Weight, and Min. Cost Designs.

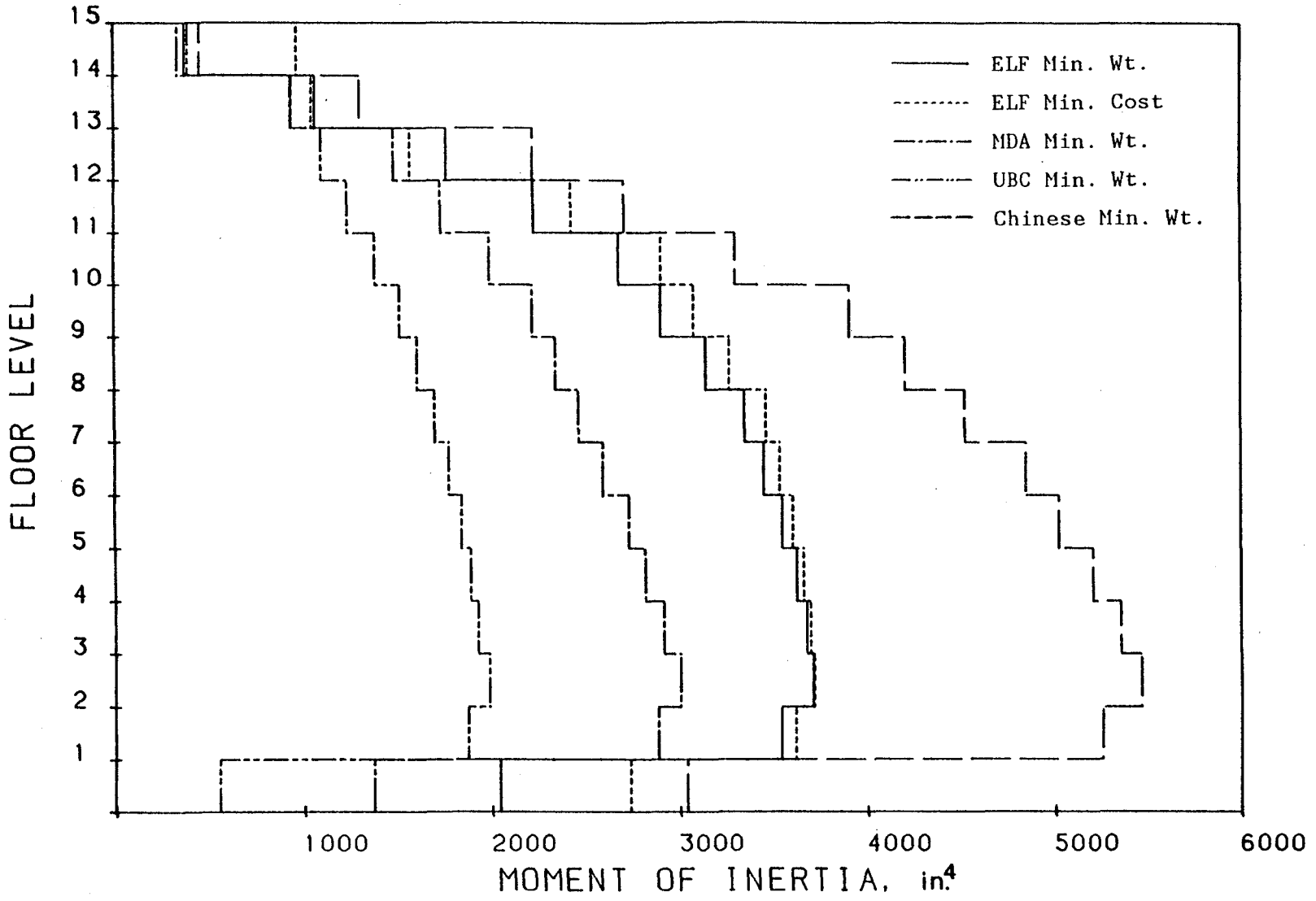

Figure 45. Moments of Inertia of the Girders of the 15-Story, Two-Bay, Unbraced Frame for the Comparison of Various Code Provisions, Min. Weight, and Min. Cost Designs. (1 in. = 2.54 cm).

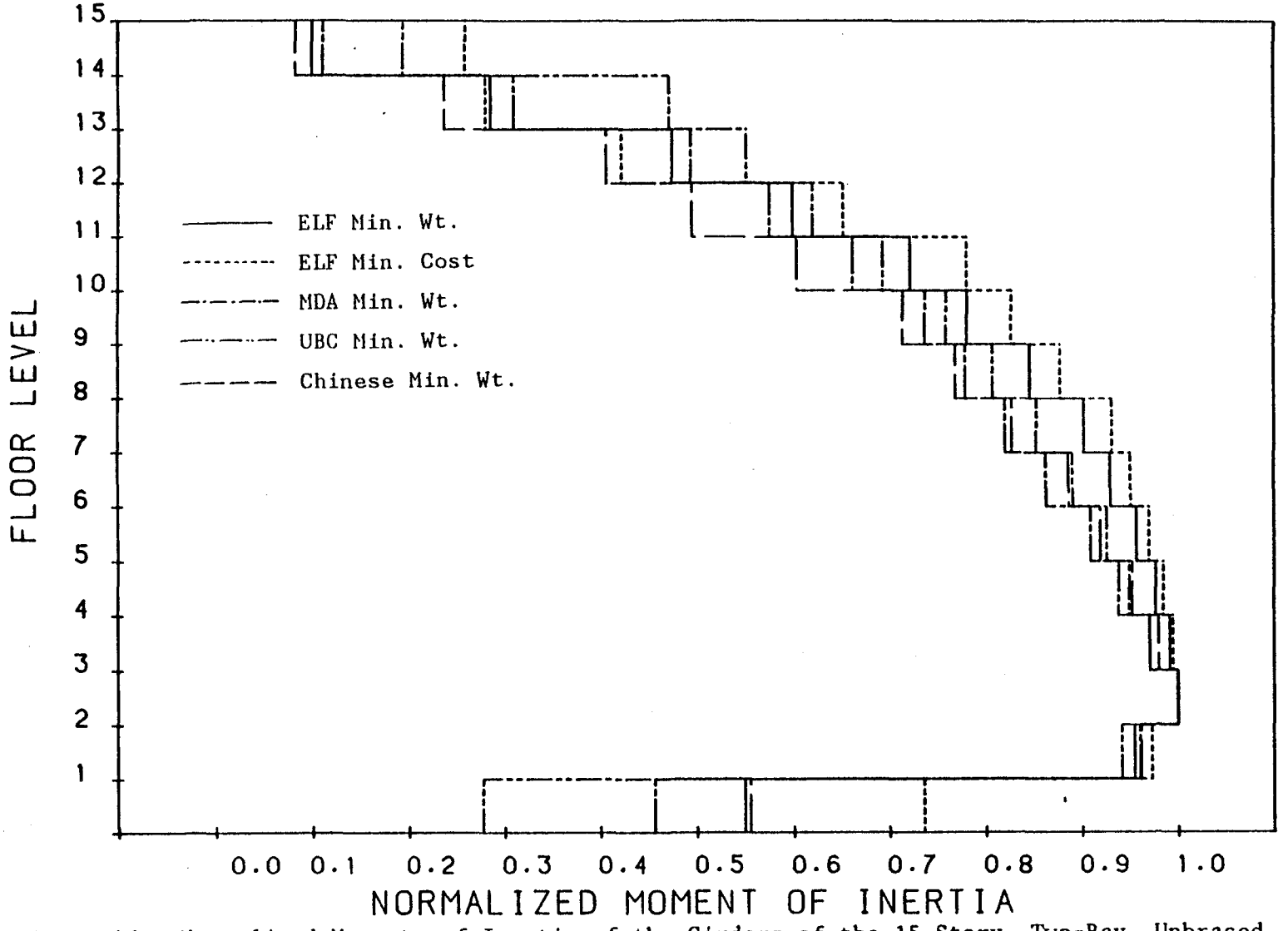

Figure 46. Normalized Moments of Inertia of the Girders of the 15-Story, Two-Bay, Unbraced Frame for the Comparison of Various Code Provisions, Min. Weight, and Min. Cost Designs.

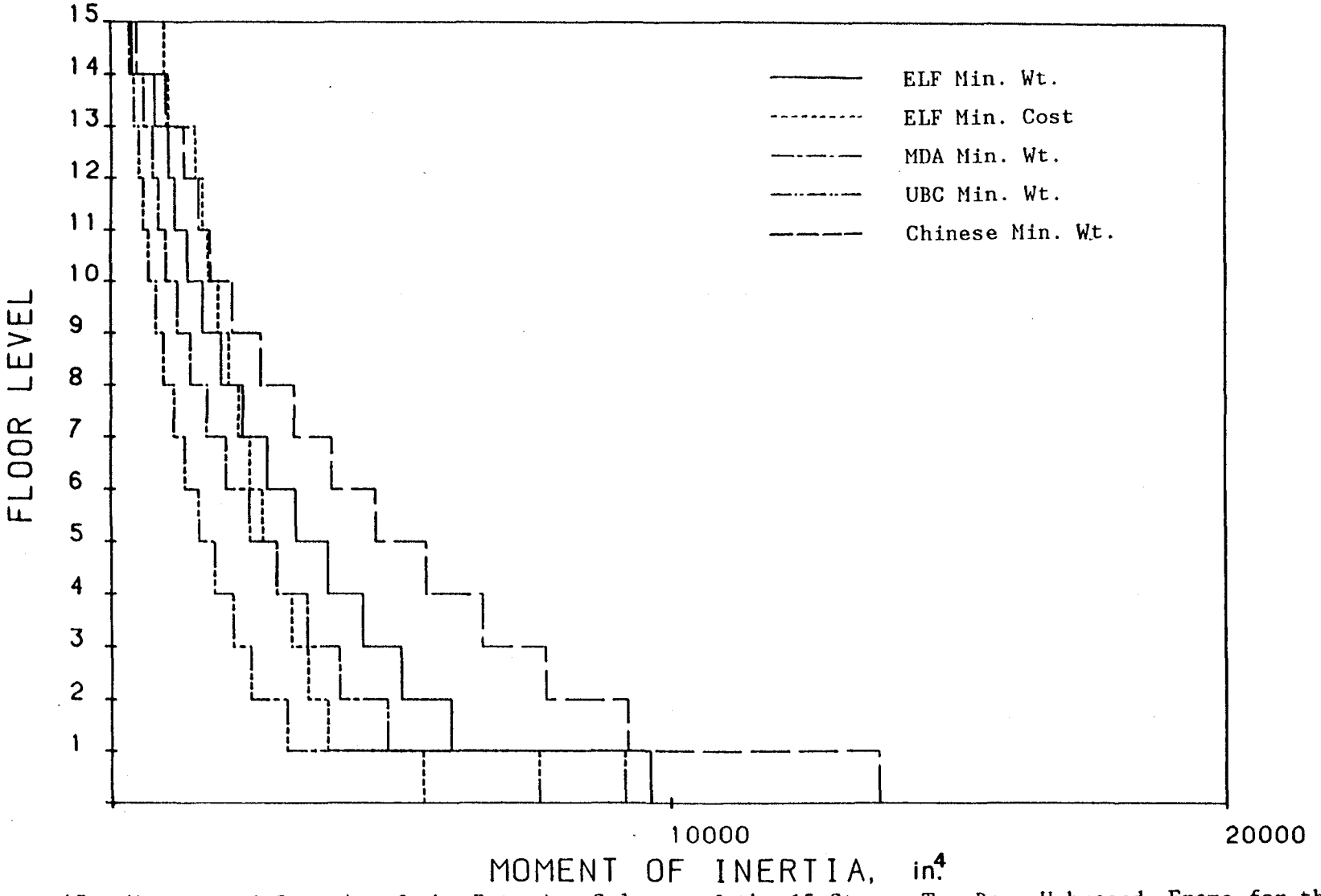

Figure 47. Moments of Inertia of the Exterior Columns of the 15-Story, Two-Bay, Unbraced, Frame for the Comparison of Various Code Provisions, Min. Weight, and Min. Cost Designs. (1 in. = 2.54 cm).

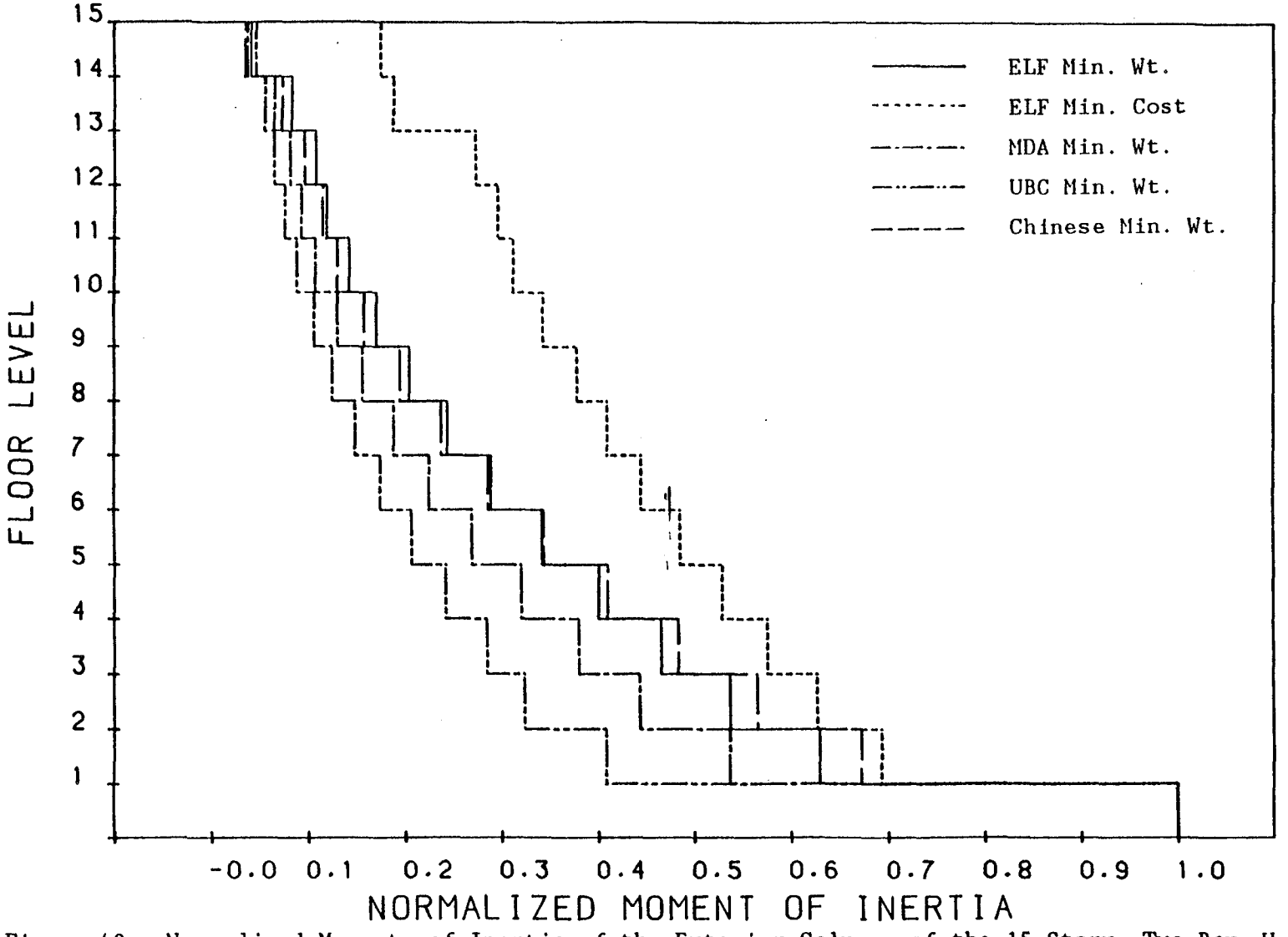

Figure 48. Normalized Moments of Inertia of the Exterior Columns of the 15-Story, Two-Bay, Unbraced Frame for the Comparison of Various Code Provisions, Min. Weight, and Min. Cost Designs.

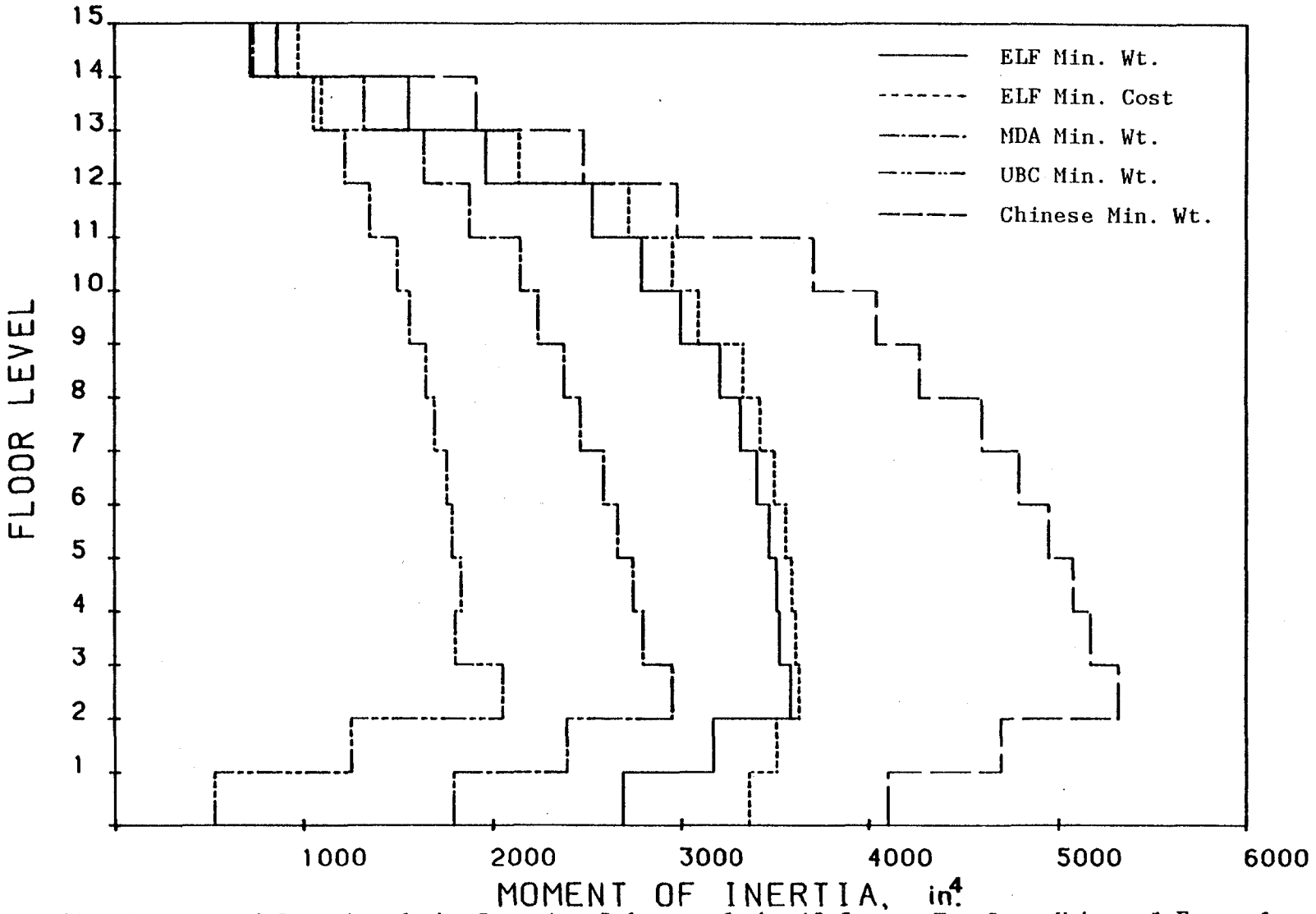

Figure 49. Moments of Inertia of the Interior Columns of the 15-Story, Two-Bay, Unbraced Frame for the Comparison of Various Code Provisions, Min. Weight, and Min. Cost Designs. (1 in. = 2.54 cm).

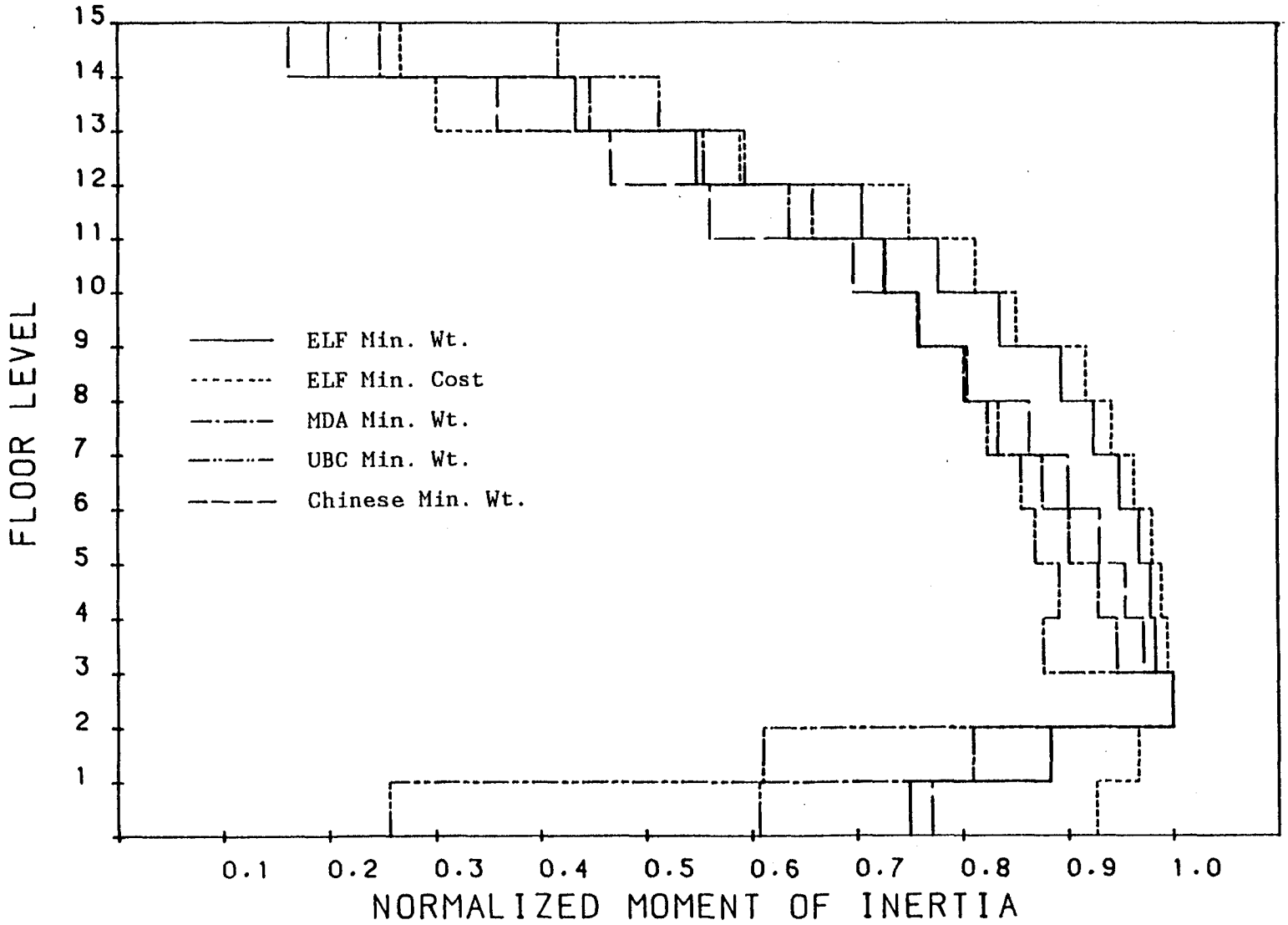

Figure 50. Normalized Moments of Inertia of the Interior Columns of the 15-Story, Two-Bay, Unbraced Frame for the Comparison of Various Code Provisions, Min. Weight, and Min. Cost Designs.

however, decreases from the third floor to the second floor and then to the first floor. The decrement from the second floor to the first floor is almost equal to the decrement from the third floor to the second floor. By comparing the moments of inertia of the members of the two cases, one finds that the moments of inertia in Case (b) are smaller than those for corresponding members in Case (a).

The displacements of the different floor levels are illustrated in Figure 51. The story drift is violated at the 10th story for Case (a) and at the 9th story for Case (b). As in the case of the one-bay frame, the lateral displacements are much smaller than the allowable displacements.

The fundamental period of Case (a) is 2.134 sec, which is greater than the upper bound, $1.2T_a$=2.064 sec, therefore the design is controlled by the upper bound. The eccentricity of Case (a) is 5.664 ft (1.726 m).

3. Fifteen-story, Two-bay, Setback Structure. The setback structure of Figure 52 was selected because, as mentioned in ATC-3-06, the equivalent lateral force method may not be adequate for the design of a structure with an irregular vertical configuration. Consequently, the modal analysis method needs to be considered. This structure was designed separately according to each design procedure for the purpose of comparison.

There are two bays for the bottom eight stories and one bay for the balance. The nonstructural weight is 50,000 lbs (222.4 kN) for each of the top seven stories and 100,000 lbs (444.8 kN) for each of the bottom eight stories. According to the final design, the

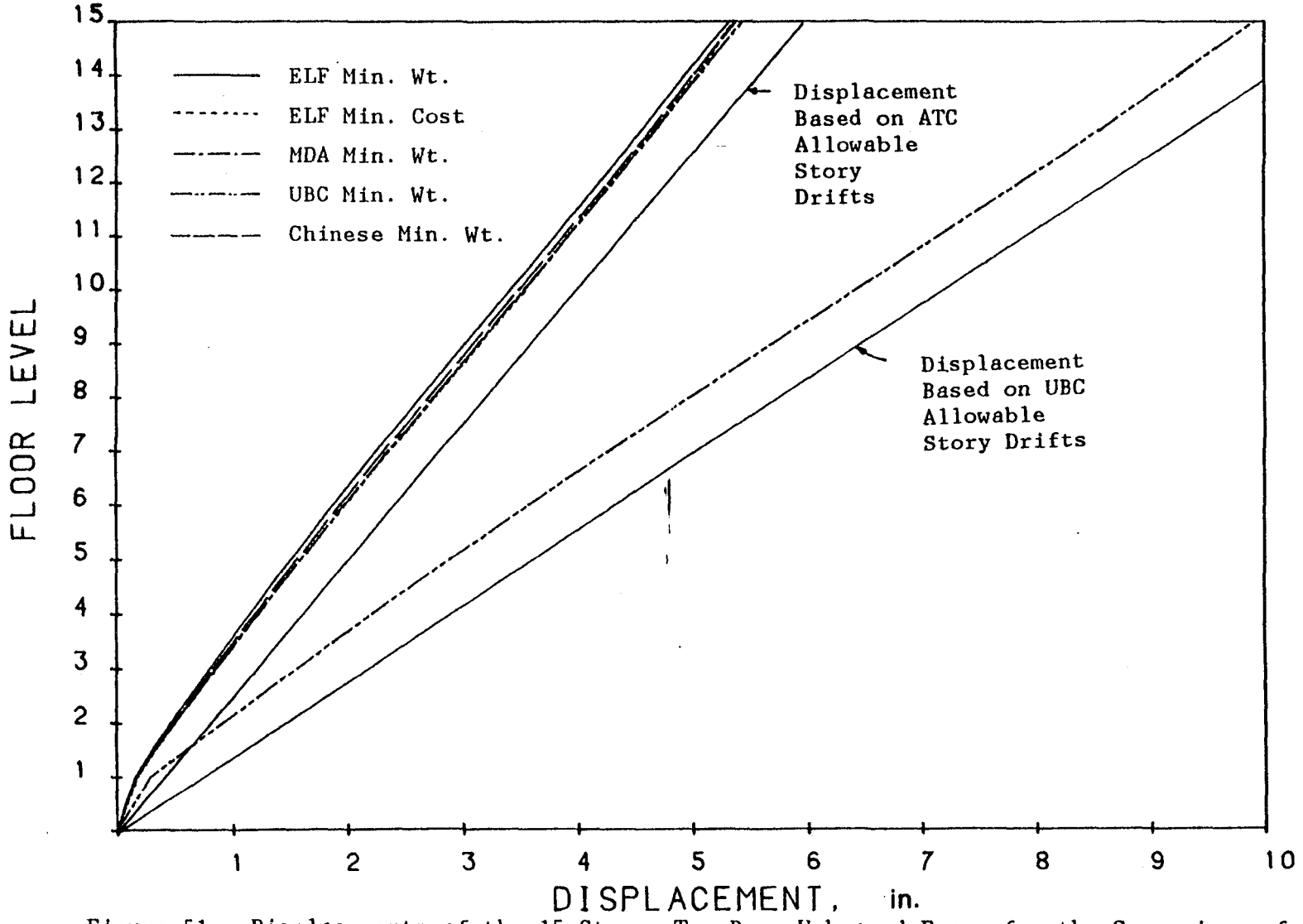

Figure 51. Displacements of the 15-Story, Two-Bay, Unbraced Frame for the Comparison of Various Code Provisions, Min. Weight, and Min. Cost Designs. (1 in. = 2.54 cm).

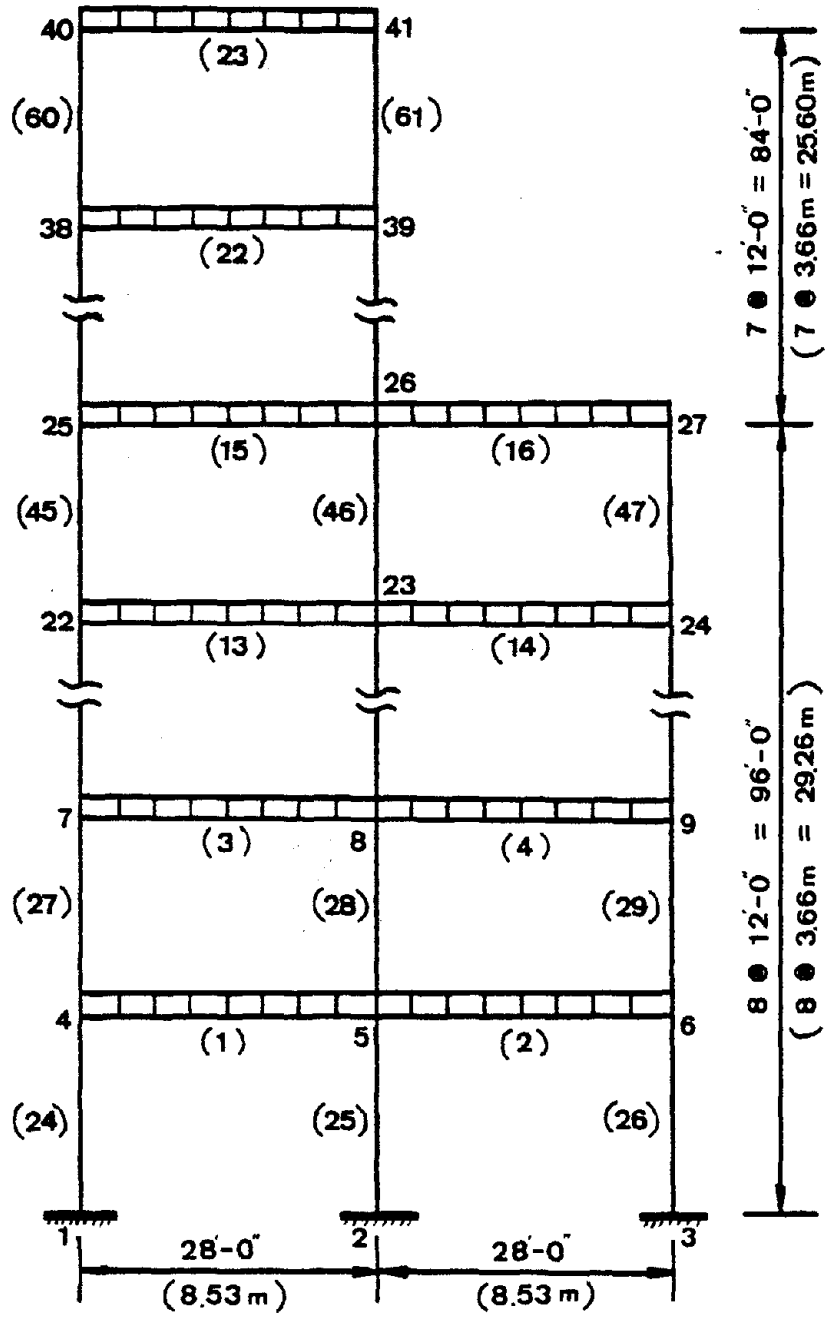

Figure 52. 15-Story, Two-Bay, Setback Structure for the Comparison of the ATC-3-06 ELF and Modal Analysis Methods.

eccentricity of Case (a) is 5.741 feet (1.750 m). The fundamental natural period is 1.754 sec, which is less than the upper bound, therefore it controls the design.

In Figure 53, the plot of the weight versus cycles of iteration is given. The optimum weight of Case (a) is 97.514 kips (433.74 kN) and 78.325 kips (348.39 kN) for Case (b). The maximum values of the stability coefficients shown in Figure 54 are 0.0171 for Case (a) and 0.0233 for Case (b). The shear envelopes shown in Figure 55 are not as smooth as those of previous examples. The envelopes decrease abruptly at the ninth story because of an approximate 50 percent reduction in story weight at the top of the seventh storey. Because of the irregular distribution of the seismic design forces, the moments of inertia of the members are not distributed as they are in structures having a regular vertical configuration. Figures 56 and 57 illustrate the distribution of moments of inertia and normalized moments of inertia of the girders. The moment of inertia at the ninth floor increases suddenly because of the reduction in number of columns at that story. A similar phenomenon is shown in Figures 58 through 61 for the distribution of the moments of inertia and normalized moments of inertia of the exterior and interior columns respectively. By comparing the curves in Figures 56 through 61, one finds that larger member sizes are required for Case (a) than for Case (b); the stiffness distributions are similar for both cases.

The lateral displacements are represented in Figure 62 which shows that in both cases there is an active story drift at the 12th story.

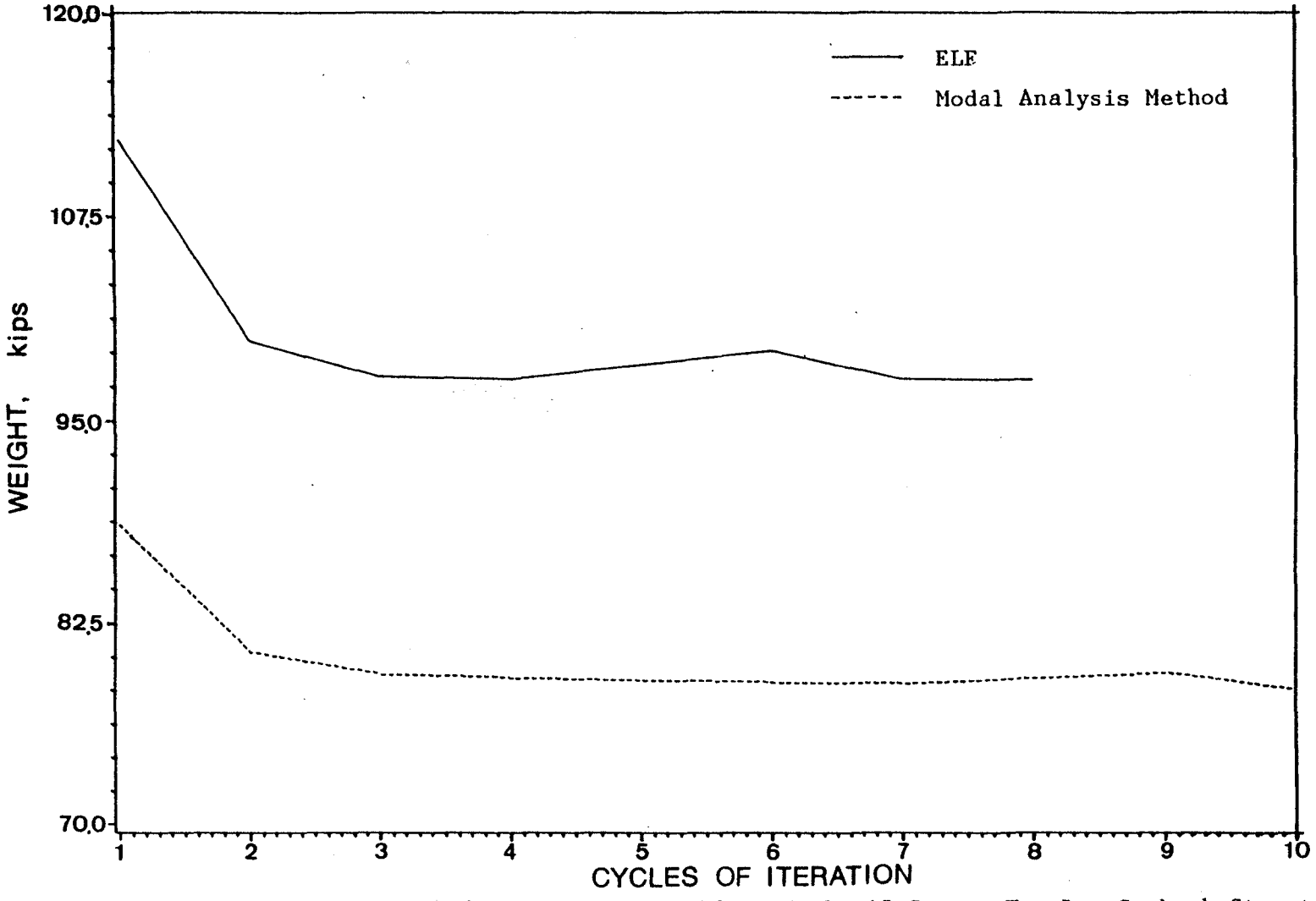

Figure 53. Weight v.s. Cycles of Iteration Plot of the 15-Story, Two-Bay, Setback Structure for the Comparison of the ATC-3-06 ELF and Modal Analysis Methods. (1 kip = 4.448 kN)

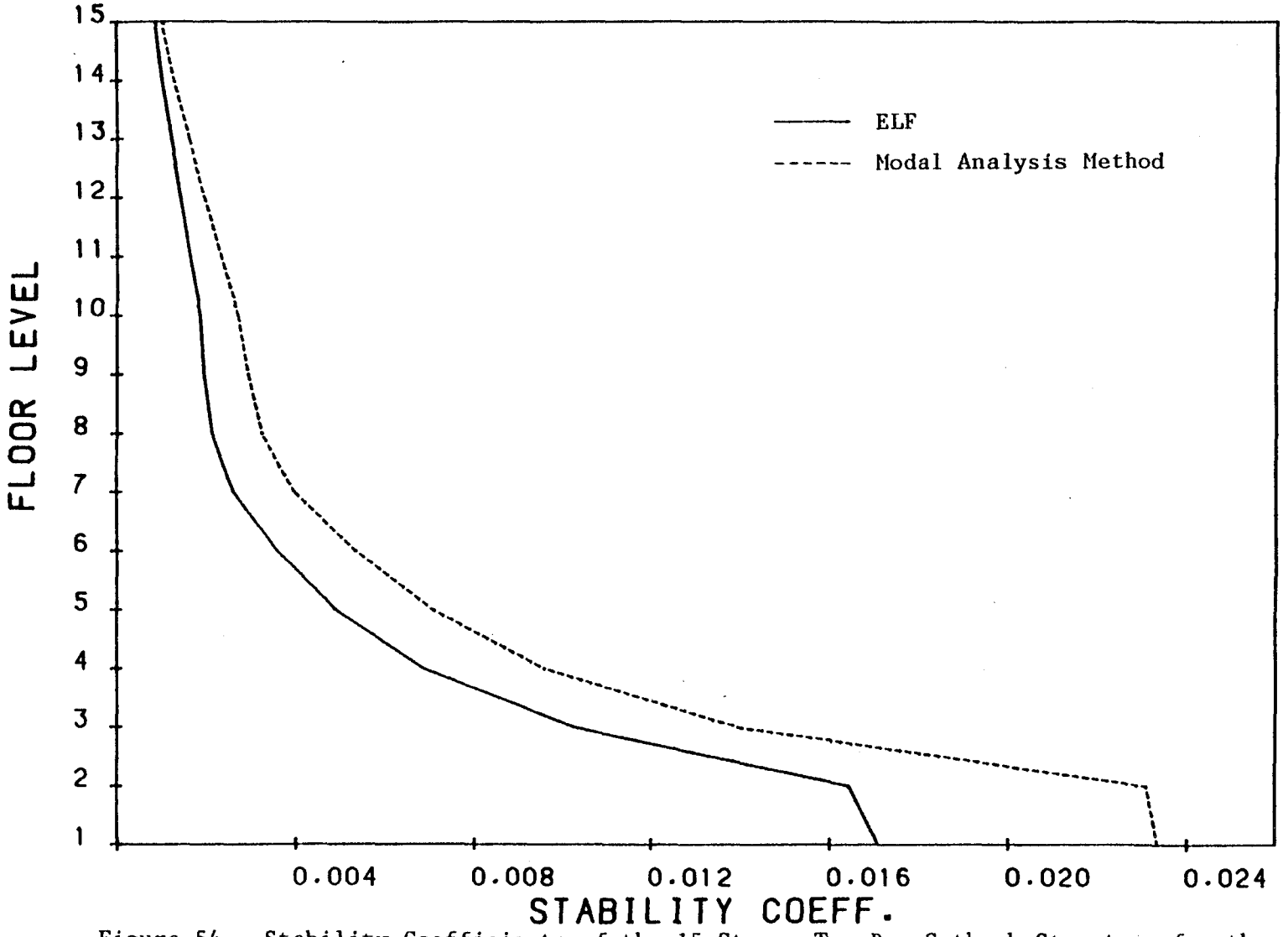

Figure 54. Stability Coefficients of the 15-Story, Two-Bay, Setback Structure for the Comparison of the ATC-3-06 ELF and Modal Analysis Methods.

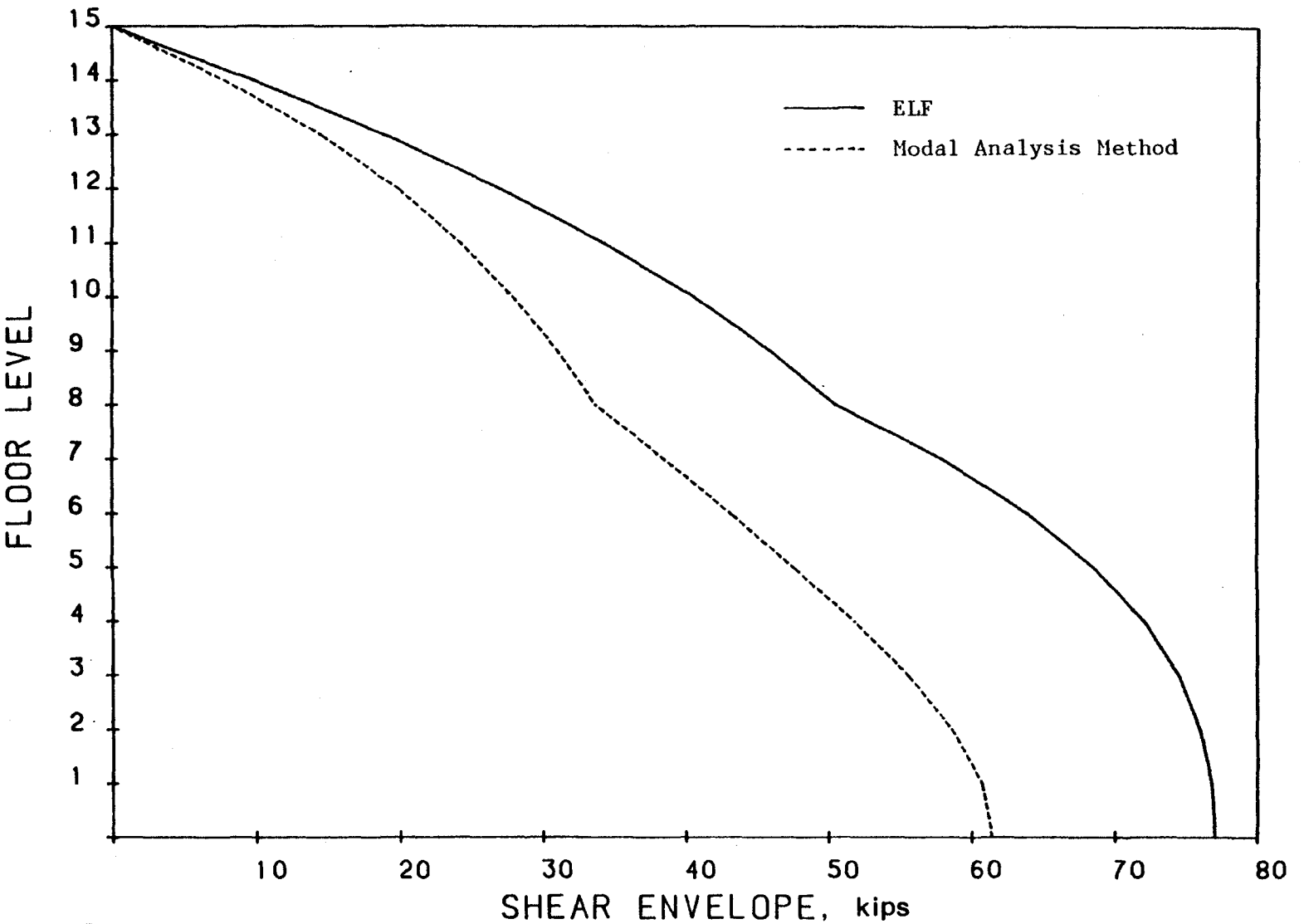

Figure 55. Shear Envelopes of the 15-Story, Two-Bay, Setback Structure for the Comparison of the ATC-3-06 ELF and Modal Analysis Methods. (1 kip = 4.448 kN).

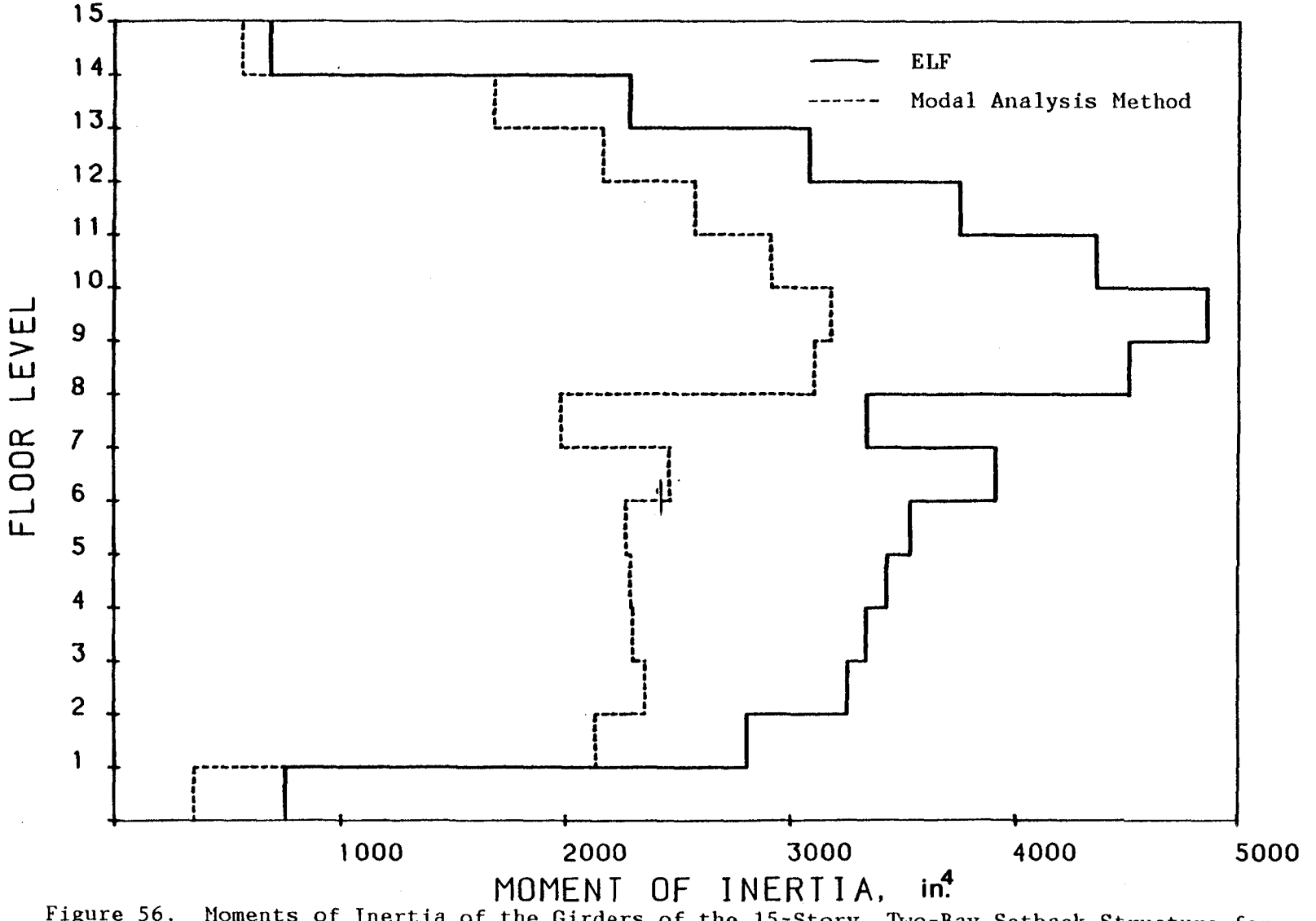

Figure 56. Moments of Inertia of the Girders of the 15-Story, Two-Bay, Setback Structure for the Comparison of the ATC-3-06 ELF and Modal Analysis Methods. (1 in. = 2.54 cm)

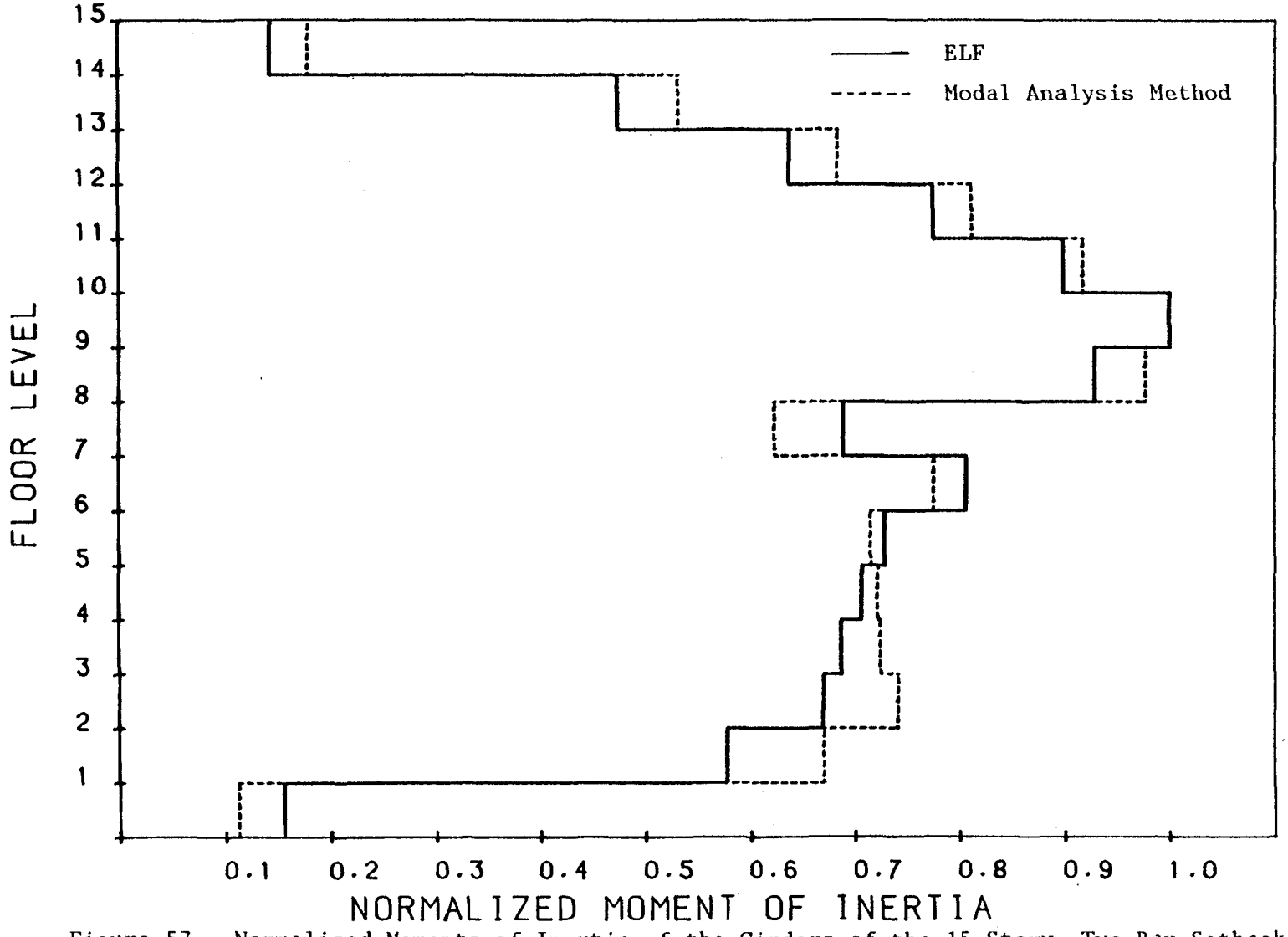

Figure 57. Normalized Moments of Inertia of the Girders of the 15-Story, Two-Bay, Setback Structure for the Comparison of the ATC-3-06 ELF and Modal Analysis Methods.

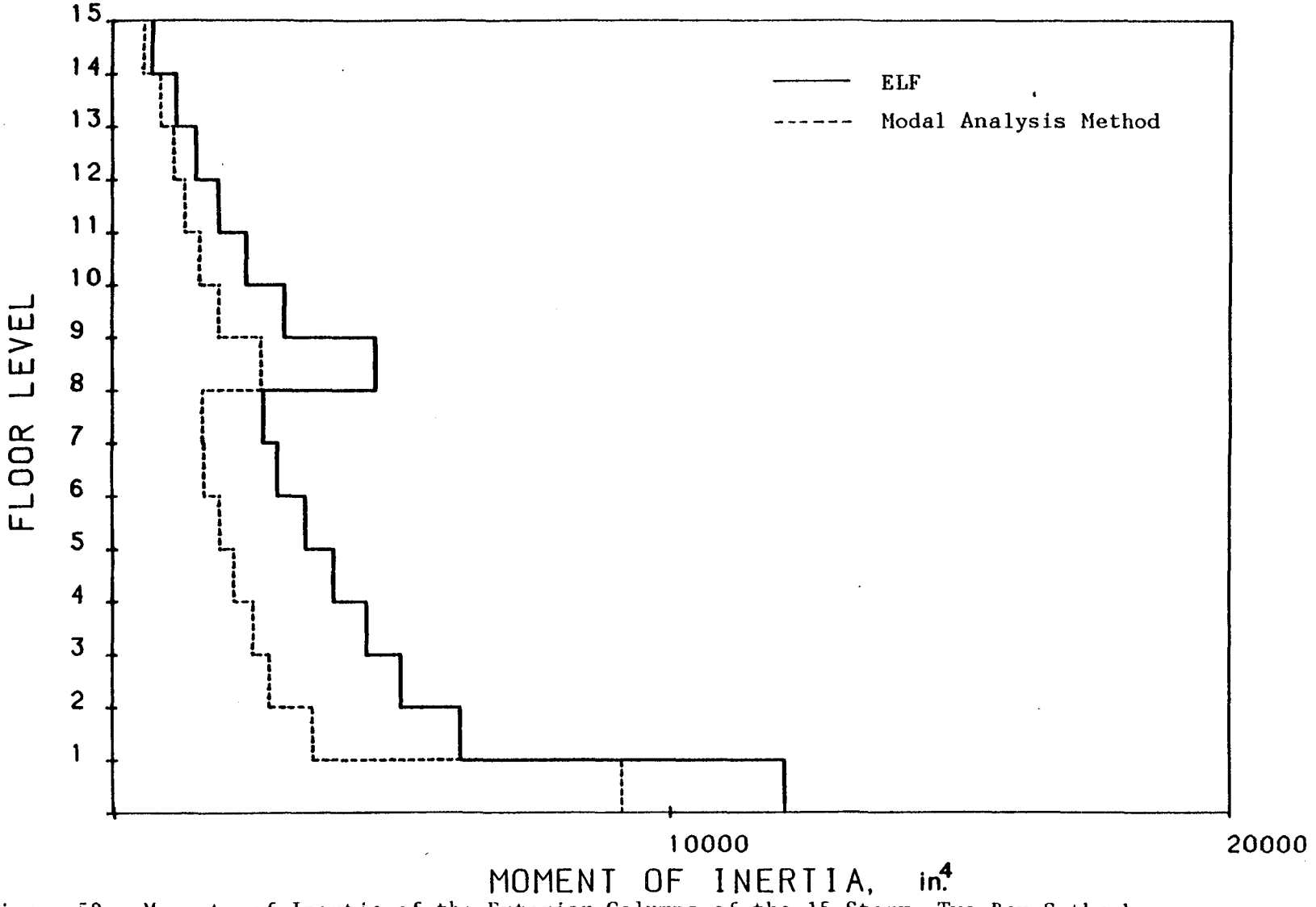

Figure 58. Moments of Inertia of the Exterior Columns of the 15-Story, Two-Bay, Setback Structure for the Comparison of the ATC-3-06 ELF and Modal Analysis Methods. (1 in. = 2.54 cm)

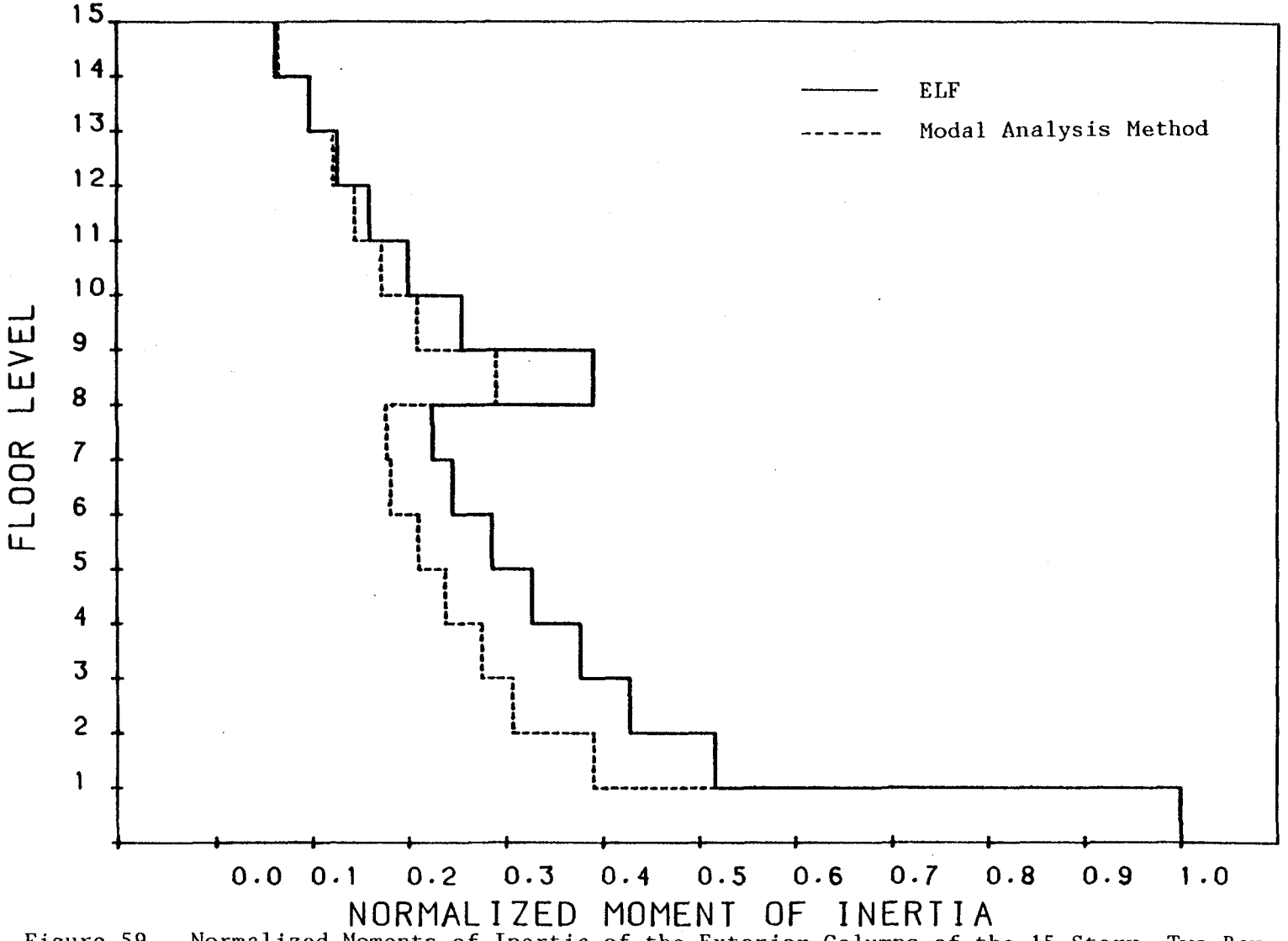

Figure 59. Normalized Moments of Inertia of the Exterior Columns of the 15-Story, Two-Bay, Setback Structure for the Comparison of the ATC-3-06 ELF and Modal Analysis Methods.

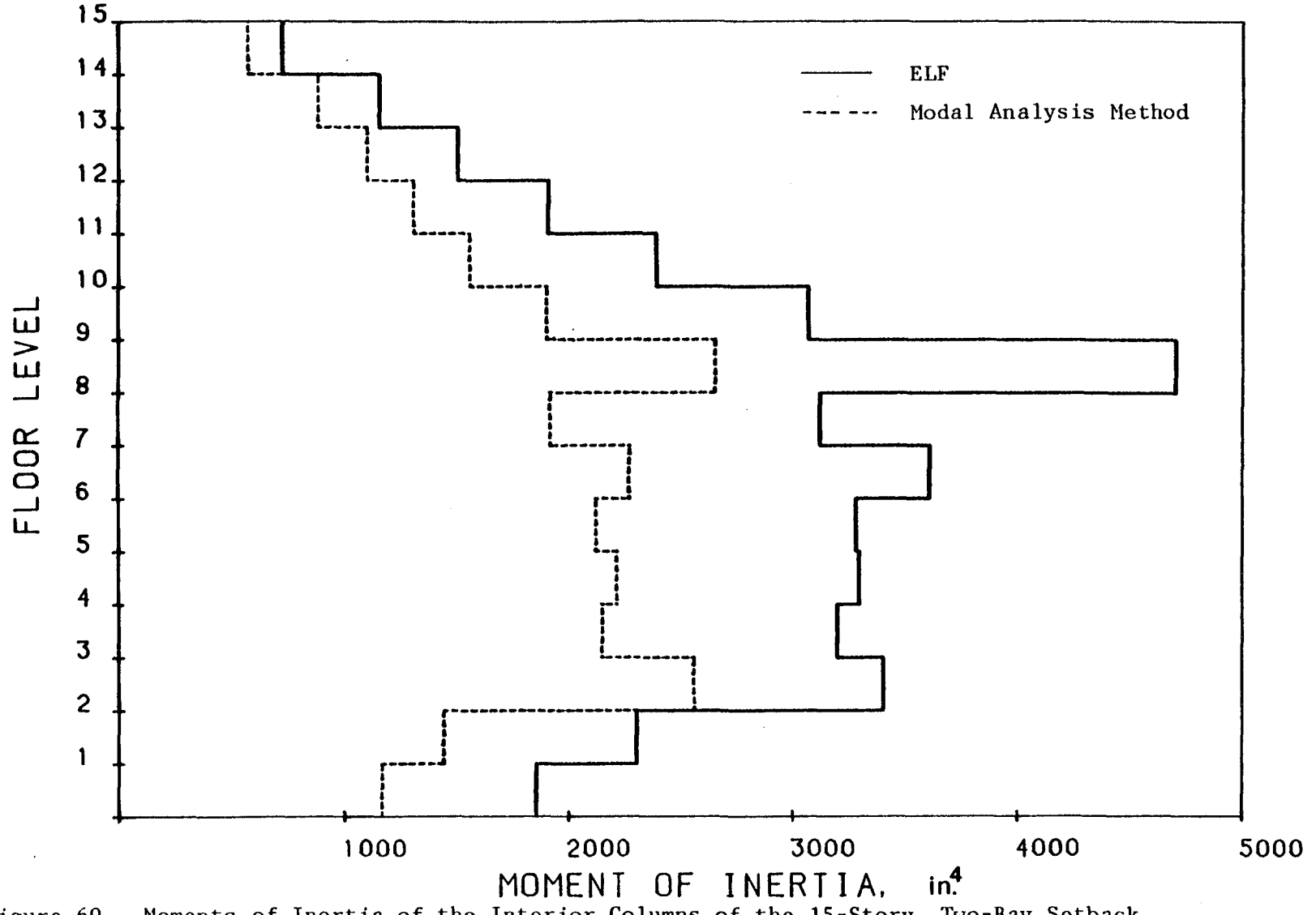

Figure 60. Moments of Inertia of the Interior Columns of the 15-Story, Two-Bay, Setback Structure for the Comparison of the ATC-3-06 ELF and Modal Analysis Methods. (1 in. = 2.54 cm)

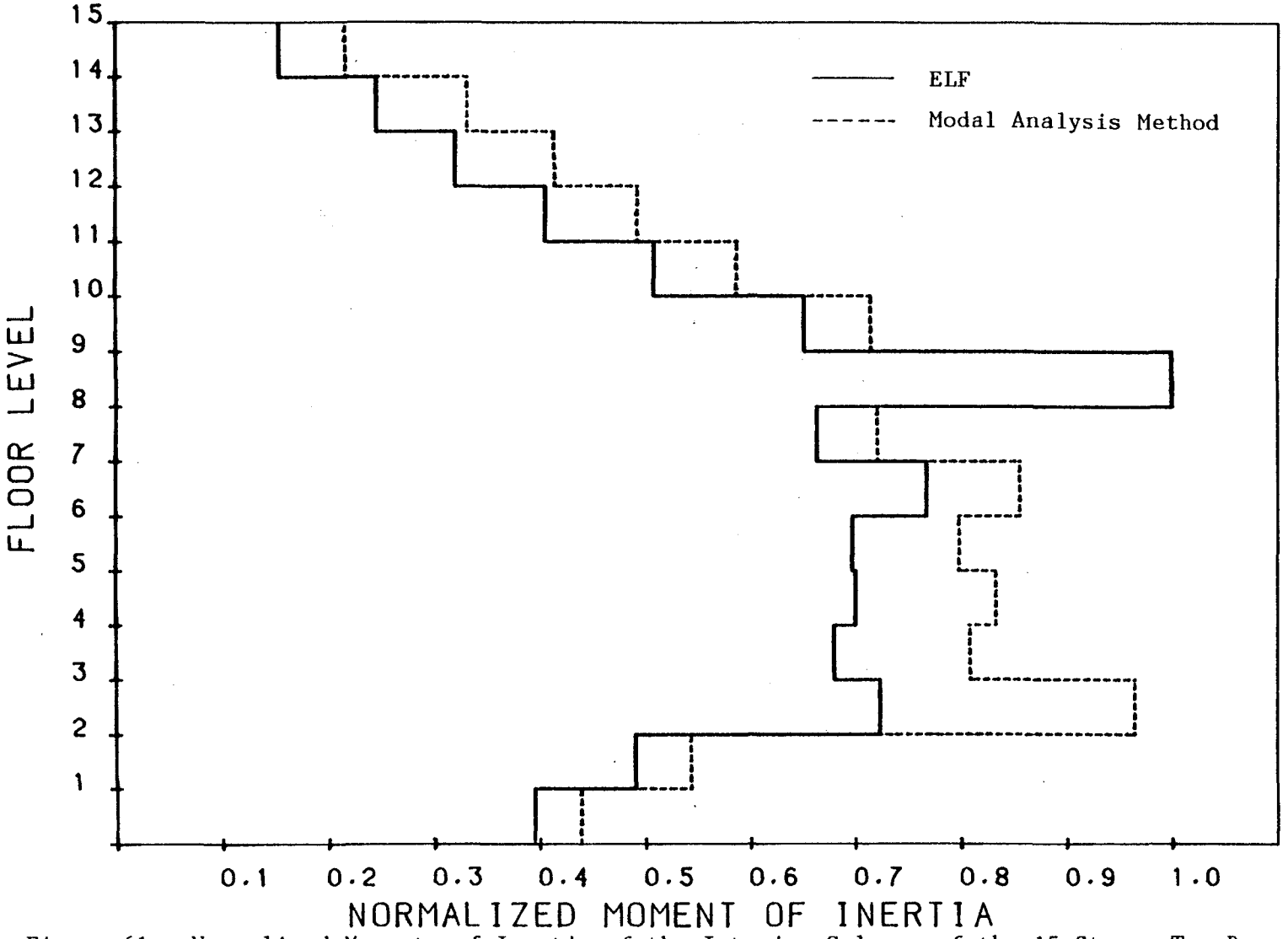

Figure 61. Normalized Moments of Inertia of the Interior Columns of the 15-Story, Two-Bay, Setback Structure for the Comparison of the ATC-3-06 ELF and Modal Analysis Methods.

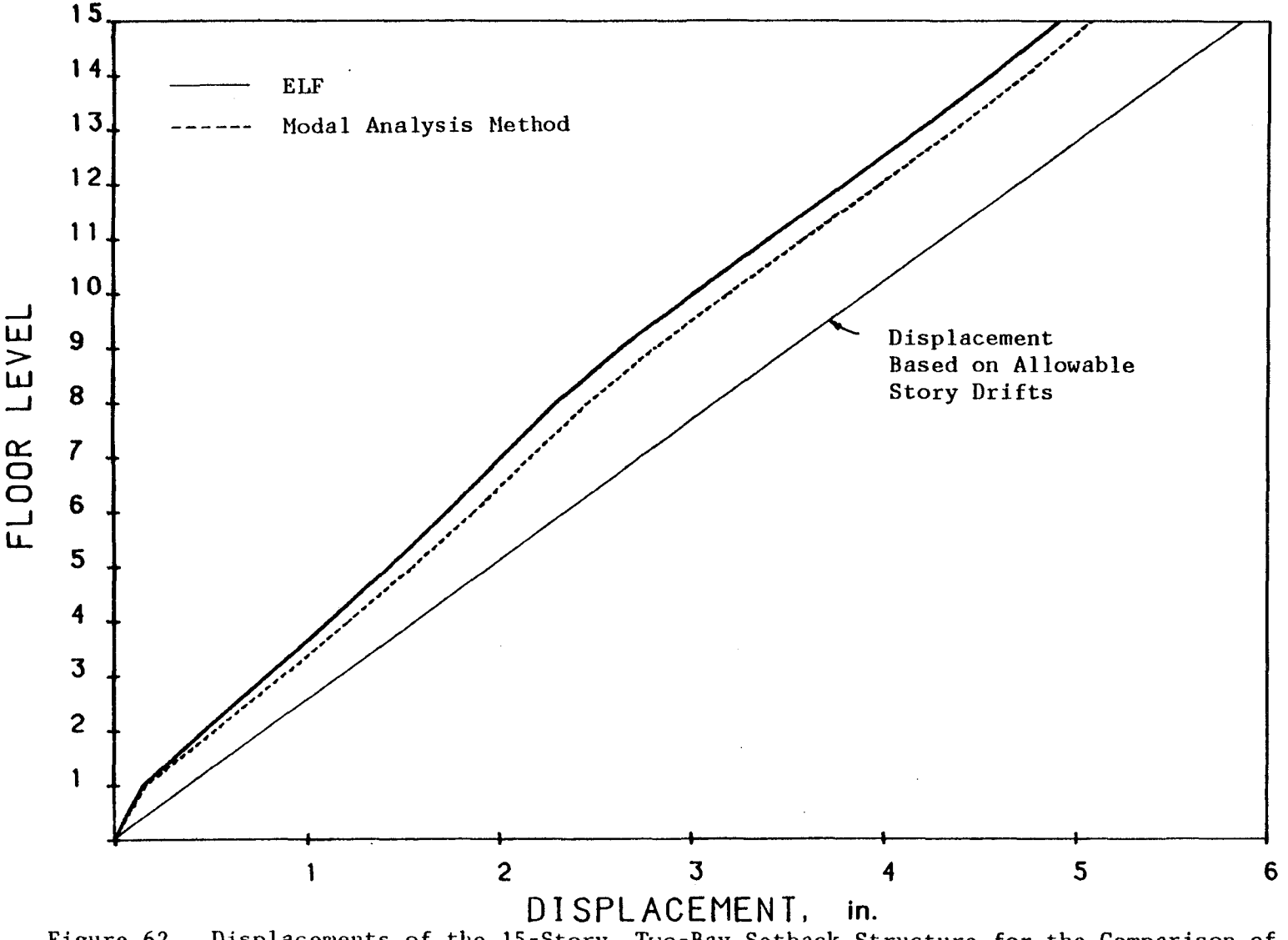

Figure 62. Displacements of the 15-Story, Two-Bay, Setback Structure for the Comparison of the ATC-3-06 ELF and Modal Analysis Methods. (1 in. = 2.54 cm)

The design results, which are summarized in Table XII, include the maximum stability coefficient, the fundamental period, the number of stories having violated drift, the final weight, and the number of design cycles. According to the results of these three design examples, the modal analysis method always provides less seismic design forces than the equivalent lateral force method. Thus, a more conservative design is developed when the design procedures of the latter are used.

D. THE EFFECT OF SOIL-STRUCTURE INTERACTION IN ATC-3-06

The first example for the study of soil-structure interaction is the two-story, seven-bay frame shown in Figure 63. It has a 4 x 4 ft (1.22 x 1.22 m) footing under each column line. The average shear wave velocity of the soil, v_{so}, was assumed to be 550 ft/sec (167.64 m/sec), the average unit weight of the soil, γ, to be 0.112 kips/ft^3 (17.593 kN/m^3), and the Poisson's ratio of the soil to be 0.45. Based on these assumed values, the lateral stiffness of the foundation, K_y, was computed as 3,307,917 lbs/in (5792.76 kN/cm) and the rocking stiffness, K_θ, as 5.73242x10^{11} lb-in/rad (6.4764 x 10^7 kN-m/rad). The building is assumed to be located in an area with A_a=7, A_v=7, and soil type 3. The response modification factor, R, was taken as 4.5 ,the response amplification factor, C_d, as 4, the allowable drift as $0.01h_{sx}/C_d$, and the uniform dead load on each floor level as 148.81 lbs/in. (260.59 N/cm). Design procedures of the equivalent lateral force method are used for two cases. In Case (a), the fixed base without soil-structure interaction was considered, and in Case (b) the

TABLE XII. THE DESIGN RESULTS OF THE 15-STORY ONE-BAY, TWO-BAY, AND SETBACK, UNBRACED FRAMES FOR THE COMPARISON OF THE ATC-3-06 ELF METHOD AND MODAL ANALYSIS METHOD.
(1 kip = 4.448 kN)

	Case (a) ELF Method			Case (b) Modal Analysis Method		
	1-Bay	2-Bay	Setback	1-Bay	2-Bay	Setback
Max. Stability Coeff.	0.0156	0.0194	0.0171	0.0186	0.0230	0.0233
Fundamental Period (sec)	2.066	2.134	1.754	2.306	2.386	2.108
No. of Story with Max. Drift	10	10	12	10	9	12
Final Weight (kips)	70.07	111.82	97.51	61.28	98.56	78.33
Cycles of Iteration	20	7	8	18	8	10

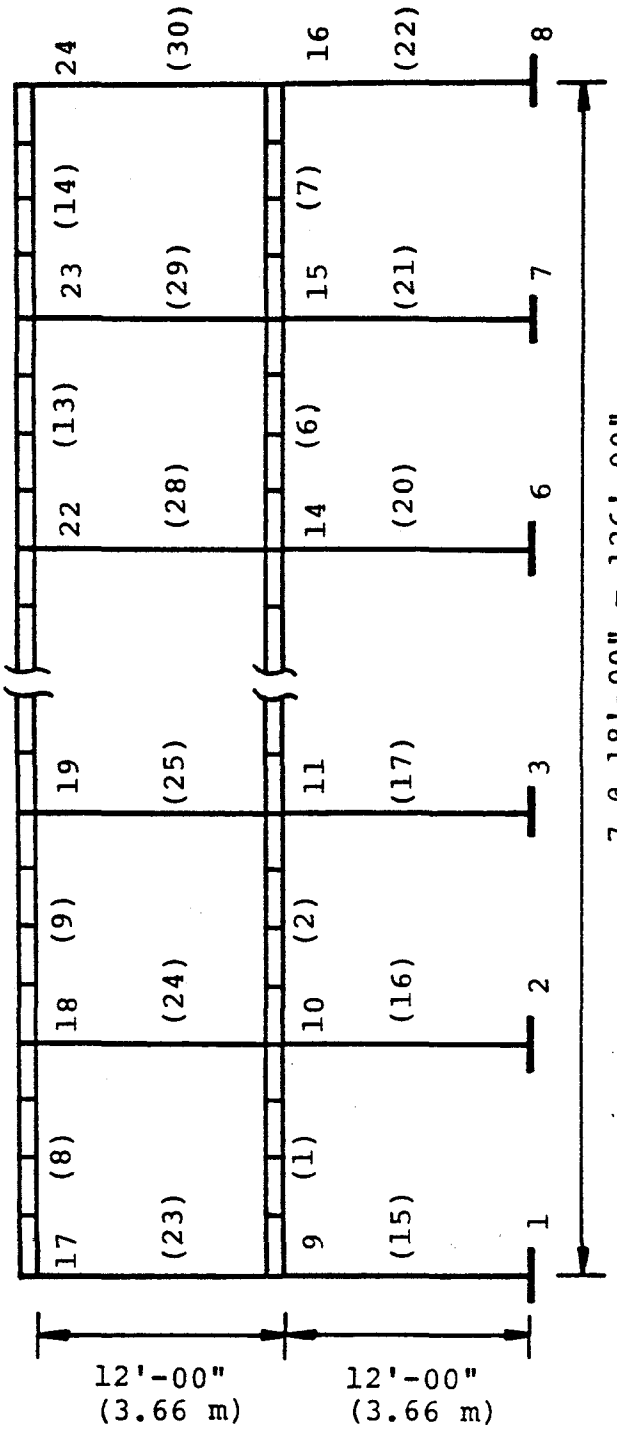

Figure 63. Two-Story, Seven-Bay, Unbraced Frame for the Study of the Effect of Soil-Structure Interaction.

effect of soil-structure interaction.

The results of both design cases that are listed in Table XIII are for the design base shear, base moment, fundamental natural period, eccentricity, and final weight of both cases. Table XIV contains the results of the moments of inertia of the members. It is obvious that the effect of soil-structure interaction reduces all the corresponding values of Case (a) as represented in Tables XIII and XIV. The upper bound of the fundamental period is 0.455 sec, which is less than the natural periods of both design cases, therefore it controls the design.

The effective damping factor of the design for Case (b) is 0.0512, which was determined in accordance with Eq. (5.14) with an effective period of 0.46877 sec, which was determined by using Eq. (5.12). Table XV contains a list of the stability coefficients, the seismic design forces, and the lateral displacements of each floor level. The stability coefficients of both design cases are less than the upper bound, and the drift at the second story is violated for both design cases.

In order to investigate the significant influence of the soil-structural interaction, the lateral stiffness of the foundation was reduced to 1.08×10^5 lbs/in. (189.13 kN/cm). This reduction in the lateral stiffness of the foundation was used to control T/T = 1.60, and effective damping factor can be increased to around 0.09. The seismic design forces were reduced to 12.94 kips (57.56 kN) on the first floor, and 25.68 kips (114.22 kN) on the second floor, those are only 50% of the fixed base case. The optimal weight was 7.66 kips

TABLE XIII. THE DESIGN PARAMETERS OF THE FINAL CYCLE OF THE TWO-STORY, SEVEN-BAY FRAME FOR THE STUDIES OF SOIL EFFECT. (1 kips = 4.448 kN, 1 ft = 0.3048 m)

	Case(a) Fixed Base	Case(b) Soil-Structure Interaction
Base Shear (kips)	82.159	81.622
Base Moment (ft-kips)	1231.03	1230.90
Fundamental Period (sec/cycle)	0.4862	0.4880
Effective Period (sec/cycle)		0.4688
Effective Damping Factor		0.0512
Eccentricity (ft)	2.6637	2.6466
Final Weight (kips)	13.977	13.950

TABLE XIV. THE MOMENTS OF INERTIA OF THE MEMBERS OF THE TWO-STORY, SEVEN-BAY FRAME FOR THE STUDIES OF THE SOIL EFFECT. (1 in. = 2.54 cm).

Member No	Moment of Inertia (in^4)	
	Case (a)	Case (b)
	Fixed Base	Soil-Structure Interaction
1,7	1334.68	1324.78
2,6	297.60	295.82
3,5	102.94	102.55
4	30.66	30.54
8,14	852.16	845.45
9,13	332.79	300.45
10,12	143.08	142.03
11	108.07	107.22
15,22	1086.75	1077.82
16,21	1058.75	1051.18
17,20	343.16	341.42
18,19	113.36	113.12
23,30	513.69	527.73
24,29	992.77	985.85
25,28	246.70	245.30
26,27	60.53	60.28

TABLE XV. THE STABILITY COEFFICIENTS, SEISMIC DESIGN FORCES, AND LATERAL DISPLACEMENTS OF THE TWO-STORY, SEVEN-BAY STRUCTURE. (1 in. = 2.54 cm, 1 kip = 4.448 kN)

	Case (a) Fixed Base			Case (b) Soil-Structure Interaction		
Floor Level	Stability Coeff.	Seismic Force (kips)	Lateral Disp. (in.)	Stability Coeff.	Seismic Force (kips)	Lateral Disp. (in.)
1	0.01126	27.54	0.2854	0.01134	27.36	0.2855
2	0.00532	54.62	0.6454	0.00535	54.27	0.6455

(34.07 kN), which is about 50% lighter than that of the fixed base case.

The second example is the fifteen-story, two-bay unbraced frame shown in Figure 41. The soil conditions and foundation size are the same as those of the previous example. The lateral stiffness of the foundation is 1.24×10^{6} lbs/in (2171.46 kN/cm), and the rocking stiffness 1.324×10^{11} lb-in/rad (1.4958 kN-m/rad). The same design loadings, constraints, the ATC-3-06 design parameters of A_a and A_v, the soil profile type, R and C_d, as those used for the example given in Section VI.C.2 are considered in the design.

Figure 64 shows the plot of the weight versus cycles of iteration. The optimum weight of Case (b) is 106.08 kips (471.84 kN), which is less than 111.82 kips (497.38 kN), the optimum weight of Case (a). The plot of stability coefficients is represented in Figure 65 in which the maximum value of Case (b) is shown as 0.0217. The eccentricity of Case (b) is 5.174 ft (1.577 m), which is less than that of Case (a). Similar to Case (a), the fundamental period of Case (b) is 2.232 sec, which is larger than the upper bound, $1.2T_a$, thus the upper bound of the fundamental period controls the design.

The effective damping factor is 0.03127, which is less than the lower bound 0.05. The lower bound of 0.05 is used to compute the effective base shears. The effective period is computed as 2.5165 sec. The plot of the shear envelopes is shown in Figure 66. Figures 67, 69 and 71 respectively illustrate the distributions of the moments of inertia of girders, exterior columns, and interior columns. The member sizes are reduced as expected because of the effect of the

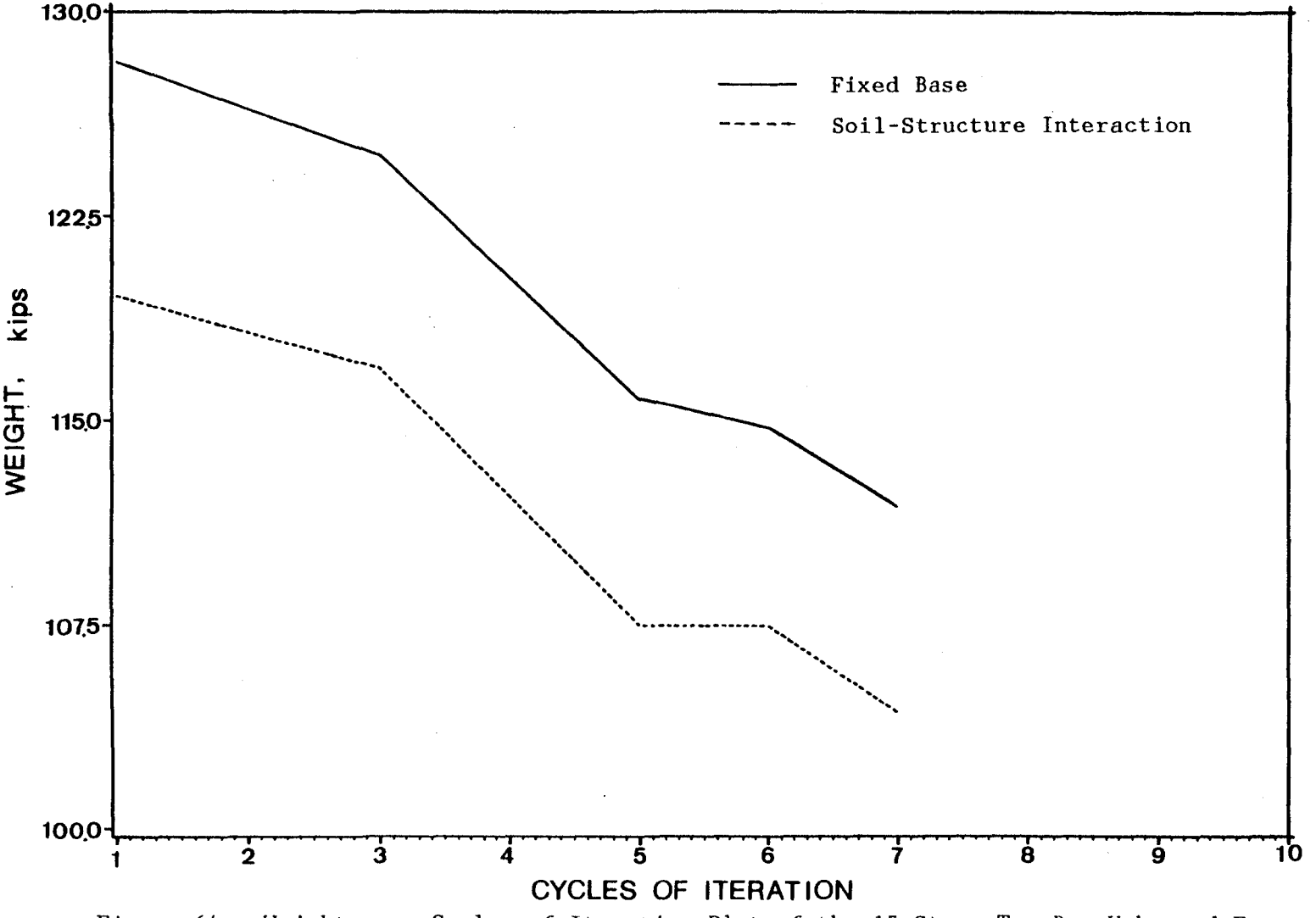

Figure 64. Weight v.s. Cycles of Iteration Plot of the 15-Story, Two-Bay, Unbraced Frame for the Study of the Effect of Soil-Structure Interaction. (1 kip = 4.448 kN).

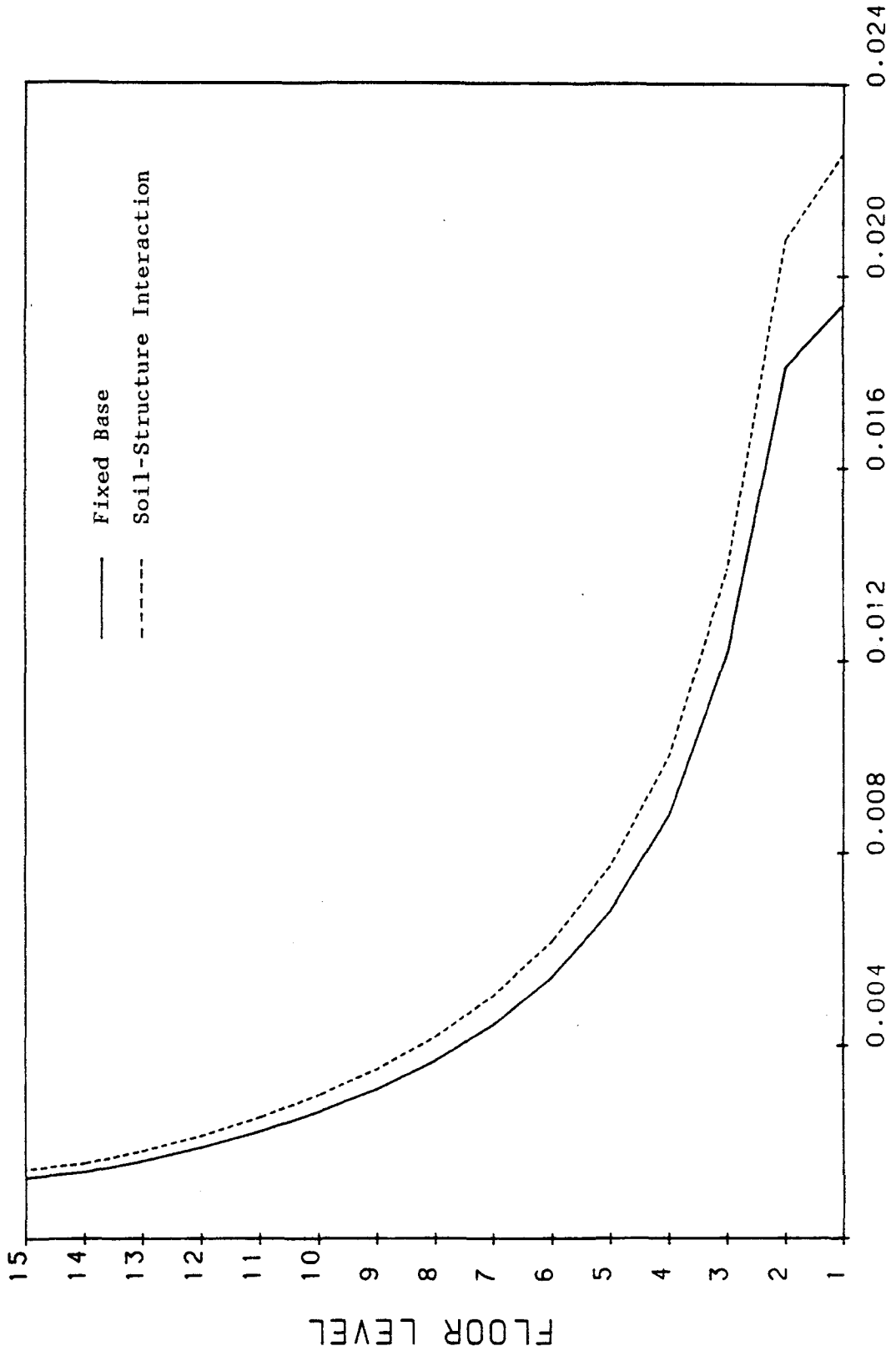

Figure 65. Stability Coefficients of the 15-Story, Two-Bay, Unbraced Frame for the Study of the Effect of Soil-Structure Interaction.

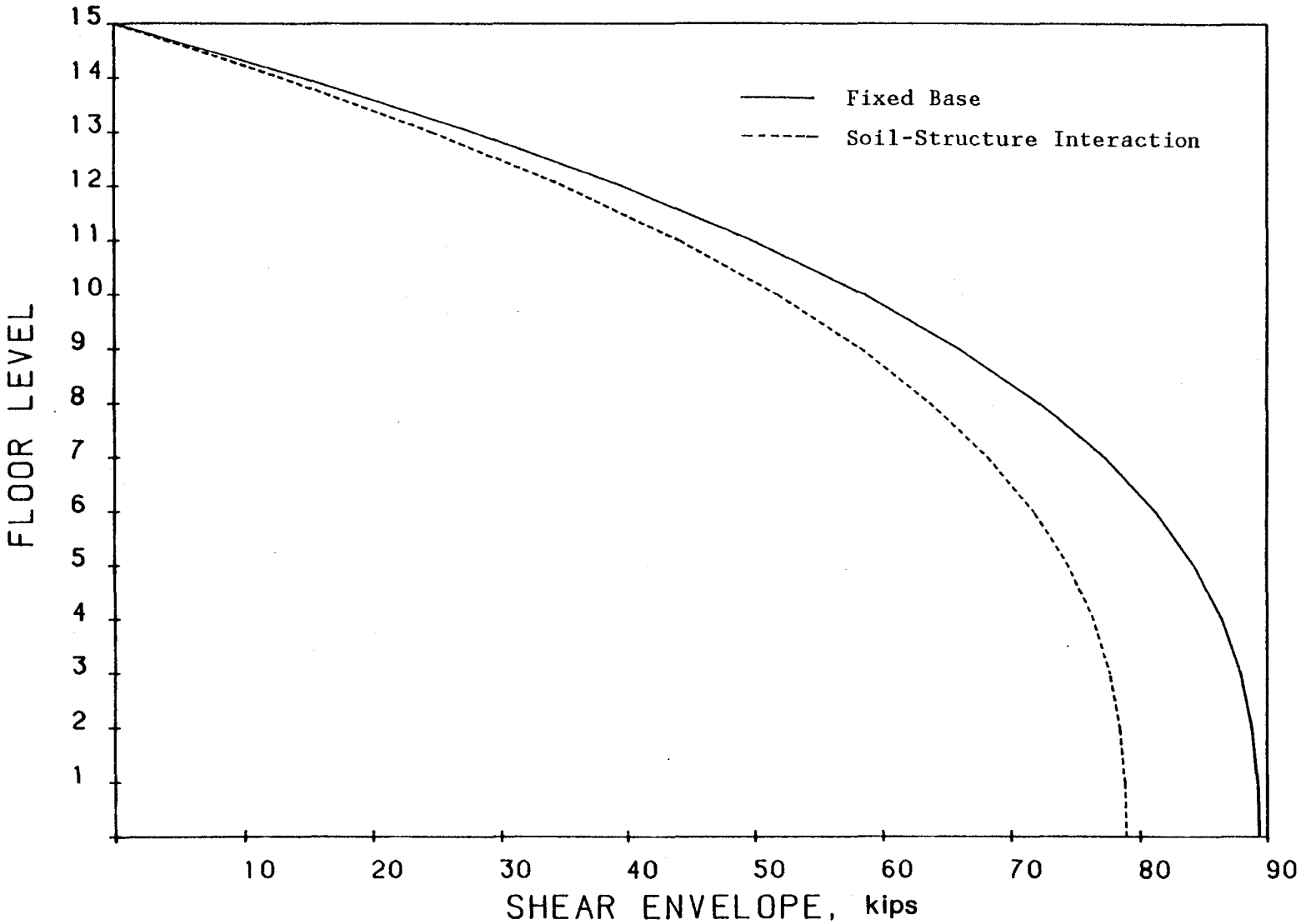

Figure 66. Shear Envelopes of the 15-Story, Two-Bay, Unbraced Frame for the Study of the Effect of Soil-Structure Interaction. (1 kip = 4.448 kN).

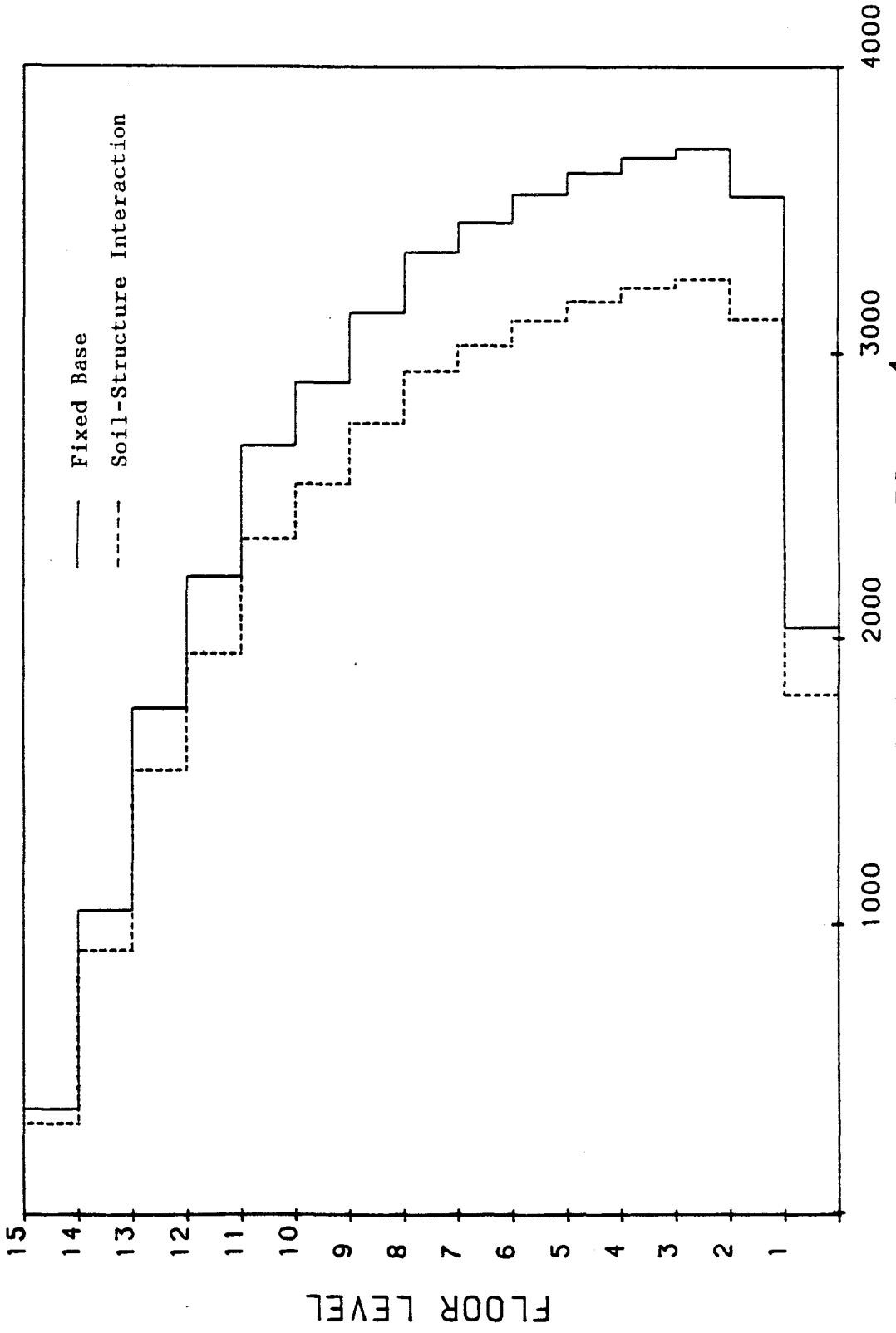

Figure 67. Moments of Inertia of the Girders of the 15-Story, Two-Bay, Unbraced Frame for the Study of the Effect of Soil-Structure Interaction. (1 in. = 2.54 cm)

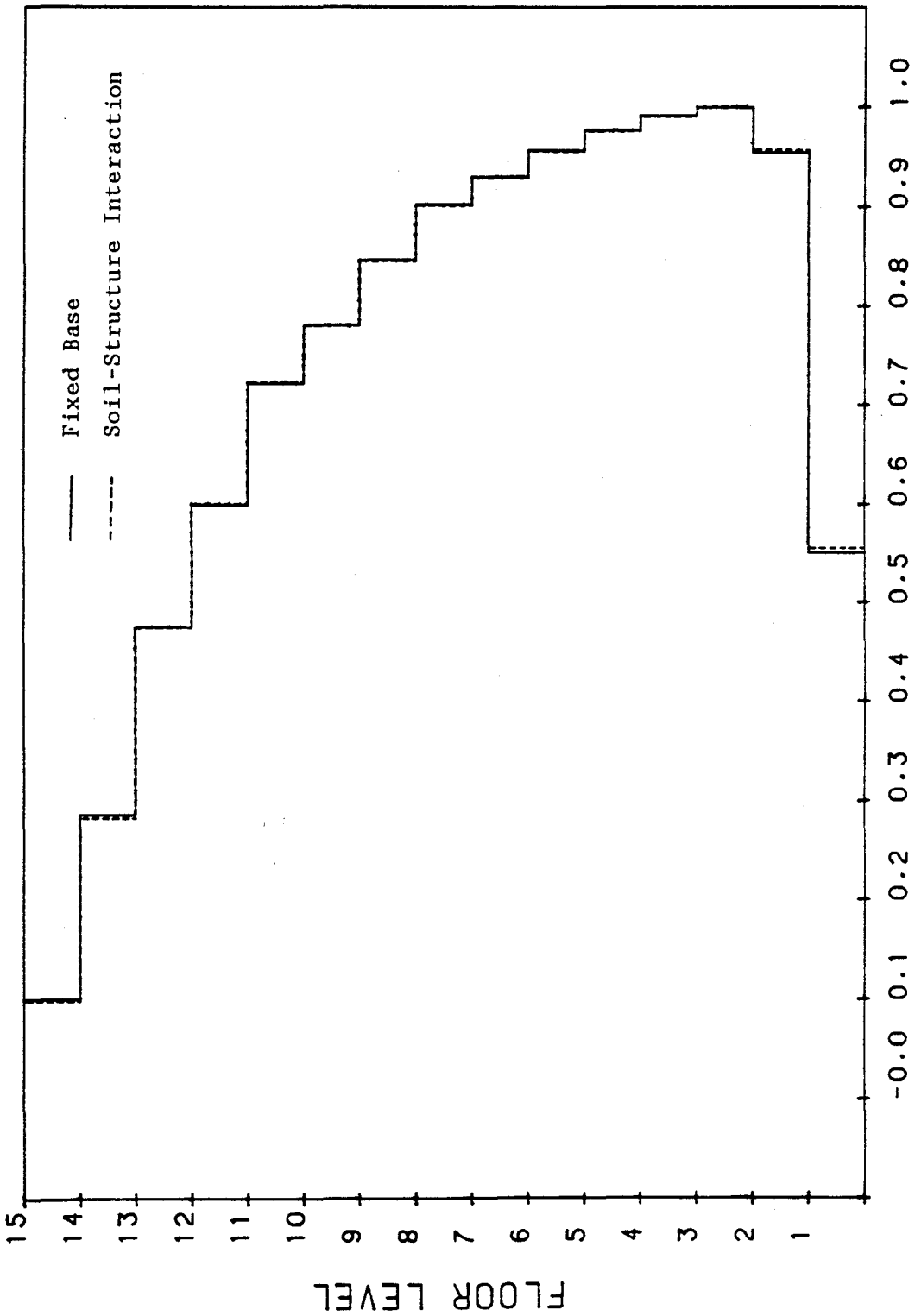

Figure 68. Normalized Moments of Inertia of the Girders of the 15-Story, Two-Bay, Unbraced Frame for the Study of the Effect of Soil-Structure Interaction.

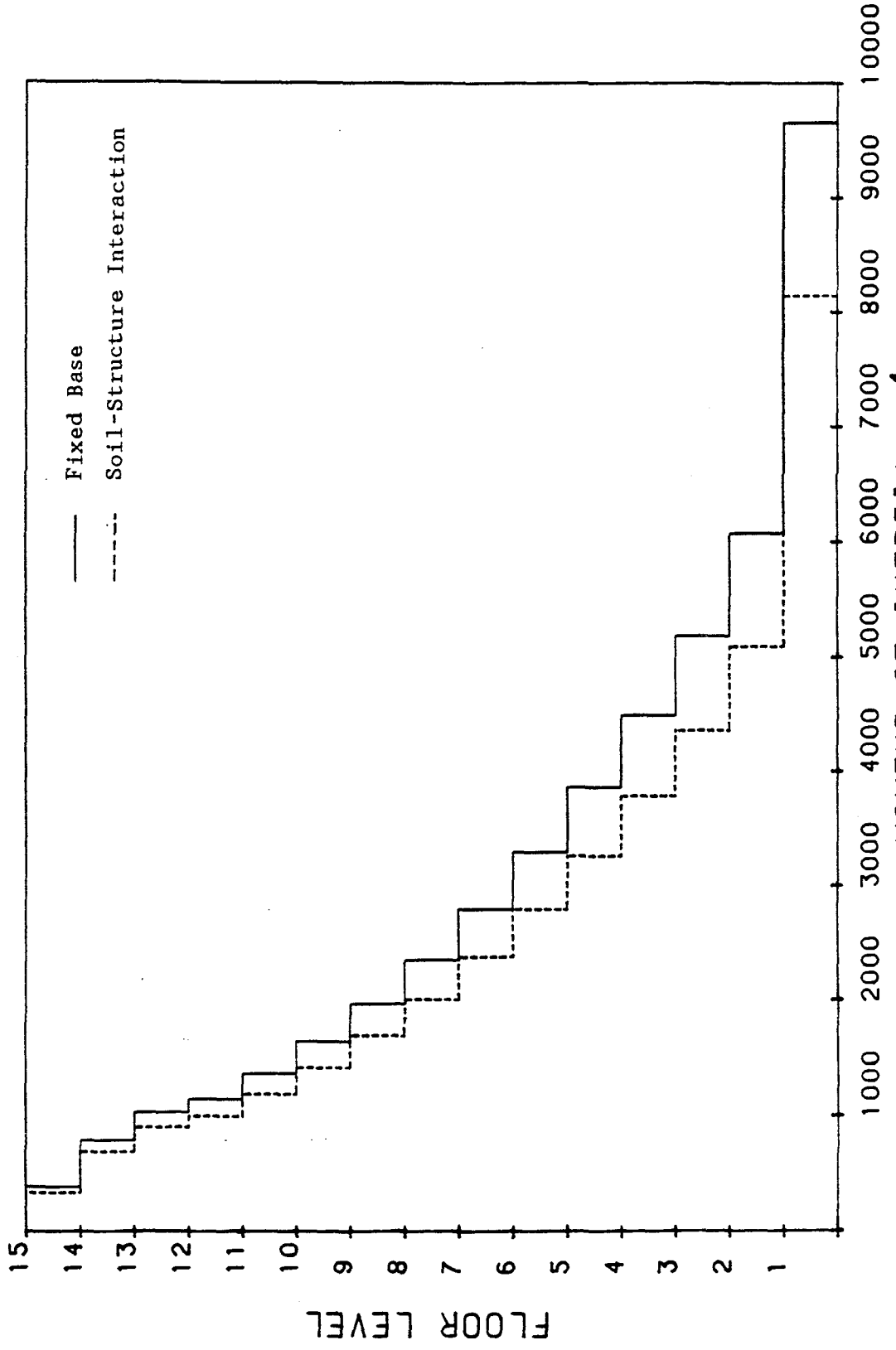

Figure 69. Moments of Inertia of the Exterior Columns of the 15-Story, Two-Bay, Unbraced Frame for the Study of the Effect of Soil-Structure Interaction. (1 in. = 2.54 cm)

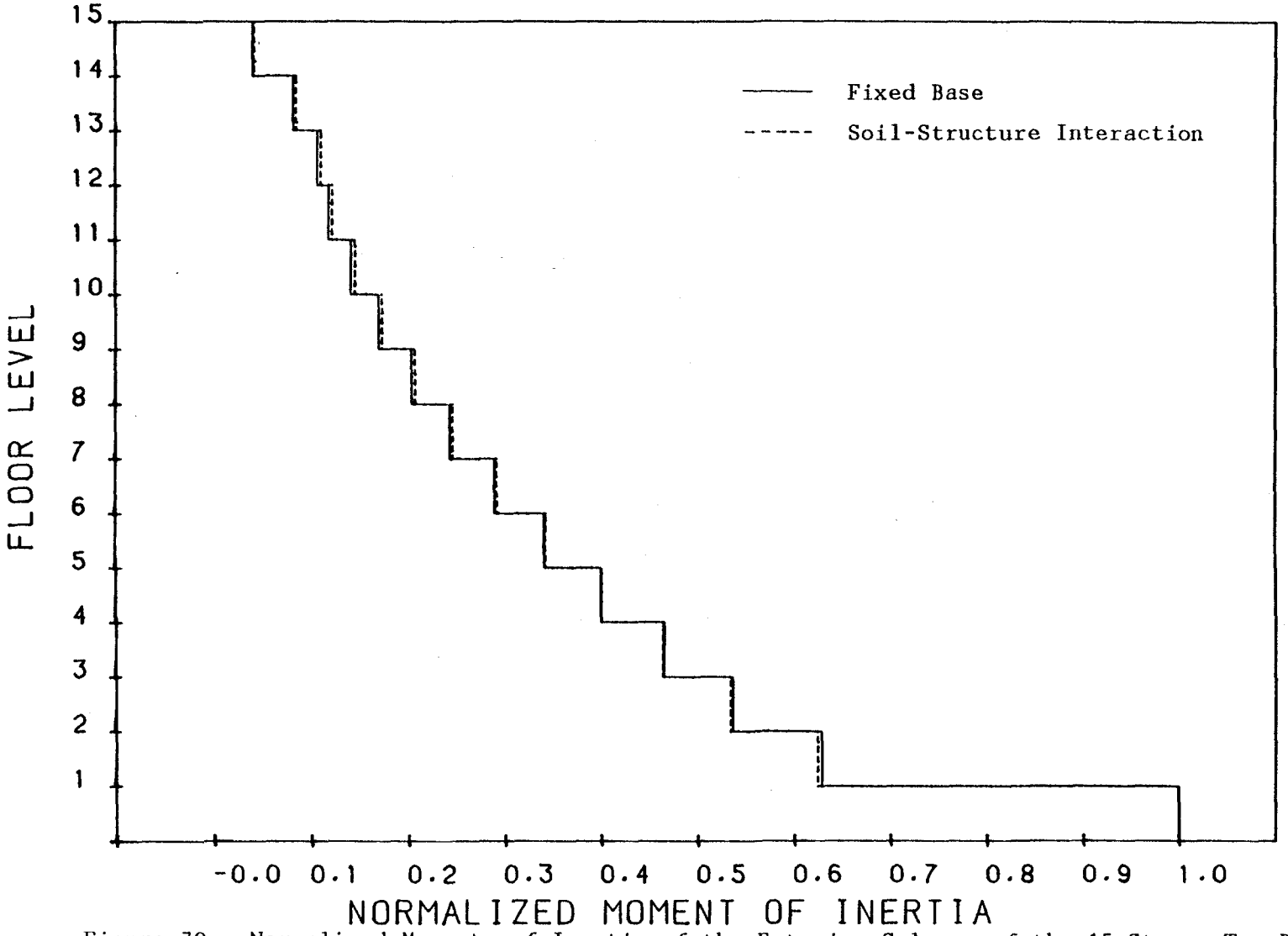

Figure 70. Normalized Moments of Inertia of the Exterior Columns of the 15-Story, Two-Bay, Unbraced Frame for the Study of the Effect of Soil-Structure Interaction.

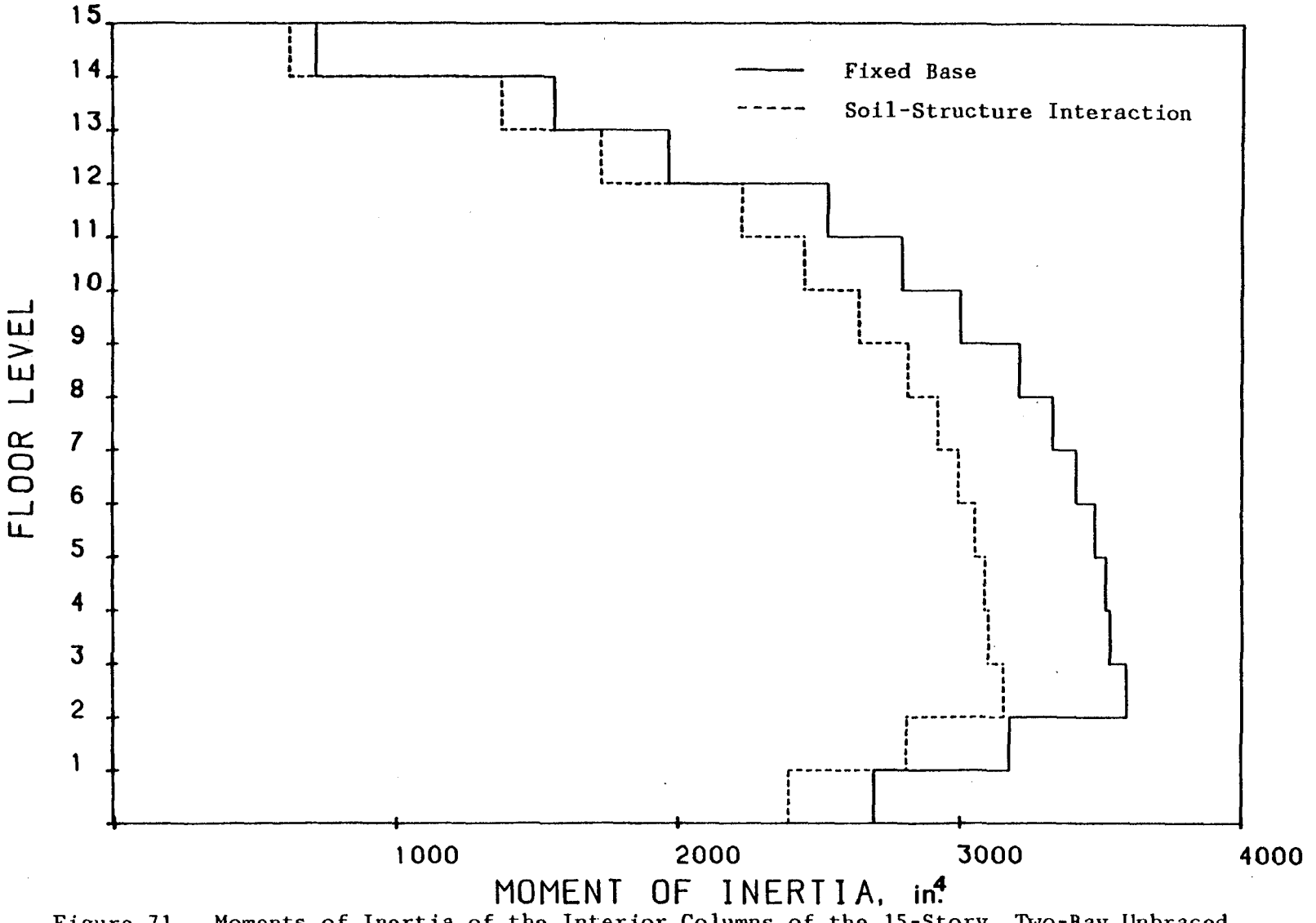

Figure 71. Moments of Inertia of the Interior Columns of the 15-Story, Two-Bay, Unbraced Frame for the Study of the Effect of Soil-Structure Interaction. (1 in. = 2.54 cm)

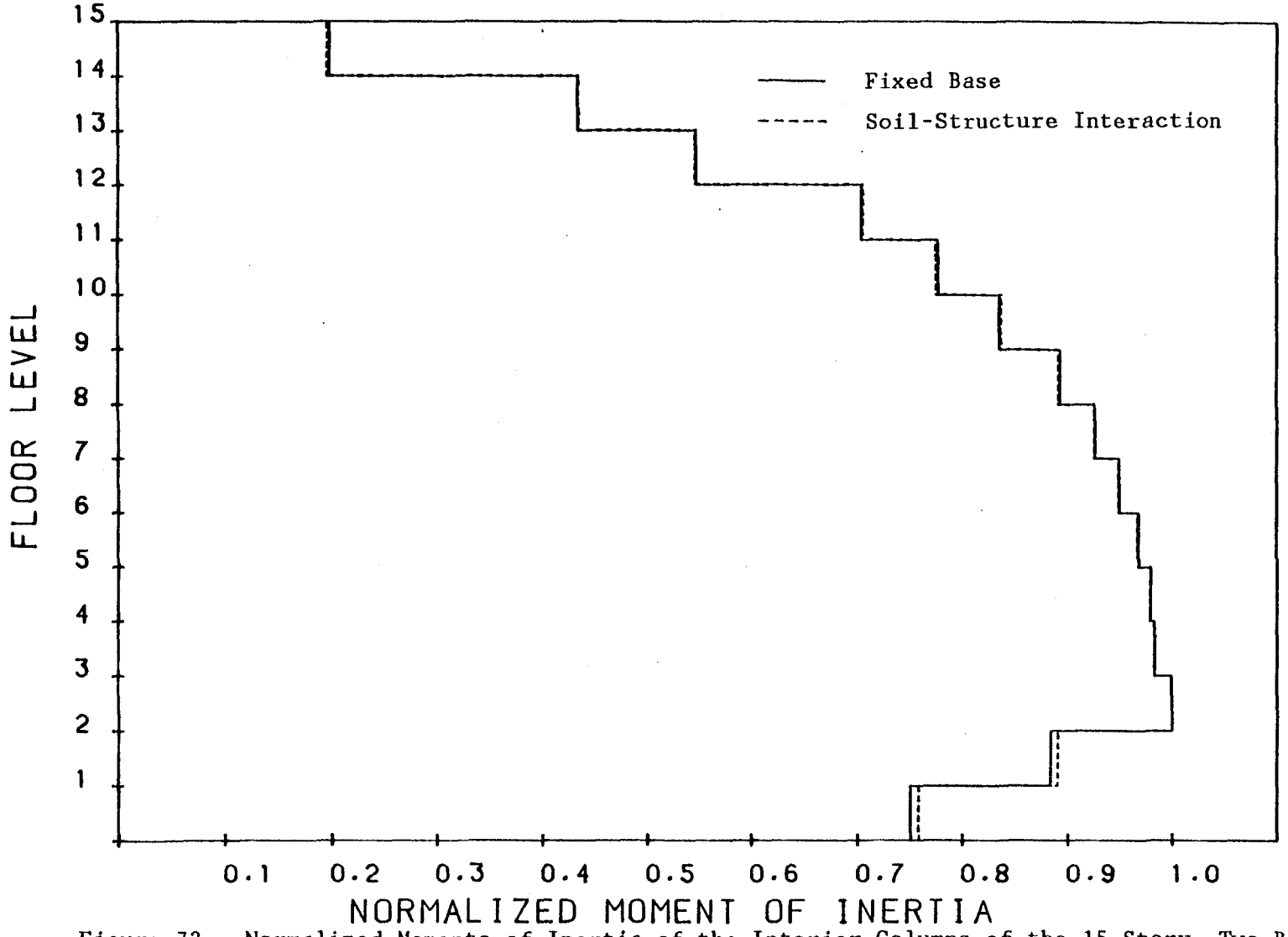

Figure 72. Normalized Moments of Inertia of the Interior Columns of the 15-Story, Two-Bay, Unbraced Frame for the Study of the Effect of Soil-Structure Interaction.

soil-structure interaction; however, the distribution in member sizes is very similar for both design cases. The normalized moments of inertia are sketched in Figures 68, 70, and 72. The shape of lateral displacements is represented in Figure 73 in which the active story drift is at the tenth story for both cases.

E. COMPARISON OF RESULTS OF MINIMUM WEIGHT AND MINIMUM COST DESIGN

The fifteen-story, two-bay structure shown in Figure 41 was redesigned for minimum cost, with the unit prices of the steel, painting, steel at the connections, and welding metal being 0.24 \$/lb (0.054 \$/N), 0.7986×10^3 \$/in^2 (0.124×10^3 \$/cm^2), 0.3 \$/lb (0.0674 \$/N), and 5.5 \$/lb (1.24 \$/N) respectively. The design was based on a ground acceleration of 0.4g. The maximum expected intensity of seismic excitations for 50 years, the lifetime of the structure, was assumed to be 0.5g. In addition, rigid connections were assumed, therefore a large value of 9×10^9 was used as the initial stiffness of the connection, k. The input parameters of ATC-3-06 equivalent lateral method were taken to be the same as those of the minimum weight design. The design results were overplotted in Figures 42 through 51 so that they can be compared with those of the minimum weight design.

In Figure 42, the distribution based on the energy distribution does not reduce the structural weight. Therefore, the constraint gradient method was used. Because the contribution based on the constraint gradients is not affected by the change of objective function, as illustrated in Figure 42, the structural weight of the first five

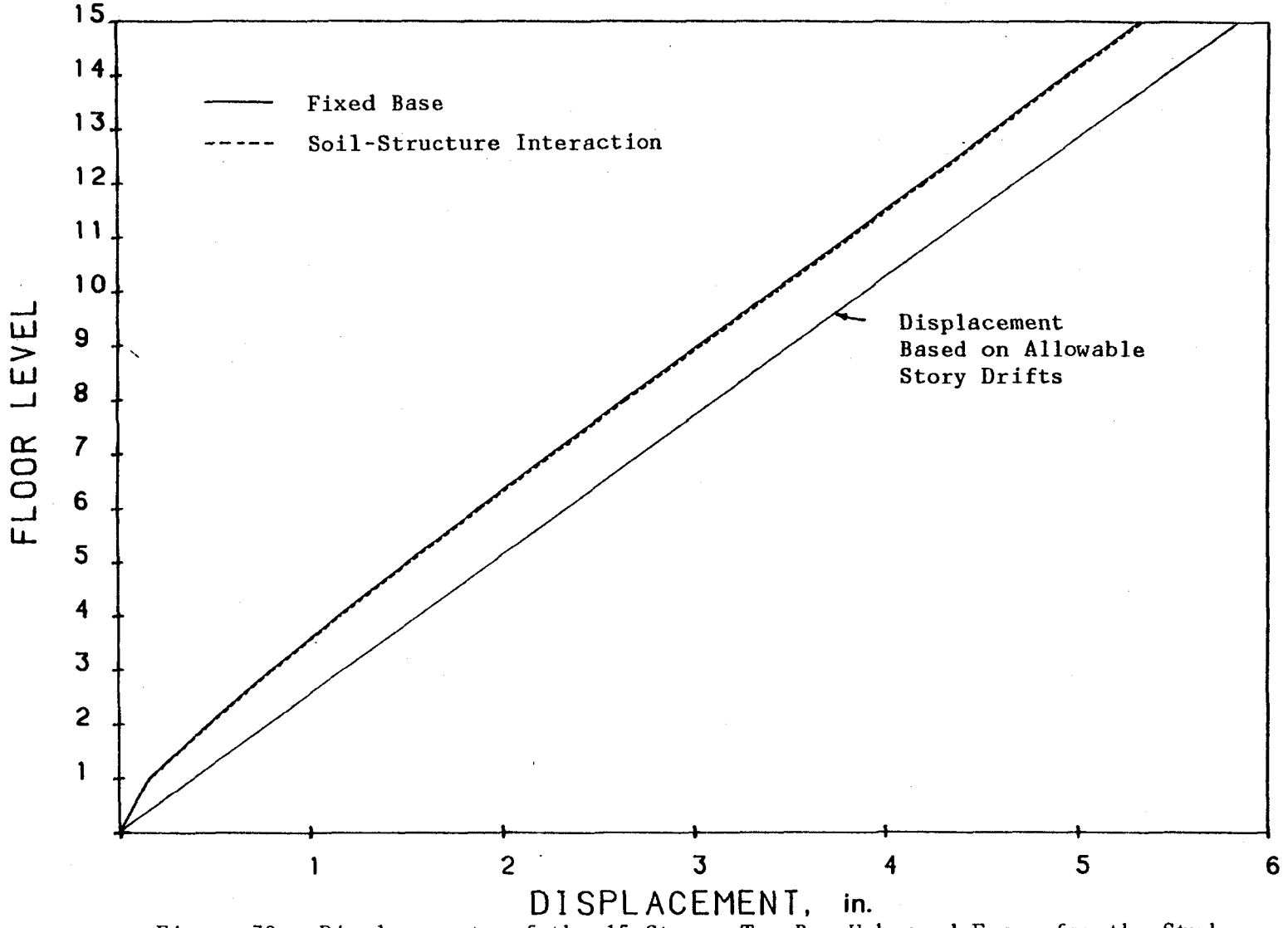

Figure 73. Displacements of the 15-Story, Two-Bay, Unbraced Frame for the Study of the Effect of Soil-Structure Interaction. (1 in. = 2.54 cm)

cycles are identical for both cases. The final weight of minimum cost design is 112.85 kips (501.96 kN), which is larger than the optimum weight of minimum weight design. The maximum stability coefficient of the minimum cost design is 0.0217, and the eccentricity is 5.669 ft (1.728 m).

The story shears of both cases are very similar as shown in Figure 43 by the shear envelopes; however, Figures 45 through 50 show the difference in the distribution of member sizes between the minimum weight and minimum cost designs. A more uniform distribution of member sizes from the bottom to the top of the building is required for minimum cost design.

The shapes of the lateral displacements are overplotted in Figure 51. For the minimum cost design, the maximum story drift is on the eighth story.

Figure 74 illustrates the plot of the costs versus cycles of iteration for each type of cost. As indicated, the total structural cost is governed by the base charge, which is the cost of the structural members. All other kinds of costs are just a small percentage of total cost. It is also worth noting that the damage cost increases whenever the total cost decreases. It is obvious that the decrease in total cost will increase the flexibility of the structure and hence enlarge the story drifts. The damage cost is therefore raised because of the increase of the story drifts.

F. COMPARISON OF VARIOUS CODE REQUIREMENTS

The structure shown in Figure 41 was redesigned for the following

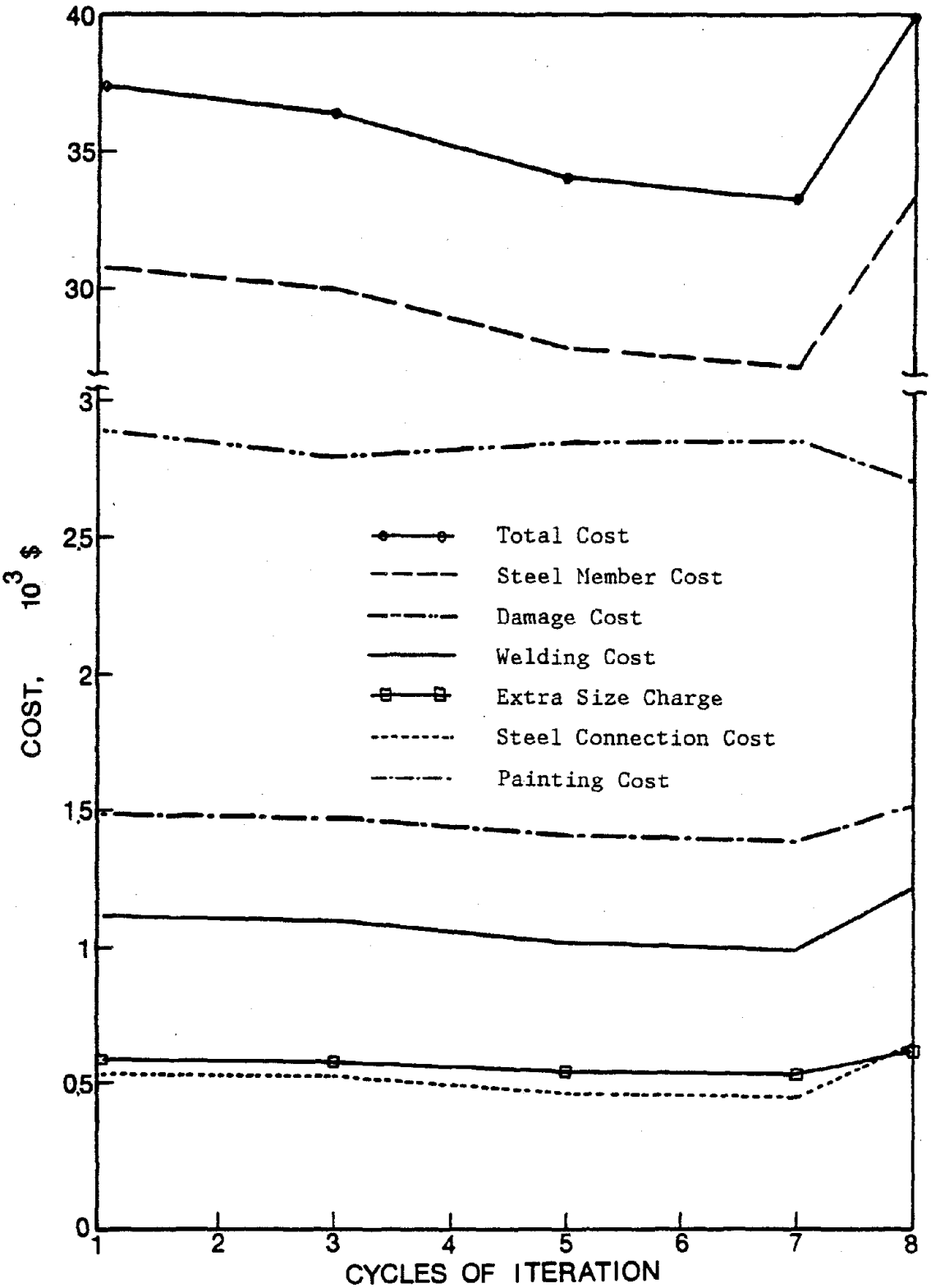

Figure 74. Costs v.s. Cycles of Iteration Plot of the 15-Story, Two-Bay, Unbraced Frame Minimum Cost Design.

two cases: 1) a seismic-resistant design according to UBC provisions and 2) a seismic-resistant design according to the Chinese Building Design Code. For the UBC, the building was assumed to be located in seismic zone 4 with the importance factor of the building being taken as I=1.5, the estimated site period as 1.0 sec, and the coefficient K as 1.0. The allowable drift was assumed to be $0.005h_{sx}$ for each story. An earthquake magnitude of 9, a site condition with soil type 3, and the structural influence coefficient, C, of 0.25 were assumed when the Chinese Building Design Code was considered. For comparative purposes, the restraint in the story drift was taken to be the same as that of ATC-3-06 provisions, $0.015h_{sx}/C_d$, although it was not considered in Chinese Building Design Code.

The results, except Figure 44, are overplotted in Figures 42 through 51 so that they can be compared with the design results based on the ATC-3-06 provisions. Figure 42 illustrates that the Chinese Code requires the heaviest design and the UBC demands the lightest because of the larger story drift allowance. The shear envelopes shown in Figure 43 represent the story shear of each floor level. The point that interrupts the smoothness of the envelope corresponding to the UBC is mainly due to the force of 0.07TV that is required at the top story when one considers the effect of the higher modes on response of long period structures where T is the fundamental period of the structure and V the design base shear. The envelope corresponding to the Chinese Code is almost linearly varied, because the effect of higher modes on responses are neglected even if the structure has a long fundamental period. It is therefore necessary to

restate that the Chinese Code limits the height of the building to 164 ft (50 m), and the stiffness from the bottom to the top of the building must be uniformly distributed. These limitations restrain the flexibility of the building so that the effect of the higher modes of response can be neglected.

The distribution of the sizes of the members is illustrated in Figures 45 through 50. These figures also show similar distributions for the girders and columns for all cases. With regard to the girders, it can be seen that a relatively small size at the first story increases suddenly at the second story. There is a small increase in size from the second floor to the third and a gradual increase in the reduction of sizes. This decreases smoothly from the third to the fourteenth floor. At the top floor, the moment of inertia abruptly decreases from the fourteenth floor. The moment of inertia of the exterior columns is the smallest at the top story. It increases smoothly from the top to the second floor and then abruptly increases at the first floor. A similar distribution of the moment of inertia exists between the interior columns and the girders; however, for the former, the moment of inertia decreases suddenly from the third floor down to the second and then down to the first with almost the same amount of decrement.

The displacements at different levels are plotted in Figure 51. Although the story drift is active, the displacements can never reach the allowable displacements.

G. THE EFFECT OF DRIFT CONSTRAINT AND DISPLACEMENT CONSTRAINT FOR UBC AND CHINESE CODE

In the previous sections, the design of all the examples were based on the drift constraint. In reviewing the plots of the lateral displacements, one can see that in almost all of the design examples the drift of the stories between the ninth and the twelfth stories was violated but that the lateral displacements are always smaller than the allowable displacements as determined on the basis of the allowable story drifts. The fifteen-story, two-bay, unbraced frame shown in Figure 41 was redesigned by using the displacement constraints instead of drift constraints as examples of the UBC and Chinese Codes for which the allowable displacements were introduced by using the allowable story drifts.

The UBC design results are overplotted in Figures 75 through 83 with the results that were determined on the basis of the drift constraint. Figure 75 shows the lateral displacements of each floor of the two design cases. For the displacement constraint case, the lateral displacement at the top floor violates the allowable displacement. However, the story drift of ninth story is 0.787 in. (1.999 cm), which exceeds the allowable drift, 0.72 in. (1.829 cm). The plot of the weight versus cycles of iteration is illustrated in Figure 76. Apparently, the design using the displacement constraint is much lighter than the design using the drift constraint. Less story shears are also obtained for the displacement constraint case as shown in the plot of shear envelopes of Figure 77. The moments of inertia and normalized moments of inertia of the girders and columns are represented in Figures 78 through 83 respectively. The

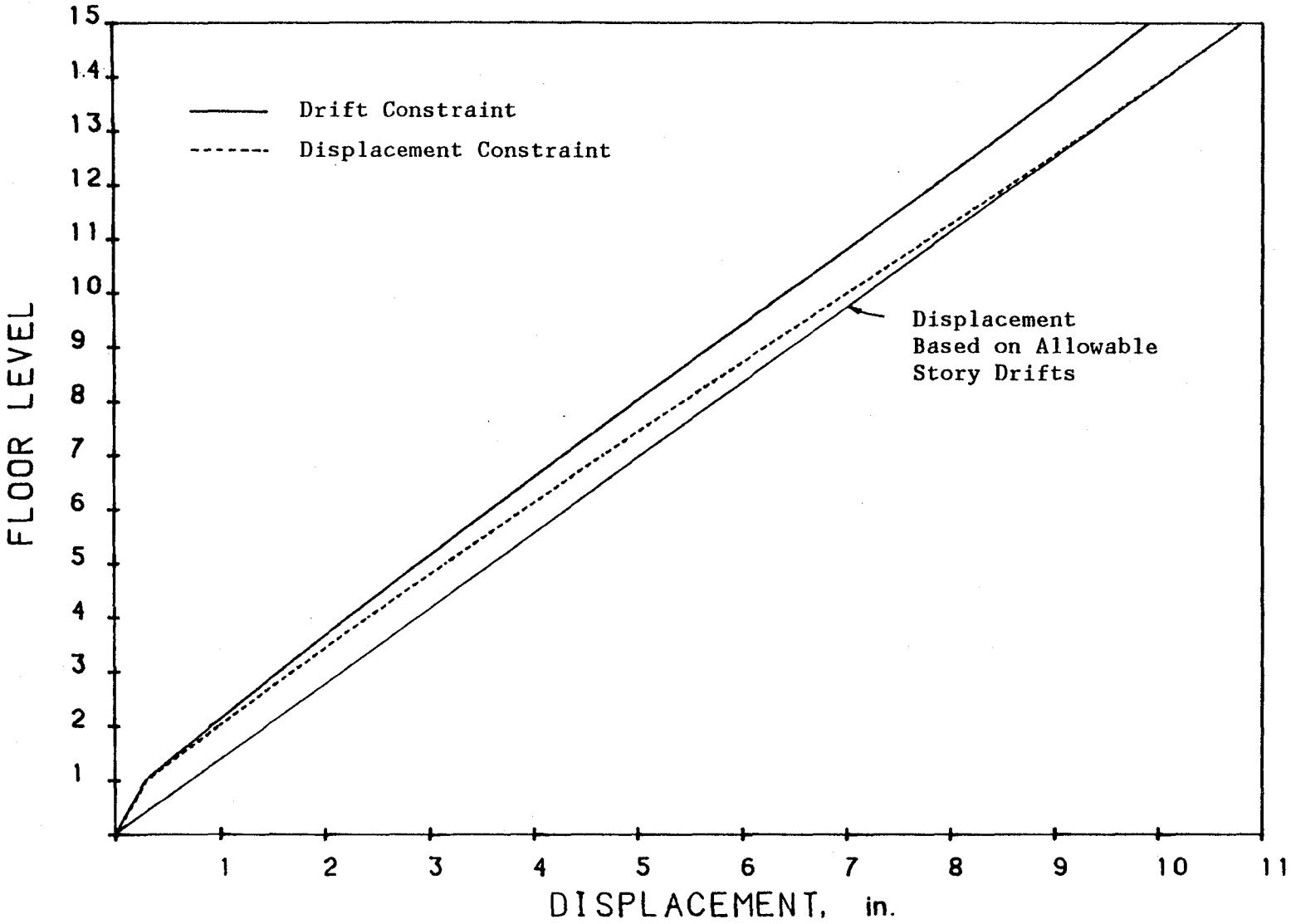

Figure 75. Displacements of the UBC Design for the Study of the Influence of Drift Constraint and Displacement Constraint. (1 in. = 2.54 cm)

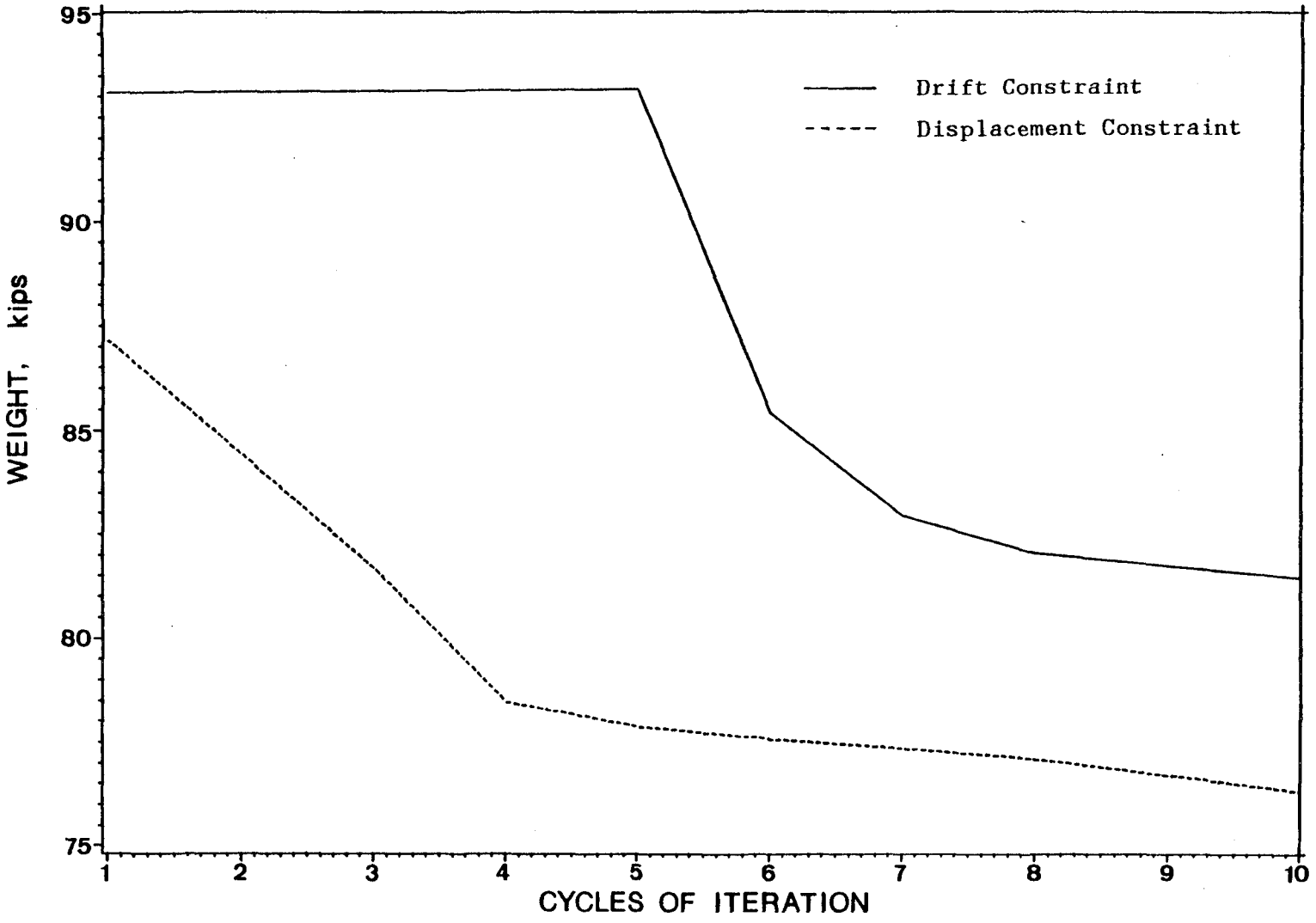

Figure 76. Weight v.s. Cycles of Iteration Plot of the UBC Design for the Study of the Influence of Drift Constraint and Displacement Constraint. (1 kip = 4.448 kN)

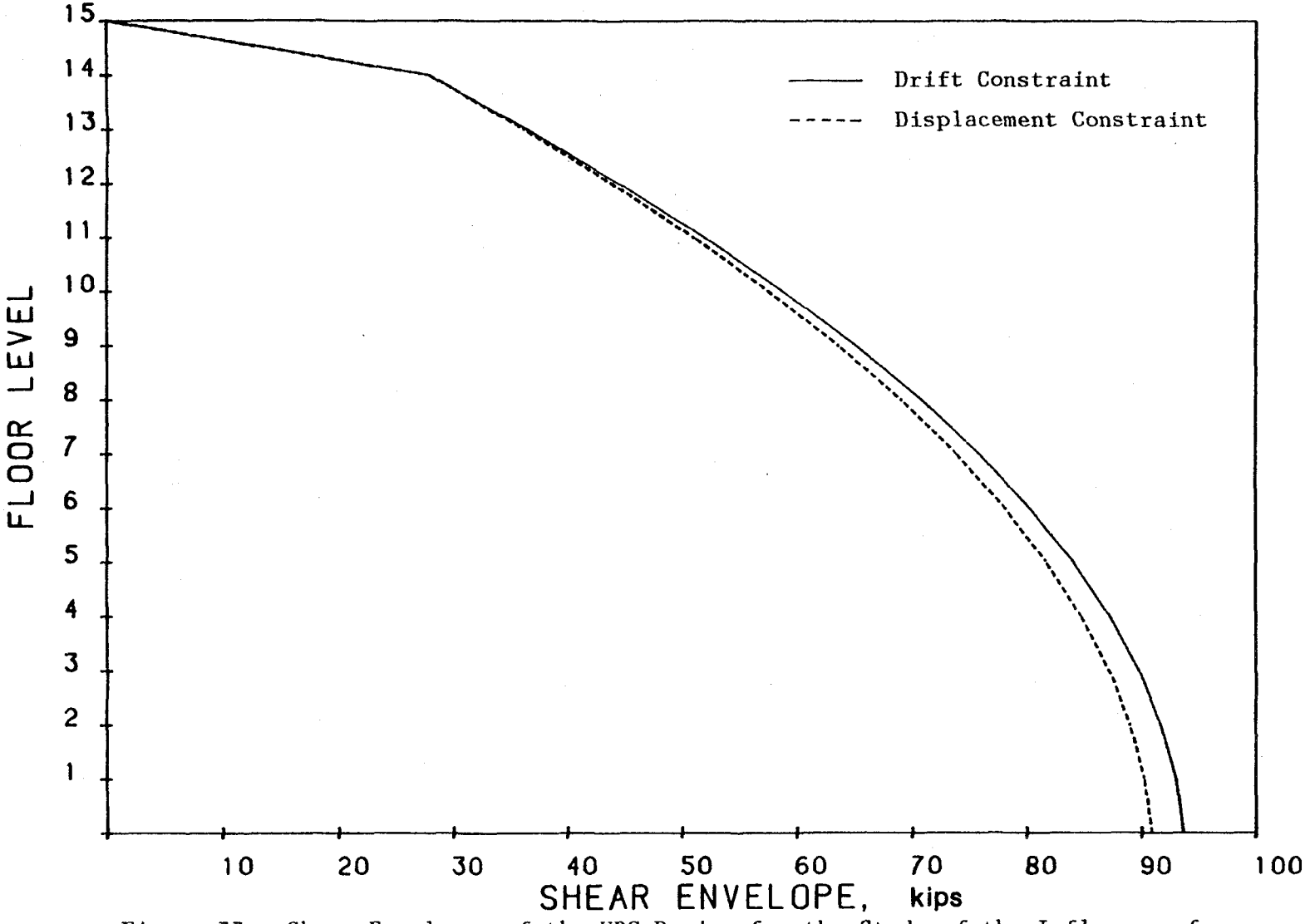

Figure 77. Shear Envelopes of the UBC Design for the Study of the Influence of Drift Constraint and Displacement Constraint. (1 kip = 4.448 kN)

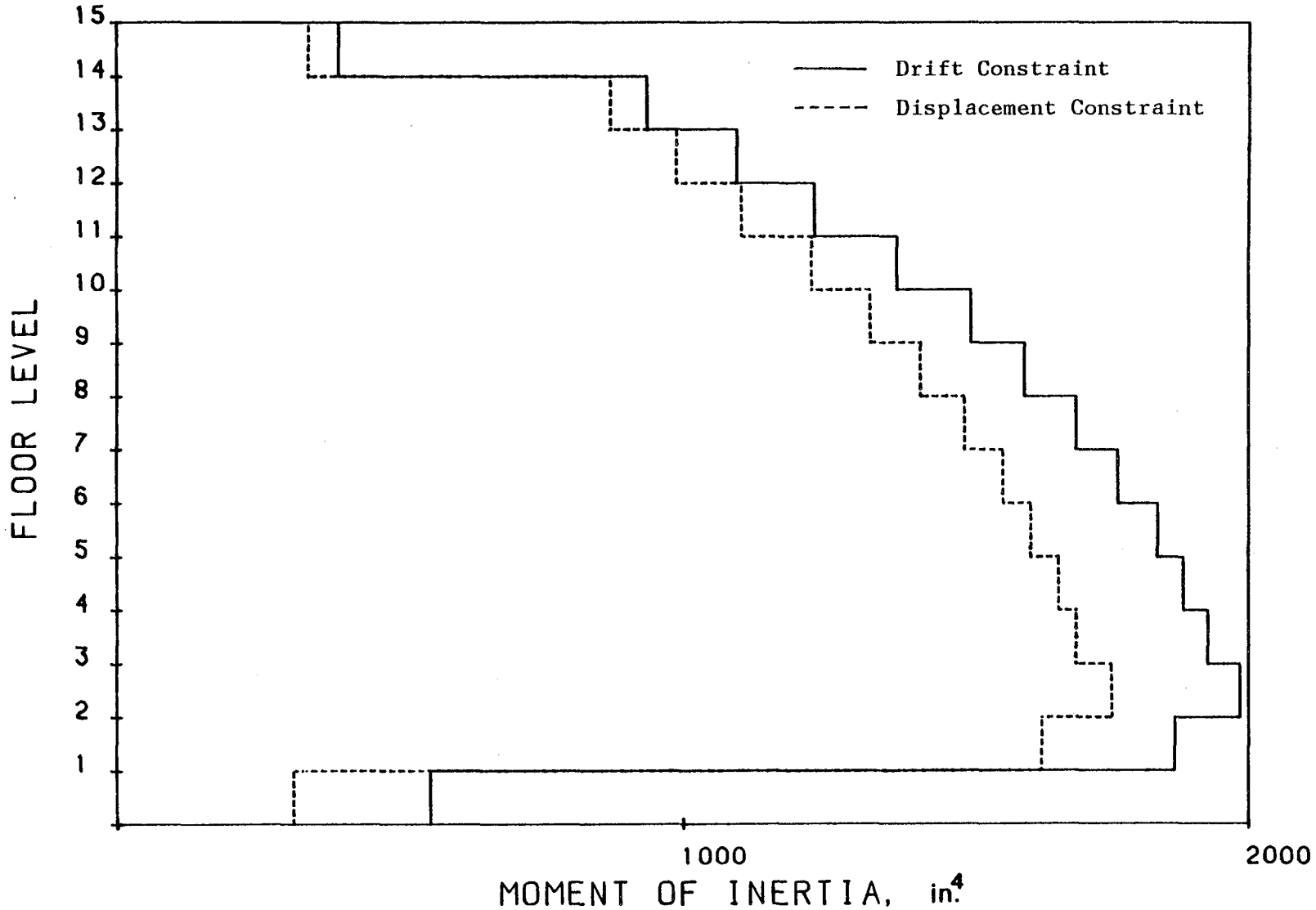

Figure 78. Moments of Inertia of the Girders of the UBC Design for the Study of the Influence of Drift Constraint and Displacement Constraint. (1 in. = 2.54 cm).

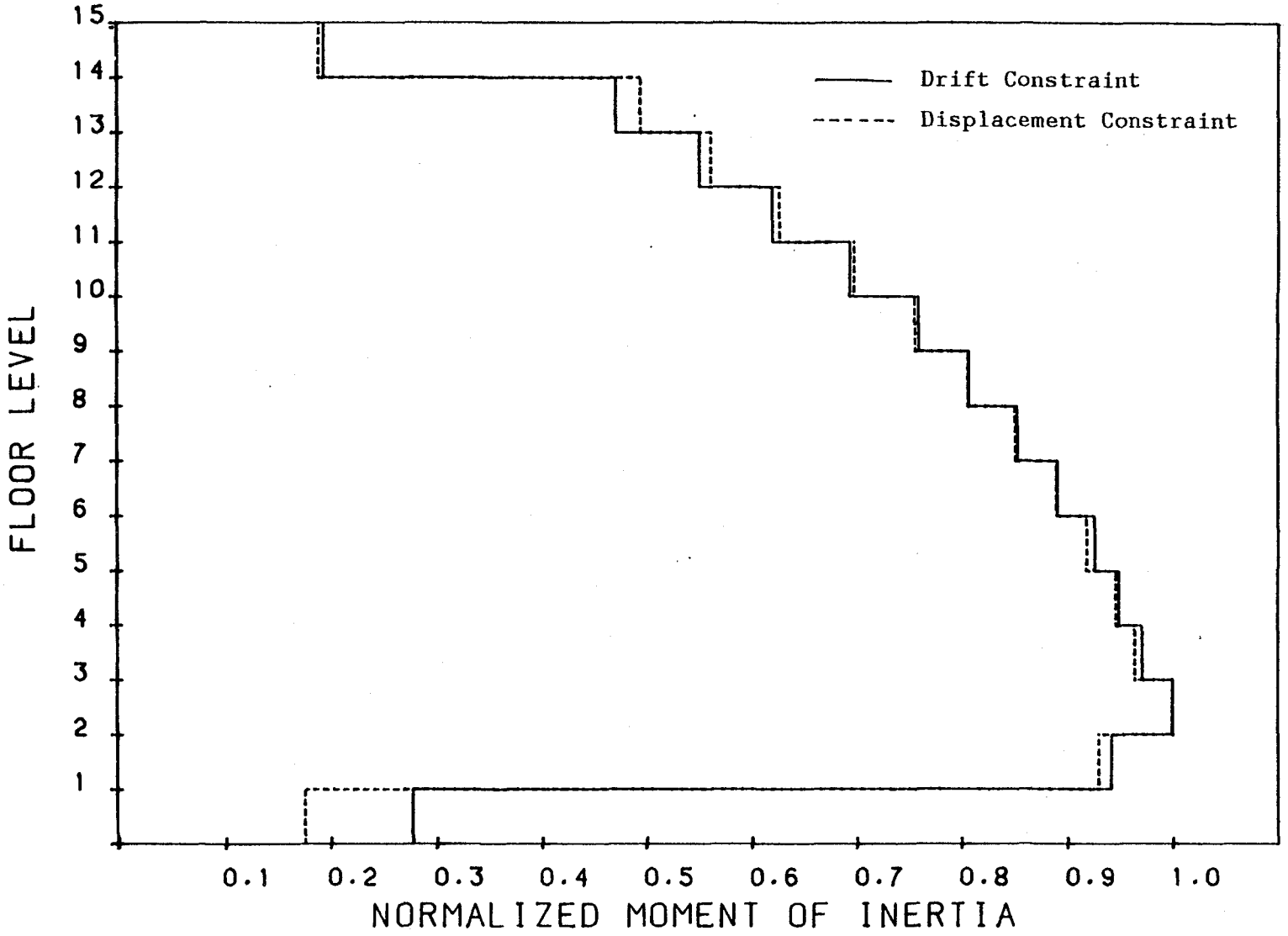

Figure 79. Normalized Moments of Inertia of the Girders of the UBC Design for the Study of the Influence of Drift Constraint and Displacement Constraint.

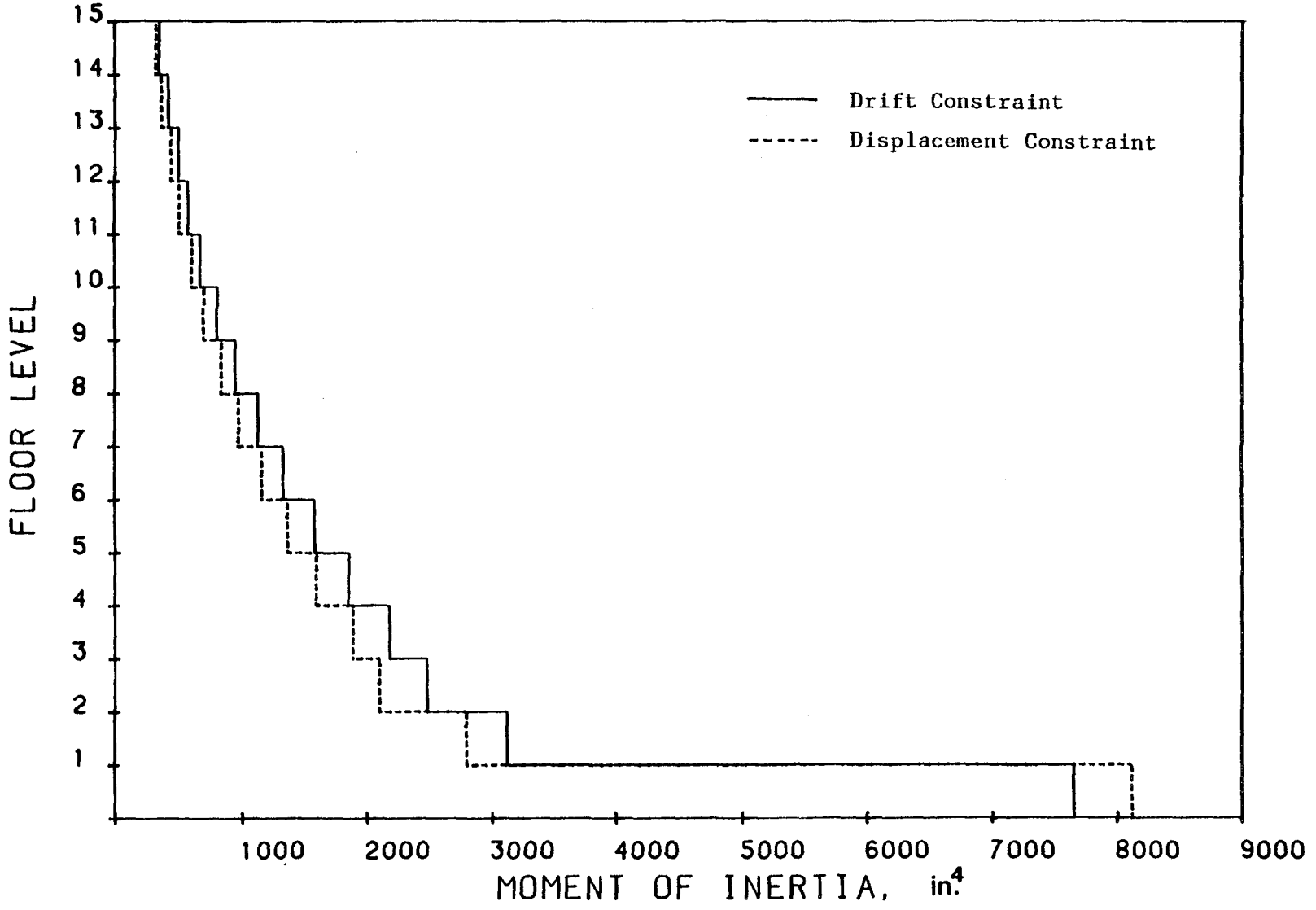

Figure 80. Moments of Inertia of the Exterior Columns of the UBC Design for the Study of the Influence of Drift Constraint and Displacement Constraint. (1 in. = 2.54 cm).

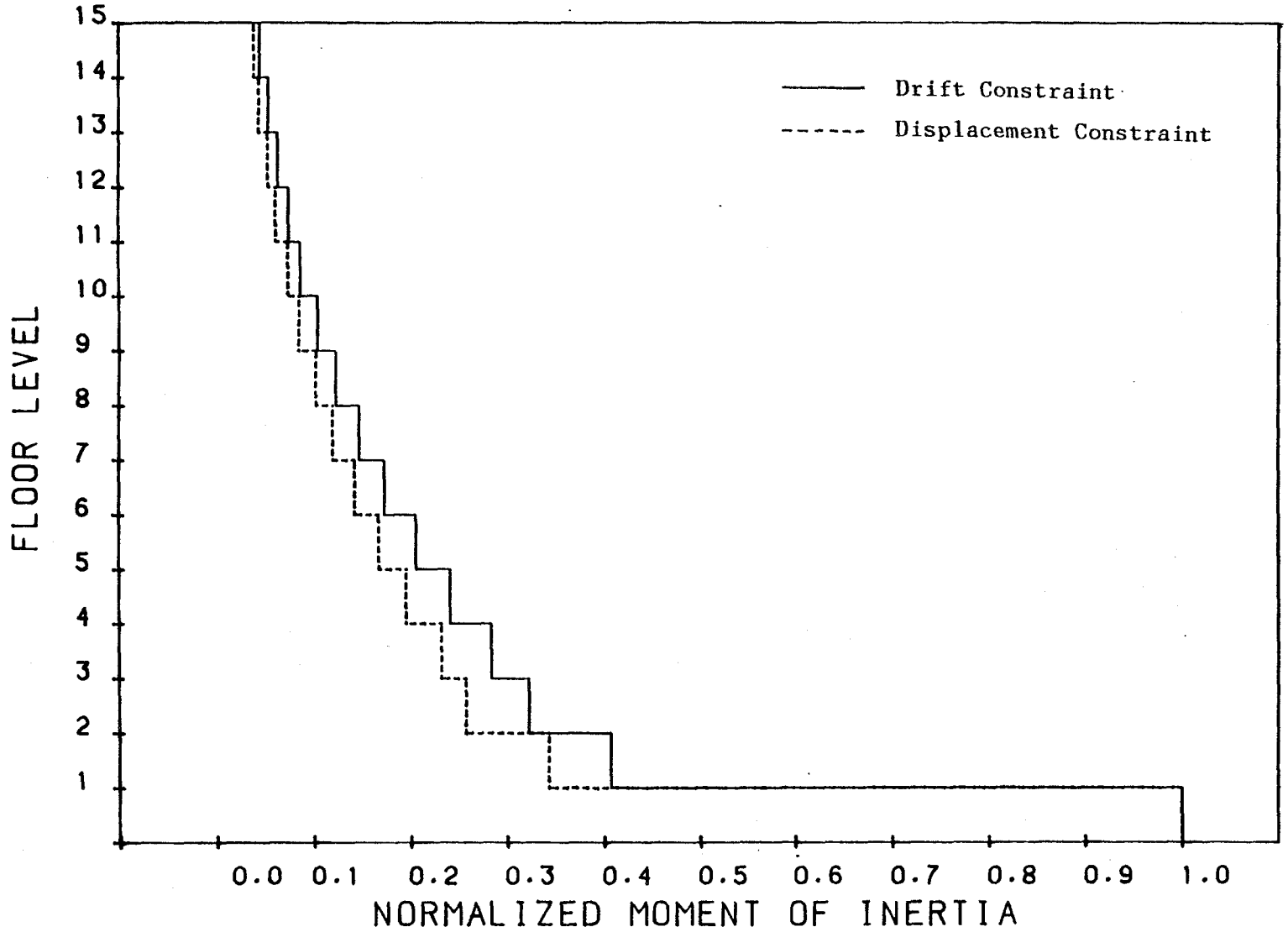

Figure 81. Normalized Moments of Inertia of the Exterior Columns of the UBC Design for the Study of the Influence of Drift Constraint and Displacement Constraint.

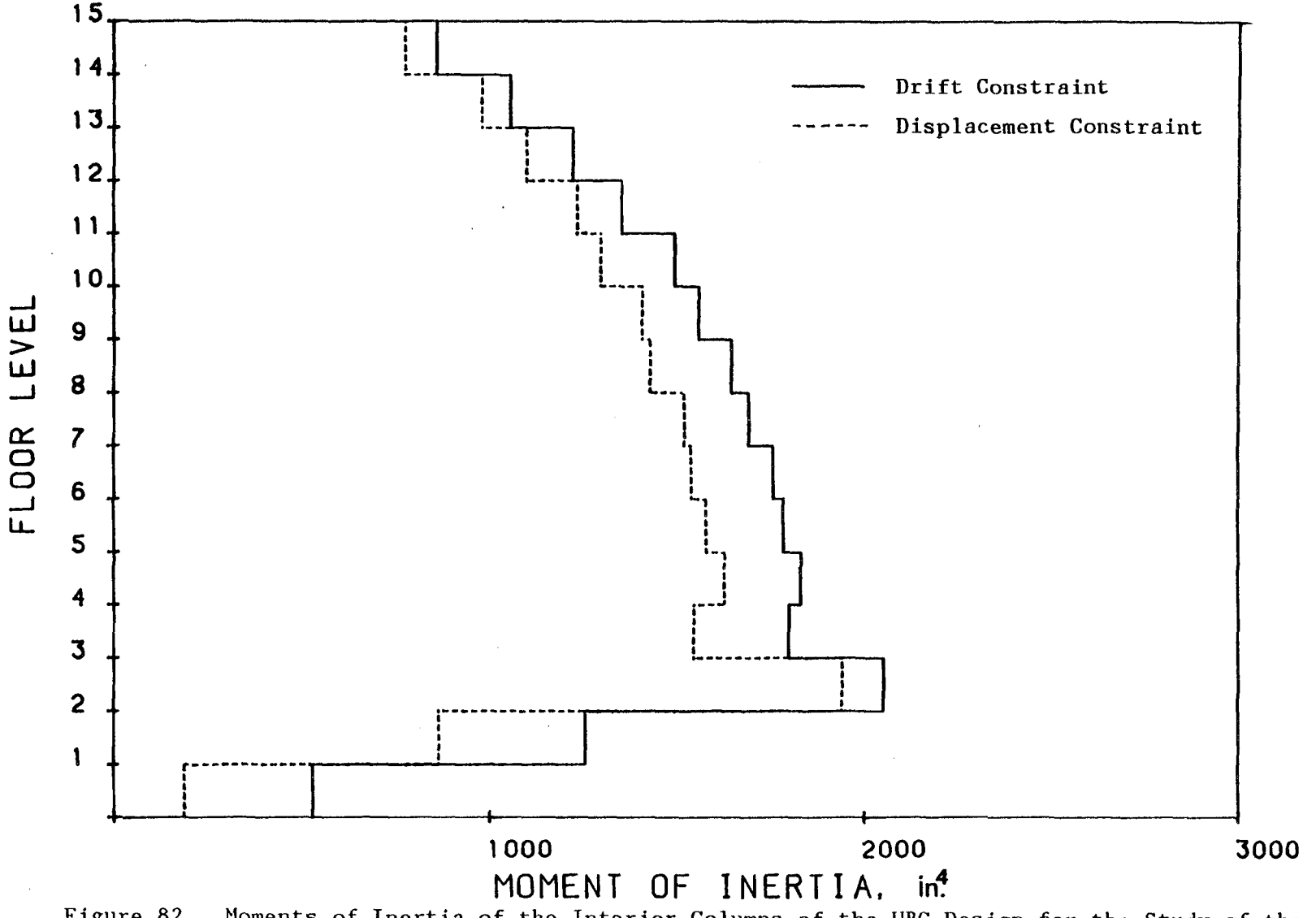

Figure 82. Moments of Inertia of the Interior Columns of the UBC Design for the Study of the Influence of Drift Constraint and Displacement Constraint. (1 in. = 2.54 cm).

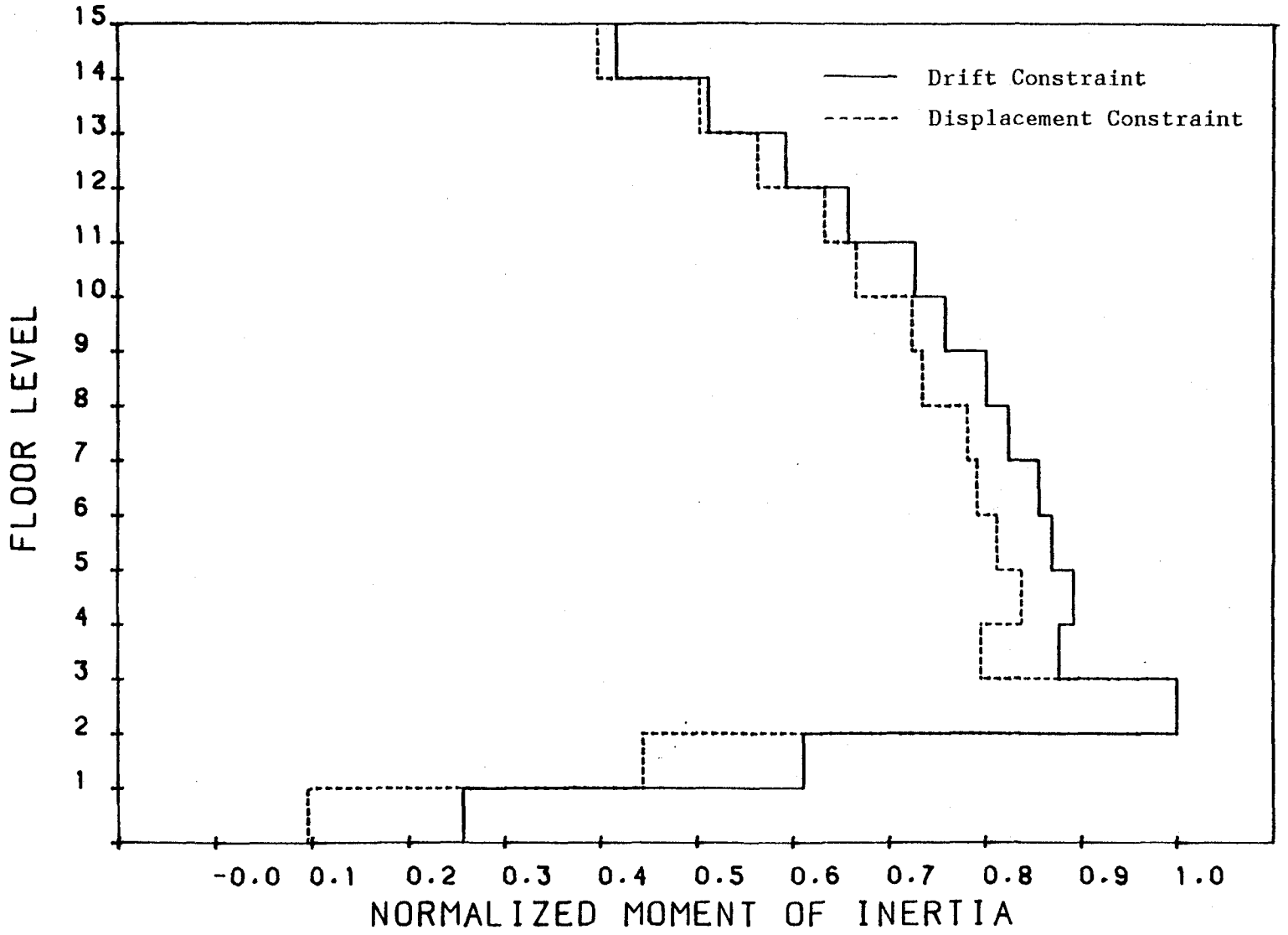

Figure 83. Normalized Moments of Inertia of the Interior Columns of the UBC Design for the Study of the Influence of Drift constraint and Displacement Constraint.

distributions of the moments of inertia of the girders and columns are similar for both cases, whereas the displacement constraint case requires smaller member sizes.

Similarly to the UBC design, the design which is based on the Chinese Code and uses the displacement constraints, requires less weight than that of the design that uses drift constraints. Figure 85 illustrates the weight versus cycles of iteration. The displacements of each floor level are shown in Figure 84. The displacement constraint case has a violated displacement at the top floor, but the story drift of the ninth story is 0.435 in. (1.105 cm), which exceeds allowable drift, 0.393 in. (0.999 cm). The plots of the shear envelopes, the moments of inertia, and the normalized moments of inertia of the girders and columns are shown in Figures 86 through 92 respectively. All these figures illustrate results similar to those discussed in the UBC design case.

The conclusion is that the design based on story drift requires a heavier design. In engineering practice, the restraint on the story drift is more important, because serious damage during an earthquake is mainly due to the collapse of columns that is brought on primarily by a large story drift.

H. THE EFFECT OF VARIOUS BRACINGS ON A SEISMIC DESIGN BASED ON ATC-3-06 ELF PROCEDURES

The fifteen-story, one-bay frame shown in Figure 21 was selected for this study. The five different bracing systems, which are classified as (a) single bracing, (b) double bracing, (c) K-bracing,

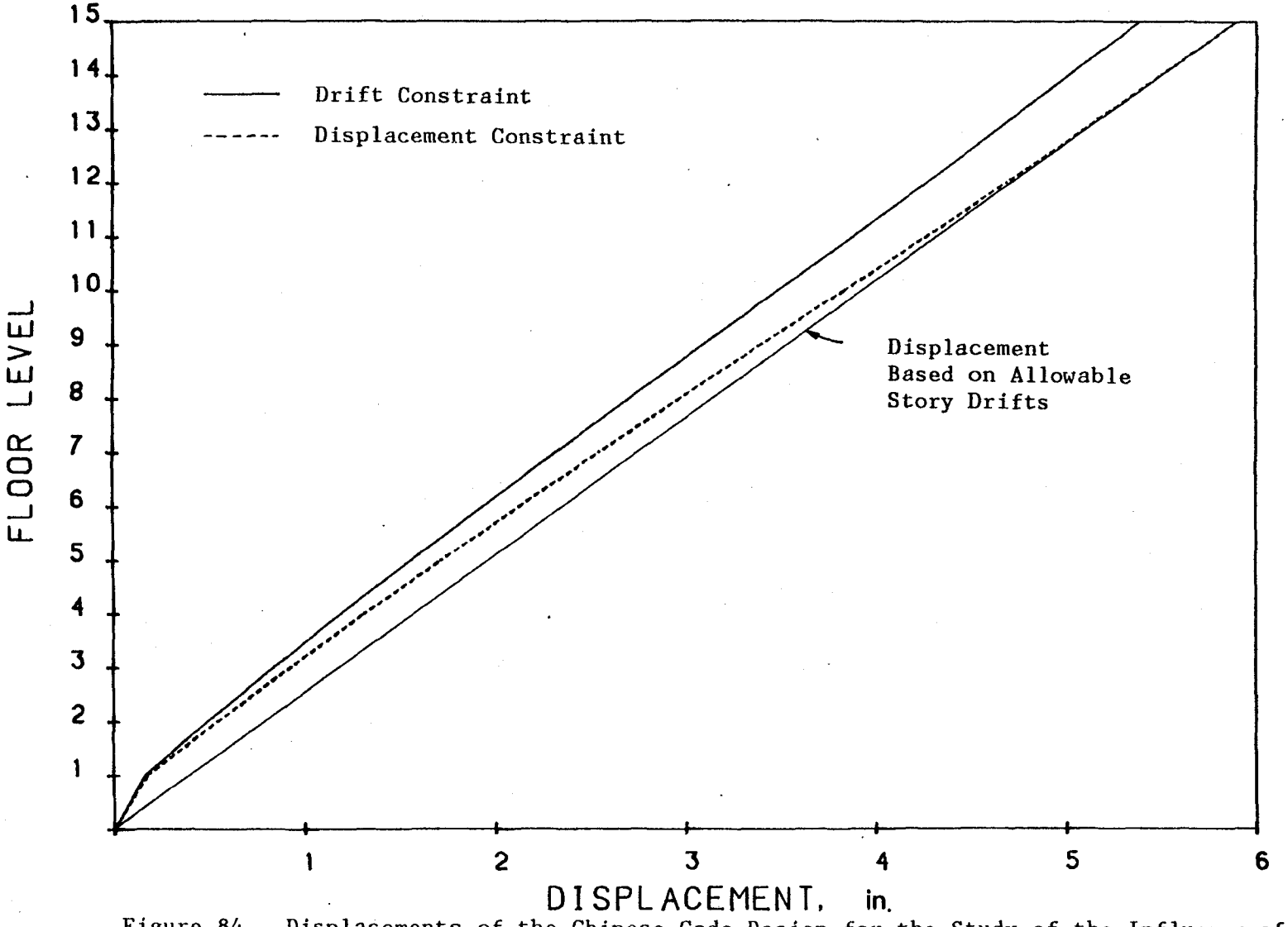

Figure 84. Displacements of the Chinese Code Design for the Study of the Influence of Drift Constraint and Displacement Constraint. (1 in. = 2.54 cm)

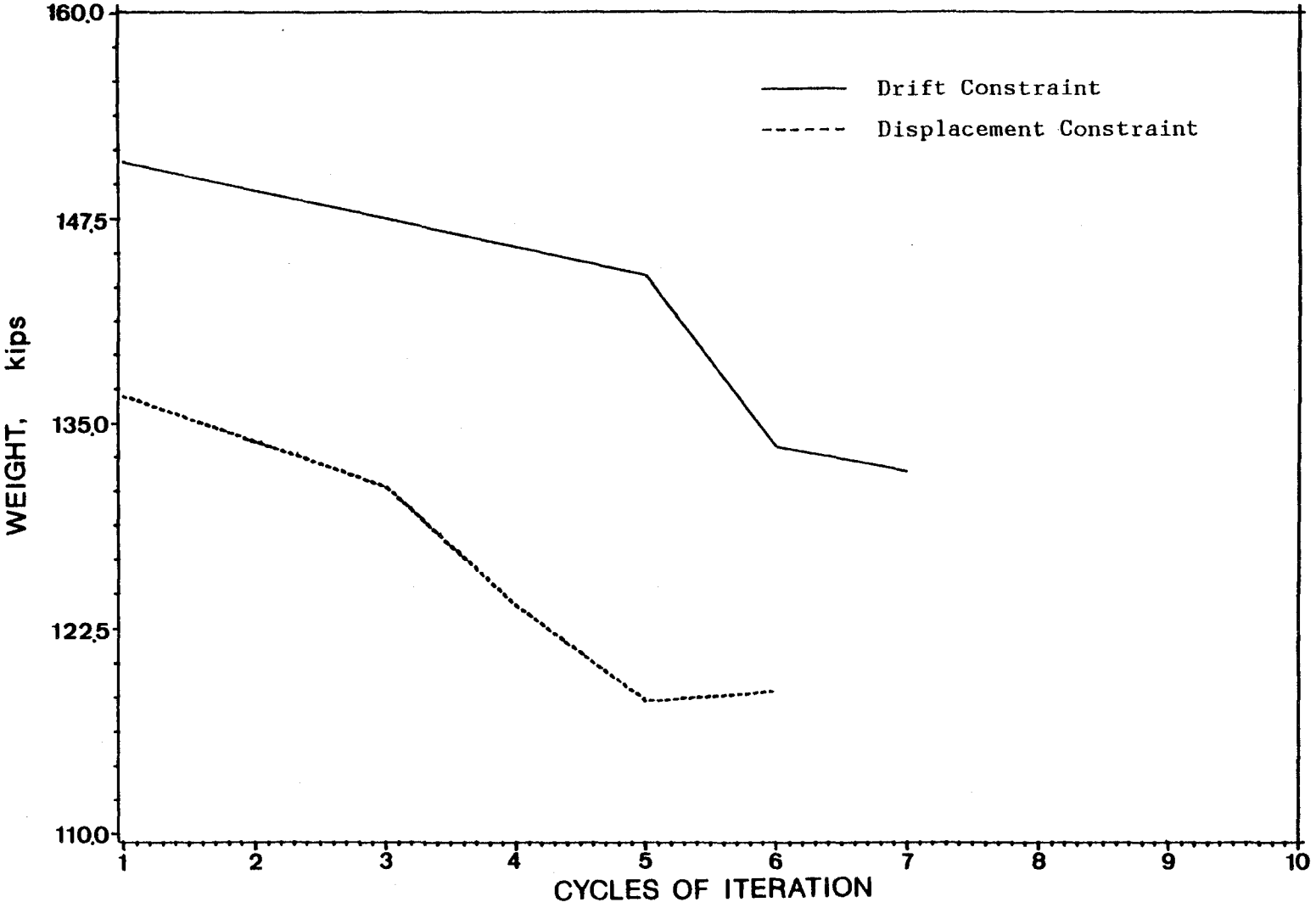

Figure 85. Weight v.s. Cycles of Iteration Plot of the Chinese Code Design for the Study of the Influence of Drift Constraint and Displacement Constraint. (1 kip = 4.448 kN)

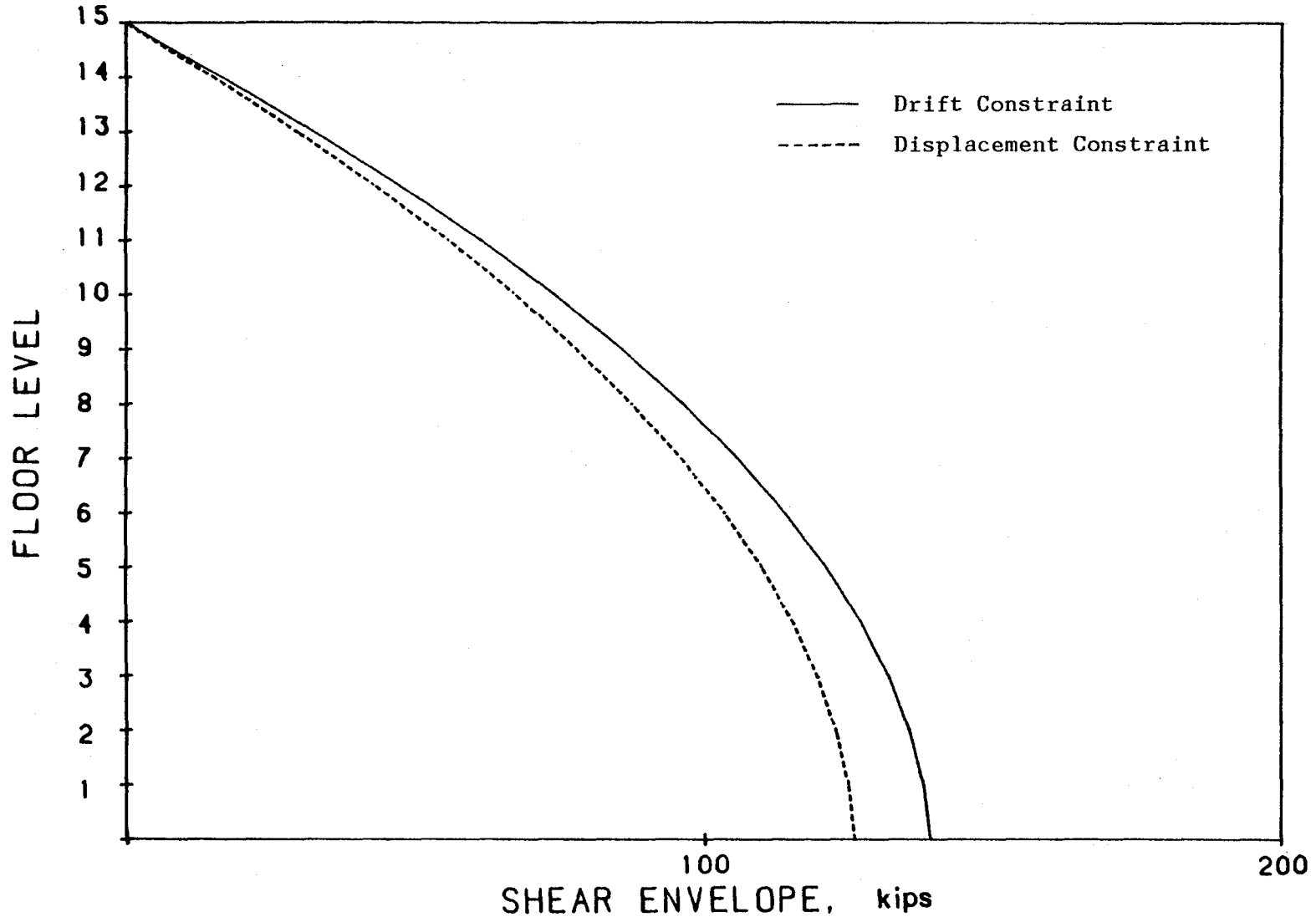

Figure 86. Shear Envelopes of the Chinese Code Design for the Study of the Influence of Drift Constraint and Displacement Constraint. (1 kip = 4.448 kN)

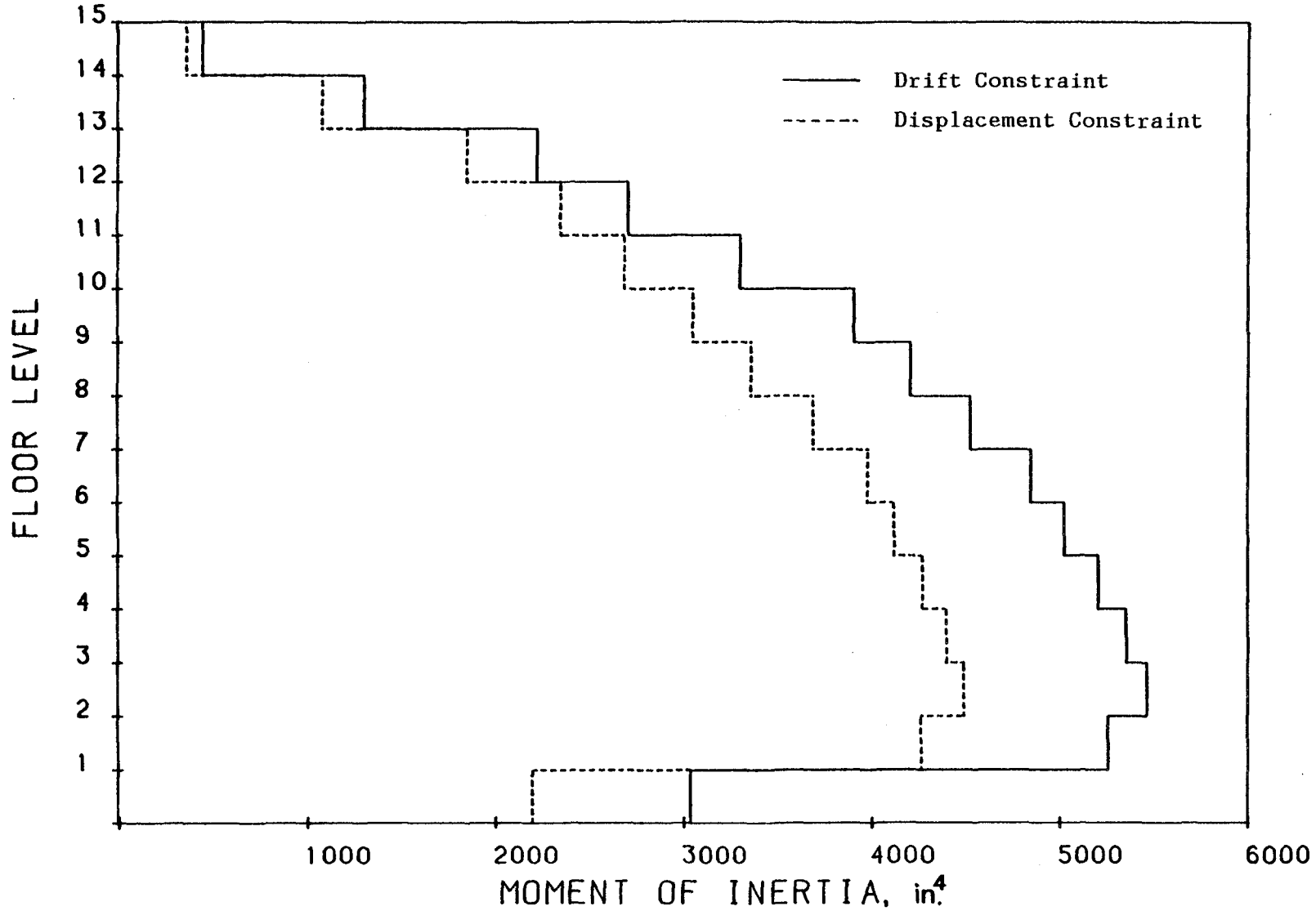

Figure 87. Moments of Inertia of the Girders of the Chinese Code Design for the Study of the Influence of Drift Constraint and Displacement Constraint. (1 in. = 2.54 cm).

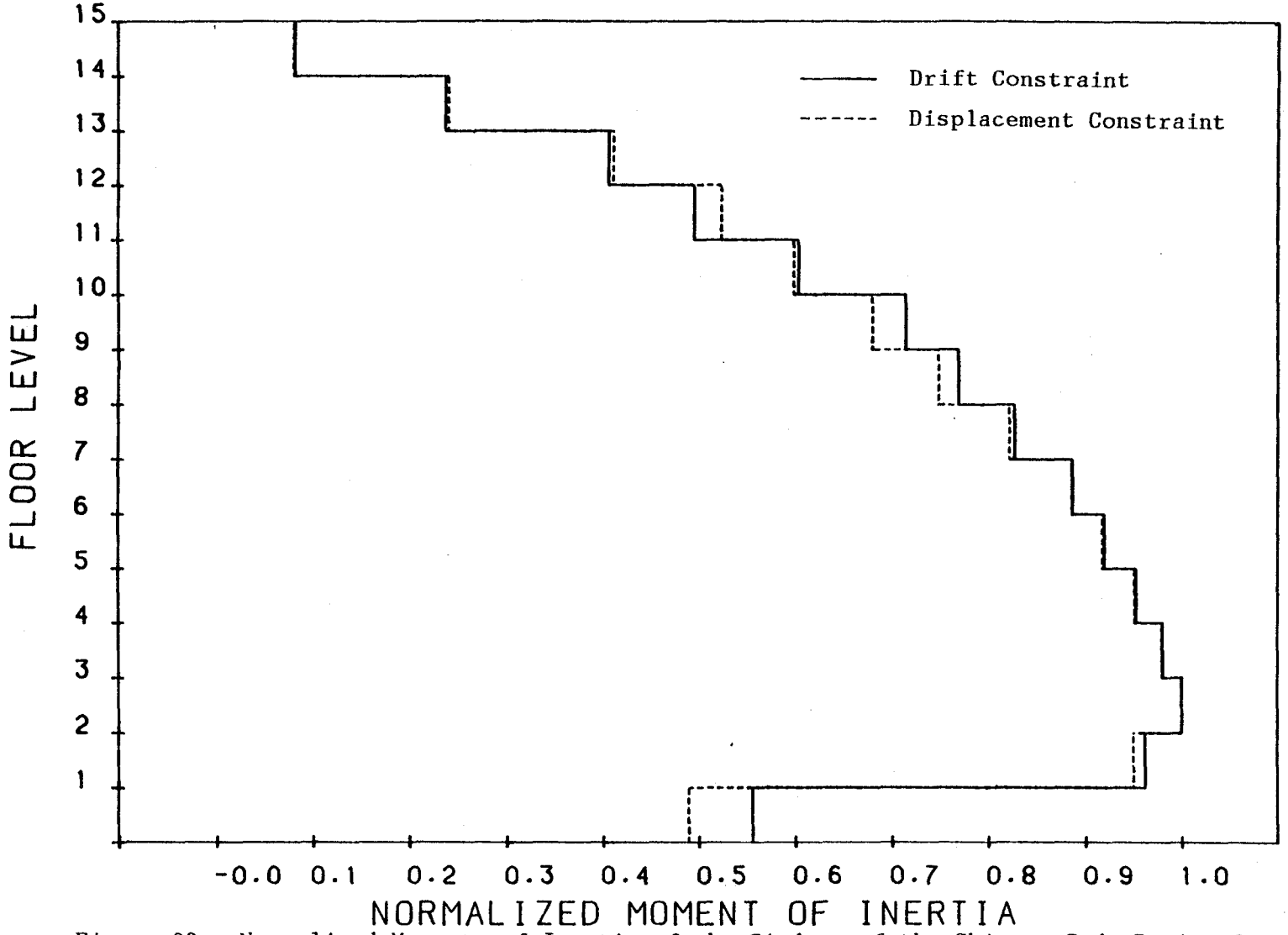

Figure 88. Normalized Moments of Inertia of the Girders of the Chinese Code Design for the Study of the Influence of Drift Constraint and Displacement Constraint.

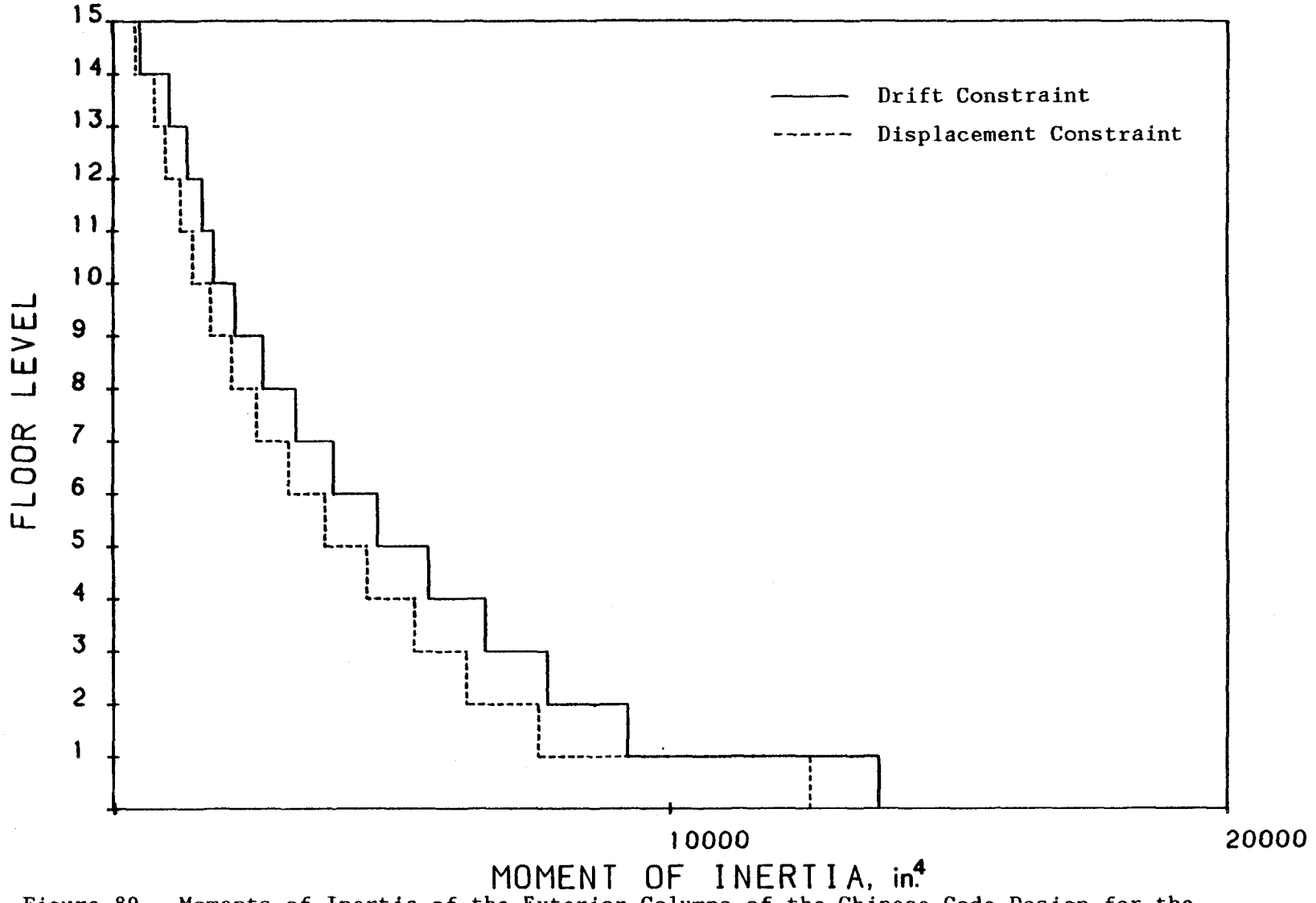

Figure 89. Moments of Inertia of the Exterior Columns of the Chinese Code Design for the Study of the Influence of Drift Constraint and Displacement Constraint. (1 in. = 2.54 cm).

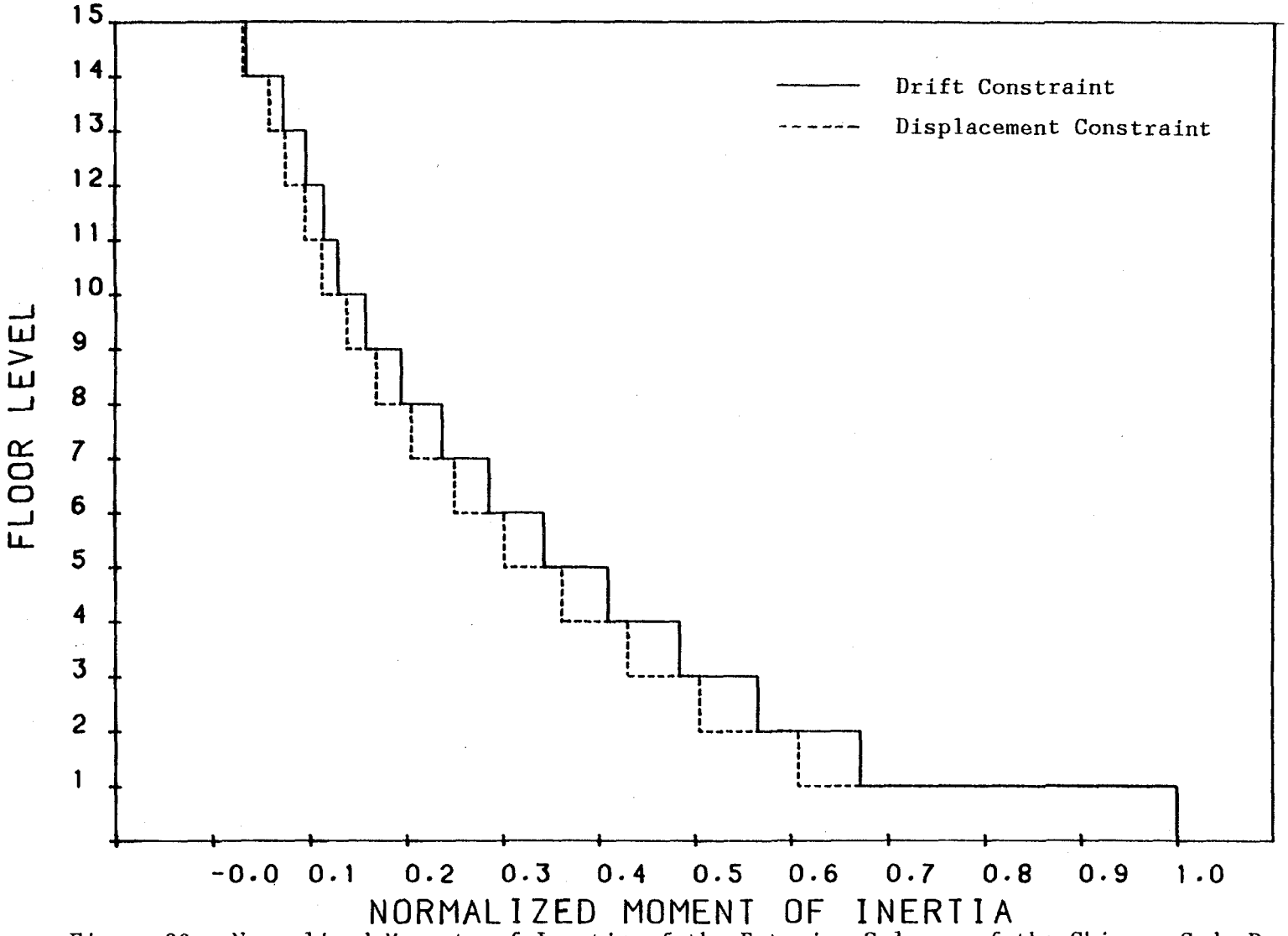

Figure 90. Normalized Moments of Inertia of the Exterior Columns of the Chinese Code Design for the Study of the Influence of Drift Constraint and Displacement Constraint.

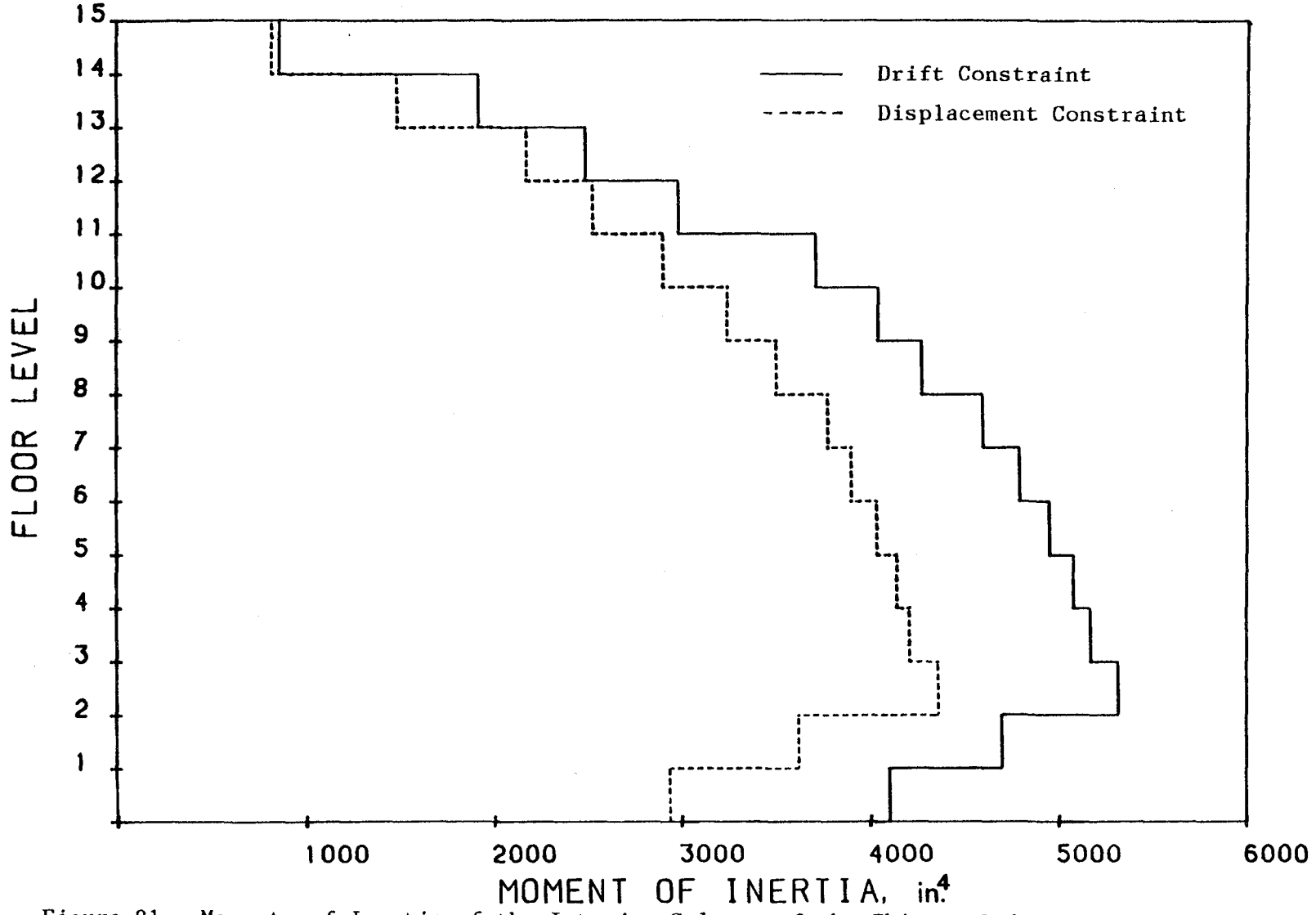

Figure 91. Moments of Inertia of the Interior Columns of the Chinese Code Design for the Study of the Influence of Drift Constraint and Displacement Constraint. (1 in. = 2.54 cm).

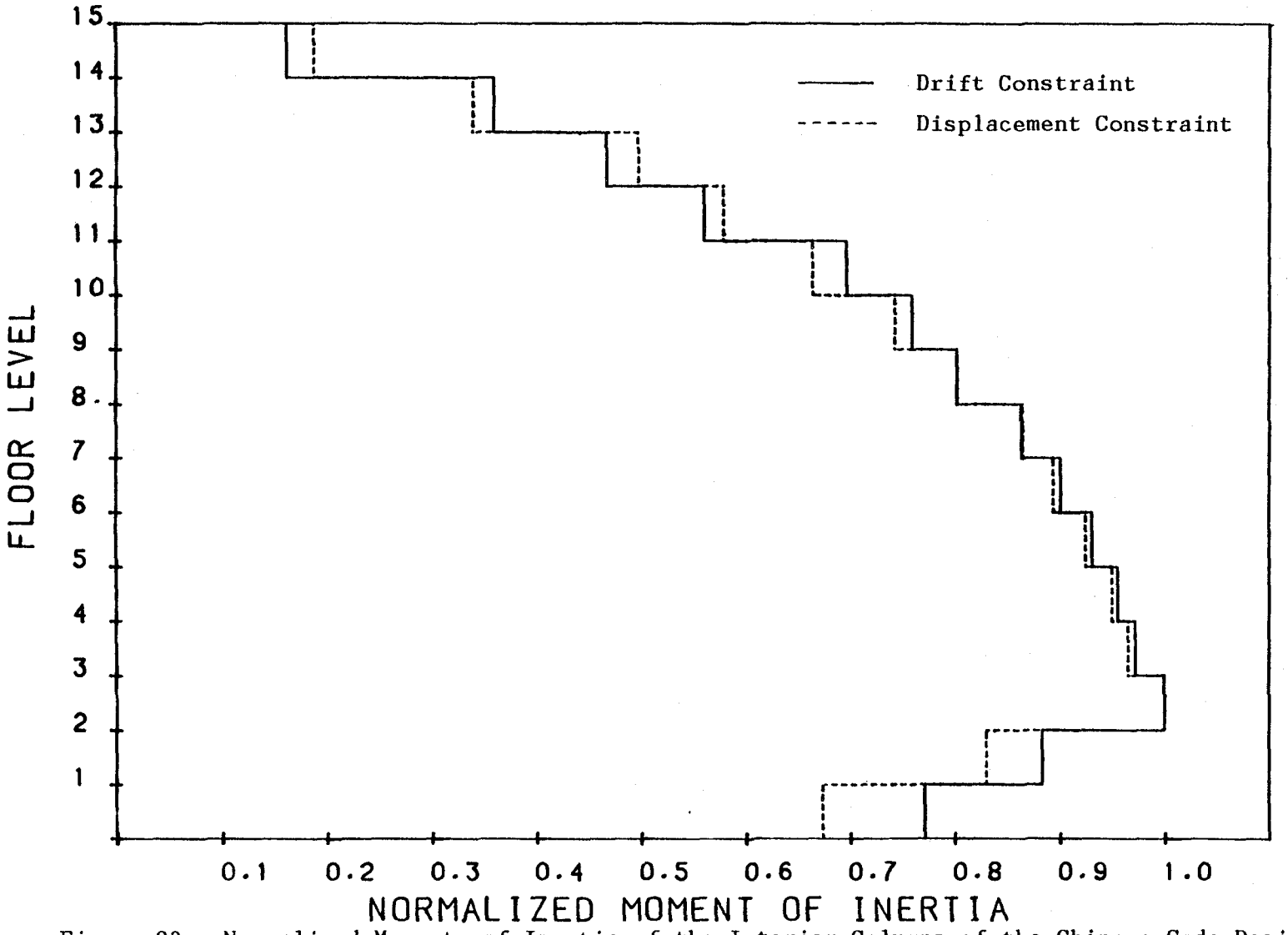

Figure 92. Normalized Moments of Inertia of the Interior Columns of the Chinese Code Design for the Study of the Influence of Drift Constraint and Displacement Constraint.

(d) eccentric K-bracing, and (e) eccentric double bracing and are shown in Figure 93, were used to design this structure for a map area of A_a=7, A_v=7, and soil type 3 associated with R=6 and C_d=5. The design loadings and the allowable story drift are the same as those used in Section VI.B.

Table XVI shows the fundamental period, eccentricity, maximum stability coefficient, the number of stories having maximum drift, and the final weight of each bracing system. All the fundamental periods of these five bracing systems exceed the upper bound, $1.2T_a$=1.493 sec. Based on the experience learned from Section VI.B, the fundamental period corresponds to areas with different A_a's, A_v's, and the soil profile types also exceed $1.2T_a$. Therefore, $1.2T_a$ will control the design no matter what values of A_a, A_v, and soil type are considered. Therefore, the seismic design coefficient, C_s, corresponds to each different combination of A_a and A_v, and the soil type can be easily detetermined. Figure 94 illustrates the seismic design coefficients of these five bracing systems when A_a is changed as 1, 3, 5, and 7, when A_v is changed as 3, 5, and 7, and the soil types are varied from 1, 2 and 3.

As shown in Table XVI, the maximum stability coefficients are all less than the upper bound of 0.1. The stability coefficient of each floor level is plotted in Figure 95. Figure 96 represents the plot of the weight versus cycles of iteration. The model (c) has the least weight, and the model (d) is the heaviest.

The moments of inertia and the normalized moments of inertia of the girders and columns are respectively shown in Figures 97, 98, 99,

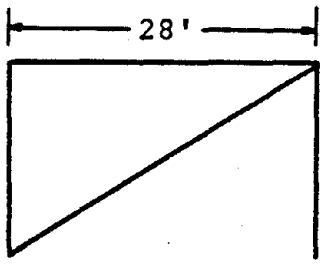

(a) Single Bracing

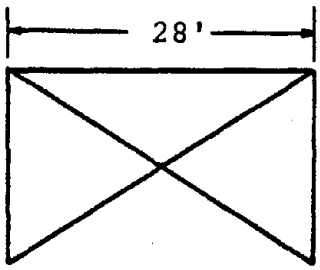

(b) Double Bracing

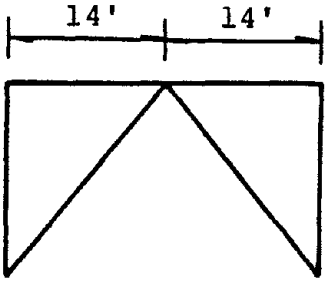

(c) K-Bracing

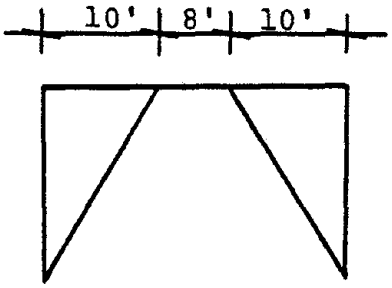

(d) Eccentric K-Bracing

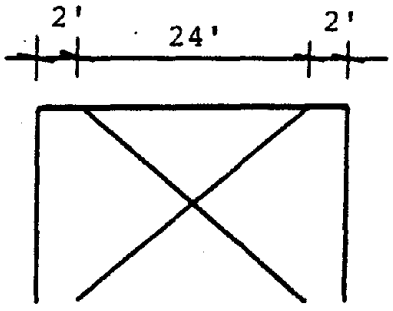

(e) Eccentric Double Bracing

Figure 93. Various Bracing Systems Used in the Design of 15-Story, One-Bay, Braced Frame Based on the ATC-3-06 ELF Procedures

Table XVI. THE DESIGN RESULTS OF VARIOUS BRACING SYSTEMS BASED ON THE ATC-3-06 ELF PROCEDURES. (1 ft = 0.3048 m, 1 kip = 4.448 kN)

	Bracing Type				
	Model (a)	Model (b)	Model (c)	Model (d)	Model (e)
Fundamental Period (sec)	1.7678	1.5935	1.5765	1.7115	1.5784
Eccentricity (ft)	8.248	8.763	8.819	8.412	8.809
Stability Coefficient	0.01358	0.00903	0.00868	0.01148	0.00805
No. of Story with Max Drift	12	13	13	12	14
Final Weight (kips)	43.38	35.06	33.01	46.98	41.25

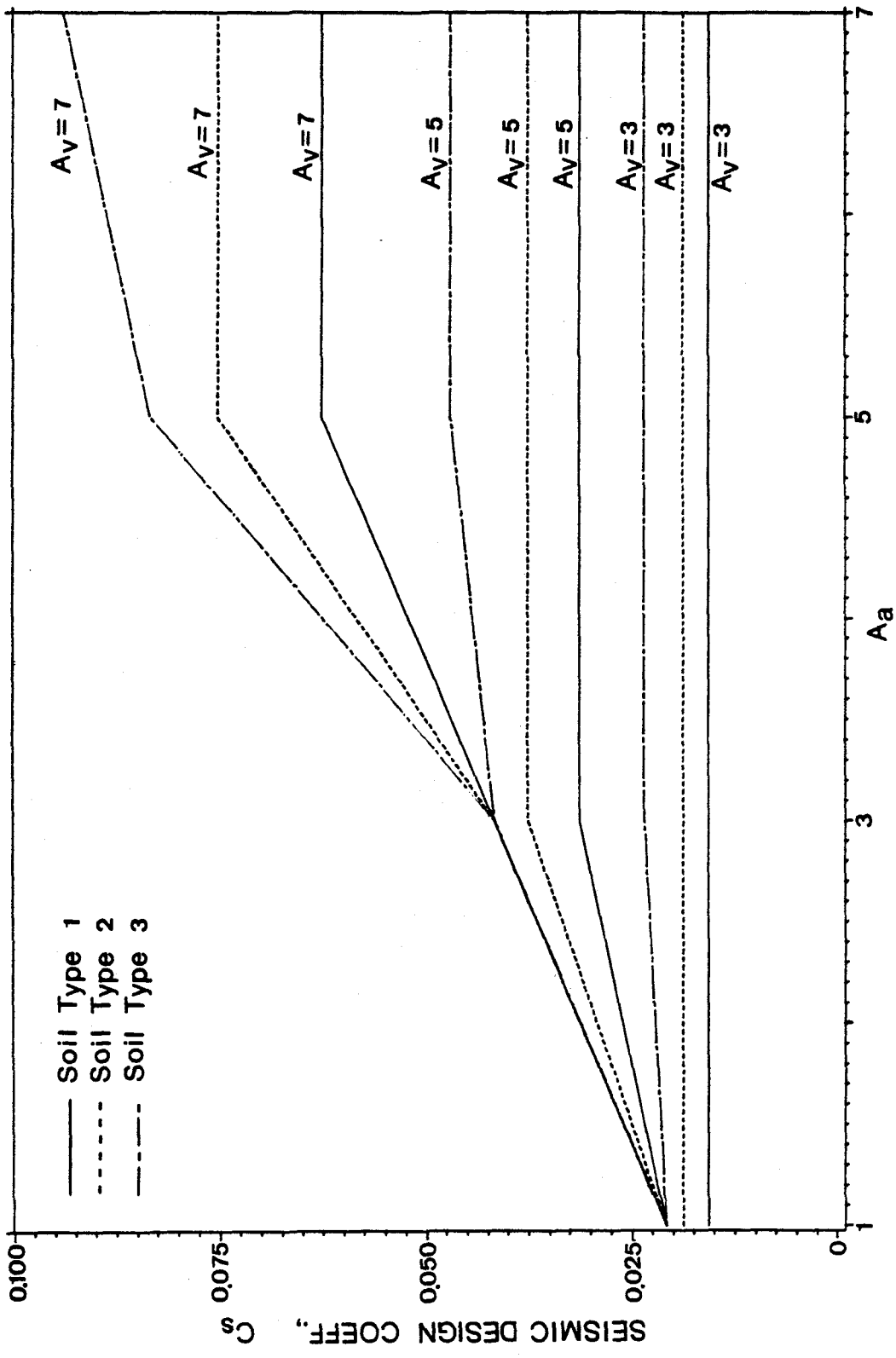

Figure 94. Seismic Design Coefficients of Braced Frames.

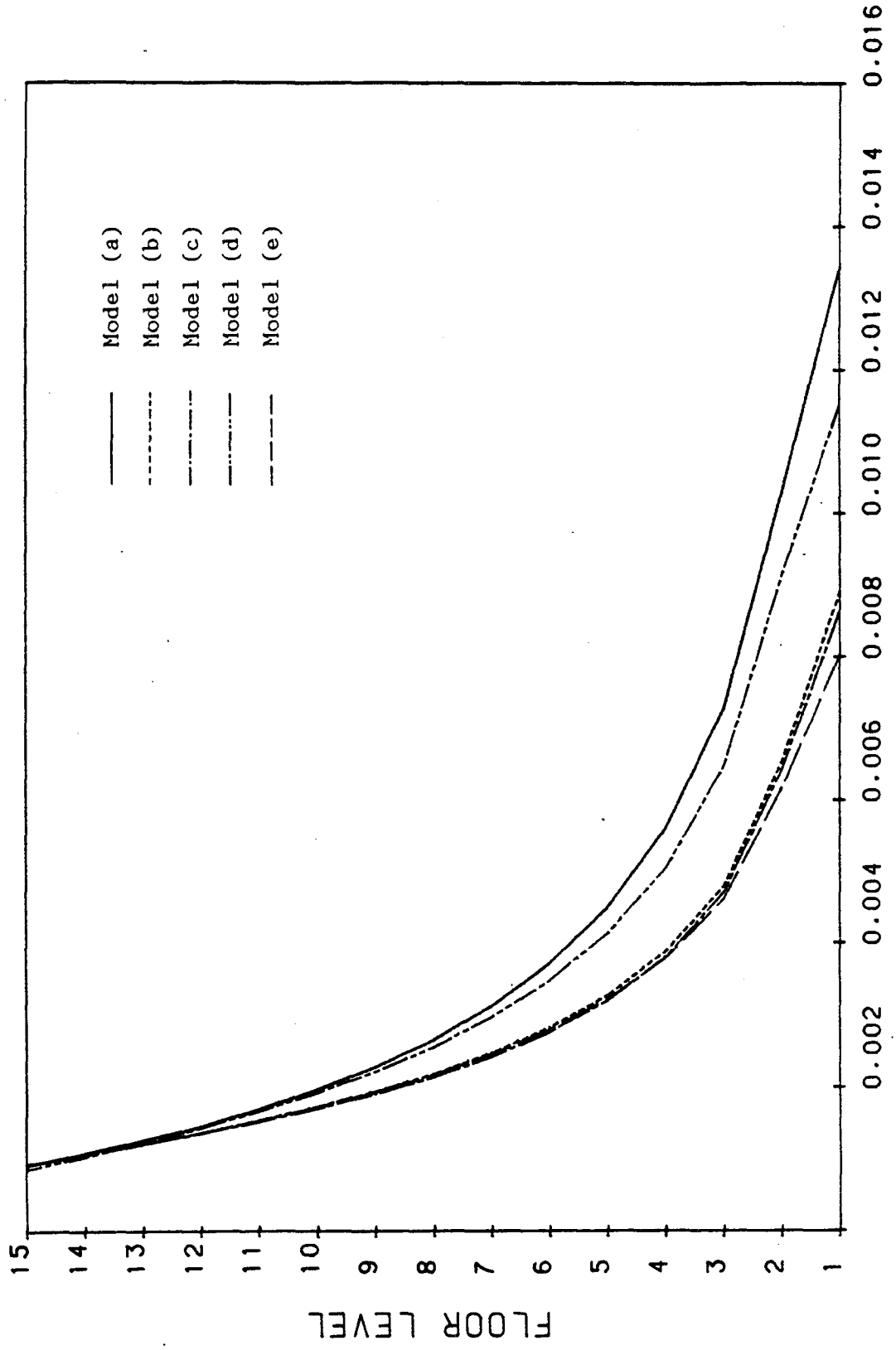

Figure 95. Stability Coefficients of the Braced Frames.

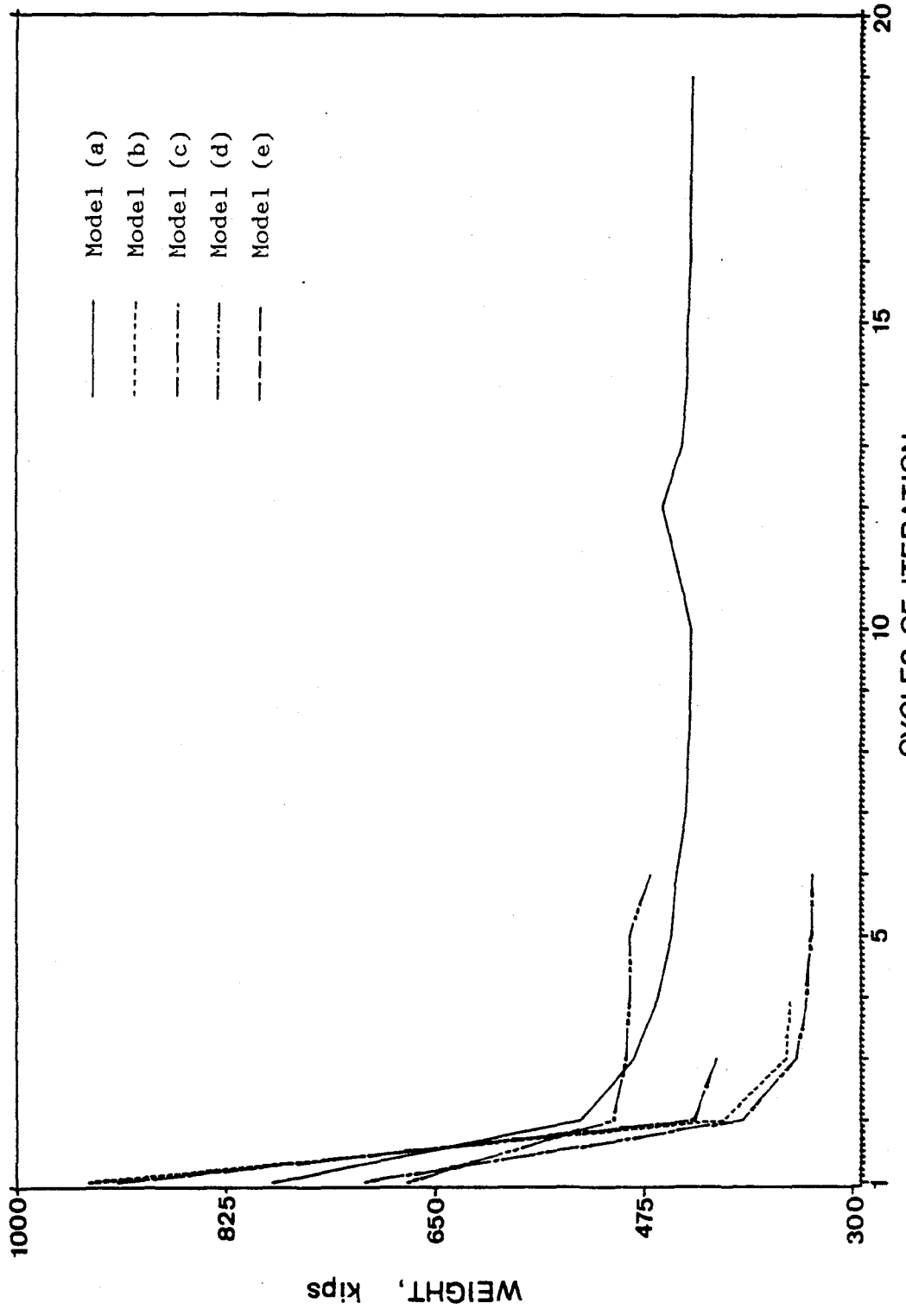

Figure 96. Weight v.s. Cycles of Iteration Plot of the Braced Frames. (1 kip = 4.448 kN)

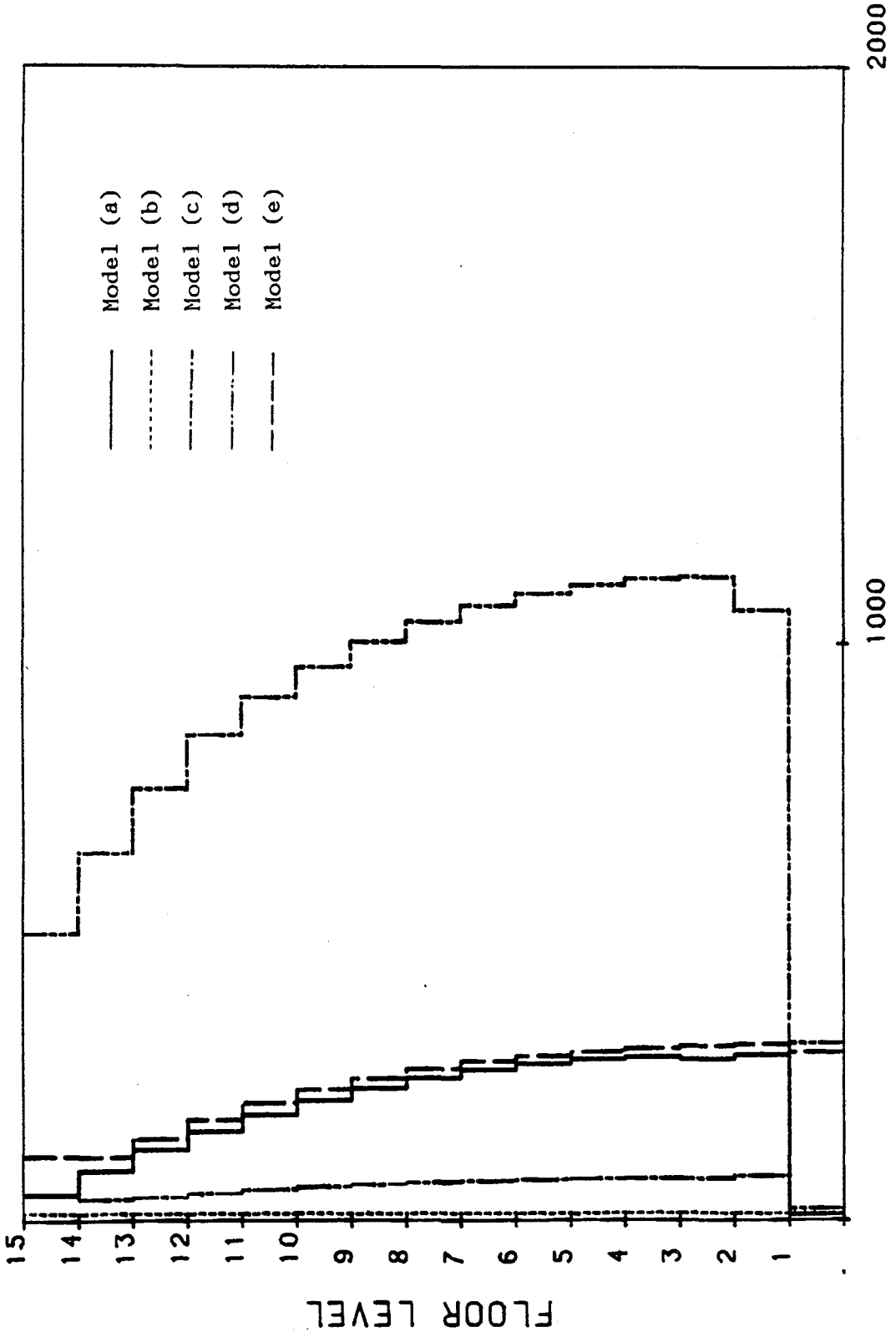

Figure 97. Moments of Inertia of the Girders of the Braced Frames. (1 in. = 2.54 cm).

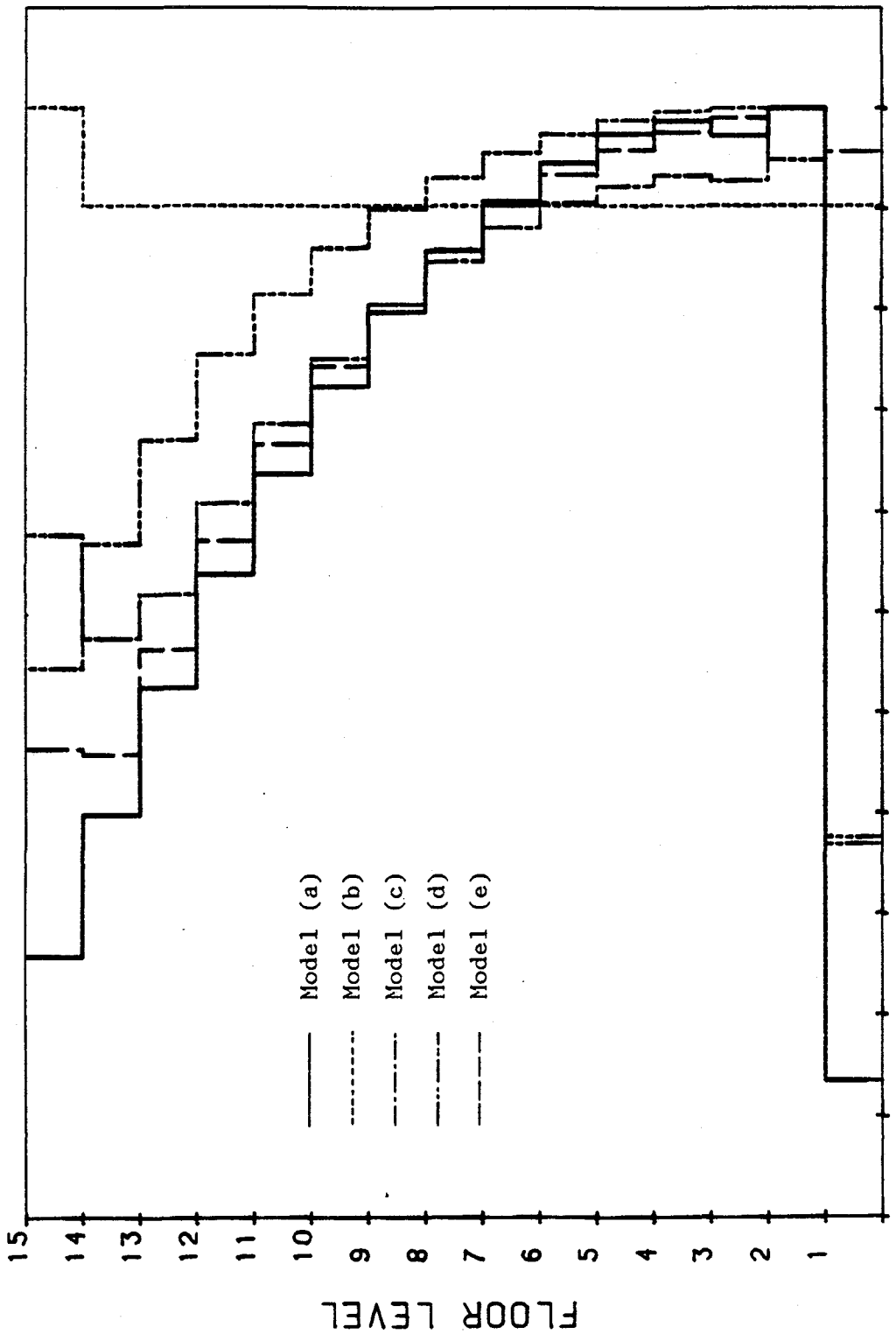

Figure 98. Normalized Moments of Inertia of the Girders of the Braced Frames.

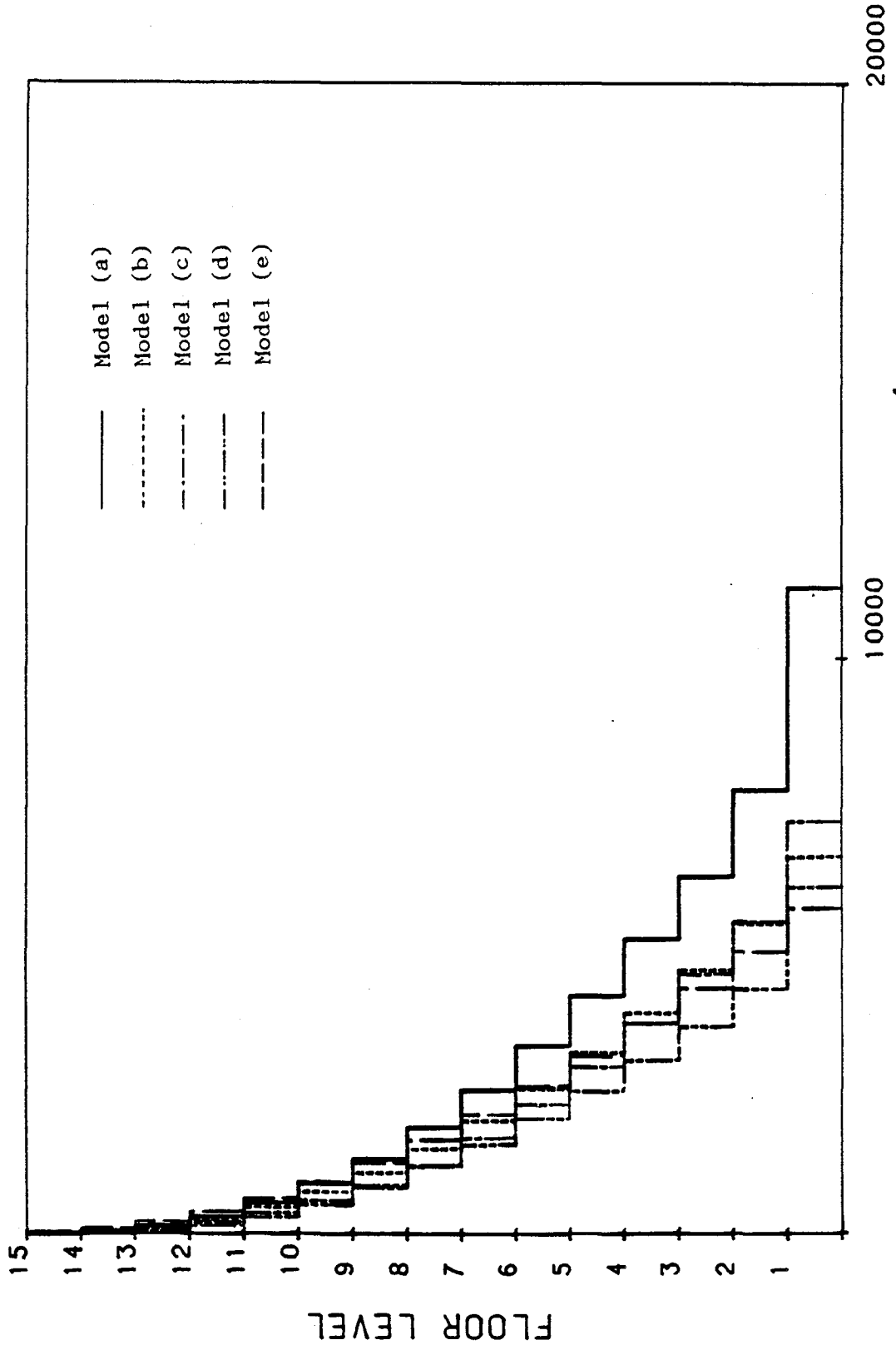

Figure 99. Moments of Inertia of the Columns of the Braced Frames. (1 in. = 2.54 cm).

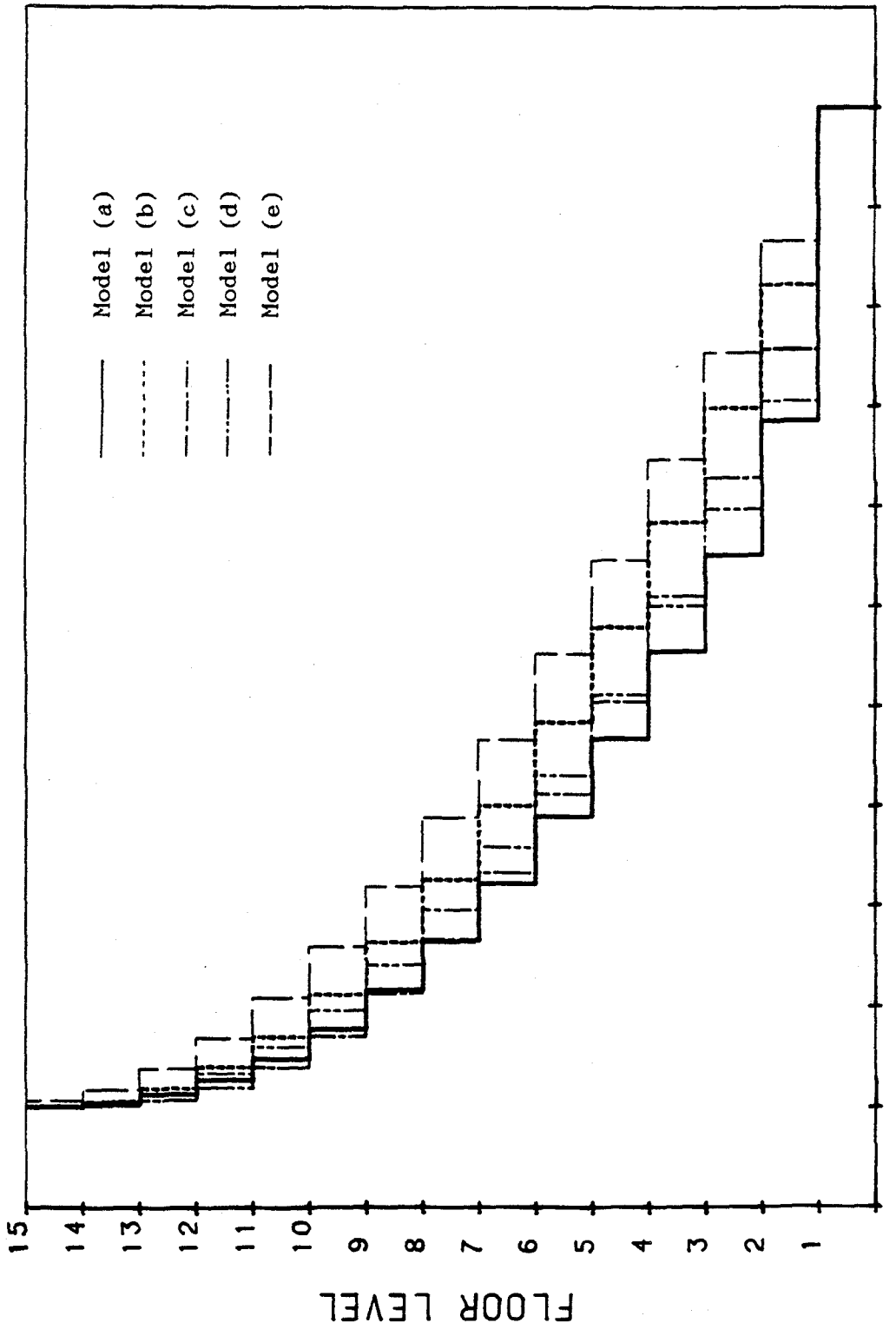

Figure 100. Normalized Moments of Inertia of the Columns of the Braced Frames.

and 100. Figures 101 and 102 illustrate the cross sectional areas and the normalized areas of bracings respectively. For model (a), there is only one bracing to resist longitudinal forces, thus it requires larger columns. On the other hand, the model (d) can provide a better resistance to the longitudinal forces because of the larger angle between the brace and girder, thus smaller columns are required. However, model (d) is worse than other bracing systems in resisting lateral forces, thus larger girders are required. As shown in Figure 97, there are relatively smaller moments of inertia for the girders than for the columns for almost all the bracing systems.

The shear envelopes and the displacement at each floor level are respectively sketched in Figures 103 and 104. The design is actually terminated, because the allowable story drift is violated before the allowable displacements are reached.

I. WIND DESIGN BASED ON UBC AND POWER LAW REQUIREMENTS

The building shown in Figure 41 was assumed to be located in an area where the basic wind speed, v_{30}, was 110 mph (177 km/h). In order to determine the wind forces according to the power law, the gradient height, h_g, for open country at an elevation of 900 feet (274.3 m) was also assumed. The power law coefficient, γ, was selected from Table IX as 1/7. The external pressure coefficient was 0.9 for a windward wall and -0.6 for a leeward wall.

To determine the wind forces in accordance with UBC provisions, a wind pressure of 31 psf (1.48 kN/m^2) corresponding to 110 mph (177 km/hr.) basic wind speed was used. The site condition of exposure

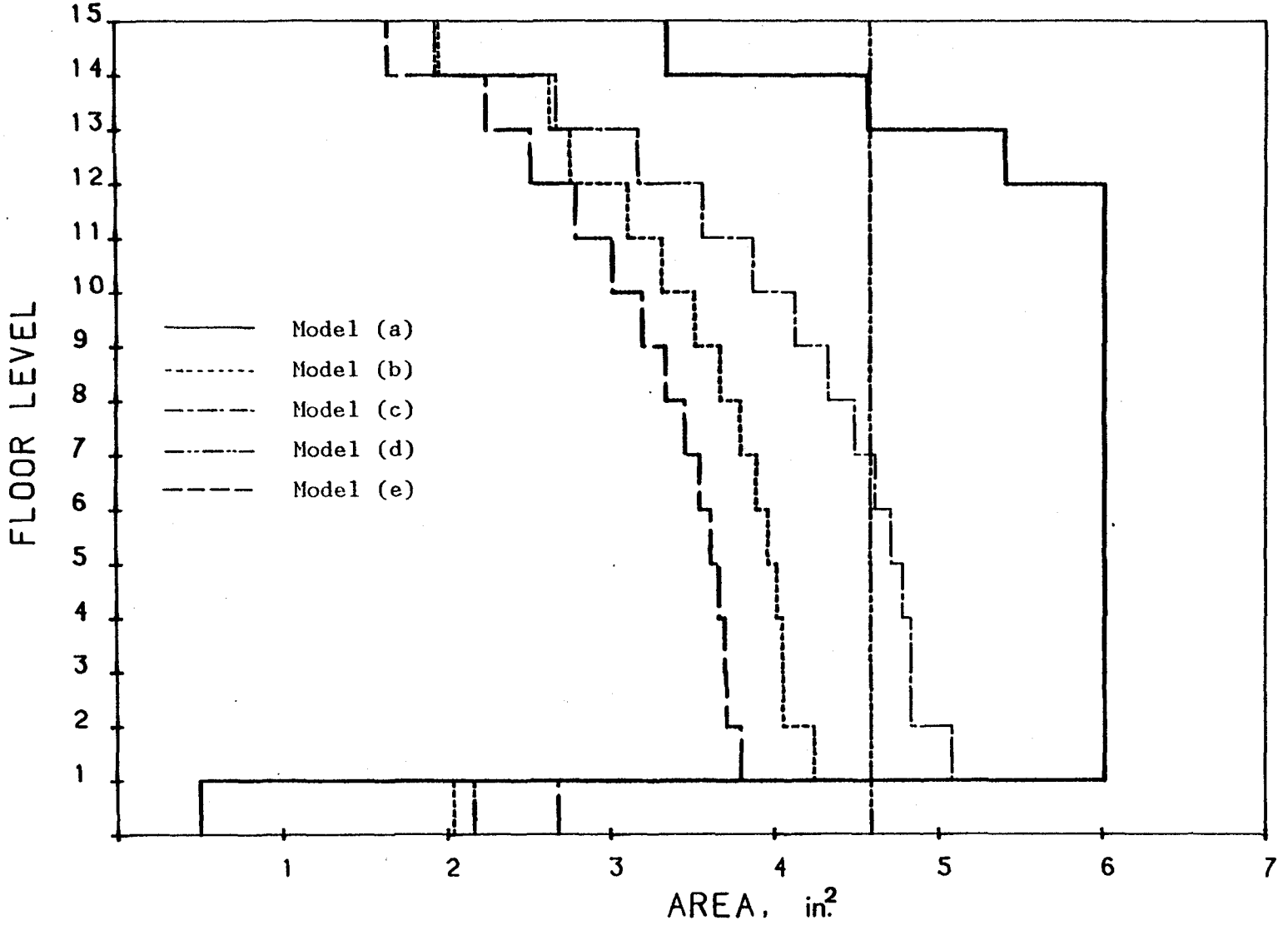

Figure 101. Cross-Sectional Areas of the Bracings of the Braced Frames. (1 in. = 2.54 cm).

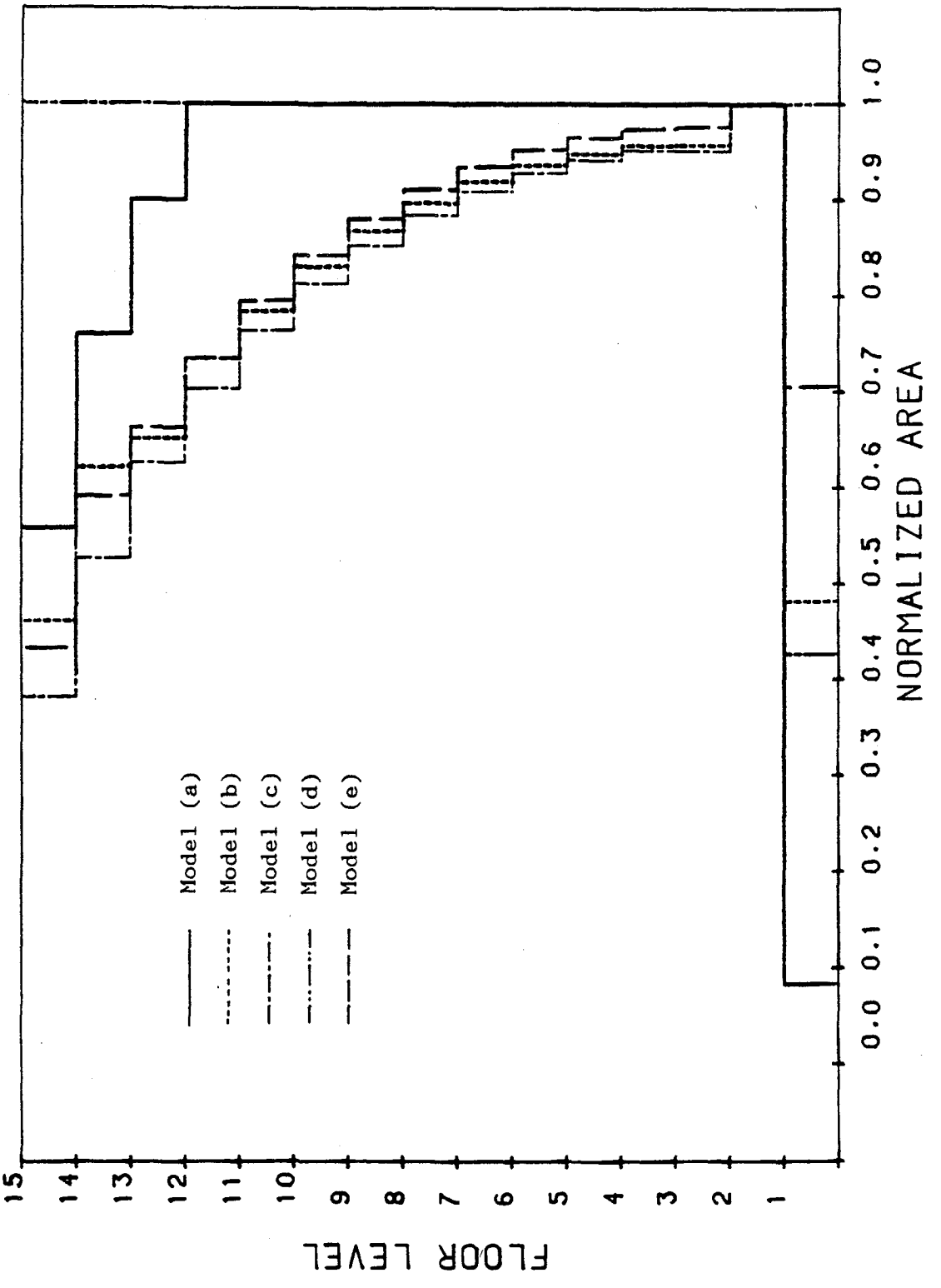

Figure 102. Normalized Cross-Sectional Areas of the Bracings of the Braced Frames.

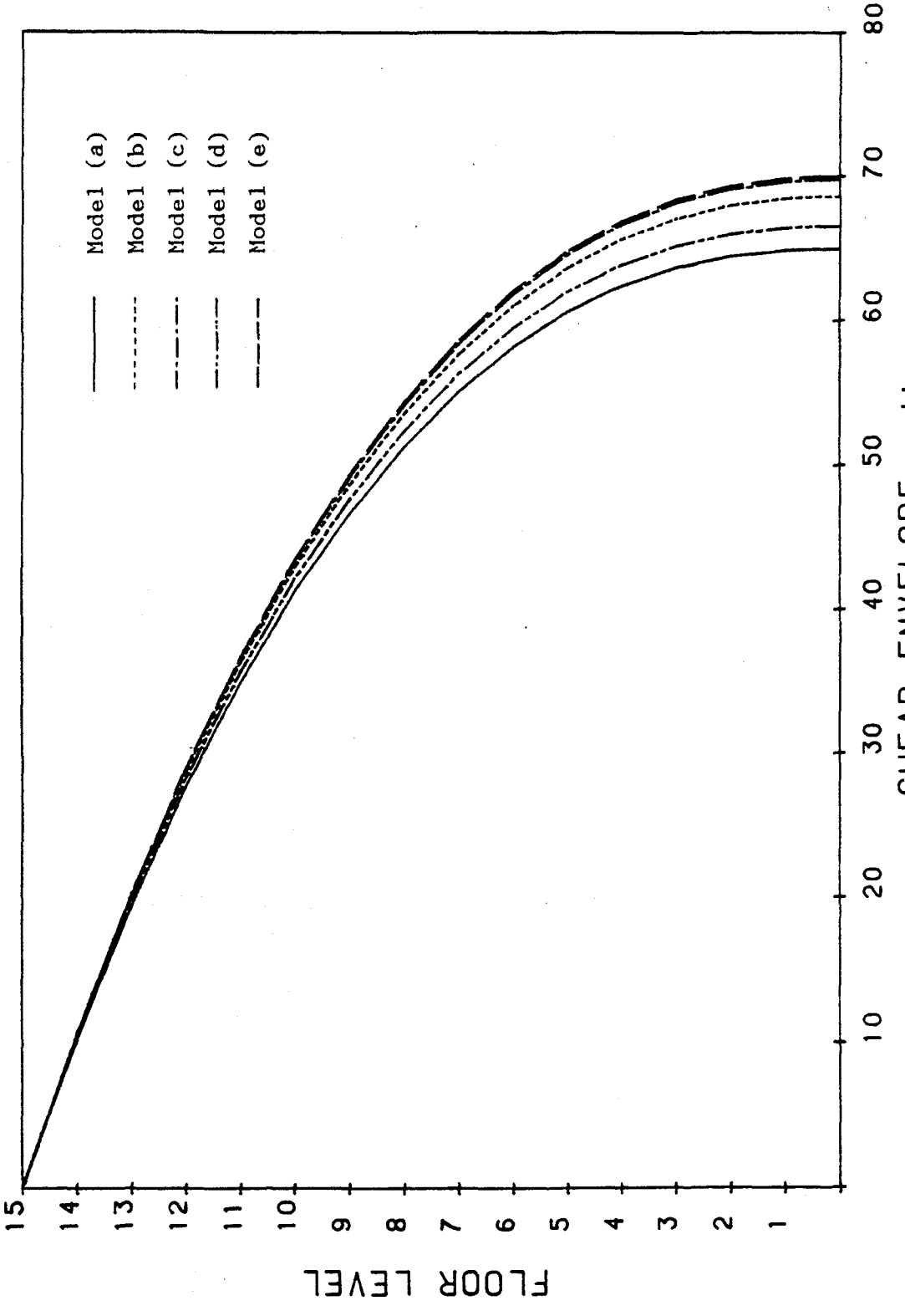

Figure 103. Shear Envelopes of the Braced Frames. (1 kip = 4.448 kN).

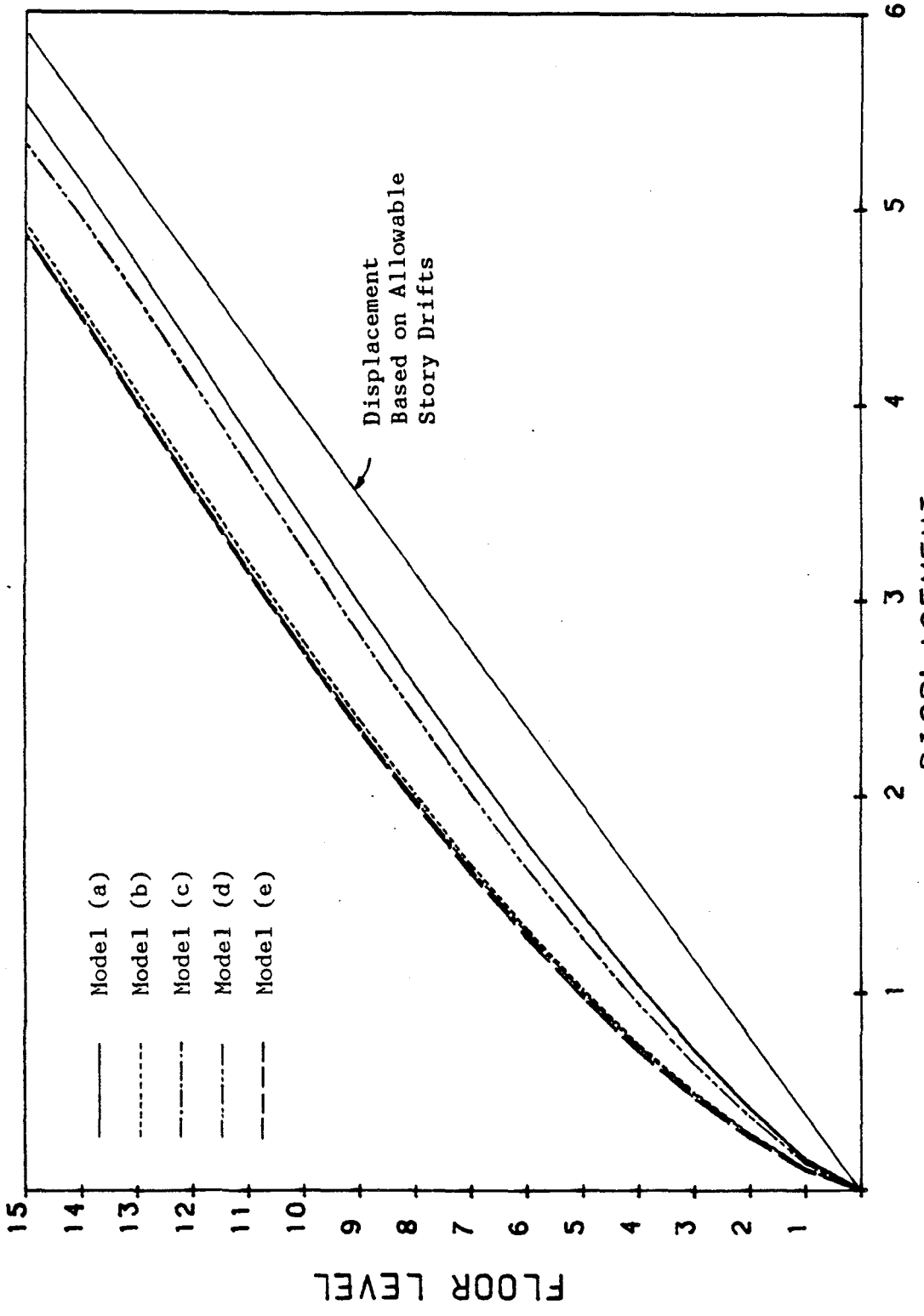

Figure 104. Displacements of the Braced Frames. (1 in. = 2.54 cm).

C corresponds with open country, and the importance factor, I, was taken to be 1.15 for an essential building. The wind pressure was determined by using the normal force method, and an allowable drift of $0.005h_{sx}$ was considered for both design cases.

Figures 105 through 113 depict the design results. As shown in Figure 105, for the first four cycles of iteration, the design, as based on the UBC provisions, is heavier than the design based on the power law, but the final design is lighter. The two shear envelopes, as illustrated in Figure 106, from the sixth floor to the top floor, almost coincide with each other, but the difference between the two envelopes gradually increases from sixth floor to the first. This difference is mainly due to the fact that the wind pressure according to UBC is assumed to be uniformly distributed throughout the height of the building; however, the power law yields a parabolically distributed wind pressure along the height.

The moments of inertia and the normalized moments of inertia of the girders are plotted in Figures 107 and 108 respectively. Figures 109 through 112 respectively illustrate the distribution of the moments of inertia and the normalized moments of inertia of exterior columns and interior columns.

The lateral displacements are shown in Figure 113. The 14th story has the violated drift for the design based on the power law and the drift of the eighth story is violated for the UBC wind design.

Apparently, the wind force determined on the basis of the UBC requirements is close to that determined on the basis of the power law.

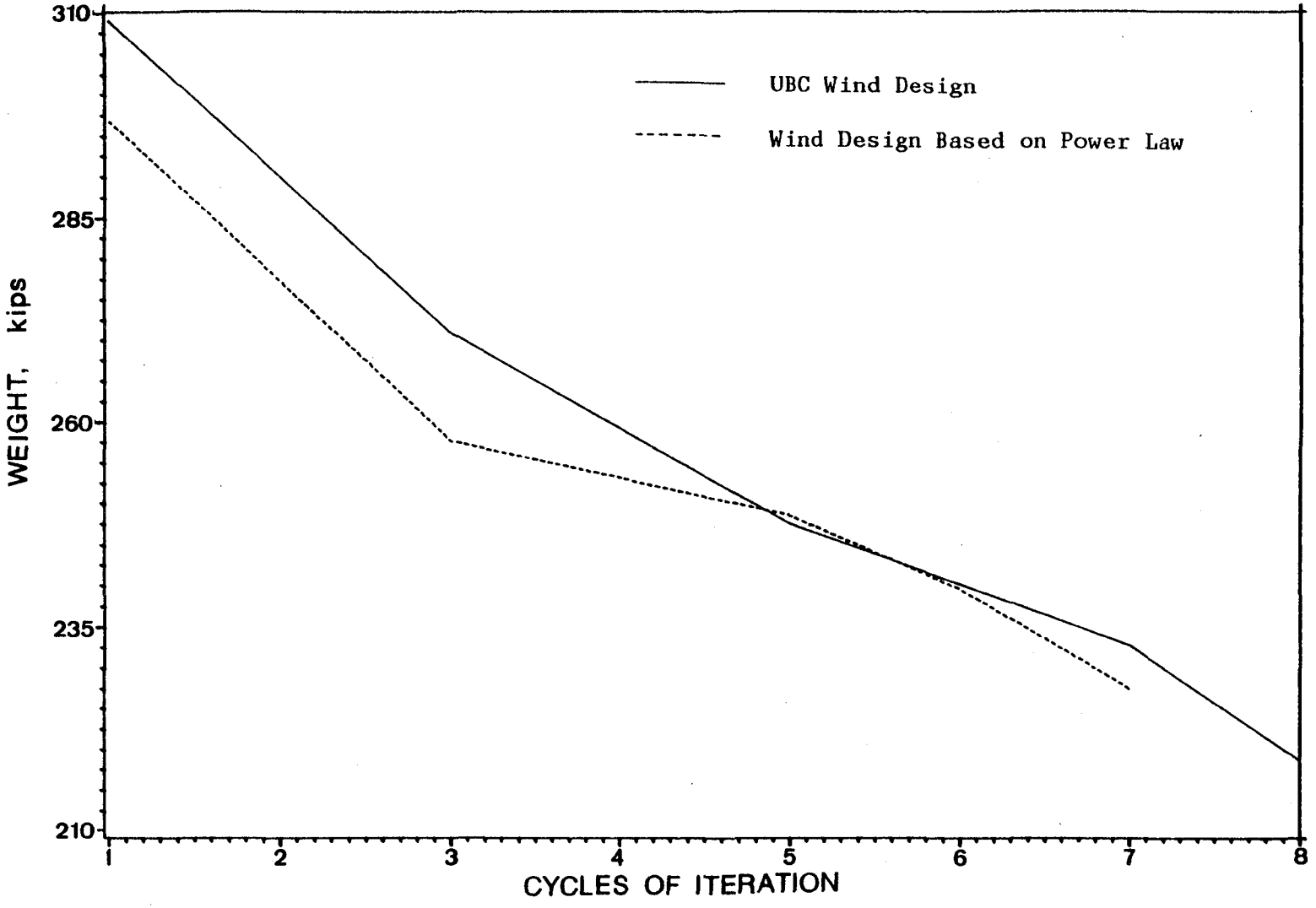

Figure 105. Weight v.s. Cycles of Iteration Plot of the 15-Story, Two-Bay Frame Wind Designs.
(1 kip = 4.448 kN)

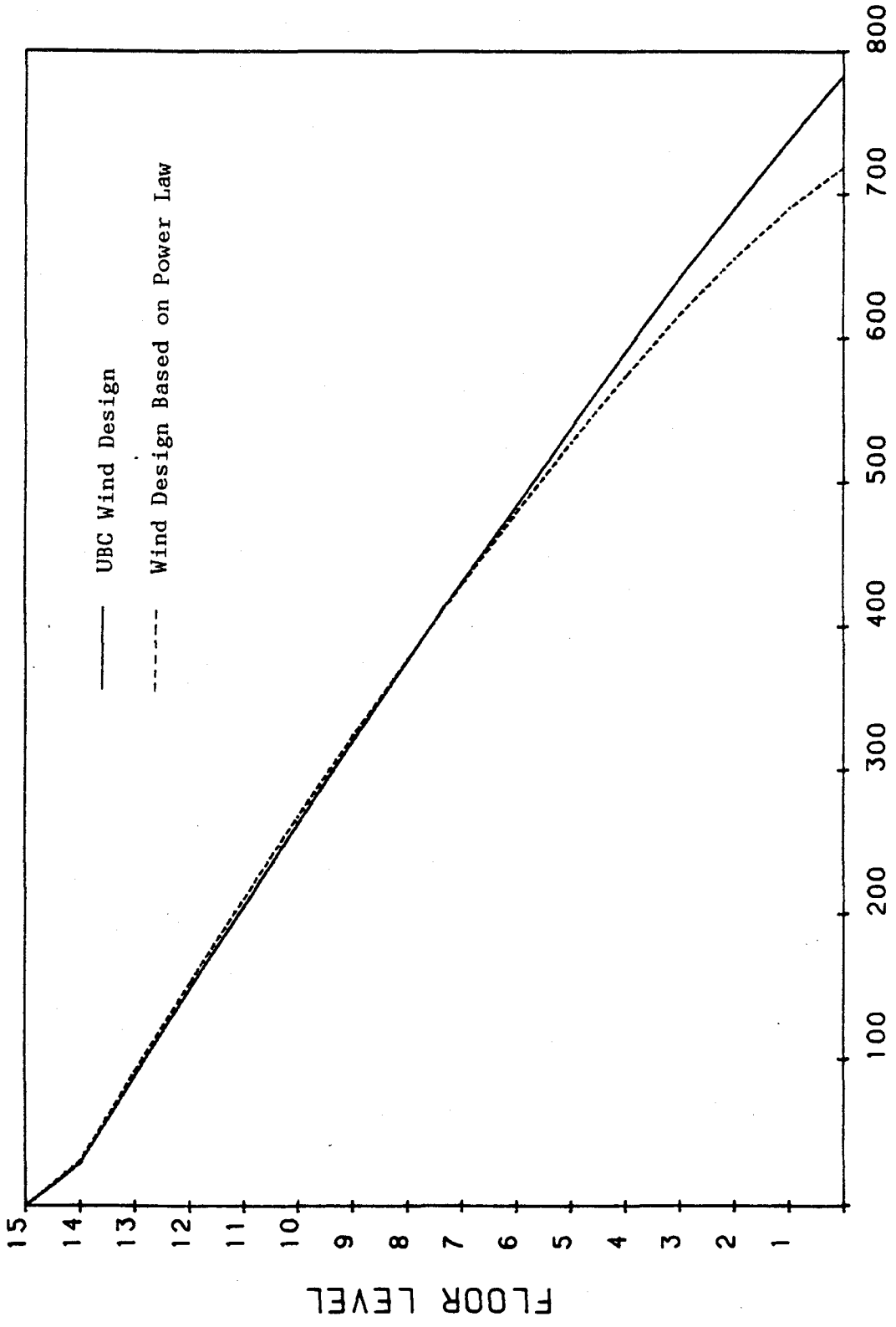

Figure 106. Shear Envelopes of the 15-Story, Two-Bay, Unbraced Frame Wind Designs.
(1 kip = 4.448 kN)

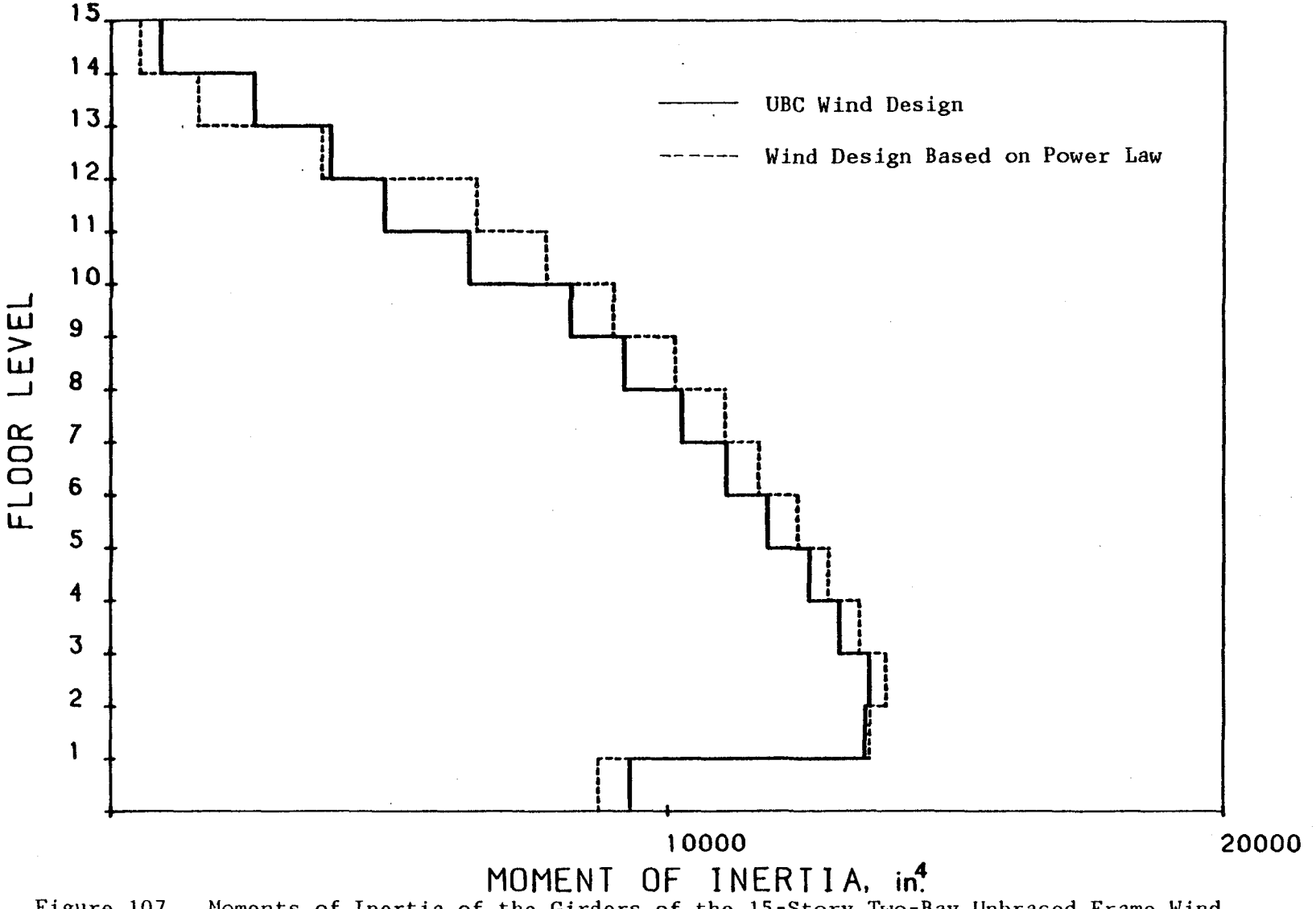

Figure 107. Moments of Inertia of the Girders of the 15-Story, Two-Bay, Unbraced Frame Wind Designs. (1 in. = 2.54 cm).

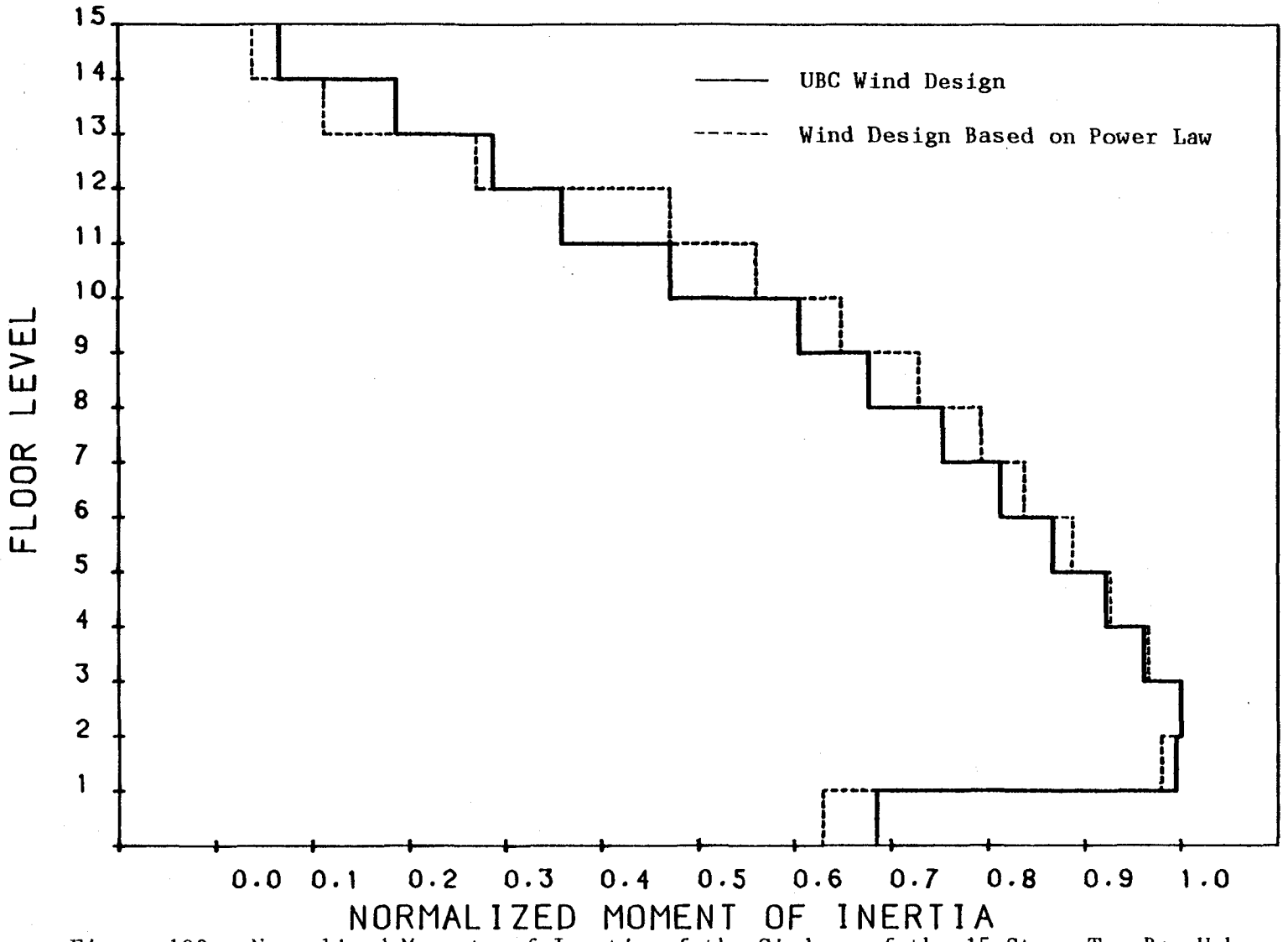

Figure 108. Normalized Moments of Inertia of the Girders of the 15-Story, Two-Bay, Unbraced Frame Wind Designs.

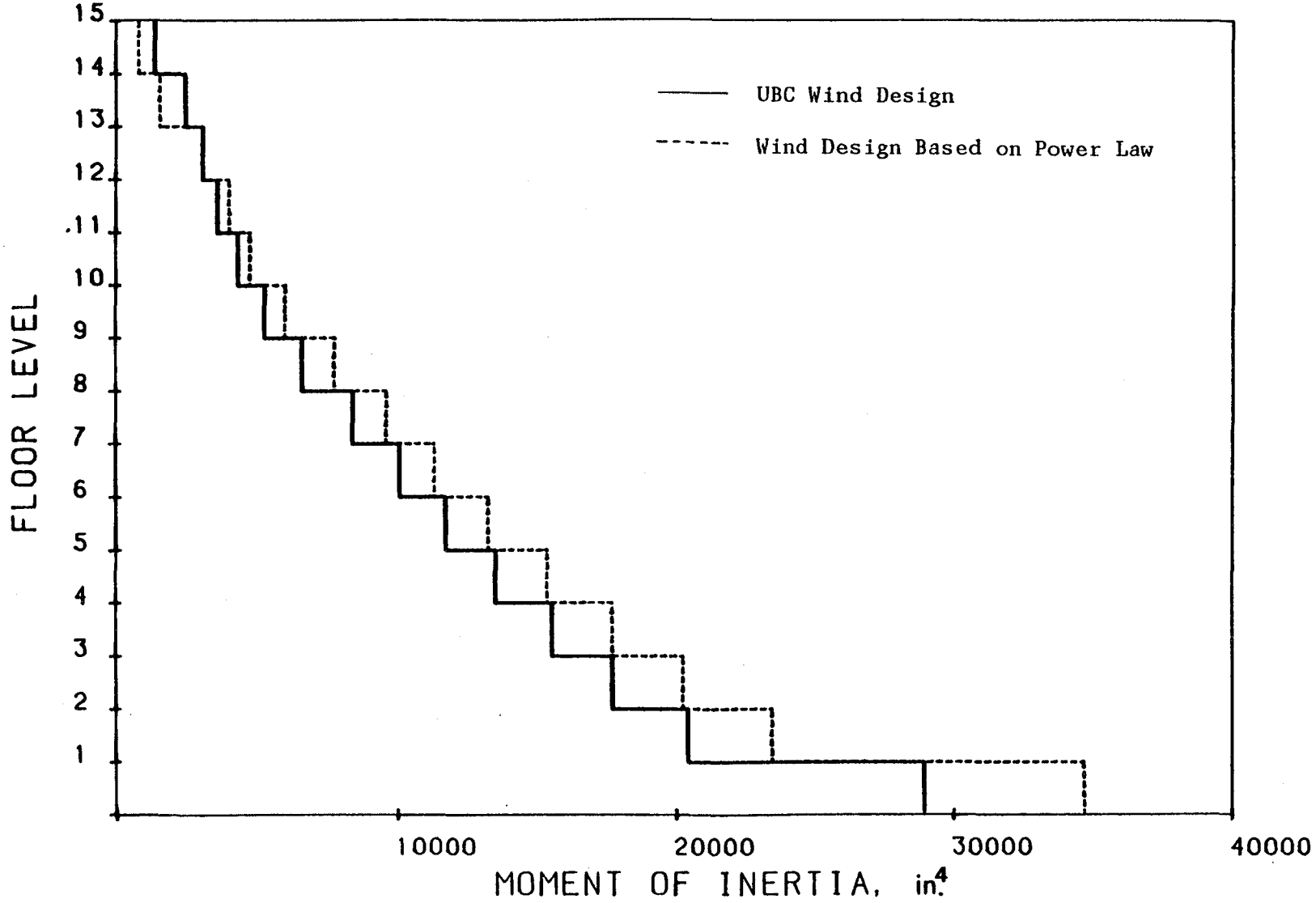

Figure 109. Moments of Inertia of the Exterior Columns of the 15-Story, Two-Bay, Unbraced Frame Wind Designs. (1 in. = 2.54 cm).

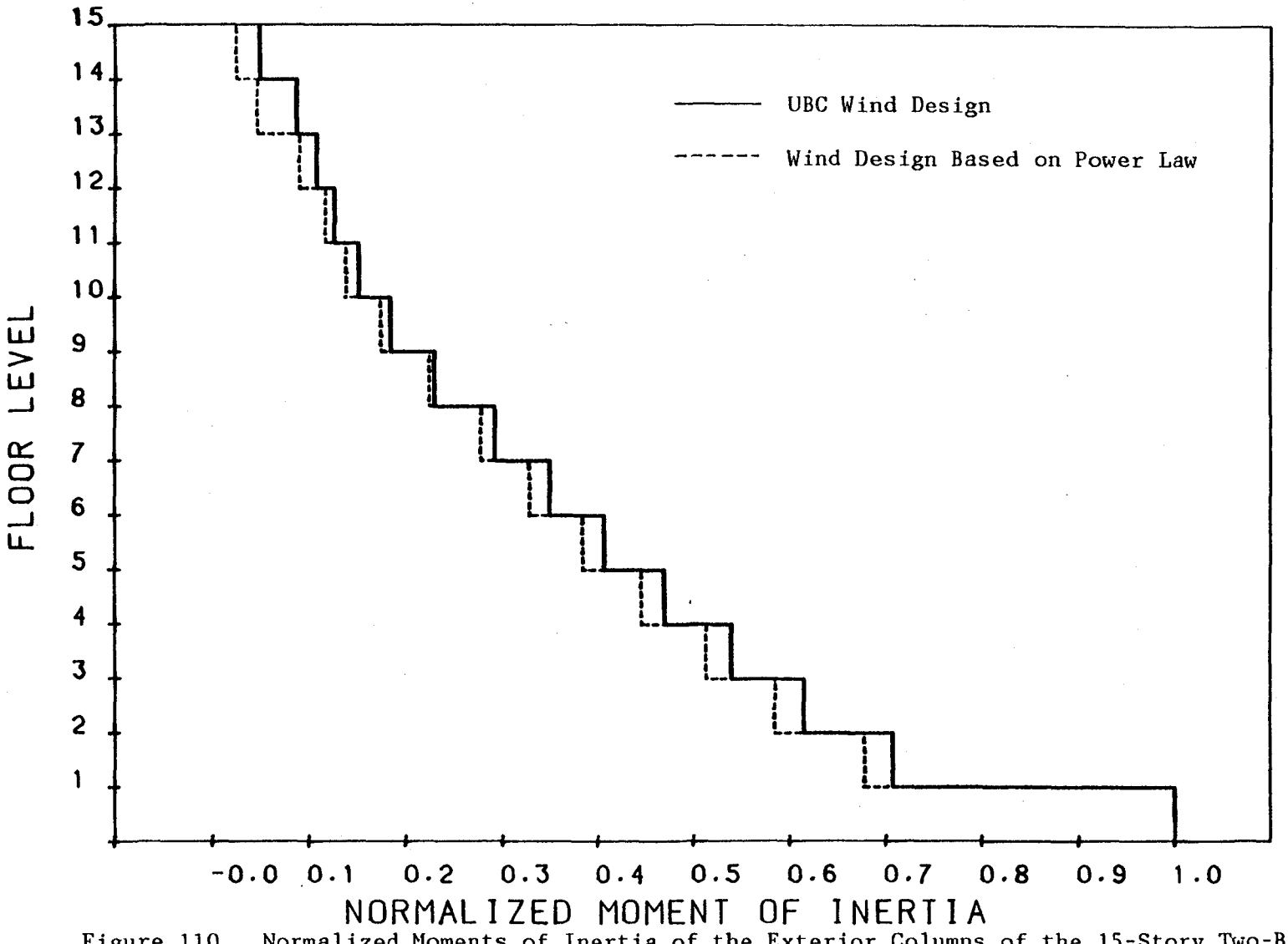

Figure 110. Normalized Moments of Inertia of the Exterior Columns of the 15-Story, Two-Bay, Unbraced Frame Wind Designs.

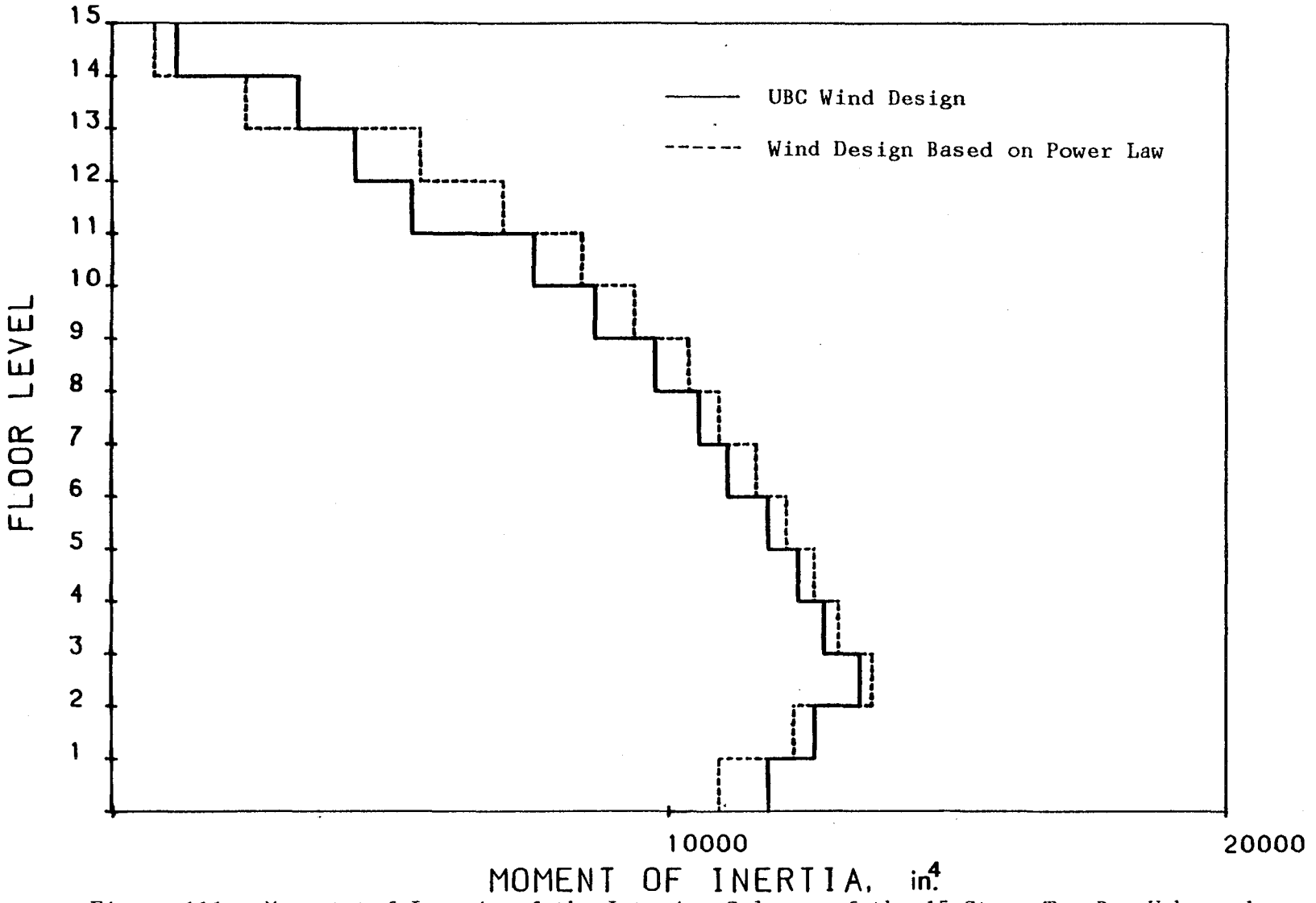

Figure 111. Moments of Inertia of the Interior Columns of the 15-Story, Two-Bay, Unbraced Frame Wind Designs. (1 in. = 2.54 cm).

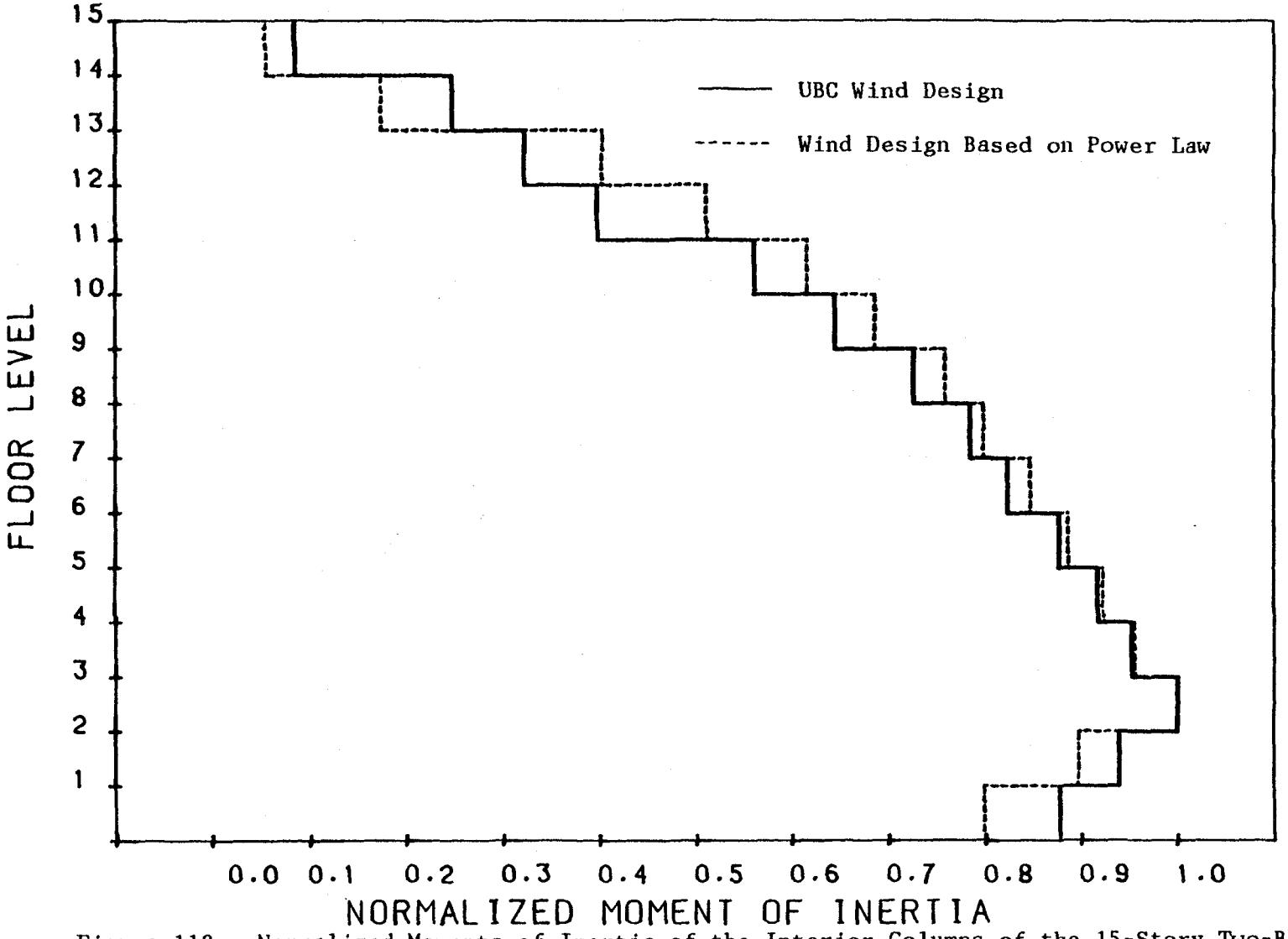

Figure 112. Normalized Moments of Inertia of the Interior Columns of the 15-Story, Two-Bay, Unbraced Frame Wind Designs.

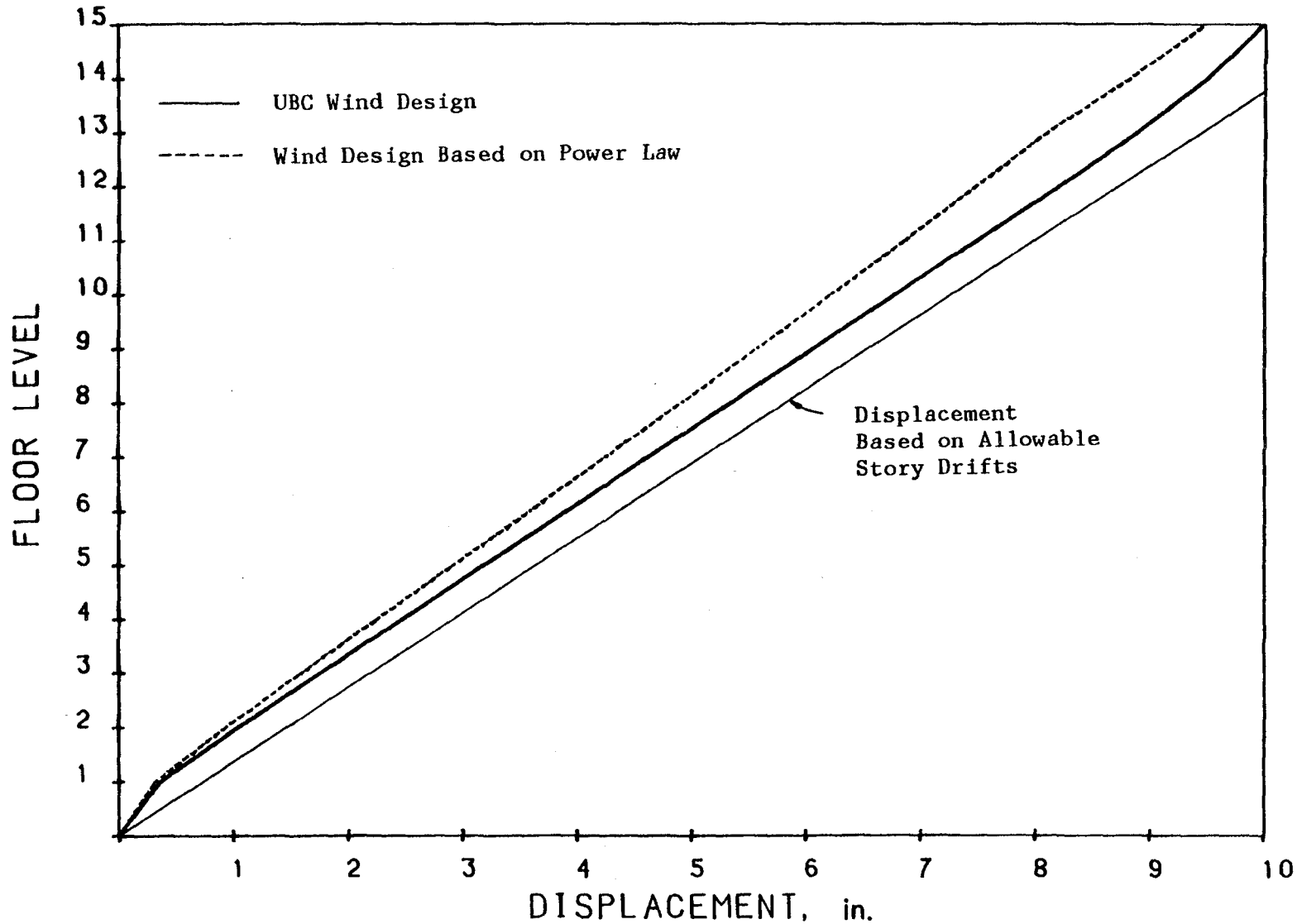

Figure 113. Displacements of the 15-Story, Two-Bay, Unbraced Frame Wind Designs. (1 in. = 2.54 cm).

J. THE INFLUENCE OF VERTICAL MOTIONS AND P-Δ EFFECT ON STRUCTURAL DESIGN

The fifteen-story, one-bay, unbraced frame shown in Figure 114 has a span length of 21 feet (6.40 m), a floor height, h_{sx}, of 12 feet (3.66 m), a dead load on each floor level, w, of 180 lbs/in (315.2 N/cm), a modulus of elasticity, E, of 29,000 ksi (19994 kN/cm^2), and a mass density of construction material, $\rho=0.283$ lb/in^3. (0.0768 N/cm^3). It also has an additional node at the midspan of the girder on each floor. All the members are designed on the basis of the AISC wide-flange sections. The ratios of the minimum moment of inertia to the maximum moment of inertia of the girders and columns are restrained to 0.1, and the minimum moment of inertia is limited to 10 in^4 (416.23 cm^4).

The design was based on spectral analysis by using the following three design spectra: 1) 90 percentile, alluvium, design spectra with 5% damping as shown in Figures 9 and 10 for the horizontal and vertical ground motions respectively for which a maximum ground motion of 0.4g, and a spectrum reduction factor of 4.5 were used, 2) the normalized response spectra recommended by ATC-3-06 as shown in Figure 13 is based on a maximum ground acceleration of 0.4g, and a soil profile type of S_3, and 3) Chinese design spectra as shown in Figures 14 and 15 for horizontal and vertical motions respectively is based on an earthquake magnitude of 9, and a spectrum reduction factor of 0.25. The spectrum reduction factors were used on the basis of the concept

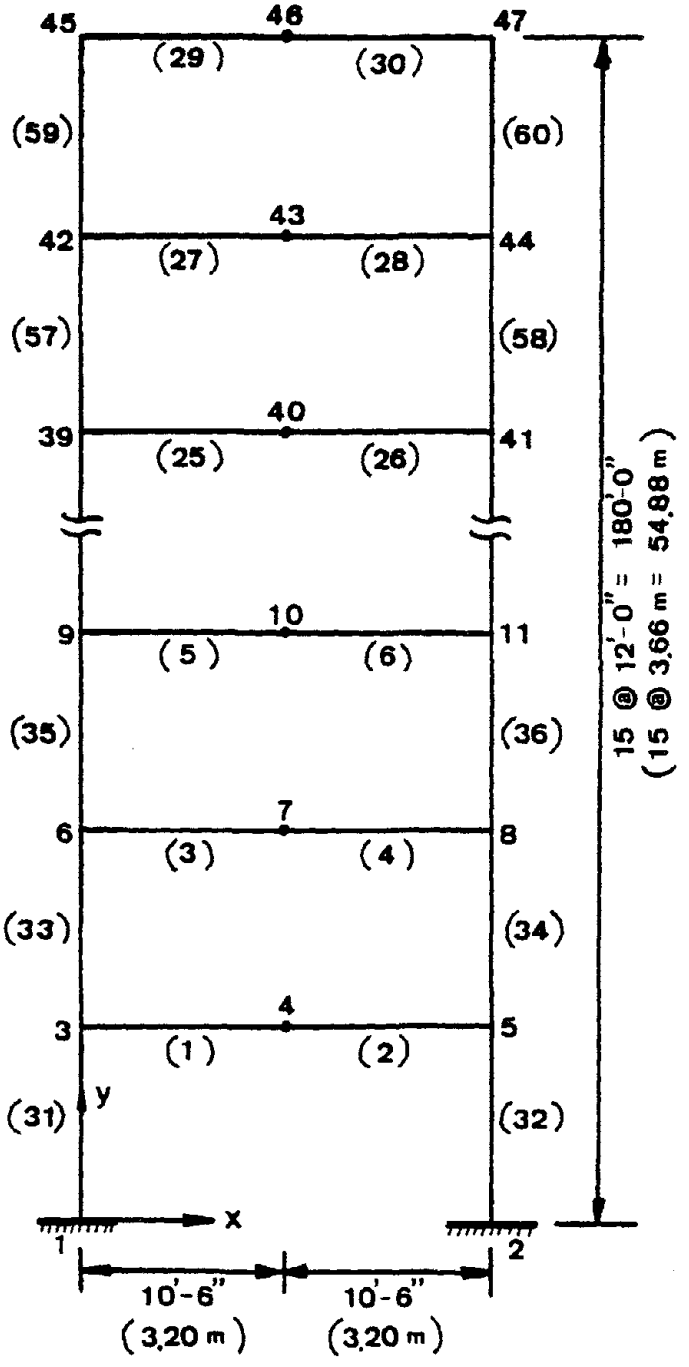

Figure 114. Fifteen-Story, One-Bay, Unbraced Frame for the Study of the Effects of Vertical Ground Motions and P-Δ Forces

of inelastic spectral analysis, which was mentioned in Section F of Chapter 4, to reduce the strength requirement. For the Newmark's spectra and ATC-3-06 normalized response spectra, the reduction factor was chosen to be equal to the response modification factor, R, of the ATC-3-06, and the spectrum reduction factor of the Chinese spectra was selected to be equal to the factor C of the Chinese Seismic Design Code. For each spectral analysis, three cases were considered in the design: a) horizontal motions only, b) horizontal ground motions plus vertical ground motions, and c) horizontal and vertical motions plus the P-Δ effect. The dynamic responses were obtained by using the root-mean-square superposition of the first five modes.

For this structure, one first considers only the stress constraint with an allowable stress of 24,000 psi (16547 N/cm^2) for all the members. Then the displacement constraints are considered. The allowable lateral displacement of each floor level is $0.00375h_x$, which is determined based on the ATC-3-06 allowable story drift, $0.015h_{sx}/C_d$. Here, h_x is the height of the floor level, x, as measured from the ground surface, and h_{sx} is the story height between level x and x-1. The design results are discussed below.

1. 90 Percentile, Alluvium, DesignSpectra with 5% Damping

a. Stress constraint only. The plot of weight versus cycles of iteration is shown in Figure 115. The final design weight indicates that inclusion of the vertical ground motions does not affect the design very significantly when the optimum weight is slightly smaller than that of a design for which the vertical motion has not been considered. Inclusion of the P-Δ effect, however, significantly

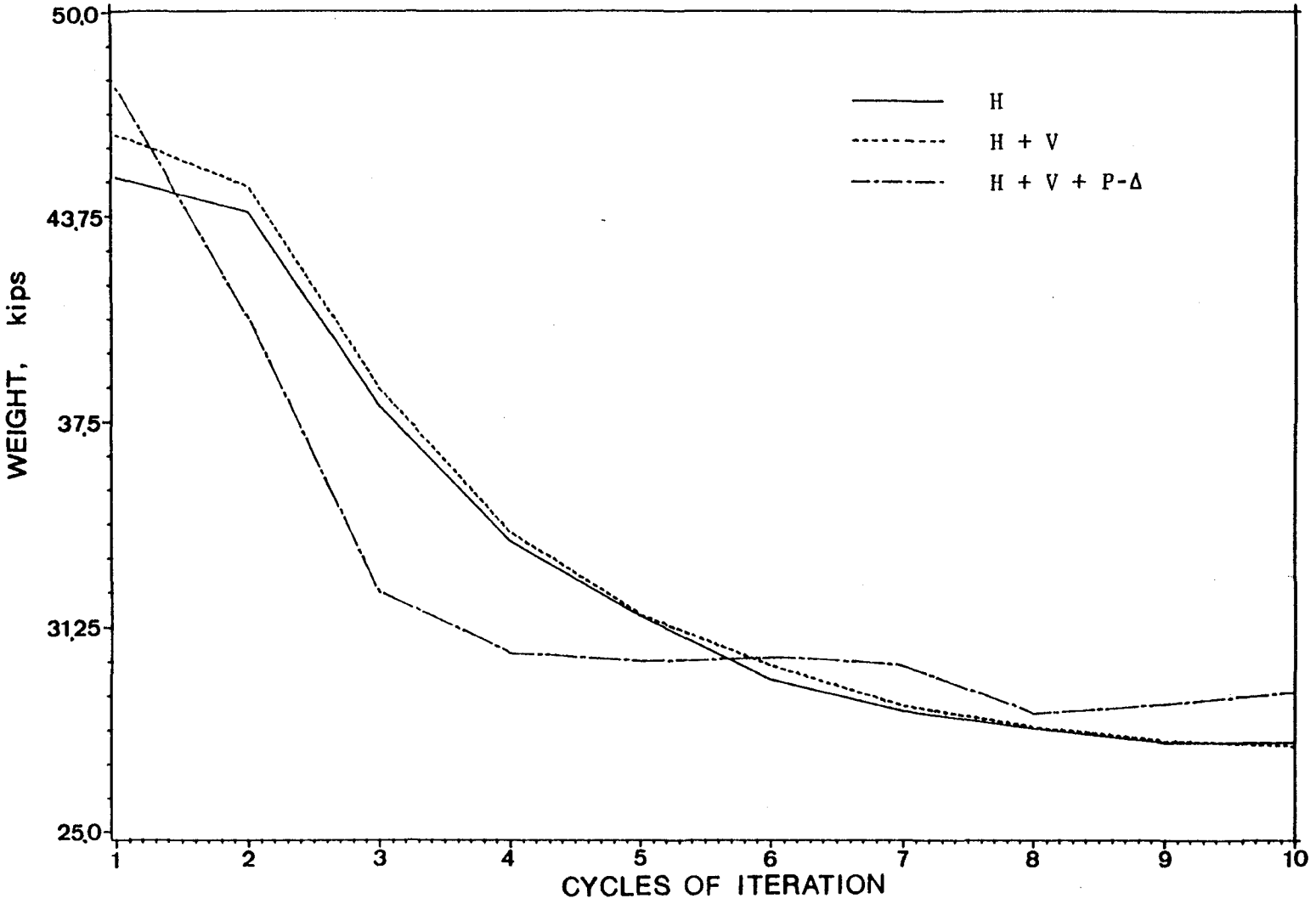

Figure 115. Weight v.s. Cycles of Iteration Plot of the Design Based on Newmark's Spectra with Stress Constraints. (1 kip = 4.448 kN).

increases the optimum weight by around 3.69% above what it would be if the P-Δ effect were not included.

The distribution of the moments of inertia of the girders and columns are illustrated in Figures 116 through 119. The moments of inertia of the members have to be much larger when the P-Δ effect is considered. When the design includes the vertical ground motions without the P-Δ effect, the smallest moments of inertia are required for the members. The moments of inertia of the girders are distributed in the same manner as those depicted in previous sections of this chapter except that the maximum moment of inertia is on the second floor. The columns on the top three stories have the same size because of the constraint on the ratio of the minimum moment of inertia to the maximum moment of inertia.

The displacements of each floor level are shown in Figure 120. The curves are very smooth from the second floor to the top floor, but at the first floor the displacement decreases suddenly because of the restraint of the rotational degree of freedom at the supports.

b. Displacement constraints only. Inclusion of vertical motions and the P-Δ effect increases the optimum weight by 1.1% and 4.15% respectively. Figure 121 shows the plots of weight versus cycles of iteration. Note that inclusion of the P-Δ effect requires the heaviest weight.

Figures 122 and 123 depict the moments of inertia and the normalized moments of inertia of the girders. The plots in these figures illustrate an exceptional case in the distribution for the design when only the horizontal ground motions are effective. As can

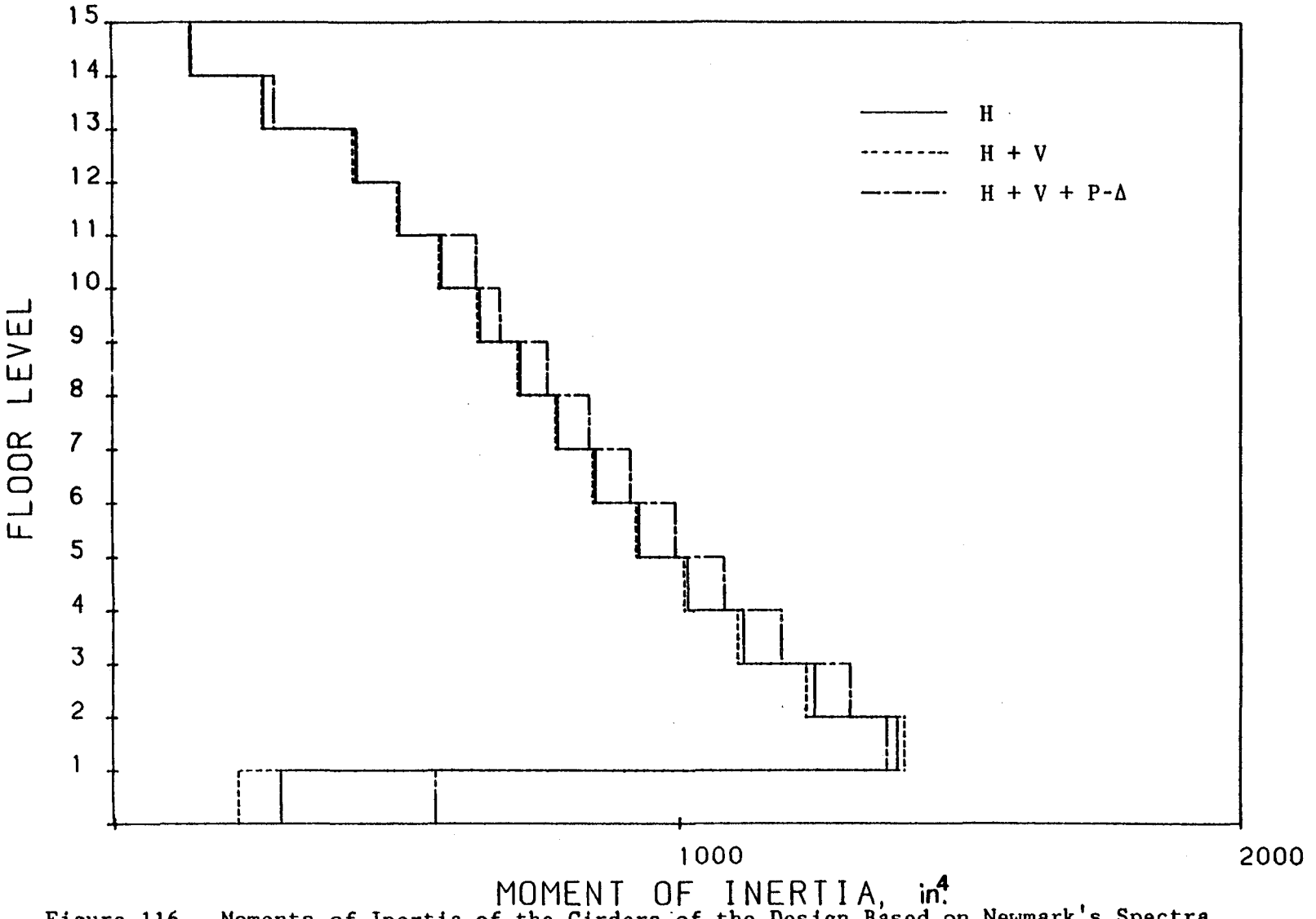

Figure 116. Moments of Inertia of the Girders of the Design Based on Newmark's Spectra with Stress Constraints. (1 in. = 2.54 cm).

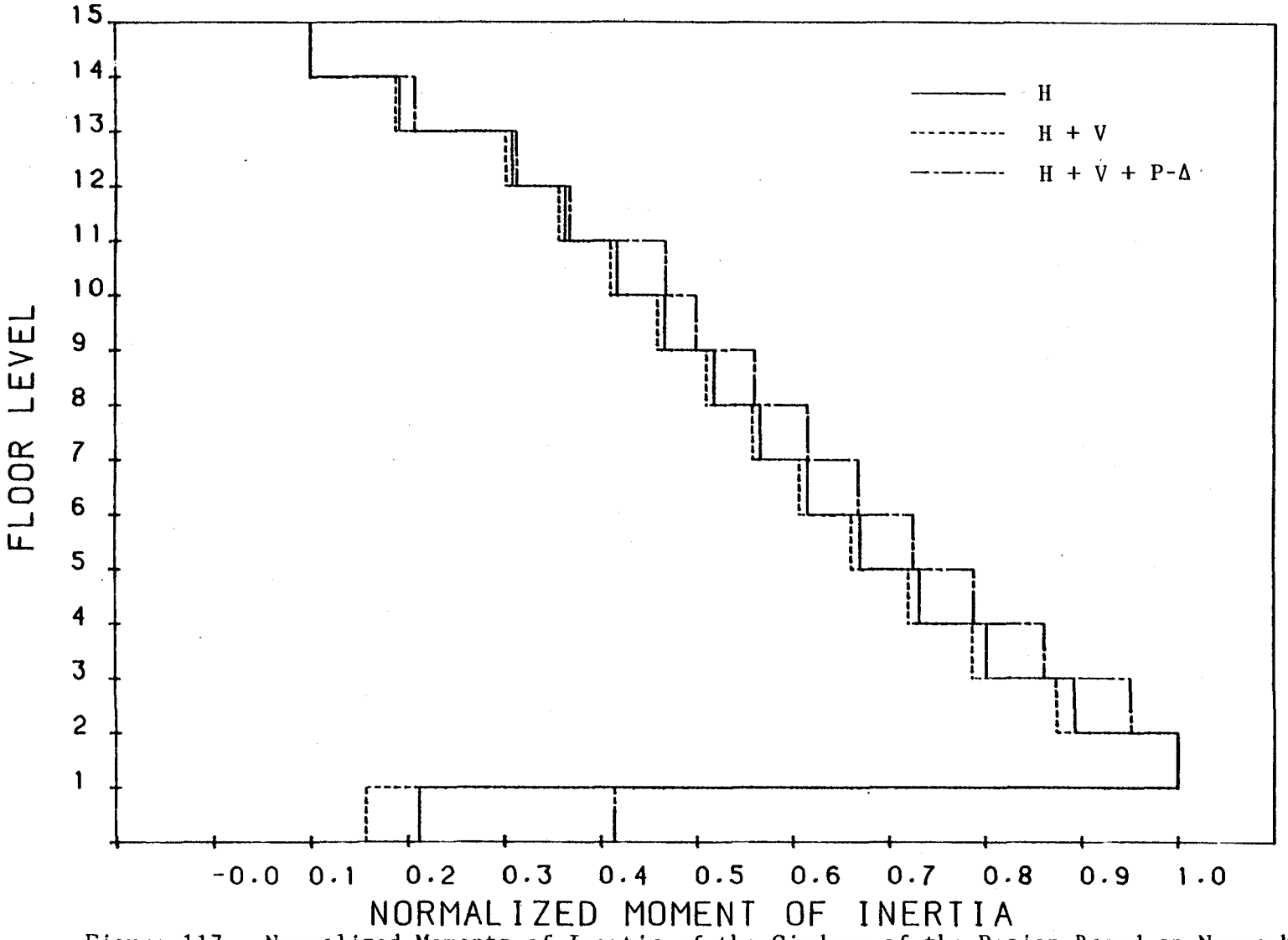

Figure 117. Normalized Moments of Inertia of the Girders of the Design Based on Newmark's Spectra with Stress Constraints.

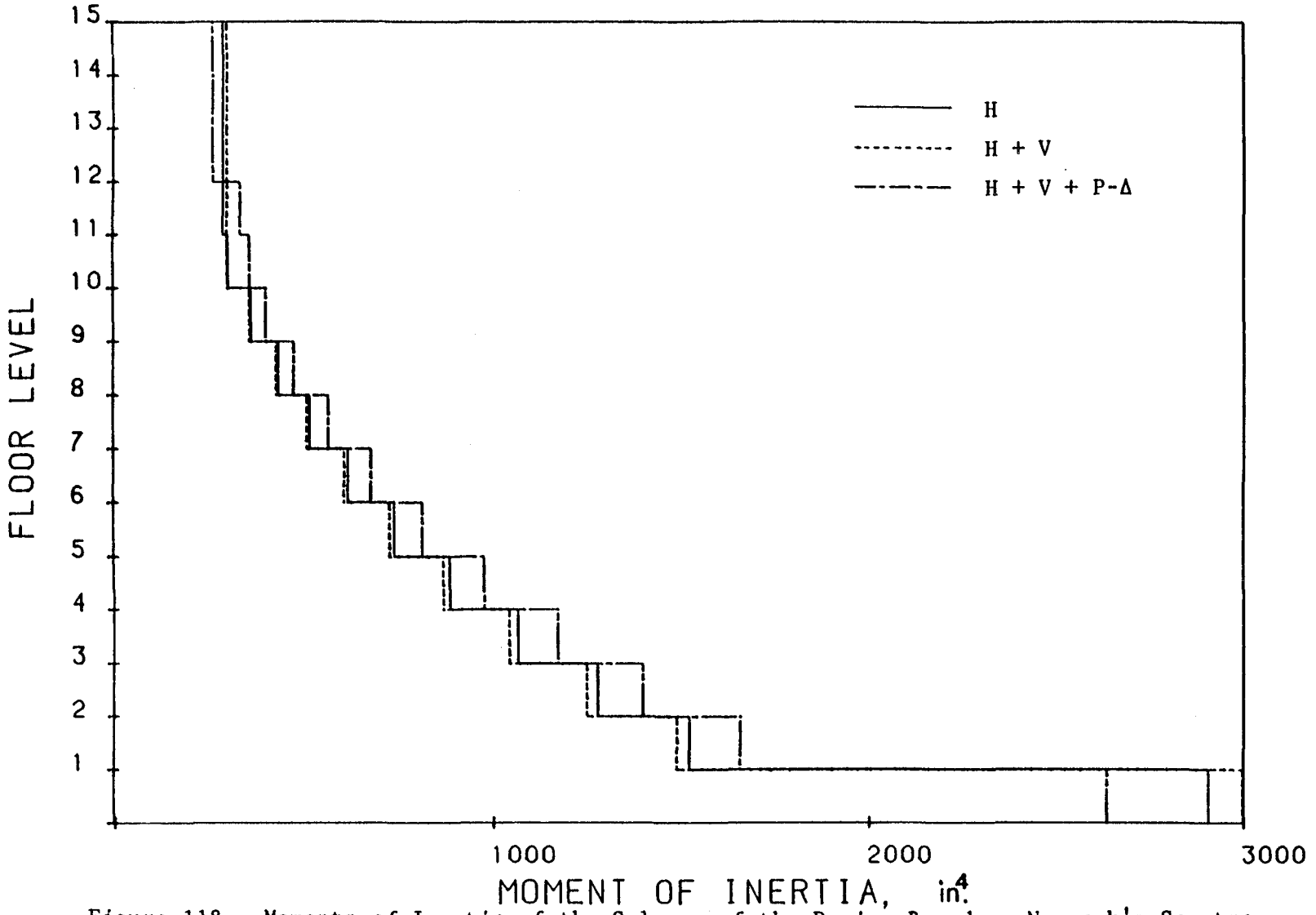

Figure 118. Moments of Inertia of the Columns of the Design Based on Newmark's Spectra with Stress Constraints. (1 in. = 2.54 cm).

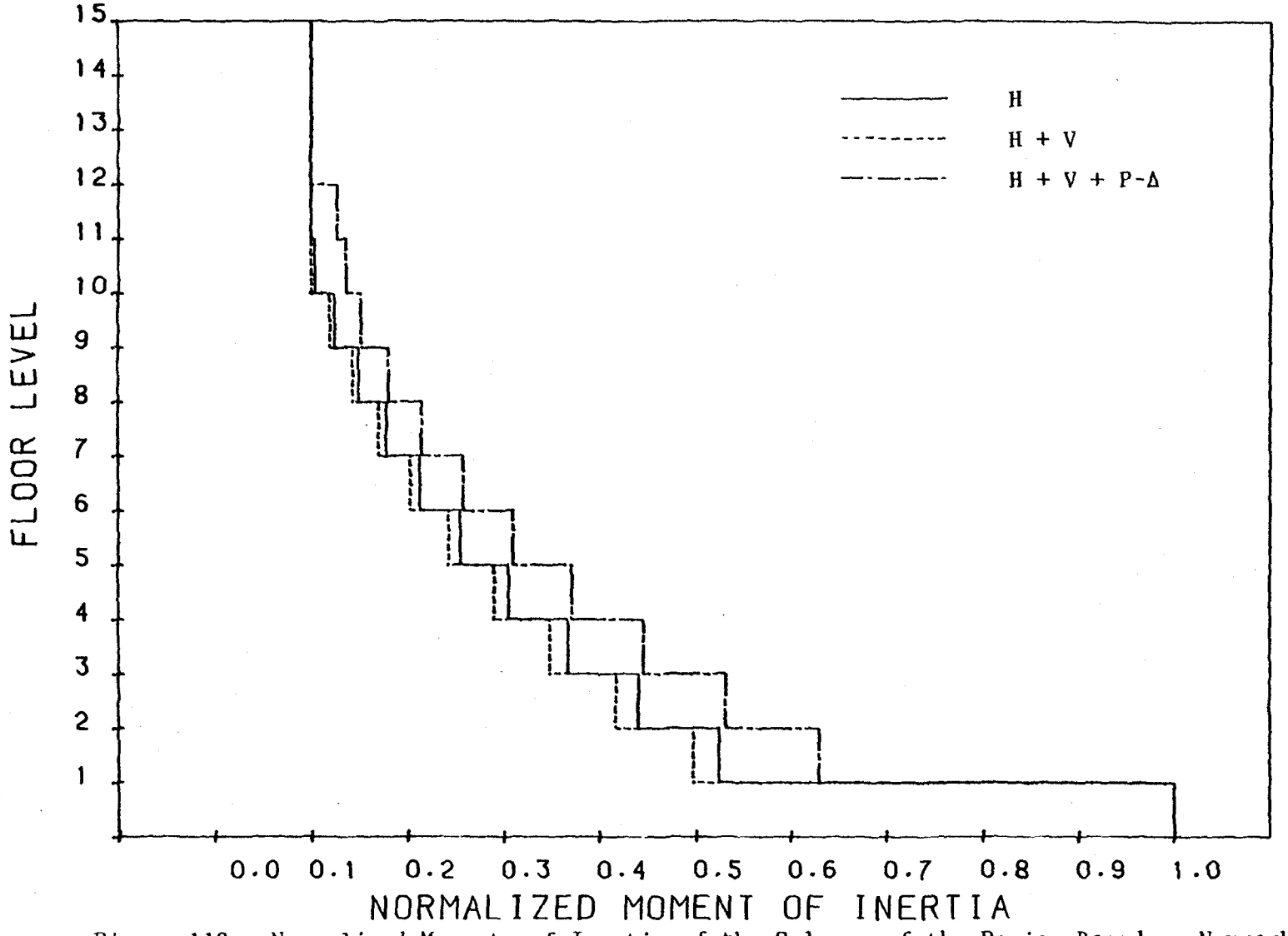

Figure 119. Normalized Moments of Inertia of the Columns of the Design Based on Newmark's Spectra with Stress Constraints.

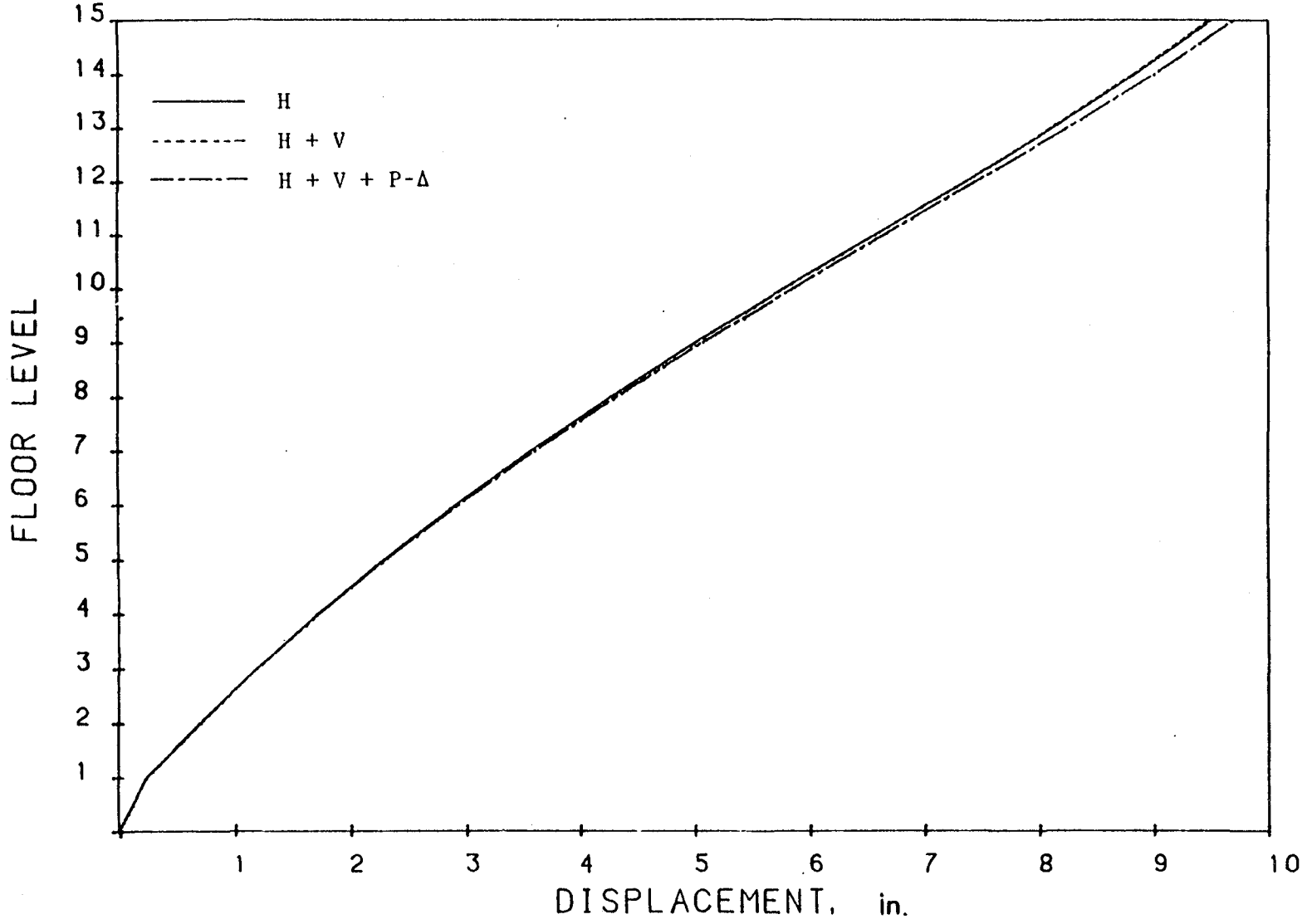

Figure 120. Displacements of the Design Based on Newmark's Spectra with Stress Constraints. (1 in. = 2.54 cm).

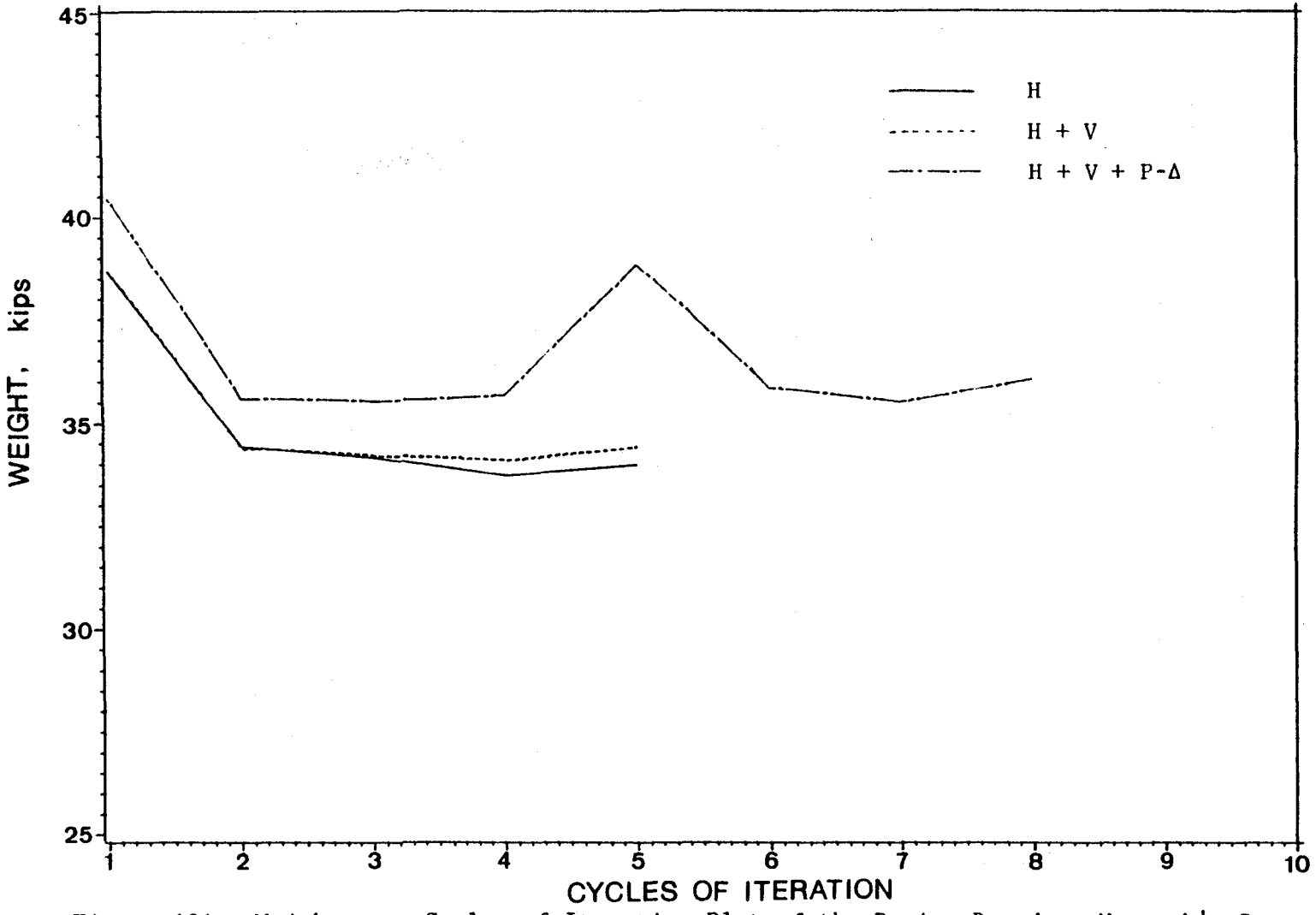

Figure 121. Weight v.s. Cycles of Iteration Plot of the Design Based on Newmark's Spectra with Displacement Constraints. (1 kip = 4.448 kN).

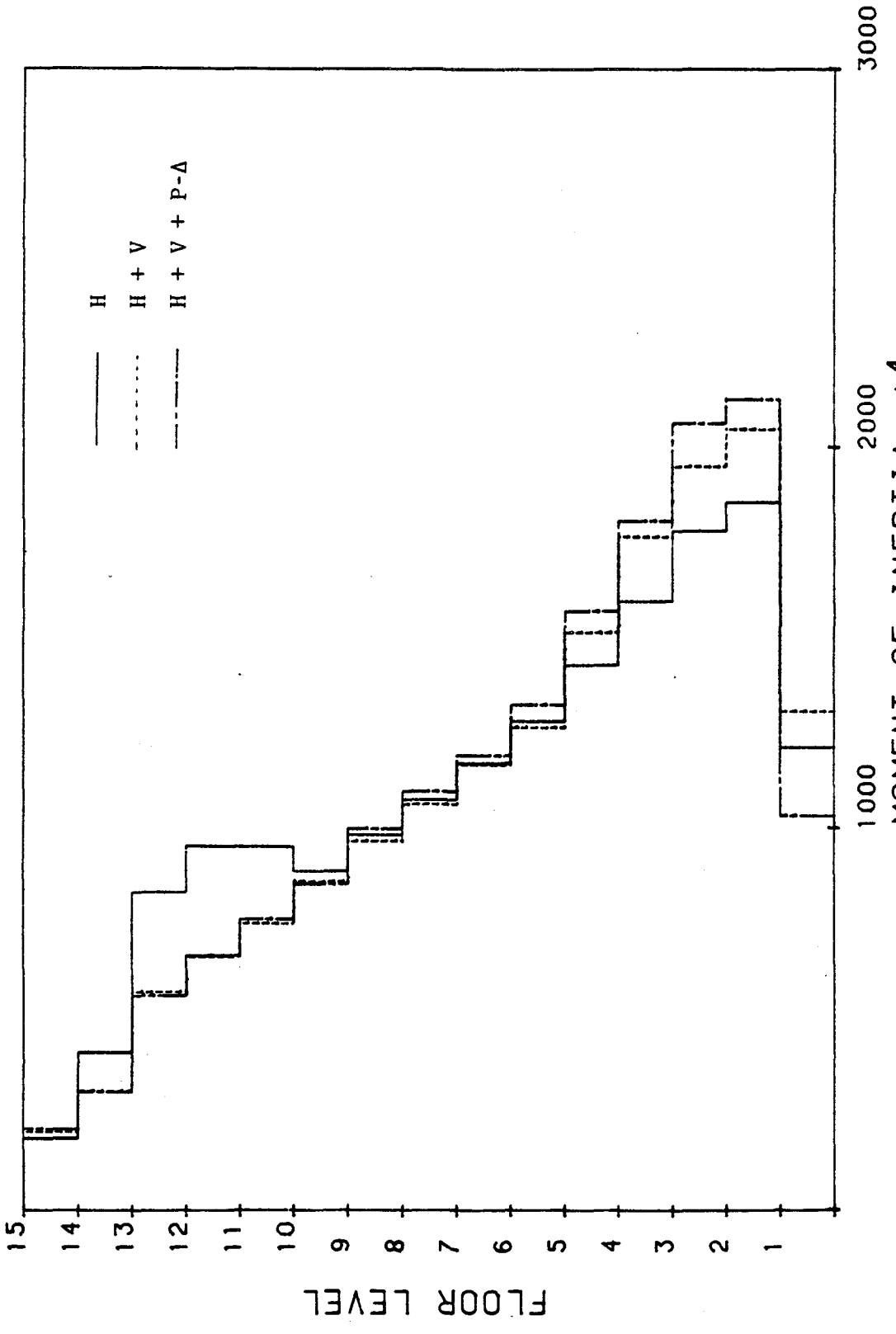

Figure 122. Moments of Inertia of the Girders of the Design Based on Newmark's Spectra with Displacement Constraints. (1 in. = 2.54 cm).

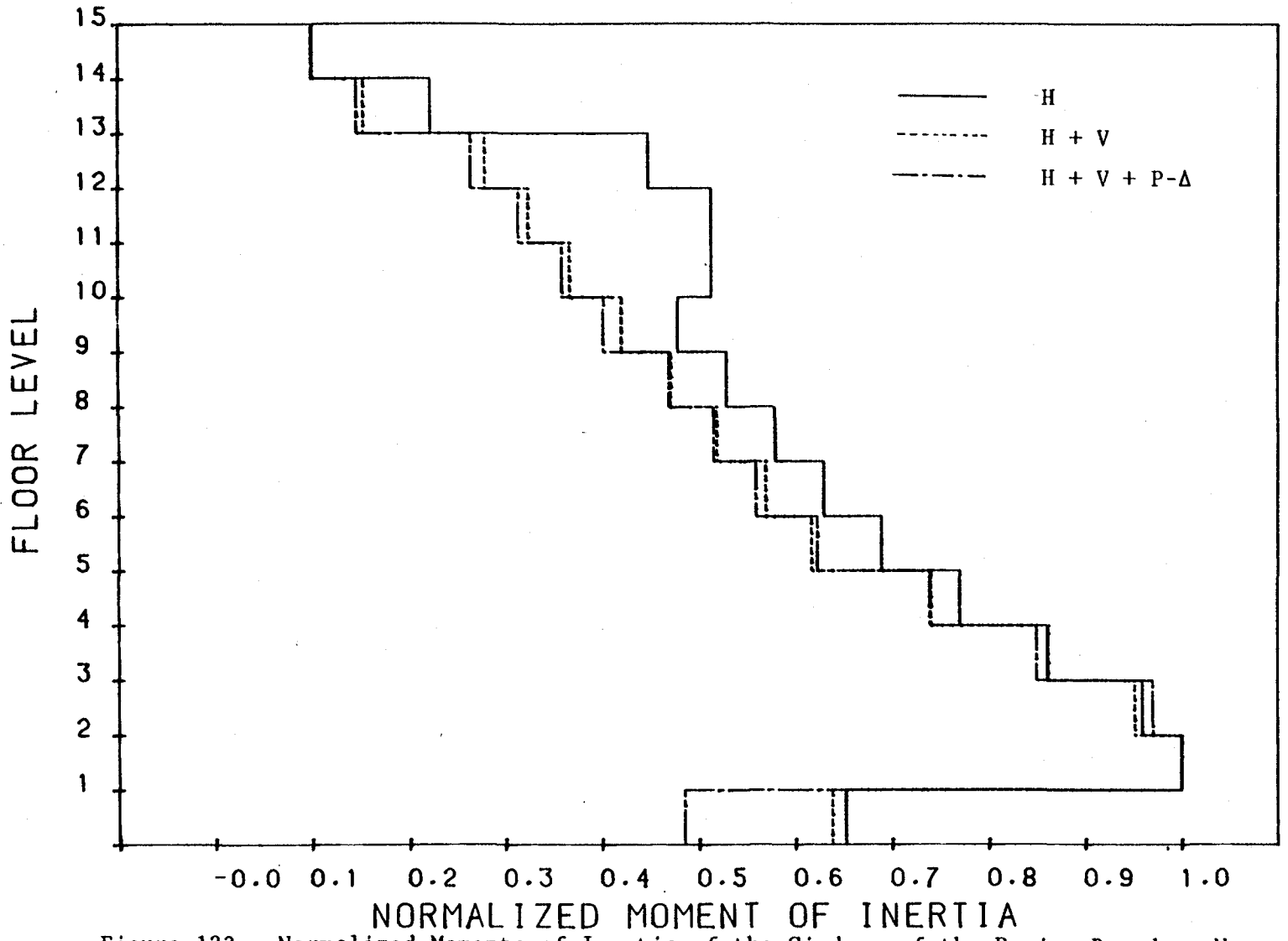

Figure 123. Normalized Moments of Inertia of the Girders of the Design Based on Newmark's Spectra with Displacement Constraints.

be seen, the distribution from the first to the tenth floor is similar to other cases, but from the tenth to the twelfth floor, the moment of inertia increases suddenly. The main reason for this increment is that the total responses are significantly affected by those of the higher modes. The redistribution, which is based on the virtual energy, changes the pattern of the distribution so that the virtual energy of the second mode of girders from tenth to twelfth floor becomes larger and controls the total virtual energies of all modes under consideration.

The distribution of the moments of inertia and the normalized moments of inertia of the columns are illustrated in Figure 124 and 125, and the displacements of each floor level are shown in Figure 126.

2. Normalized Design Spectra Recommended by ATC-3-06

a. Stress constraint only. The weight versus cycles of iteration are plotted in Figure 127. Inclusion of the vertical ground motions induces an optimum weight increment of 3.16% over that of a design for which the vertical motions are not included. When the P-Δ effect is included, the increment in the optimum weight is 2.46%.

The moments of inertia and the normalized moments of inertia of the girders and columns are plotted in Figures 128 through 131. The distribution of the girders and columns are similar to that of the previous examples.

Figure 132 shows the displacements of each floor level. Obviously, the displacements reflect the total stiffness of the structure.

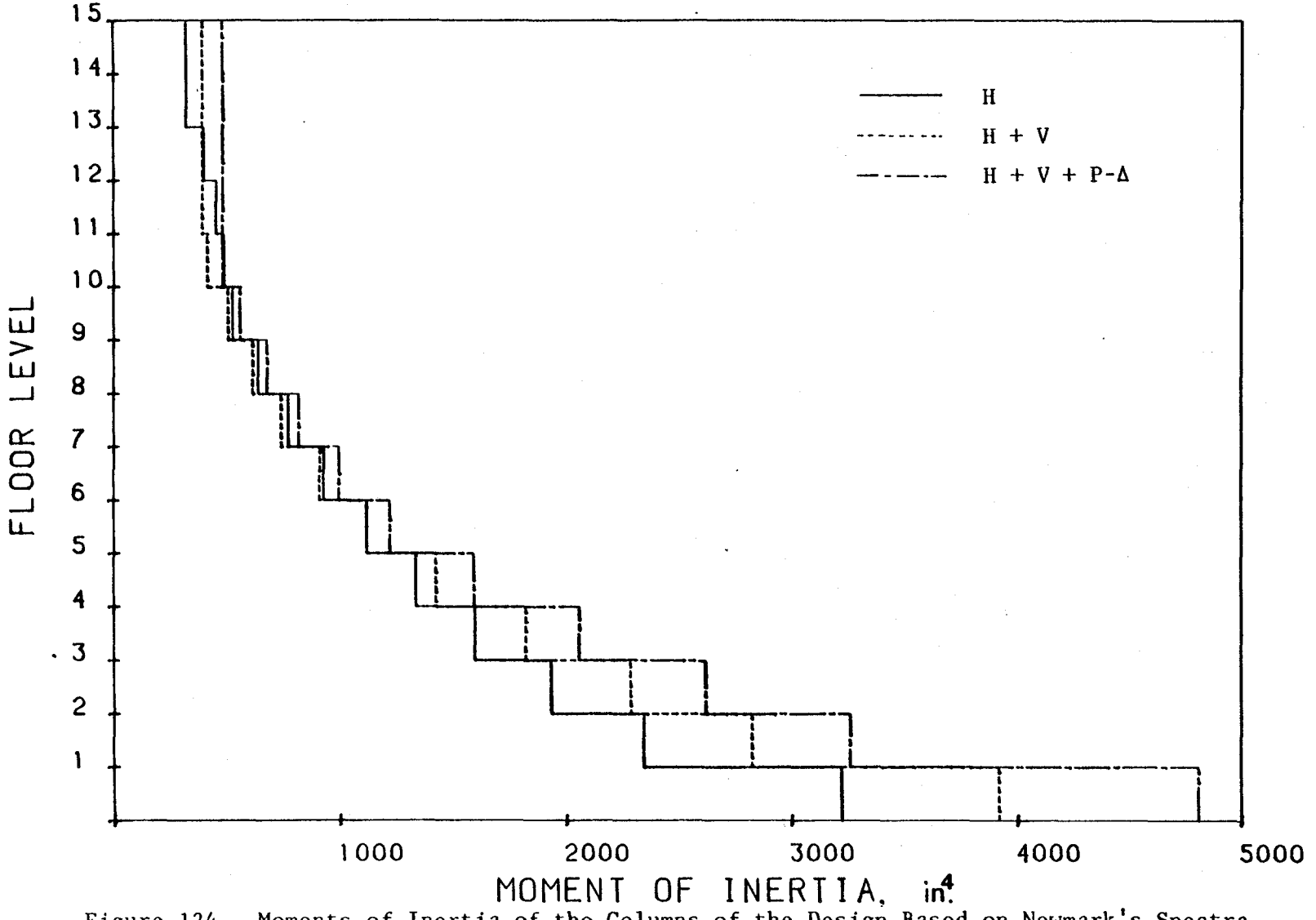

Figure 124. Moments of Inertia of the Columns of the Design Based on Newmark's Spectra with Displacement Constraints. (1 in. = 2.54 cm).

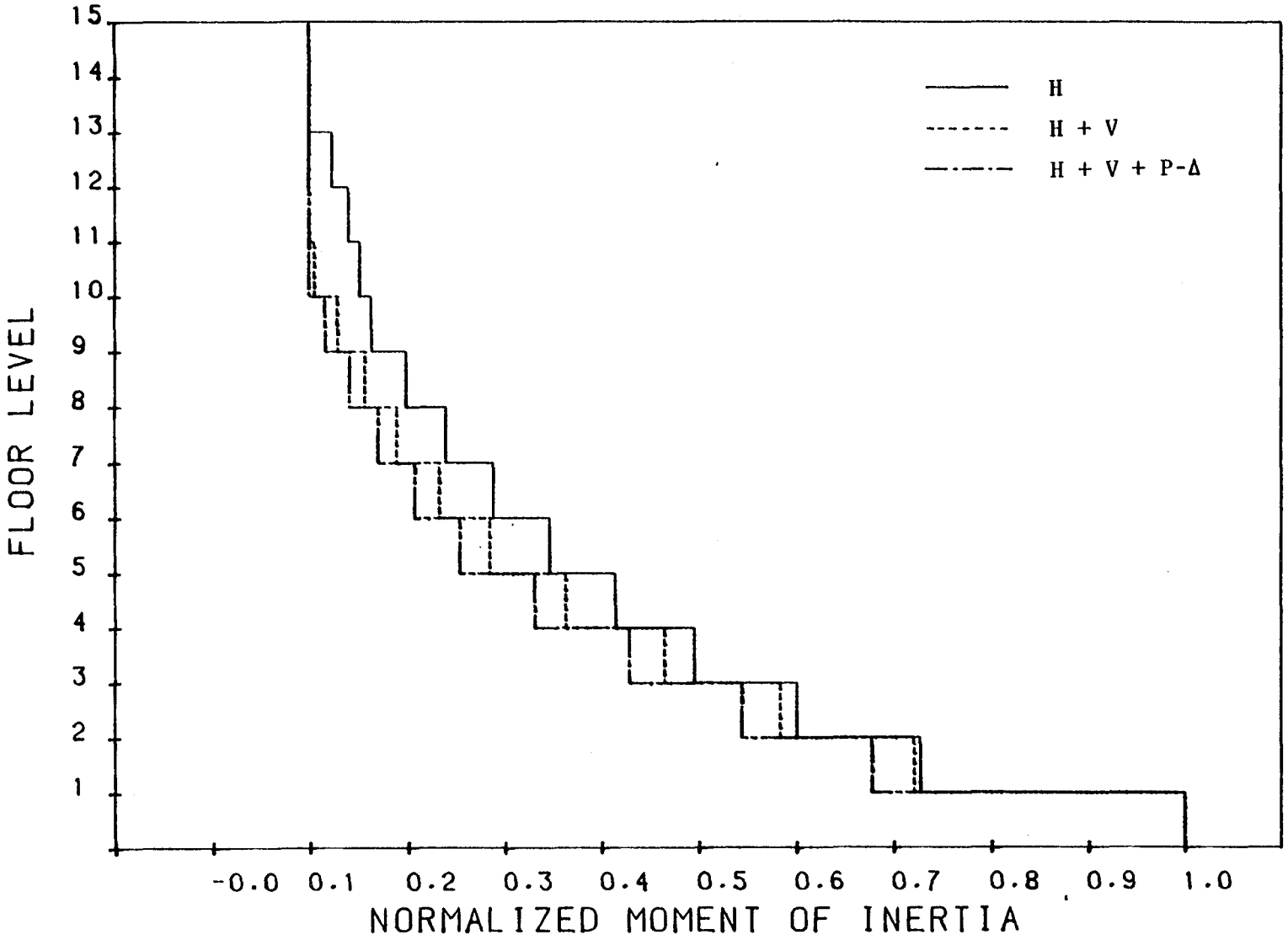

Figure 125. Normalized Moments of Inertia of the Columns of the Design Based on Newmark's Spectra with Displacement Constraints.

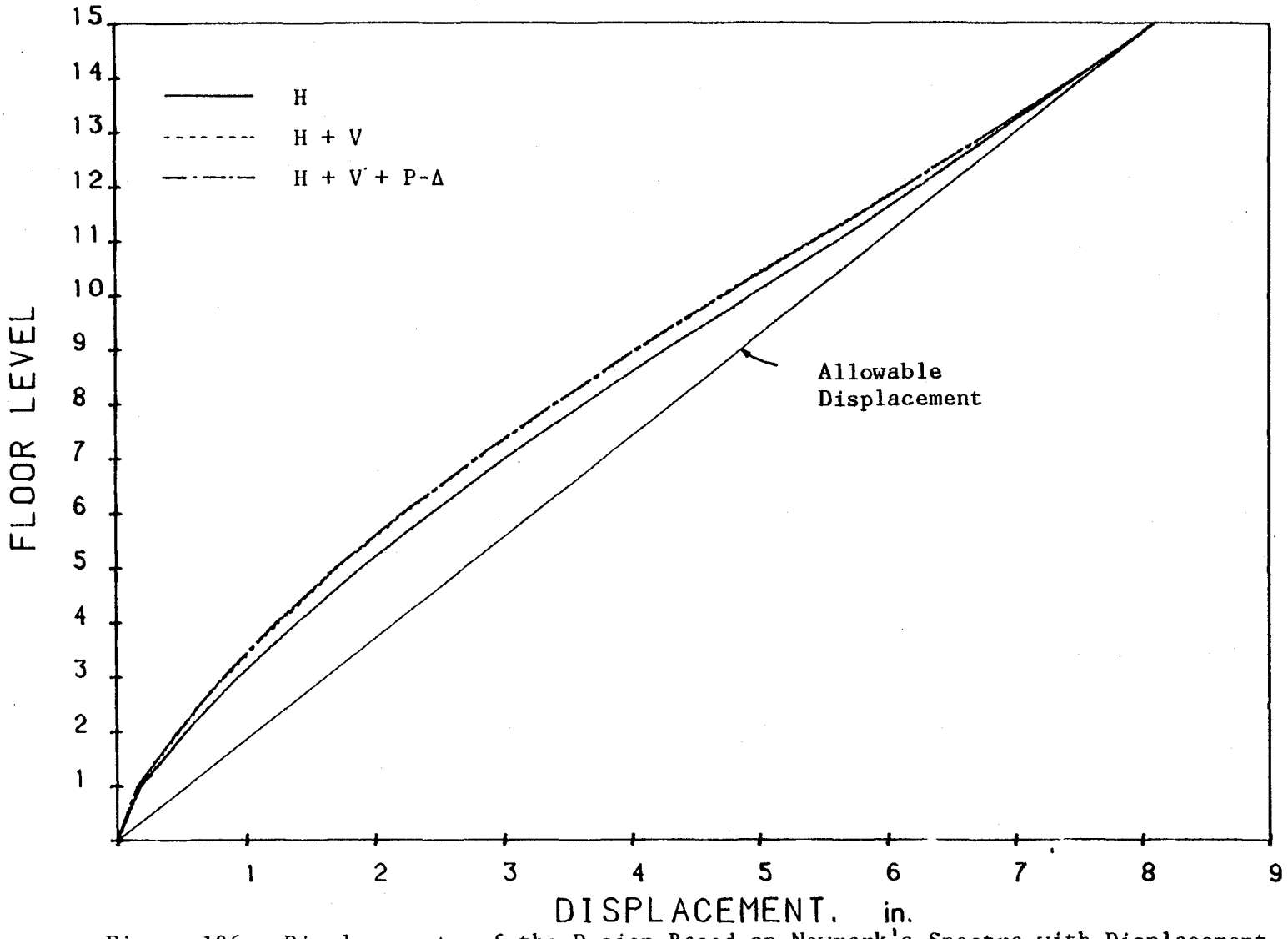

Figure 126. Displacements of the Design Based on Newmark's Spectra with Displacement Constraints. (1 in. = 2.54 cm).

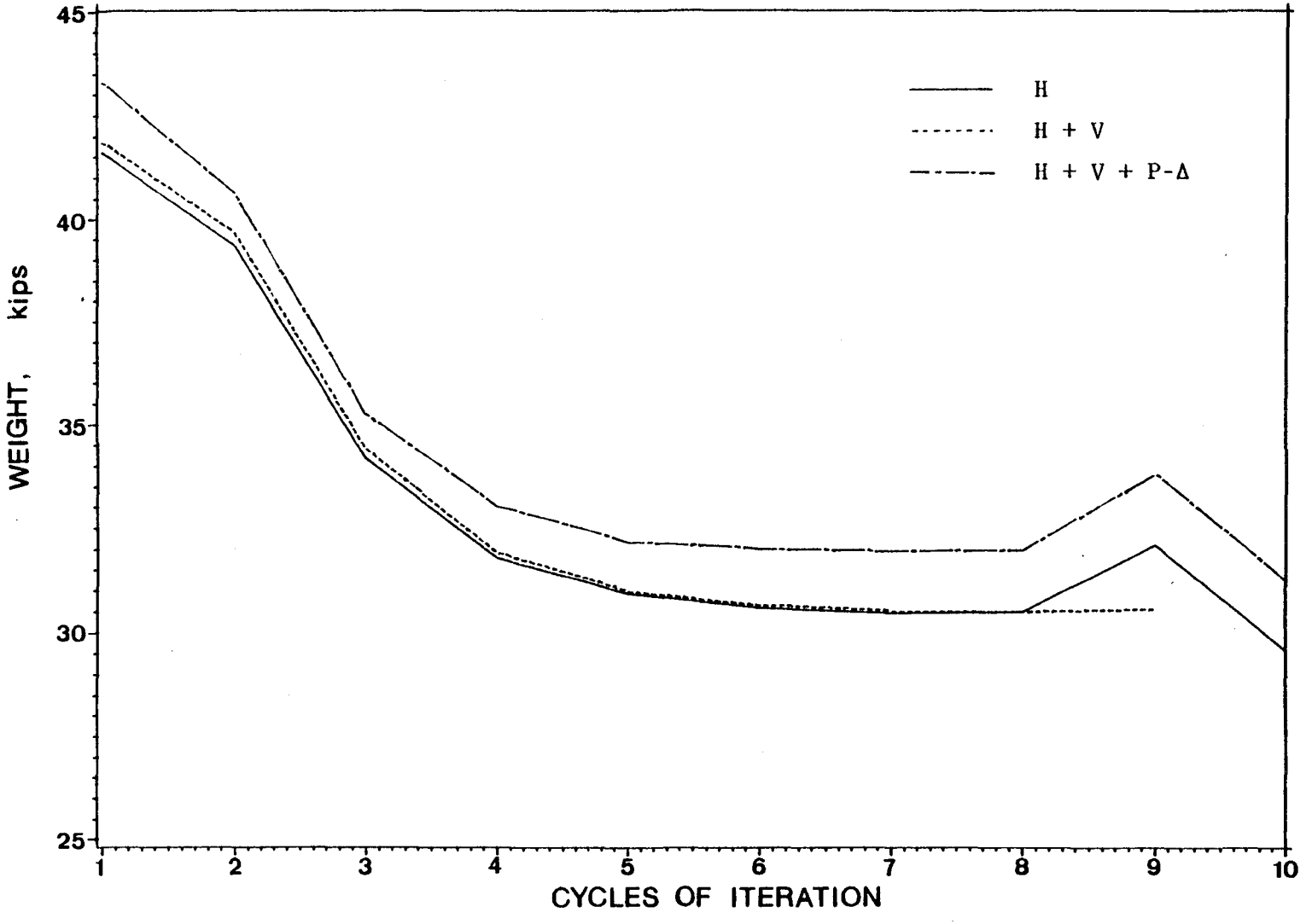

Figure 127. Weight v.s. Cycles of Iteration Plot of the Design Based on ATC Design Spectra with Stress Constraints. (1 kip = 4.448 kN).

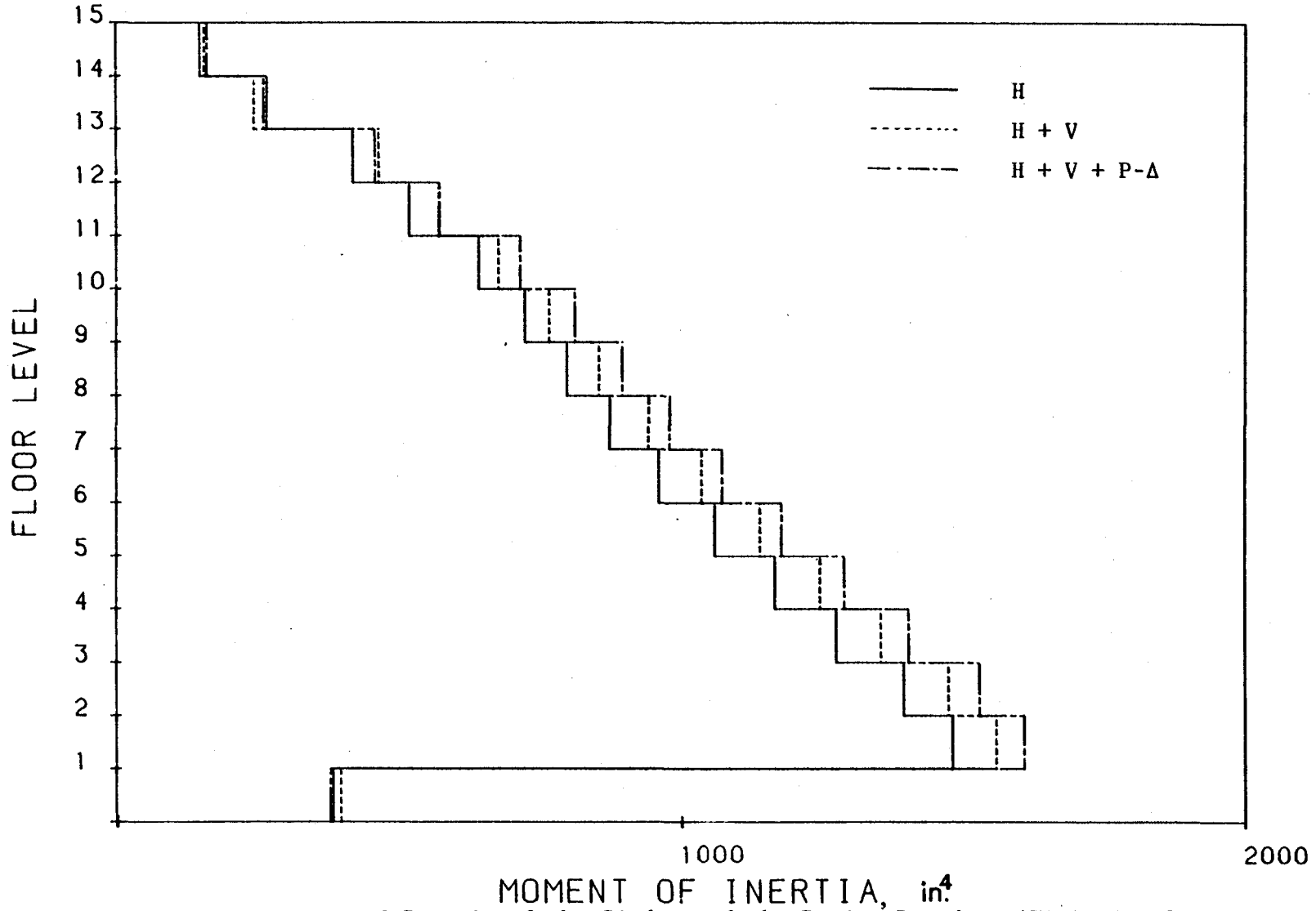

Figure 128. Moments of Inertia of the Girders of the Design Based on ATC Design Spectra with Stress Constraints. (1 in. = 2.54 cm).

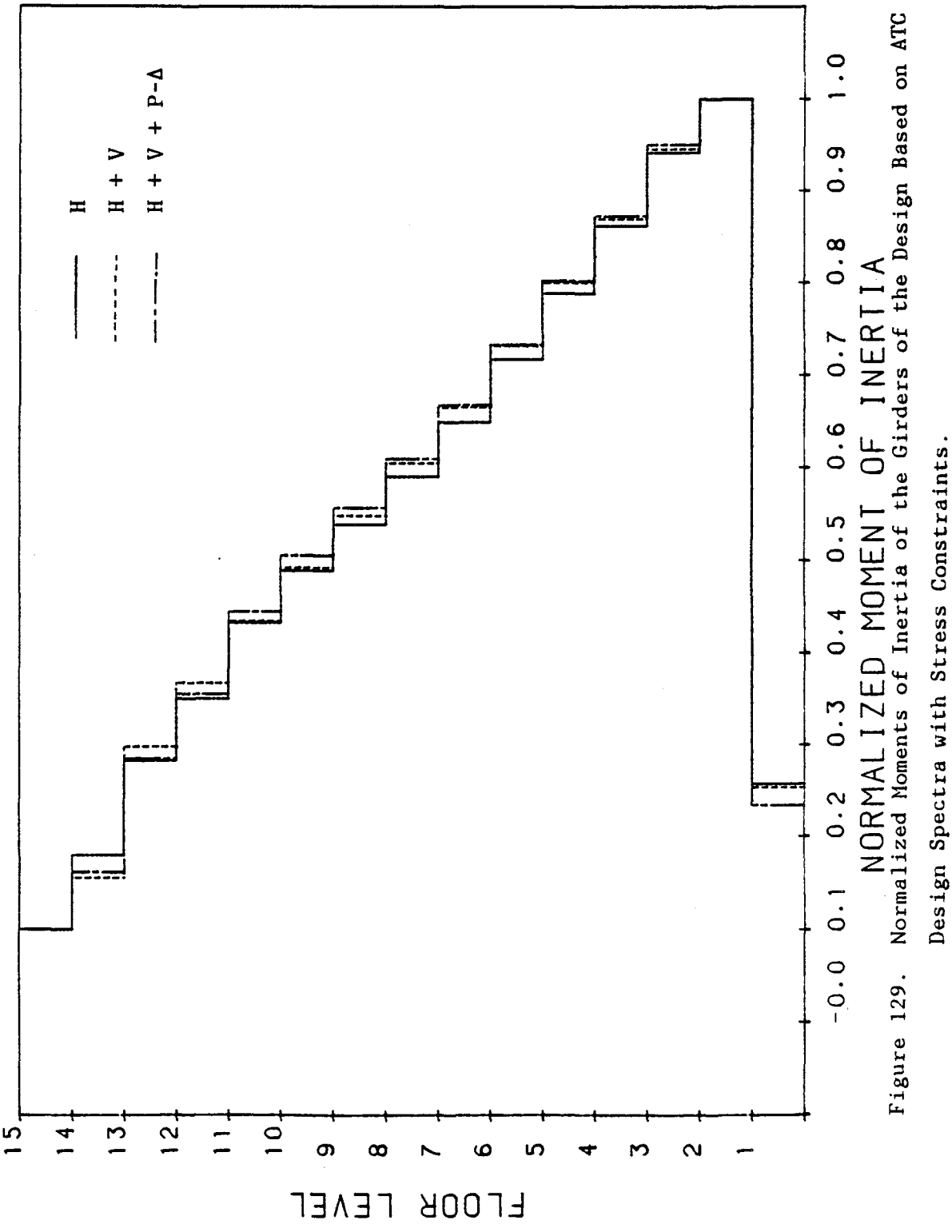

Figure 129. Normalized Moments of Inertia of the Girders of the Design Based on ATC Design Spectra with Stress Constraints.

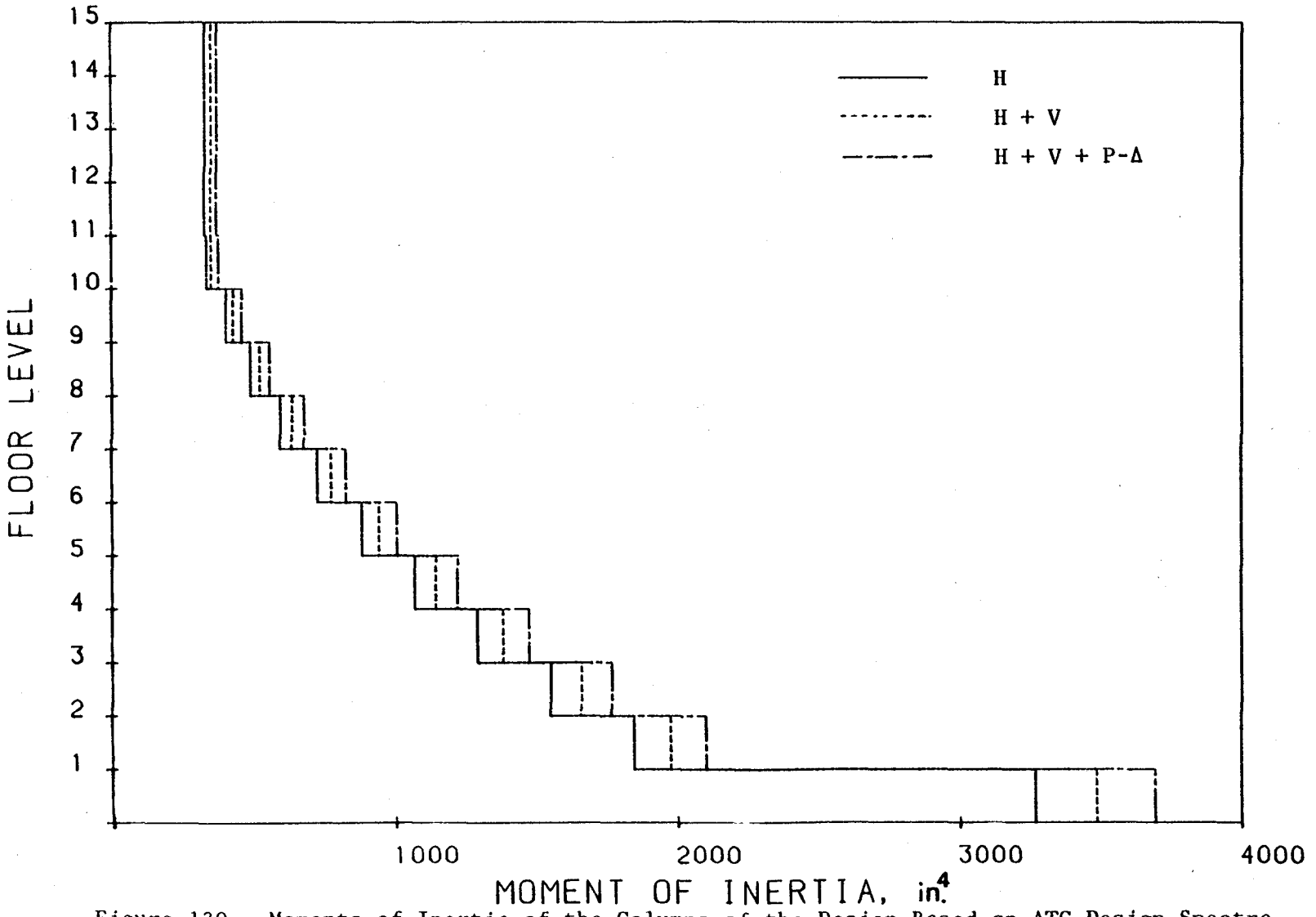

Figure 130. Moments of Inertia of the Columns of the Design Based on ATC Design Spectra with Stress Constraints. (1 in. = 2.54 cm).

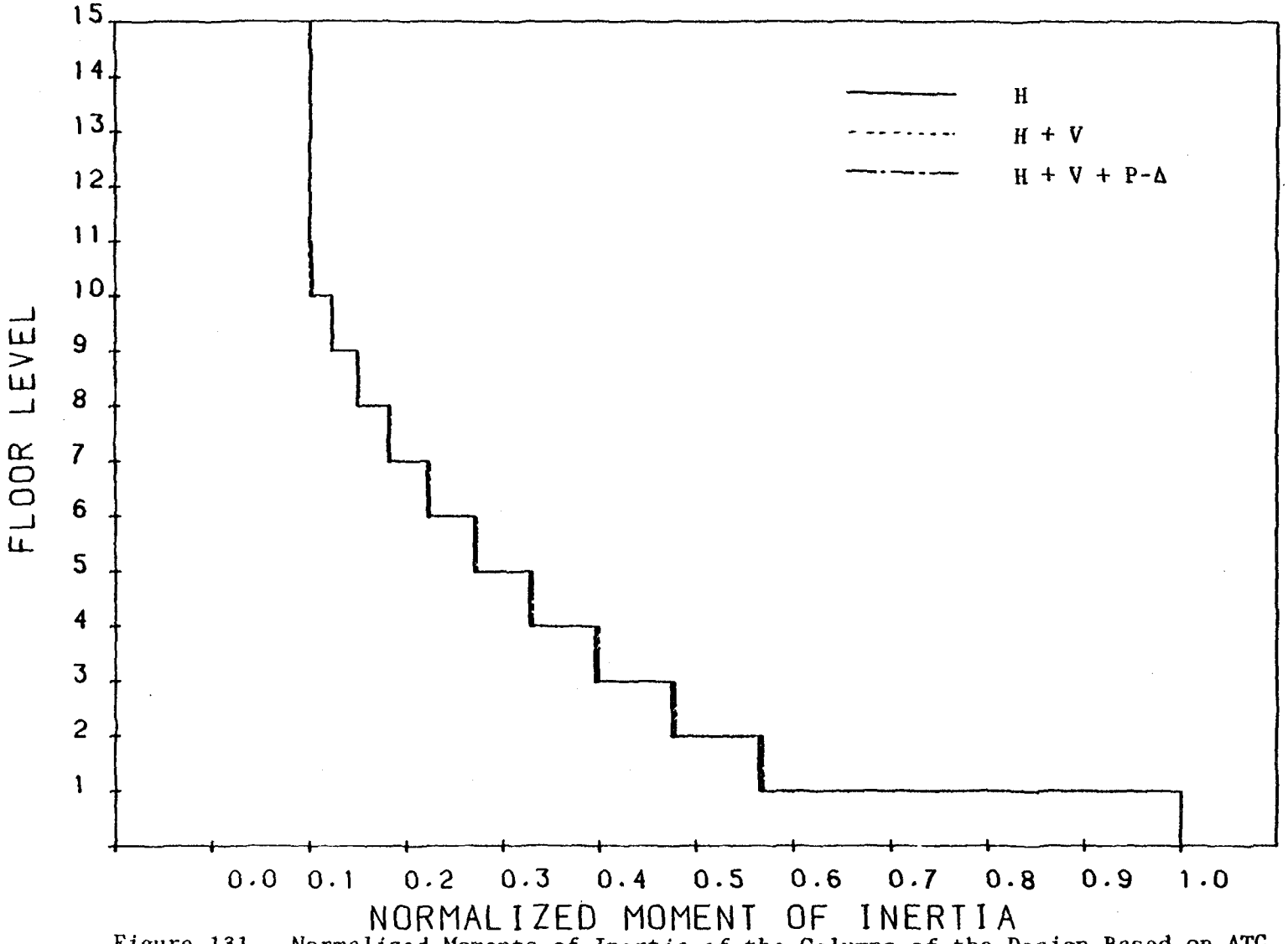

Figure 131. Normalized Moments of Inertia of the Columns of the Design Based on ATC Design Spectra with Stress Constraints.

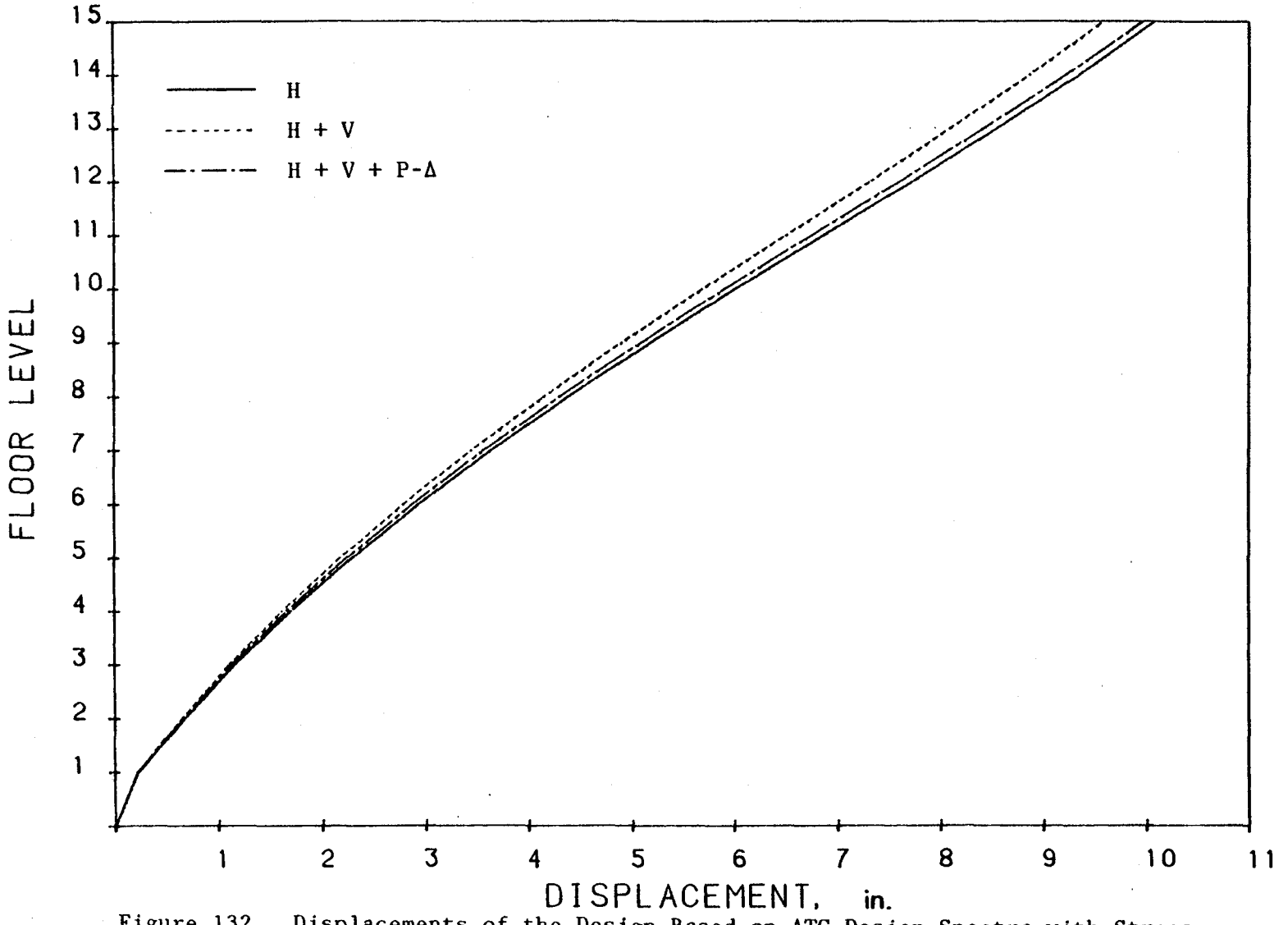

Figure 132. Displacements of the Design Based on ATC Design Spectra with Stress Constraints. (1 in. = 2.54 cm).

b. Displacement constraint only. Figure 133 represents the plots of weight versus cycles of iteration. Inspection of the final weight shows that it has an increment of 0.22% because of the inclusion of the vertical ground motions. Inclusion of the P-Δ effect produces a significant 3.37% increment in the optimum weight over that of a design without the P-Δ effect.

The distributions of the moments of inertia of the girders and columns are depicted in Figures 134 and 136, and the normalized moments of inertia of the girders and columns are shown in Figures 135 and 137 respectively.

Figure 138 shows the lateral displacements of each floor level in which the displacement of the top floor is violated in all cases.

3. Chinese Design Spectra

a. Stress constraint only. As shown in Figure 139, inclusion of the vertical ground motions decreases the final weight by 0.18%, but the P-Δ effect still significantly increases the optimum weight by 4.914%.

The distribution of the moments of inertia and the normalized moments of inertia of the girders and columns are delineated in Figures 140 through 143 respectively. Similar distributions for the girders and columns were obtained as previously illustrated.

Figure 144 shows the displacements of each floor level.

b. Displacement constraint only. Figure 145 represents the plot of weight versus cycles of iteration. There is a 0.167% increment in optimum weight occasioned by the inclusion of vertical ground motions. Inclusion of the P-Δ effect yields an important

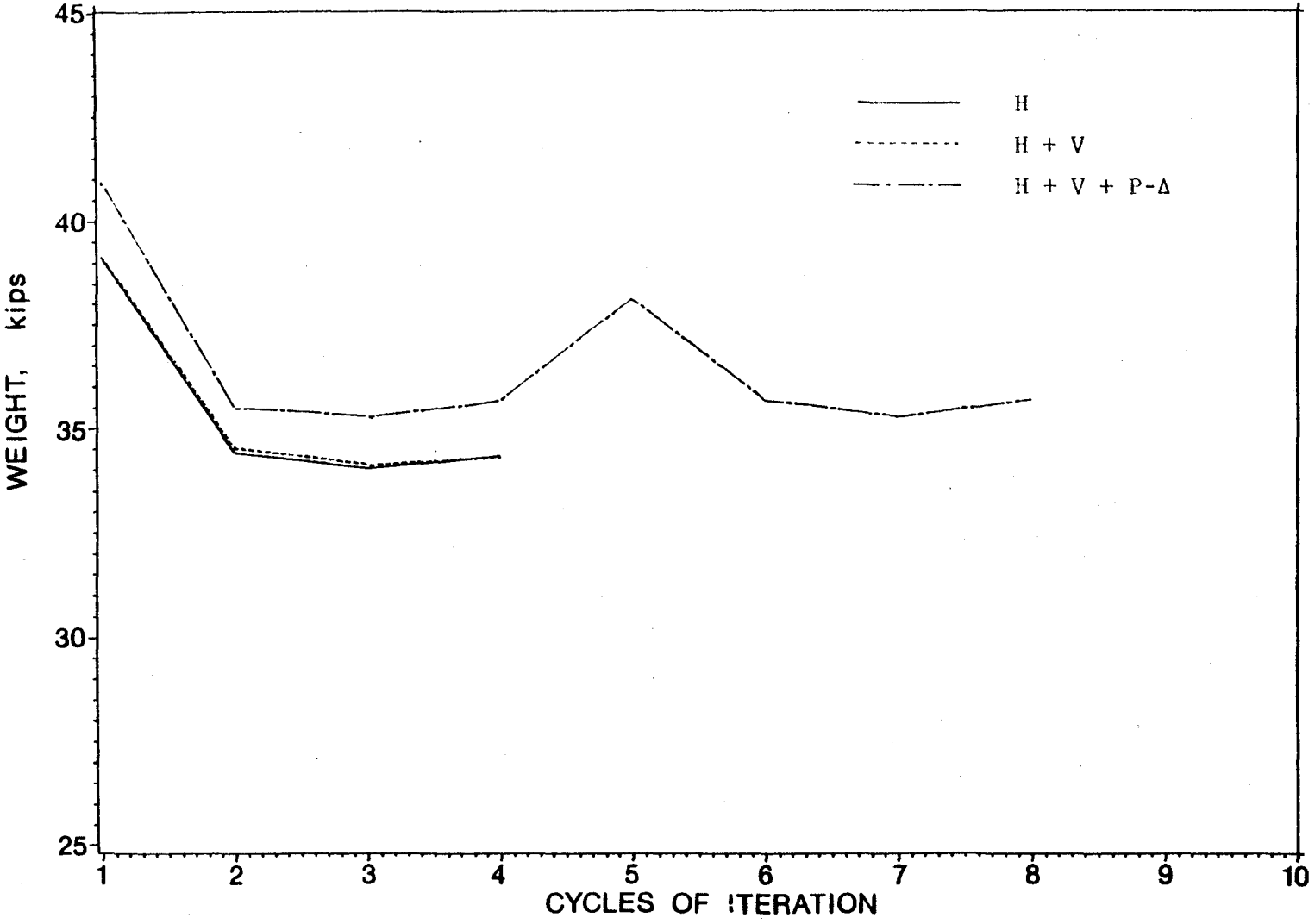

Figure 133. Weight v.s. Cycles of Iteration Plot of the Design Based on ATC Design Spectra with Displacement Constraints. (1 kip = 4.448 kN).

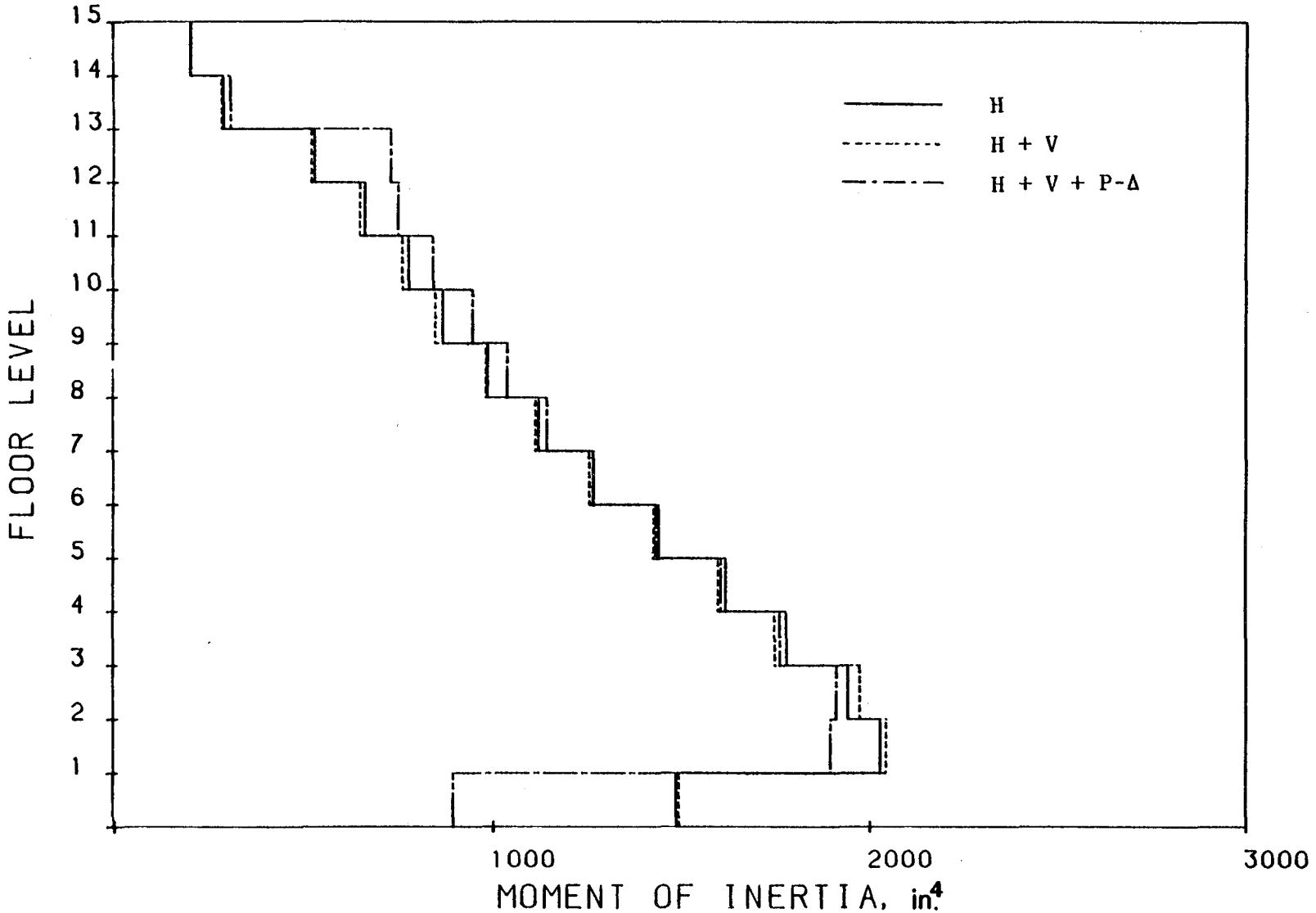

Figure 134. Moments of Inertia of the Girders of the Design Based on ATC Design Spectra with Displacement Constraints. (1 in. = 2.54 cm).

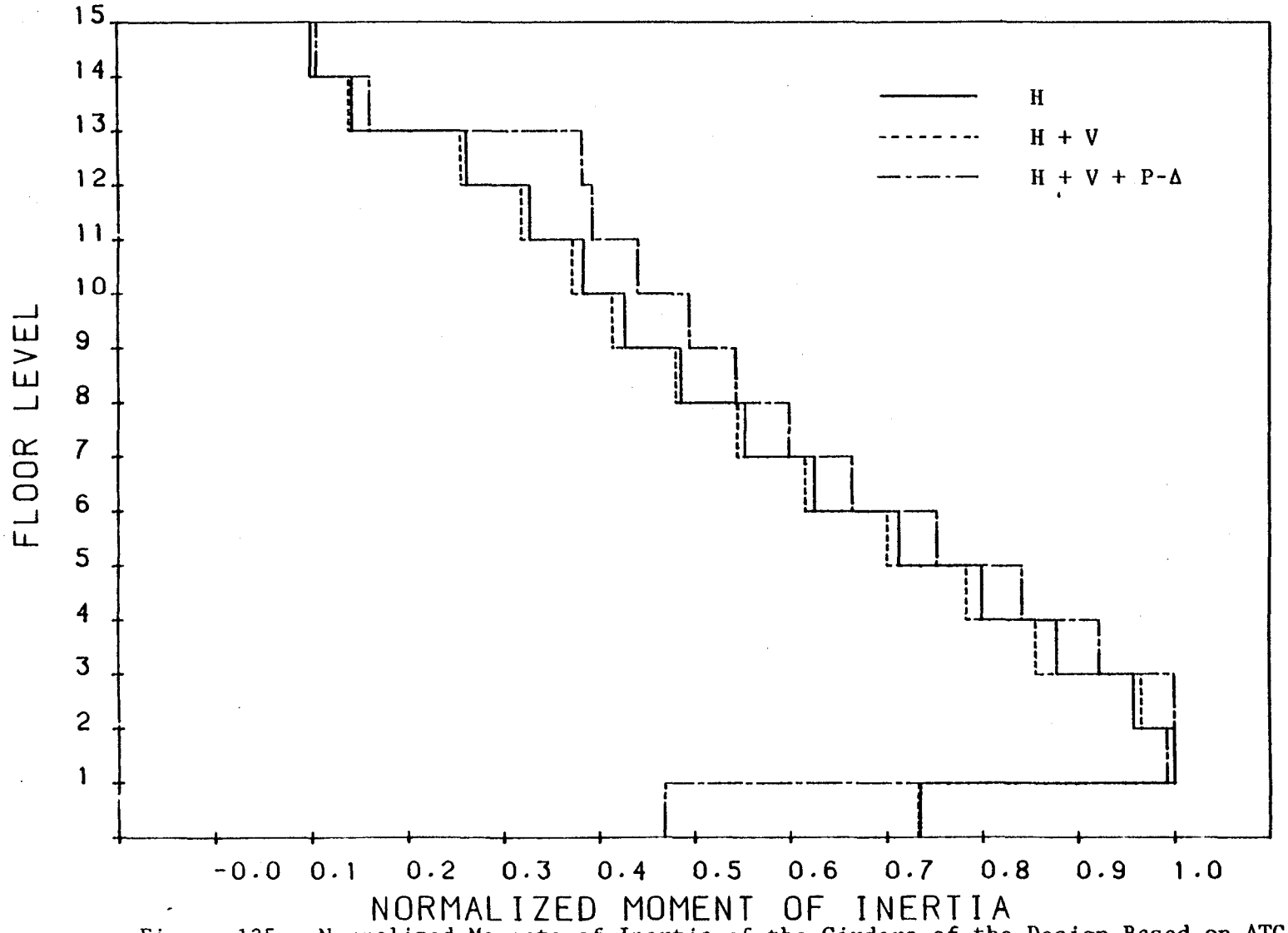

Figure 135. Normalized Moments of Inertia of the Girders of the Design Based on ATC Design Spectra with Displacement Constraints.

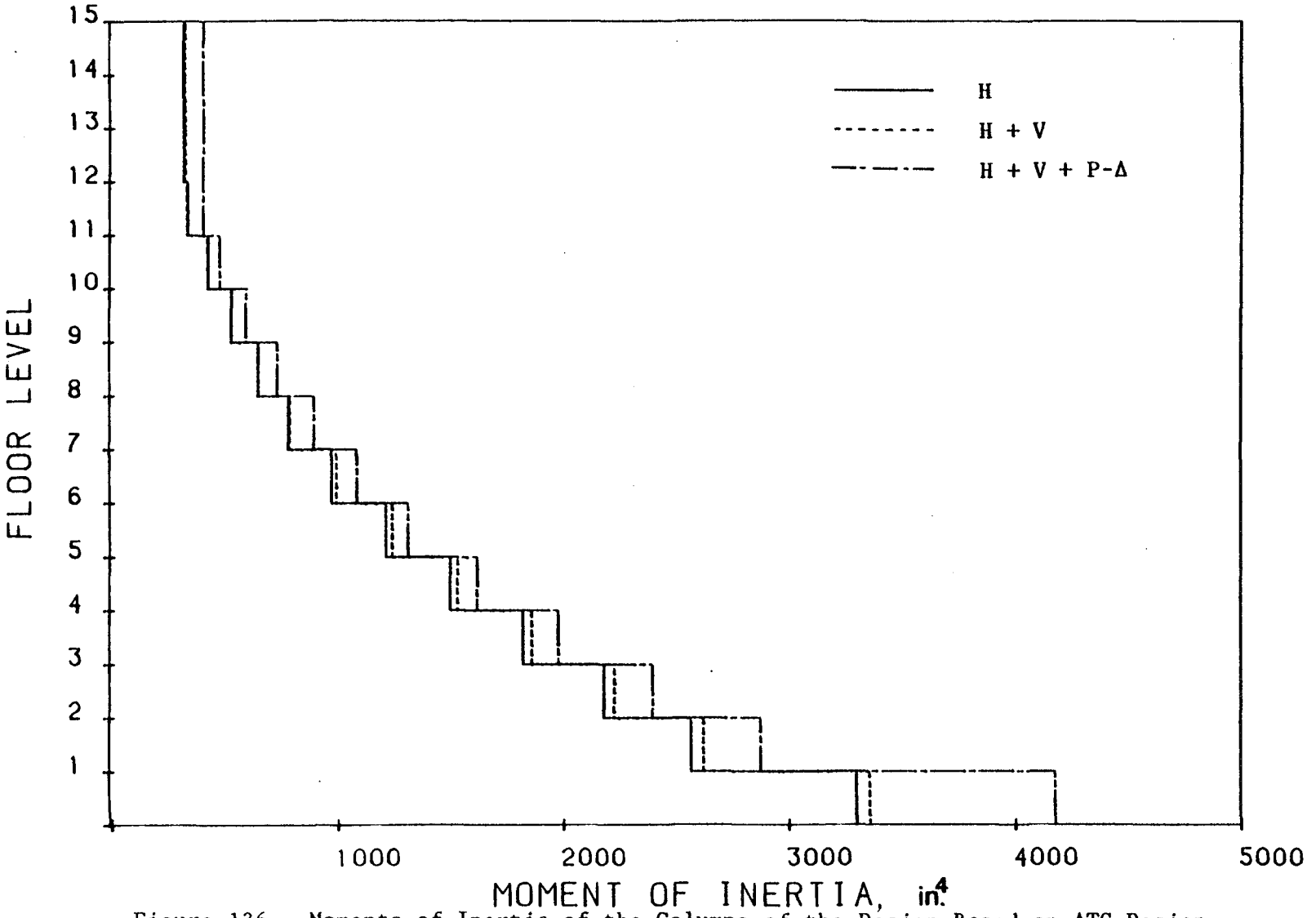

Figure 136. Moments of Inertia of the Columns of the Design Based on ATC Design Spectra with Displacement Constraints. (1 in. = 2.54 cm).

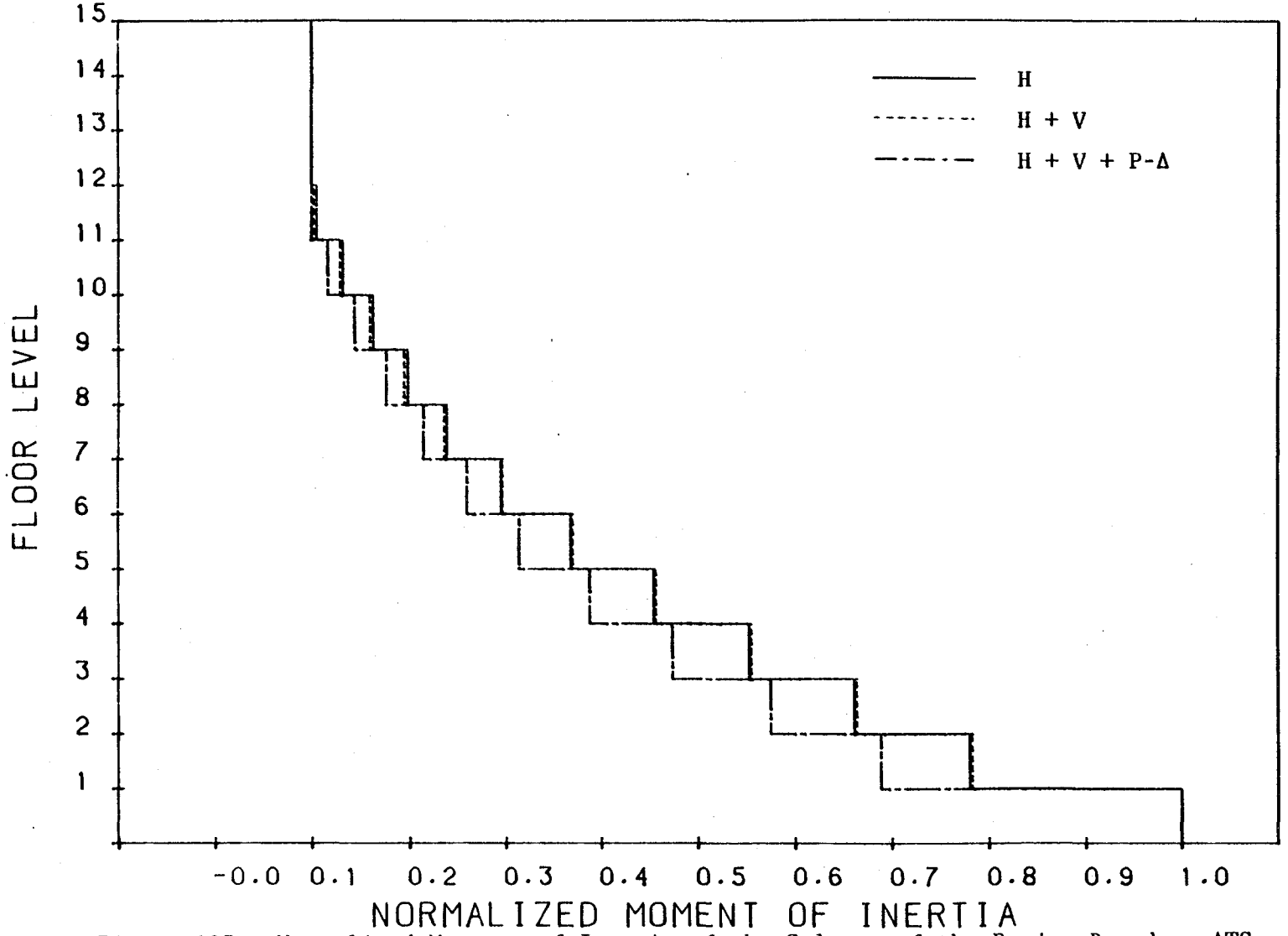

Figure 137. Normalized Moments of Inertia of the Columns of the Design Based on ATC Design Spectra with Displacement Constraints.

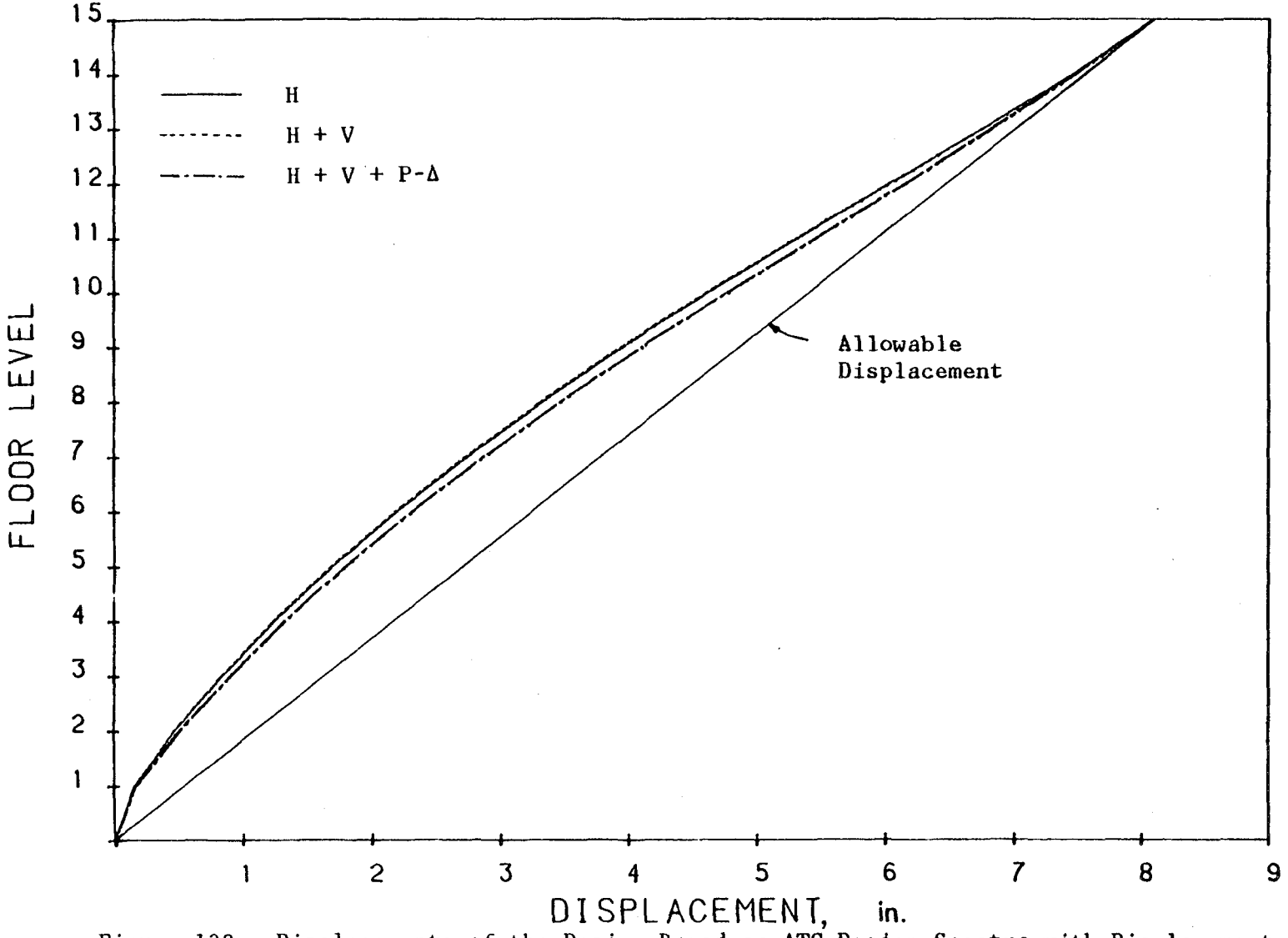

Figure 138. Displacements of the Design Based on ATC Design Spectra with Displacement Constraints. (1 in. = 2.54 cm).

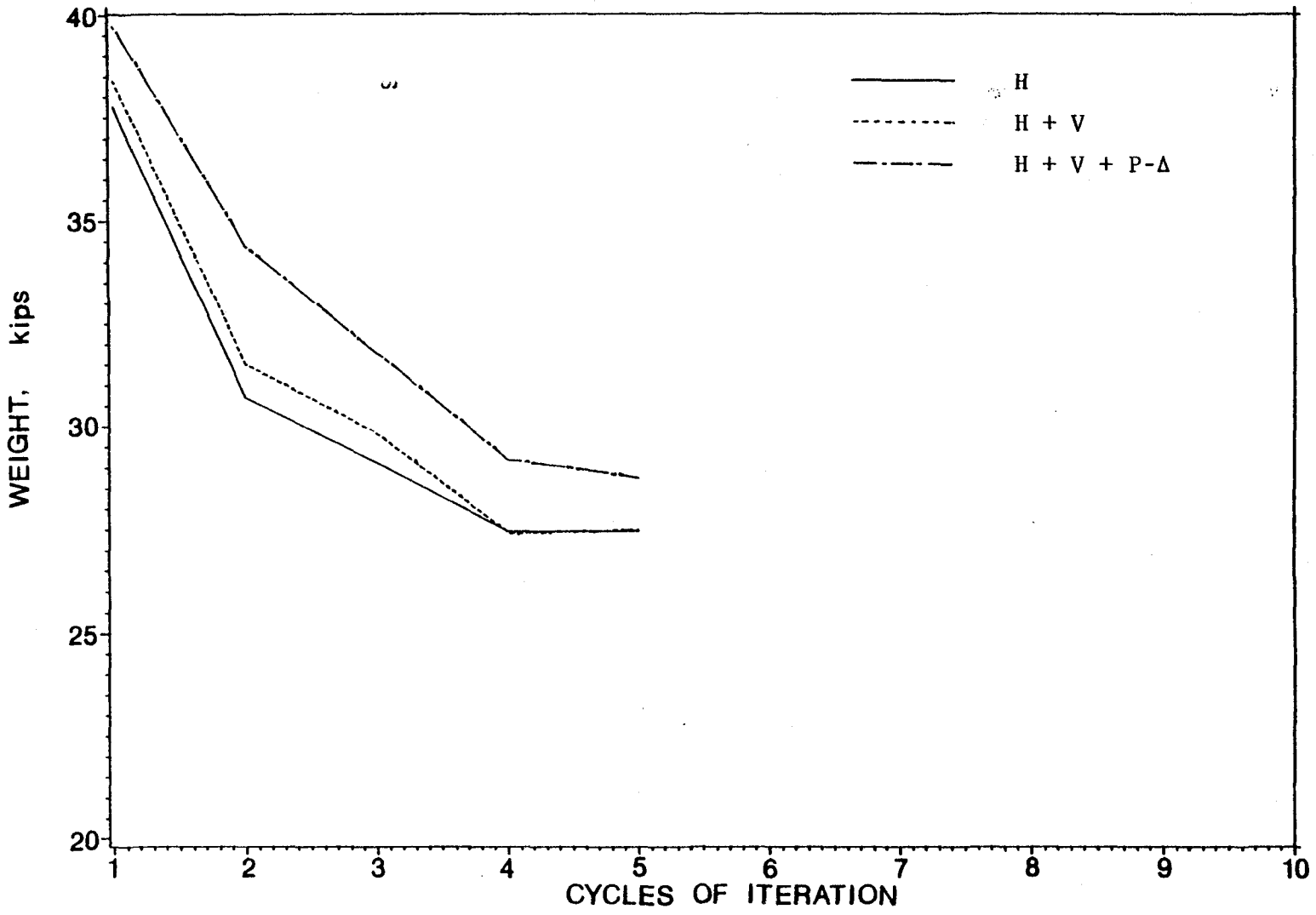

Figure 139. Weight v.s. Cycles of Iteration Plot of the Design Based on Chinese Spectra with Stress Constraints. (1 kip = 4.448 kN).

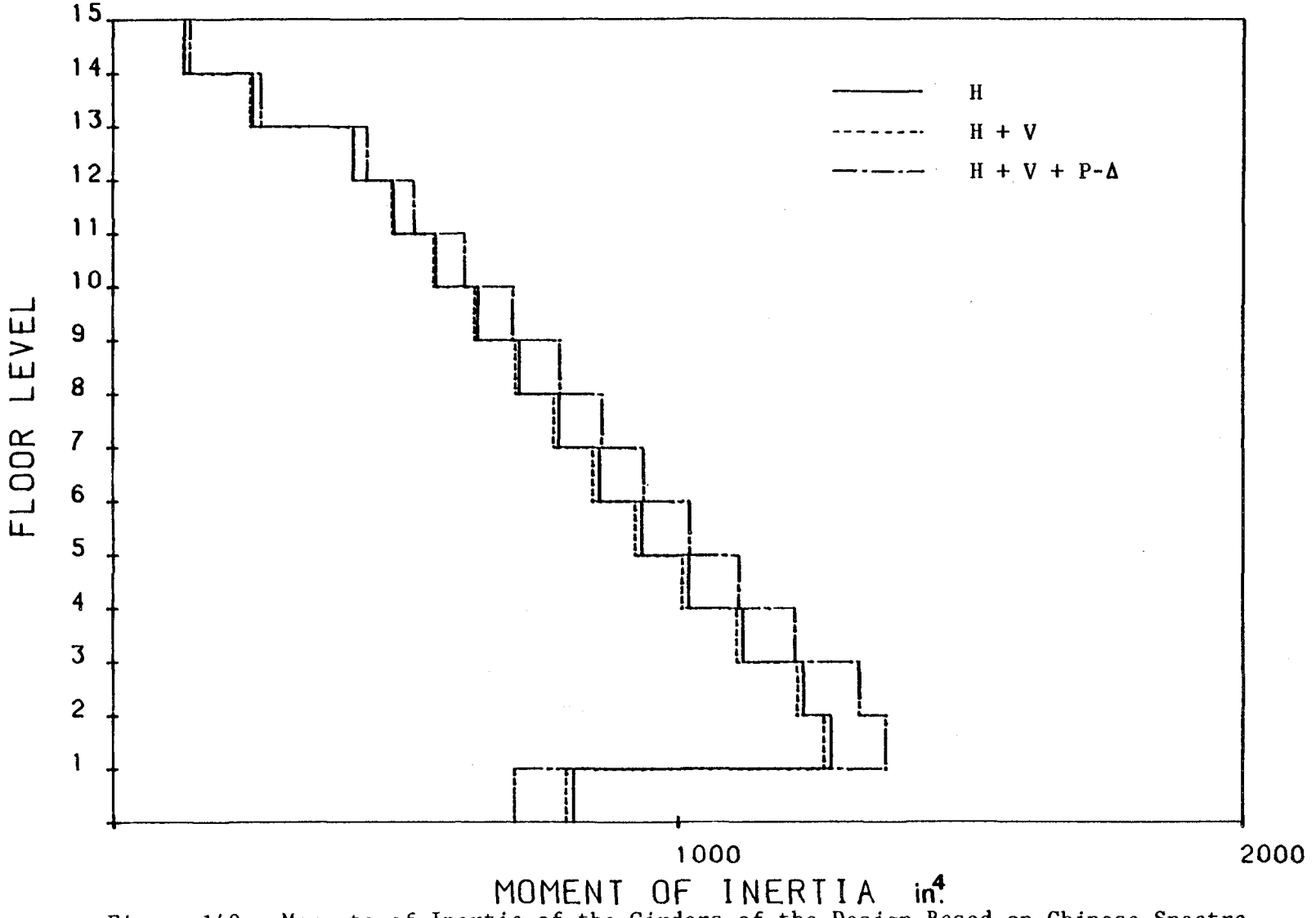

Figure 140. Moments of Inertia of the Girders of the Design Based on Chinese Spectra with Stress Constraints. (1 in. = 2.54 cm).

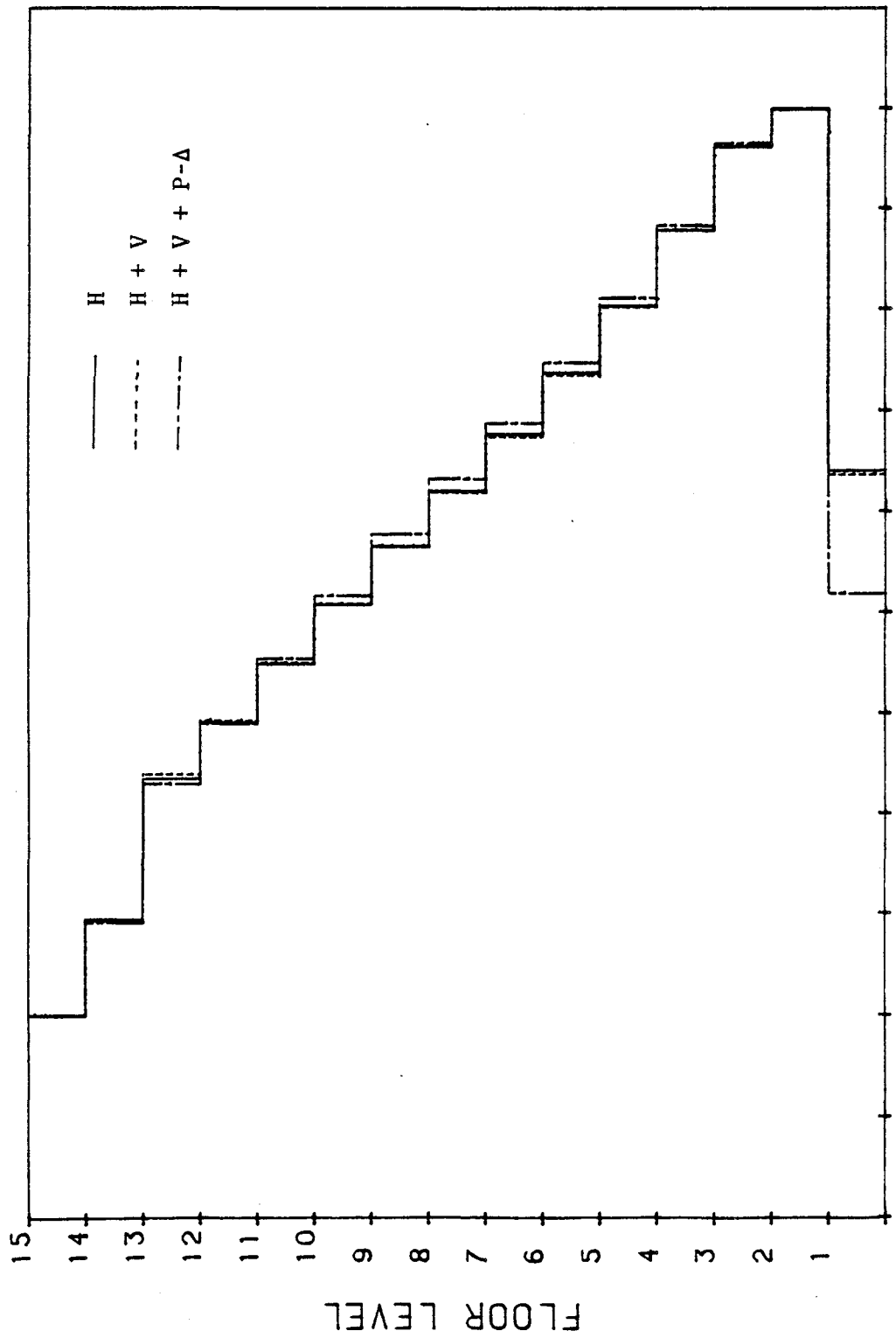

Figure 141. Normalized Moments of Inertia of the Girders of the Design Based on Chinese Spectra with Stress Constraints.

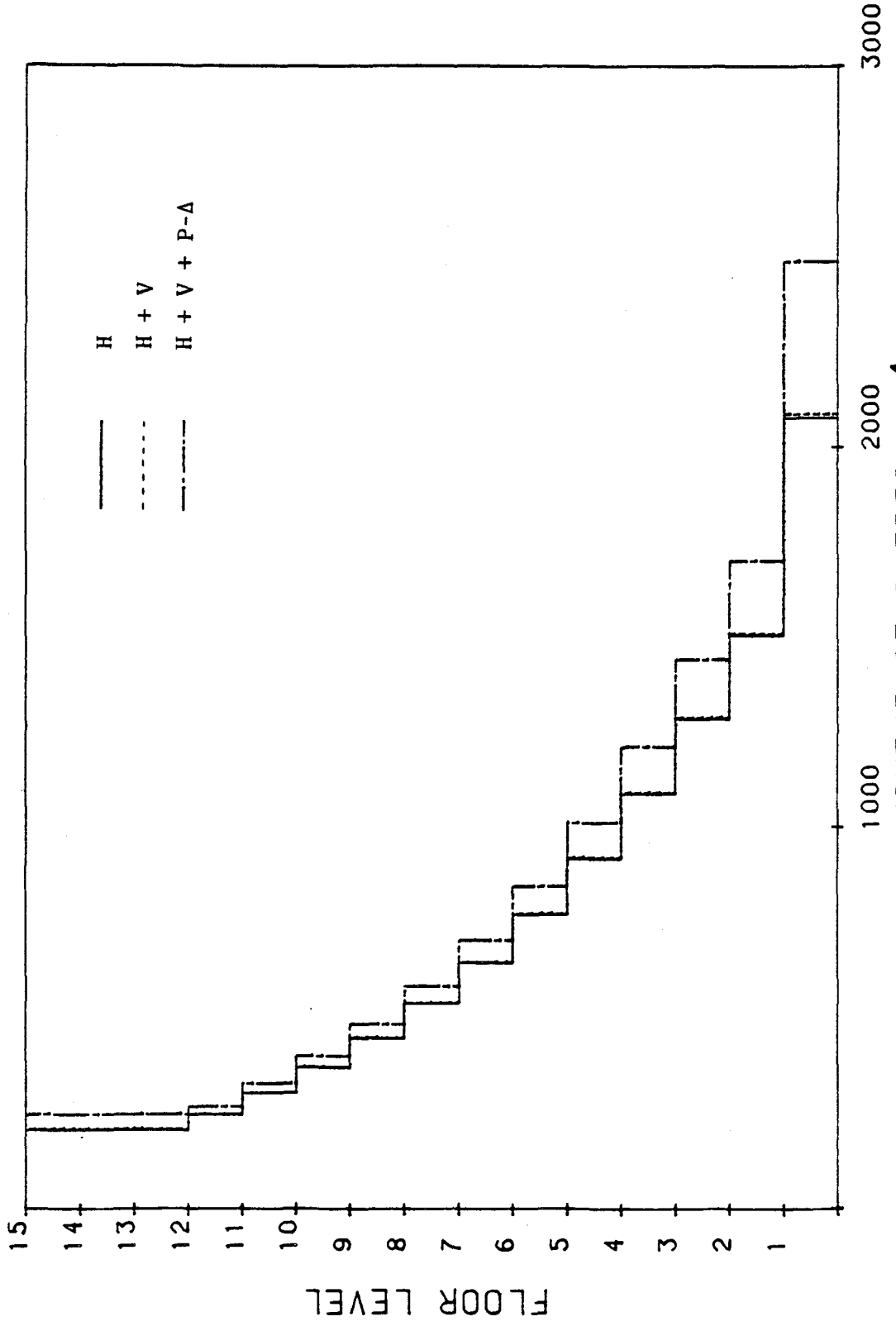

Figure 142. Moments of Inertia of the Columns of the Design Based on Chinese Spectra with Stress Constraints. (1 in. = 2.54 cm).

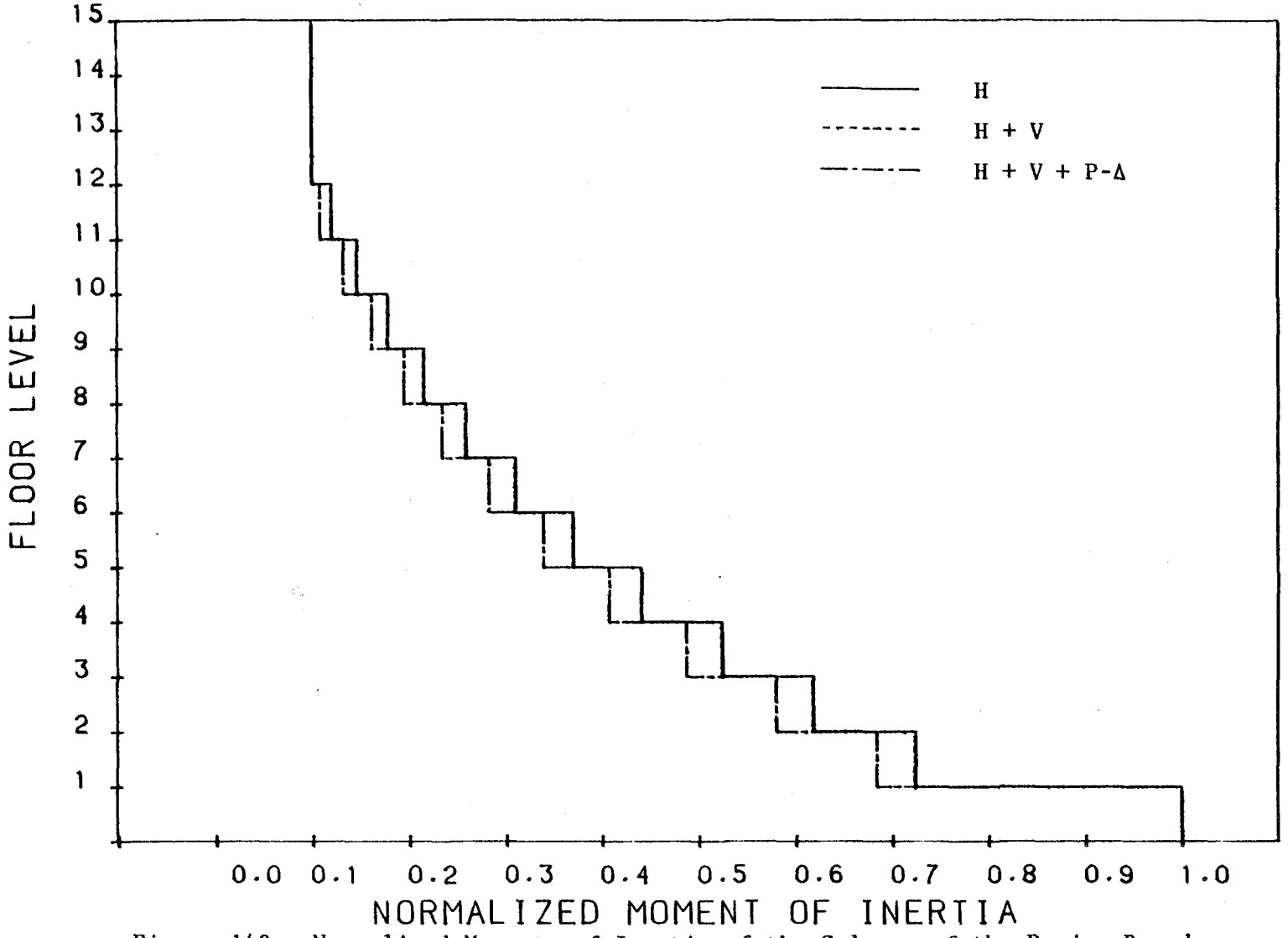

Figure 143. Normalized Moments of Inertia of the Columns of the Design Based on Chinese Spectra with Stress Constraints.

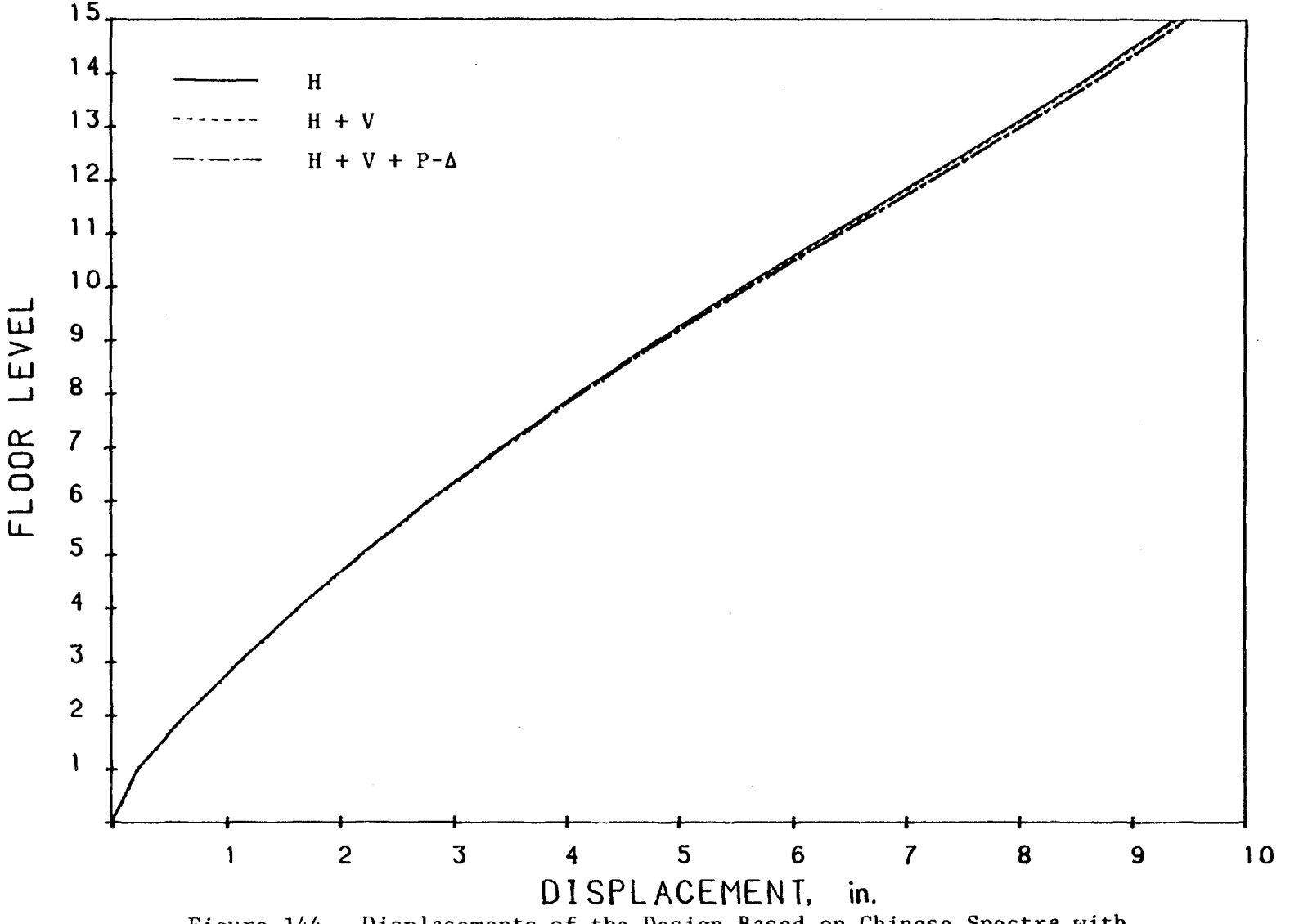

Figure 144. Displacements of the Design Based on Chinese Spectra with Stress Constraints. (1 in. = 2.54 cm).

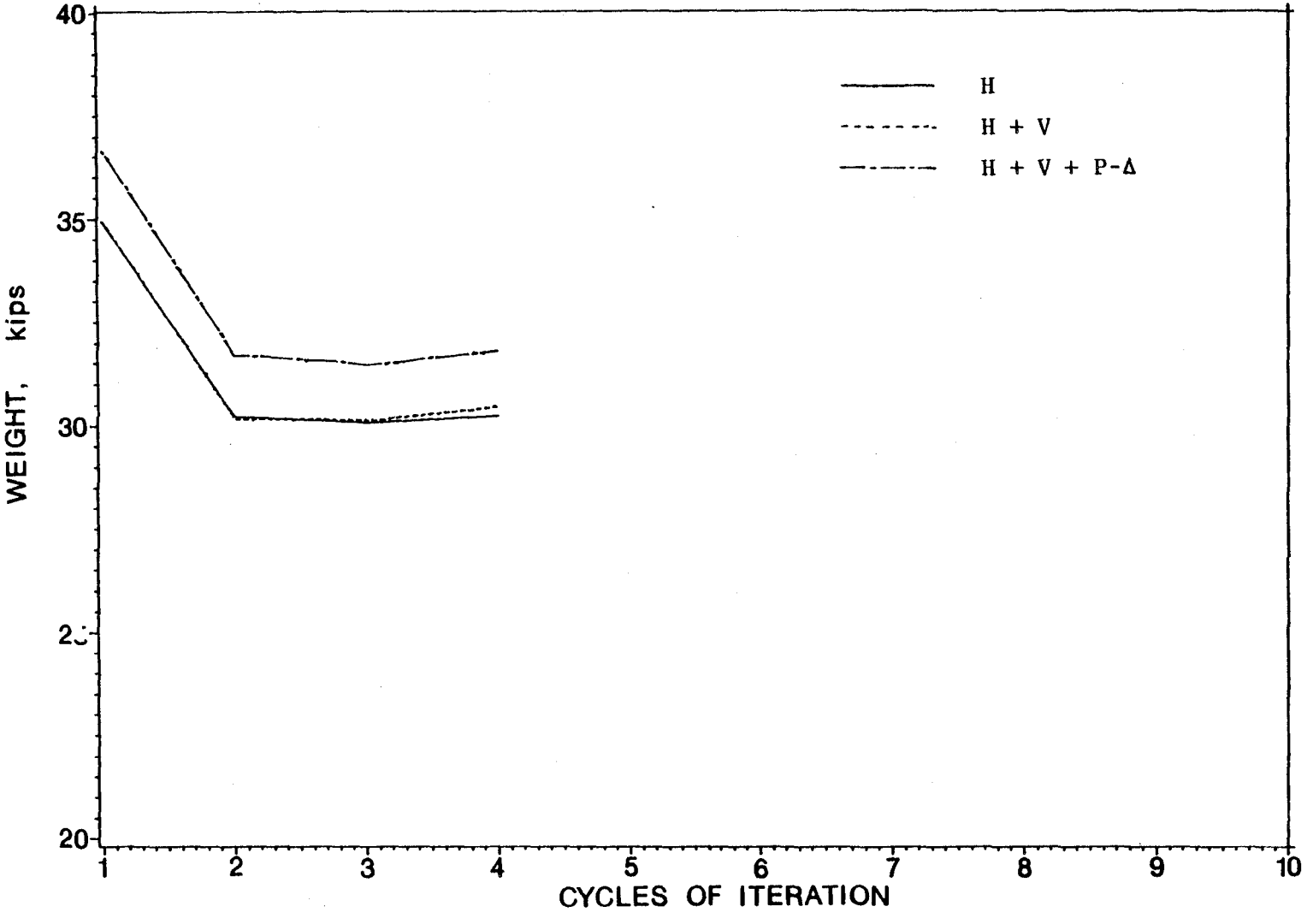

Figure 145. Weight v.s. Cycles of Iteration Plot of the Design Based on Chinese Spectra with Displacement Constraints. (1 kip = 4.448 kN).

increment in optimum weight of 4.518%.

The moments of inertia and normalized moments of inertia of the girders and columns are shown respectively in Figures 146 through 149. Note that the moment of inertia of a girder on the twelfth floor is larger than that of a girder on the eleventh floor.

The displacements at each floor are sketched in Figure 150. In this instance, all of the cases have violated displacement at the top floor.

All of the design results are summarized in Tables XVII and XVIII in which the natural periods, the final weight, the increments occasioned by the inclusion of vertical motions and P-Δ effect, and cycles of iteration are listed. It is apparent that when multi-component ground motions combine with P-Δ forces, there can be an incremental of yield nearly 3% to 4% in structural weight over that of a design in which the P-Δ effect is not included. However, the influence of vertical motions can only produce around 0.2% increment or even induce a decrease in weight.

K. THE INFLUENCE OF FIXED SUPPORT CONDITIONS ON THE FIRST-FLOOR-GIRDER RIGIDITY

As illustrated in the previous sections of this chapter, the moment of inertia of a girder on the first floor of a structure is decidedly less than the moment of inertia of a girder on the second floor. This phenomenon is mainly due to the fixed support conditions. Because rotational degrees of freedom are restrained at supports, the displacement on the first floor is affected slightly as shown in the

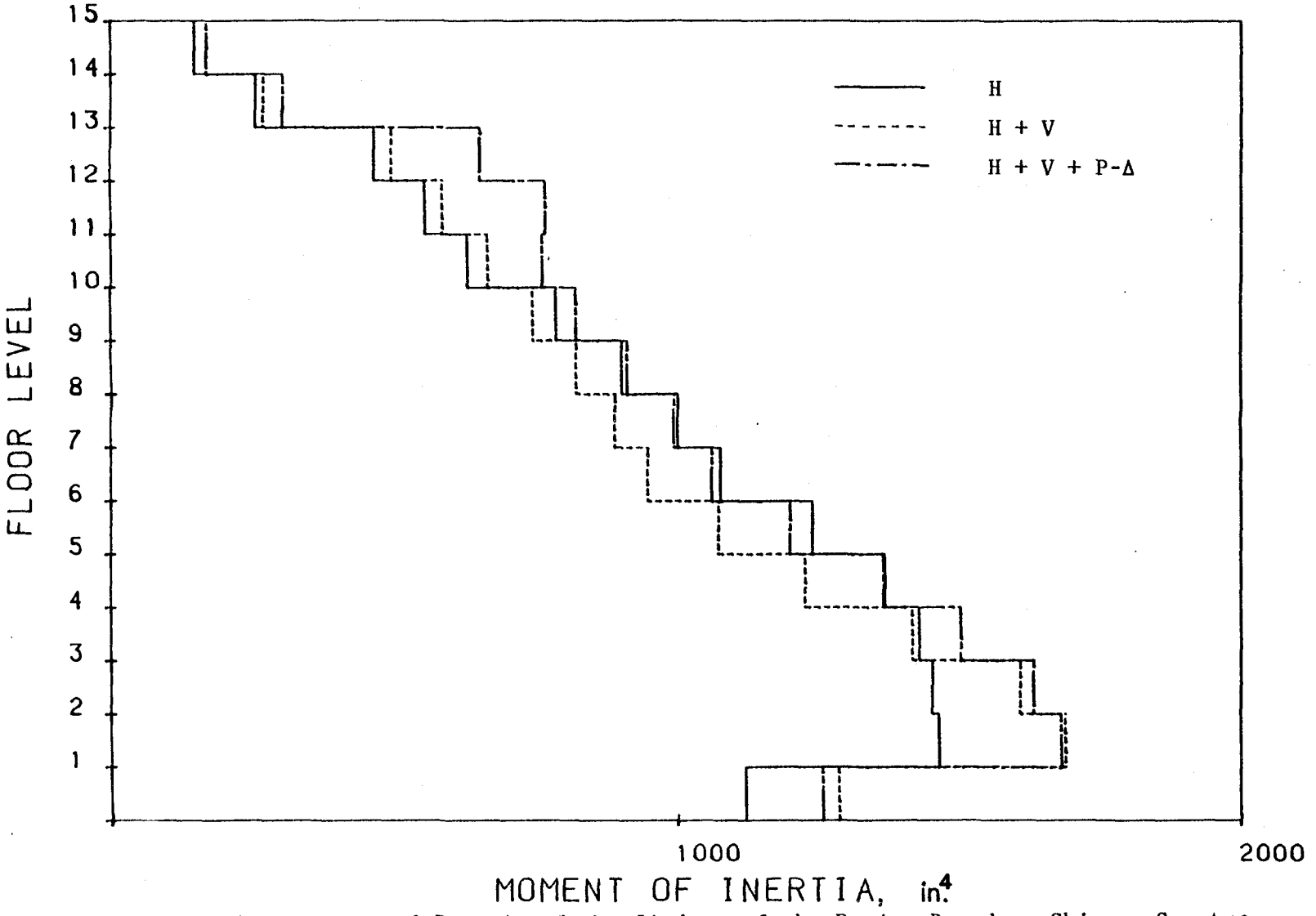

Figure 146. Moments of Inertia of the Girders of the Design Based on Chinese Spectra with Displacement Constraints. (1 in. = 2.54 cm).

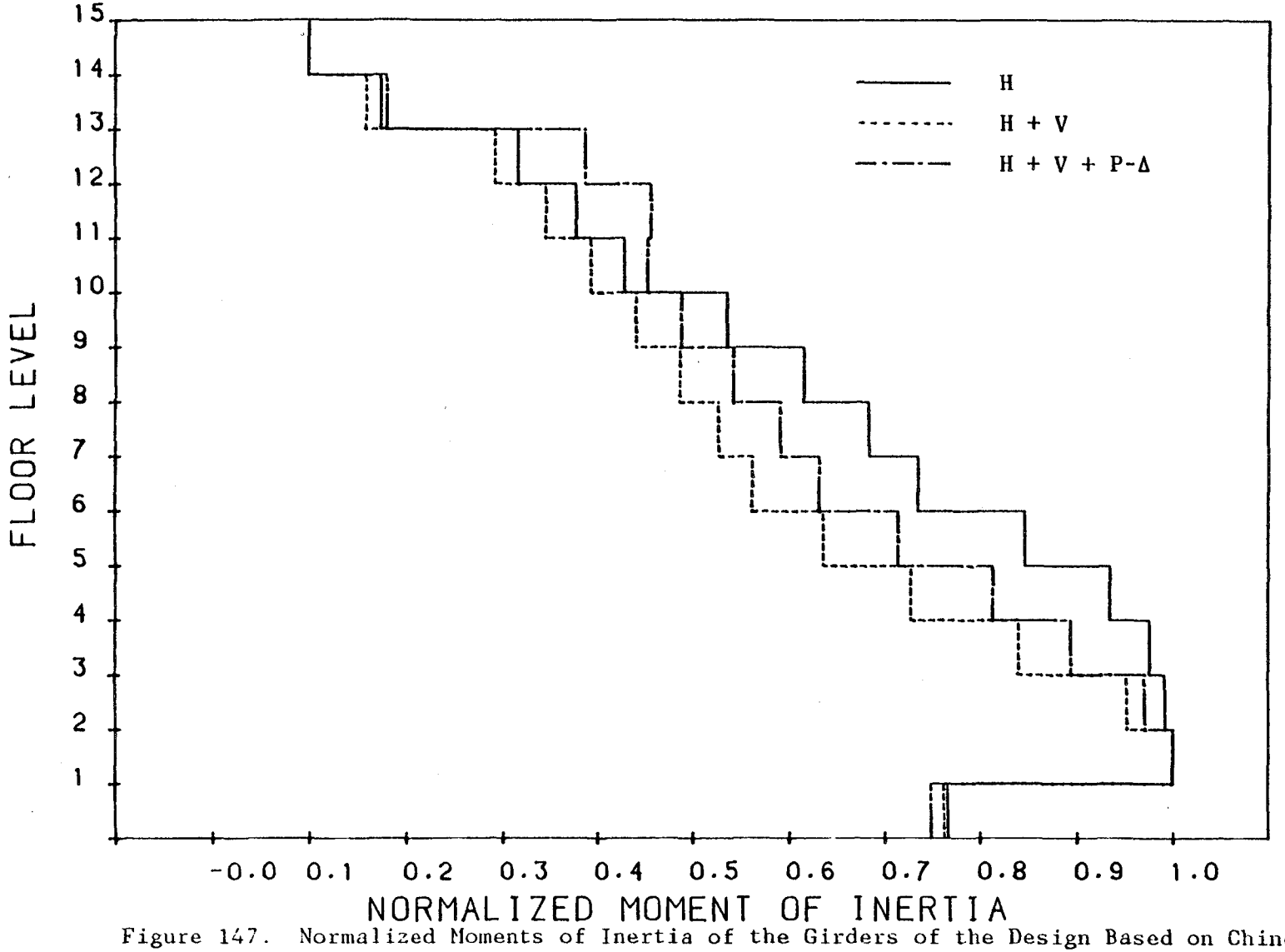

Figure 147. Normalized Moments of Inertia of the Girders of the Design Based on Chinese Spectra with Displacement Constraints.

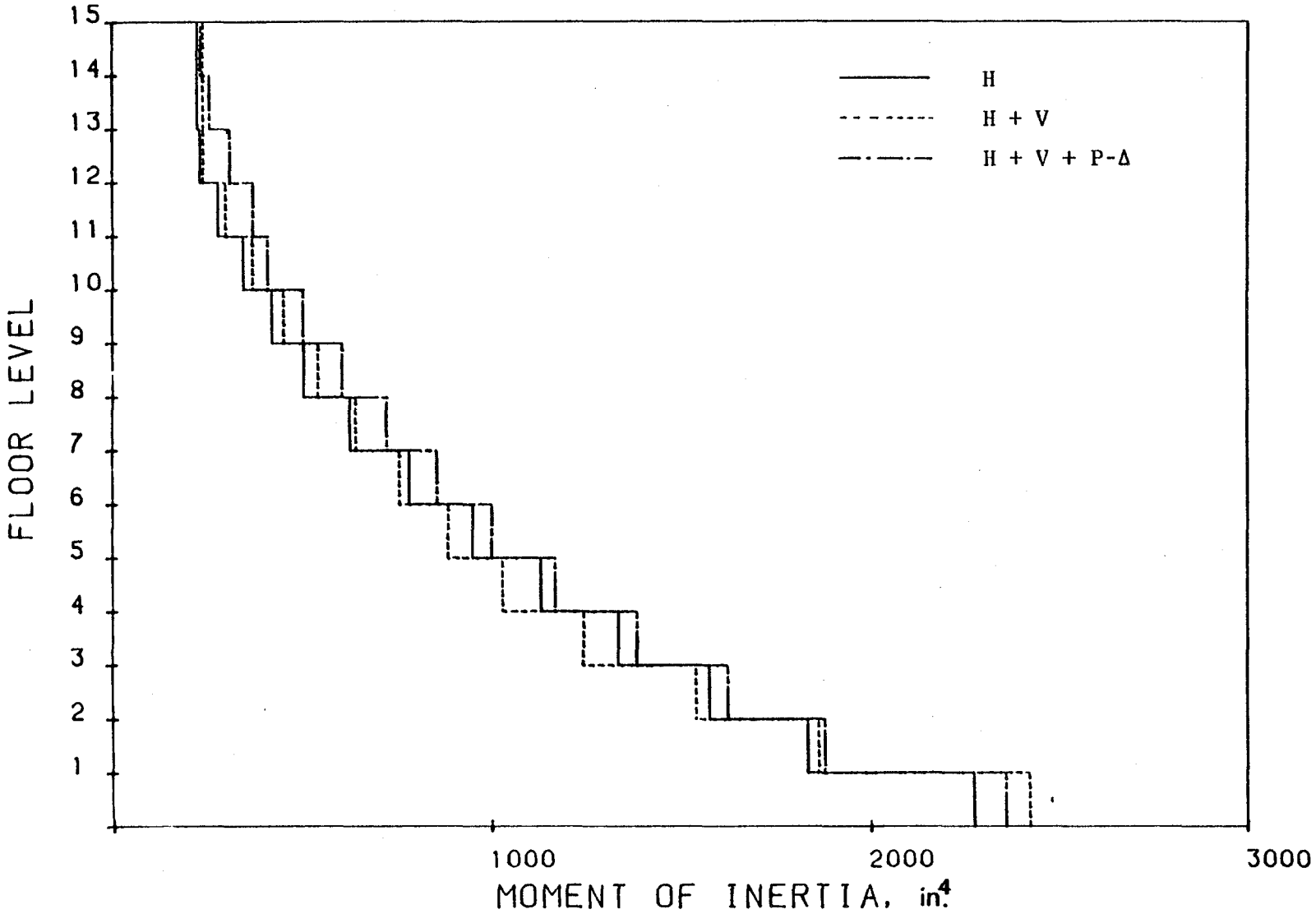

Figure 148. Moments of Inertia of the Columns of the Design Based on Chinese Spectra with Displacement Constraints. (1 in. = 2.54 cm).

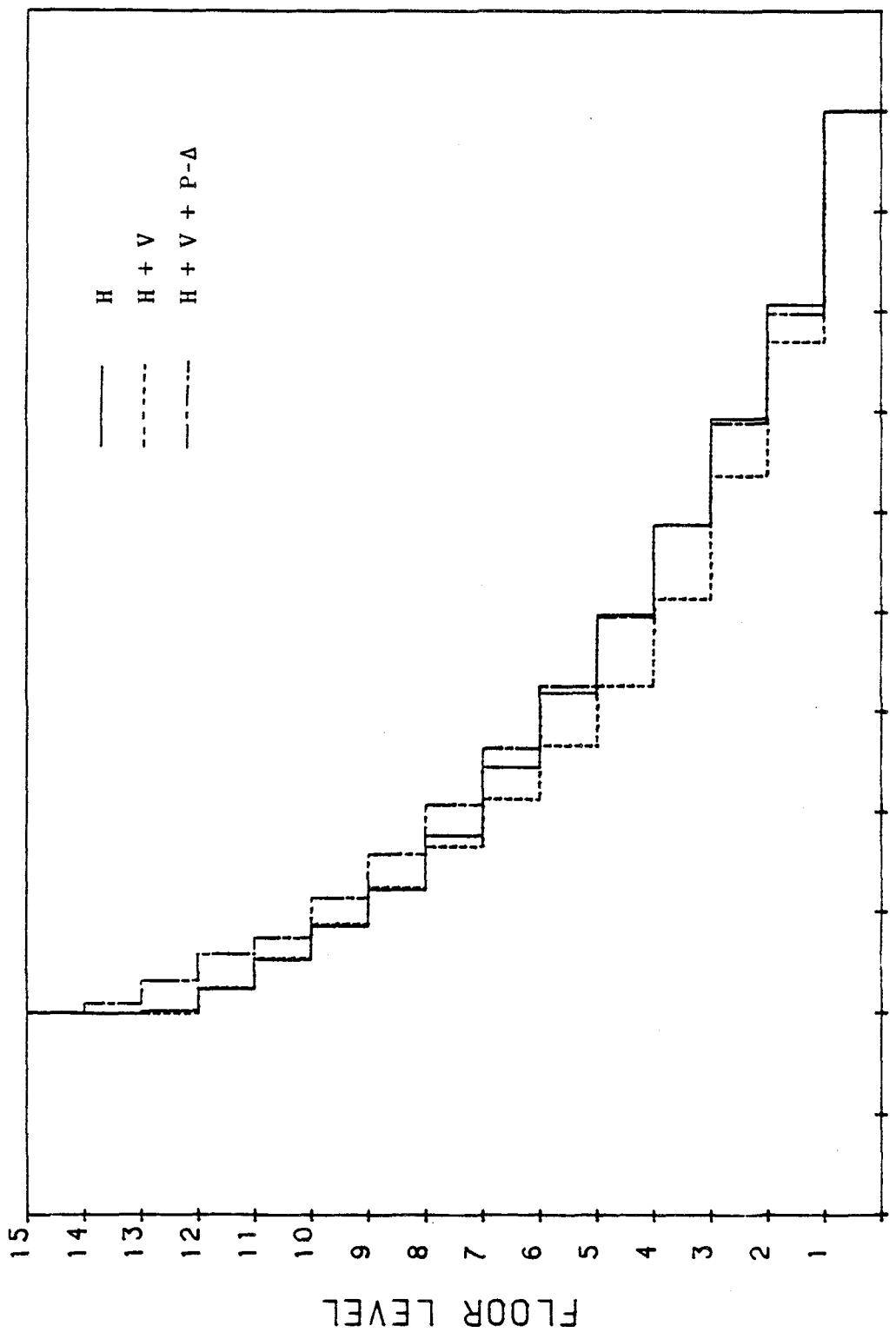

Figure 149. Normalized Moments of Inertia of the Columns of the Design Based on Chinese Spectra with Dispiacement Constraints.

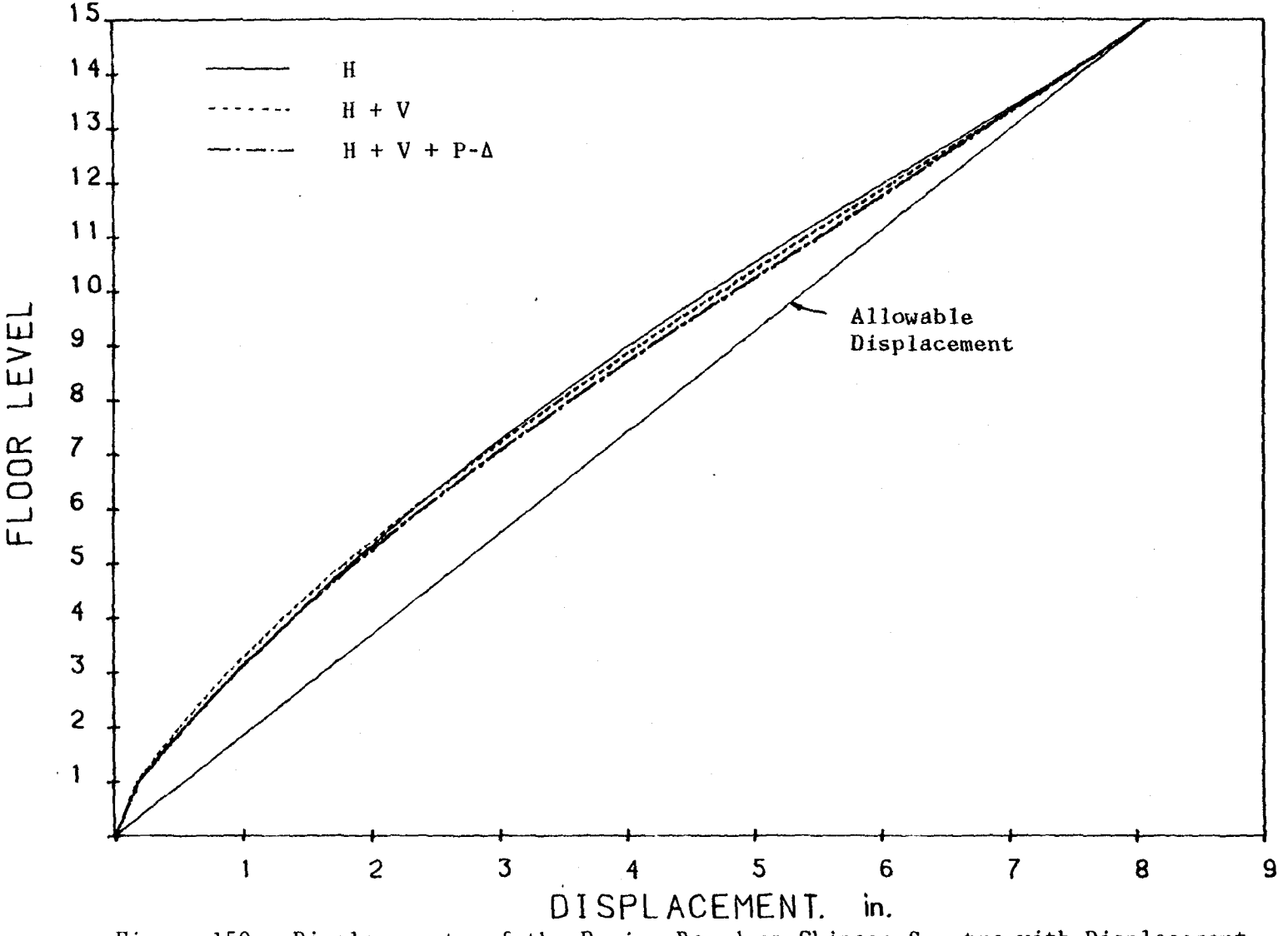

Figure 150. Displacements of the Design Based on Chinese Spectra with Displacement Constraints. (1 in. = 2.54 cm).

TABLE XVII. THE NATURAL PERIODS, THE FINAL WEIGHT, THE INCREMENTAL WEIGHT, AND DESIGN CYCLES OF THE 15-STORY, ONE-BAY FRAME FOR THE STUDIES OF THE INFLUENCE OF VERTICAL MOTIONS AND THE P-Δ EFFECT BASED ON STRESS CONSTRAINTS. (1 kip = 4.448 kN).

		Natural Period (sec/cycle)					Final Weight	Incremental	Cycles
		1	2	3	4	5	(kips)	of Weight	
90 Percentile,	H	3.778	1.287	0.741	0.518	0.386	27.758	-0.484%	9
Alluvium, 5% Damp-	H+V	3.788	1.294	0.743	0.520	0.387	27.624	3.690%	10
ing Design Spectra	H+V+PΔ	3.832	1.295	0.744	0.514	0.386	28.643		8
ATC-3-06	H	3.582	1.229	0.711	0.492	0.366	29.577	3.160%	10
Design	H+V	3.497	1.201	0.696	0.483	0.358	30.512	2.458%	8
Spectra	H+V+PΔ	3.558	1.208	0.696	0.479	0.355	31.262		10
Chinese	H	3.771	1.307	0.756	0.528	0.396	27.462	-0.180%	4
Design	H+V	3.765	1.306	0.755	0.530	0.395	27.412	4.914%	4
Spectra	H+V+PΔ	3.805	1.298	0.745	0.520	0.388	28.759		5

TABLE XVIII. THE NATURAL PERIODS, THE FINAL WEIGHT, THE INCREMENTAL WEIGHT, AND DESIGN CYCLES OF THE 15-STORY, ONE-BAY FRAME FOR THE STUDIES OF THE INFLUENCE OF VERTICAL MOTIONS AND THE P-Δ EFFECT BASED ON DISPLACEMENT CONSTRAINTS. (1 kip = 4.448 kN).

		Natural Period (sec/cycle)					Final Weight (kips)	Incremental of Weight	Cycles
		1	2	3	4	5			
90 Percentile,	H	3.229	1.058	0.619	0.431	0.321	33.719	1.100%	4
Alluvium, 5% Damp-	H+V	3.212	1.082	0.627	0.439	0.325	34.080	4.146%	4
ing Design Spectra	H+V+PΔ	3.212	1.075	0.623	0.432	0.317	35.493		7
ATC-3-06	H	3.196	1.093	0.633	0.440	0.327	34.039	0.220%	3
Design	H+V	3.196	1.094	0.633	0.440	0.327	34.113	3.370%	3
Spectra	H+V+PΔ	3.197	1.072	0.617	0.430	0.318	35.263		7
Chinese	H	3.500	1.221	0.707	0.492	0.367	30.066	0.167%	3
Design	H+V	3.507	1.195	0.695	0.486	0.364	30.117	4.518%	3
Spectra	H+V+PΔ	3.526	1.169	0.682	0.475	0.353	31.478		3

plots of displacements. The deformations as well as the internal forces of a girder on the first floor are therefore much smaller than those of a girder on the second floor. Based on the energy requirement, a girder on the first floor requires a smaller moment of inertia than a girder on the second floor.

The frame shown in Figure 114 was redesigned by changing the fixed supports to hinged supports as shown in Figure 151. The structure was designed by using the Chinese design spectra for which both the horizontal and vertical motions were included. All the other design conditions are the same as those used in Section VI.J.

As expected, the moment of inertia of the girder on the first floor is larger than that of the girder on the second floor. The distribution of the moments of inertia of the girders is shown in Figure 153. In this case, the girder at the top floor is the smallest. The moment of inertia increases almost linearly from the top to the second floor and increases abruptly at the first floor. This type of distribution is similar to that of the columns as depicted in Figures 155 and 156.

Figure 157 illustrates the displacements of each floor level. Because of the release of restraints on the rotational degrees of freedom at the supports, the lateral displacement varies almost linearly from the bottom to the top of the building.

The optimum weight is also as expected much heavier than that of a frame having fixed supports. Figure 152 represents the plot of the weight versus cycles of iteration.

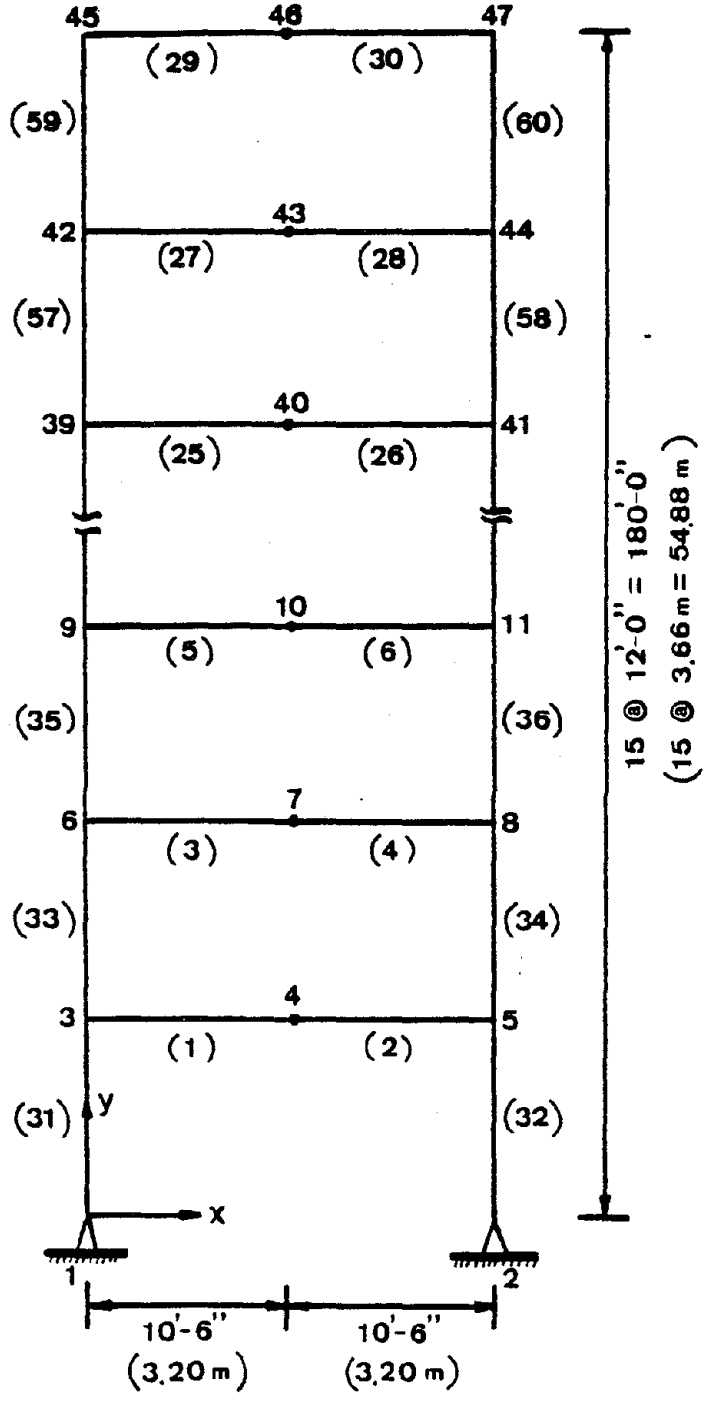

Figure 151. 15-Story, One-Bay, Unbraced Frame with Hinge Supports for the Study of the Influence of Different Supports on the First-Floor-Rigidity.

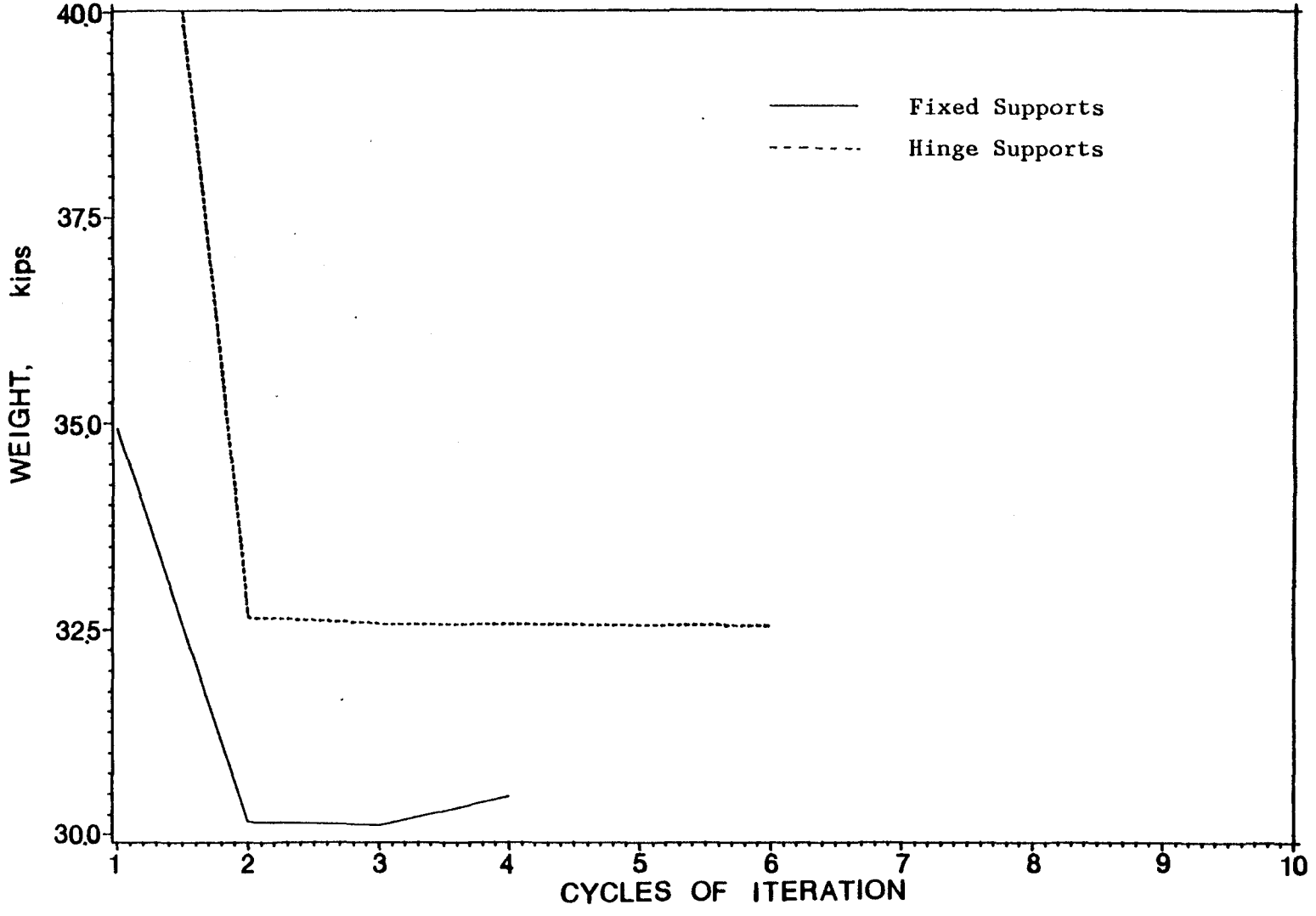

Figure 152. Weight v.s. Cycles of Iteration Plot of the 15-Story, One-Bay, Unbraced Frame for the Study of the Influence of Different Supports on the First-Floor-Rigidity. (1 kip = 4.448 kN).

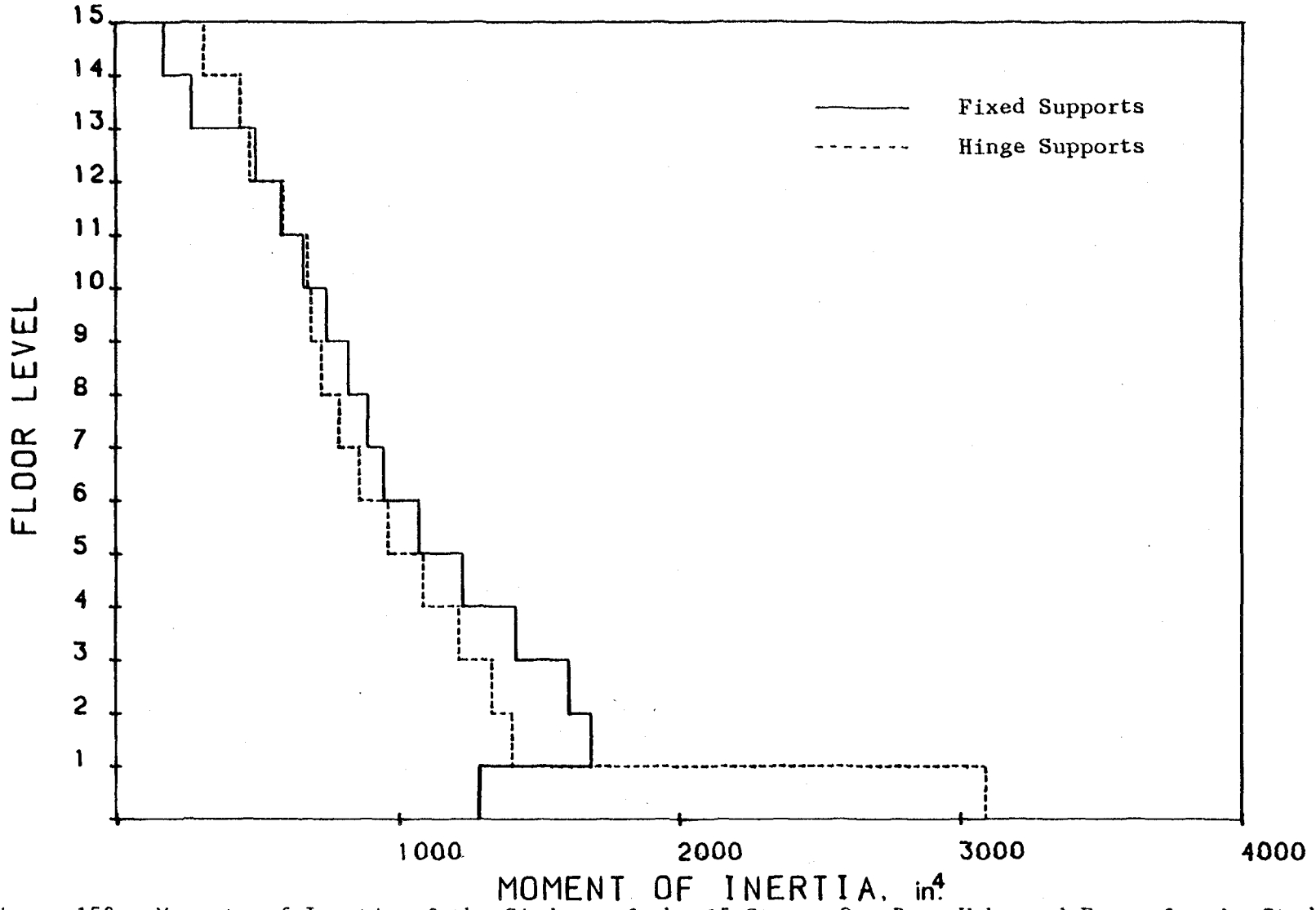

Figure 153. Moments of Inertia of the Girders of the 15-Story, One-Bay, Unbraced Frame for the Study of the Influence of Different Supports on the First-Floor-Rigidity. (1 in. = 2.54 cm).

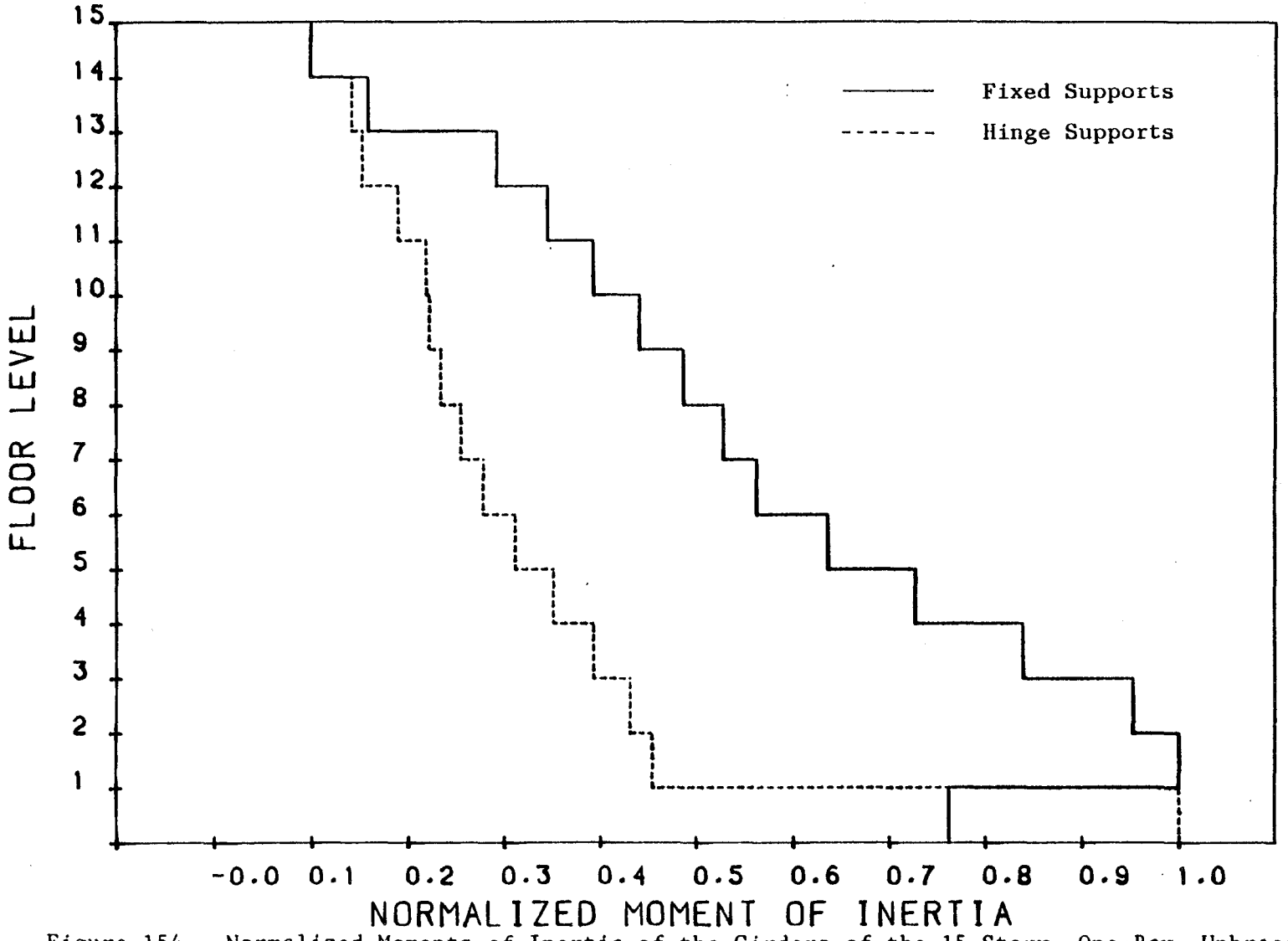

Figure 154. Normalized Moments of Inertia of the Girders of the 15-Story, One-Bay, Unbraced Frame for the Study of the Influence of Different Supports on the First-Floor-Rigidity.

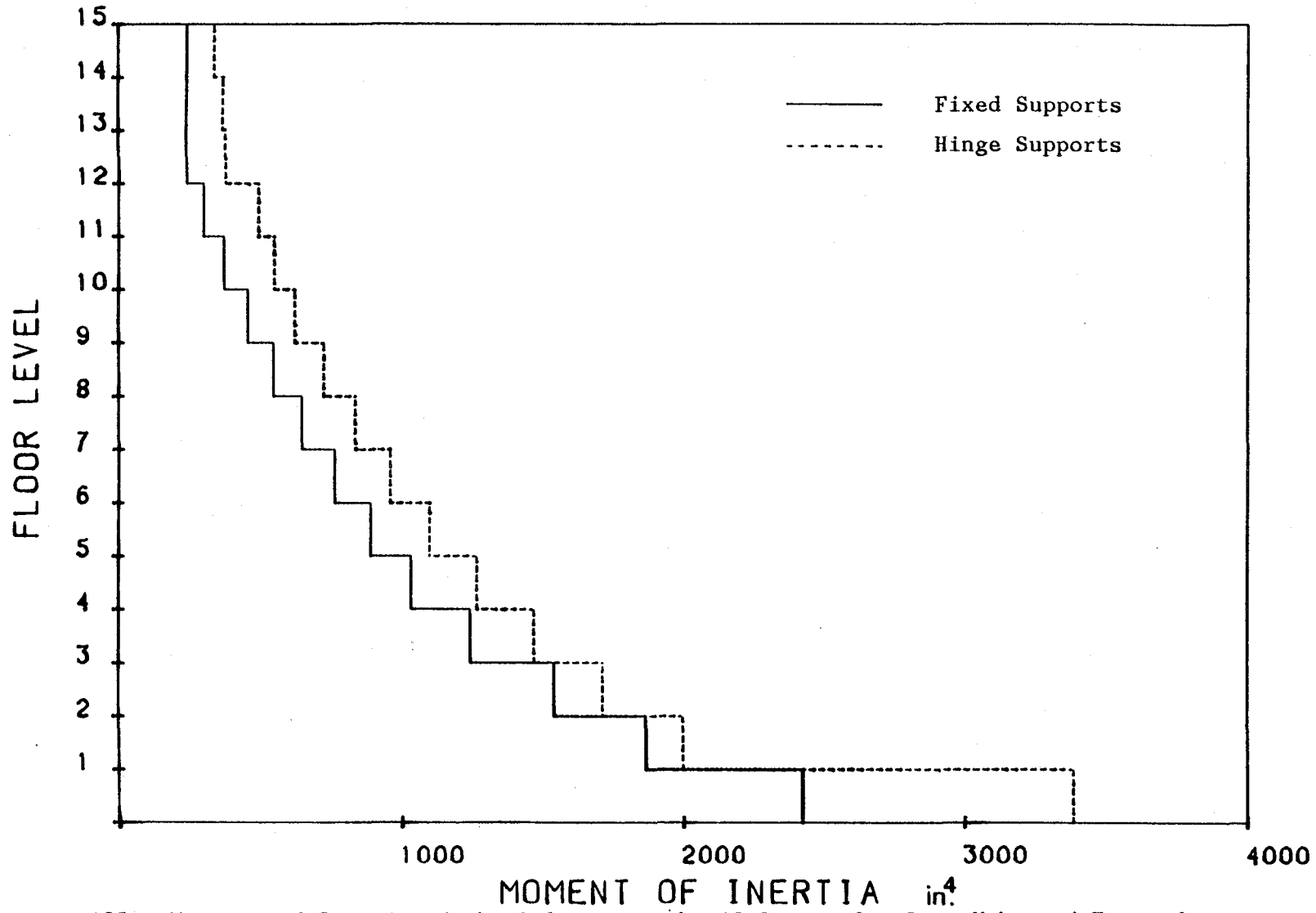

Figure 155. Moments of Inertia of the Columns of the 15-Story, One-Bay, Unbraced Frame for the Study of the Influence of Different Supports on the First-Floor-Rigidity. (1 in. = 2.54 cm).

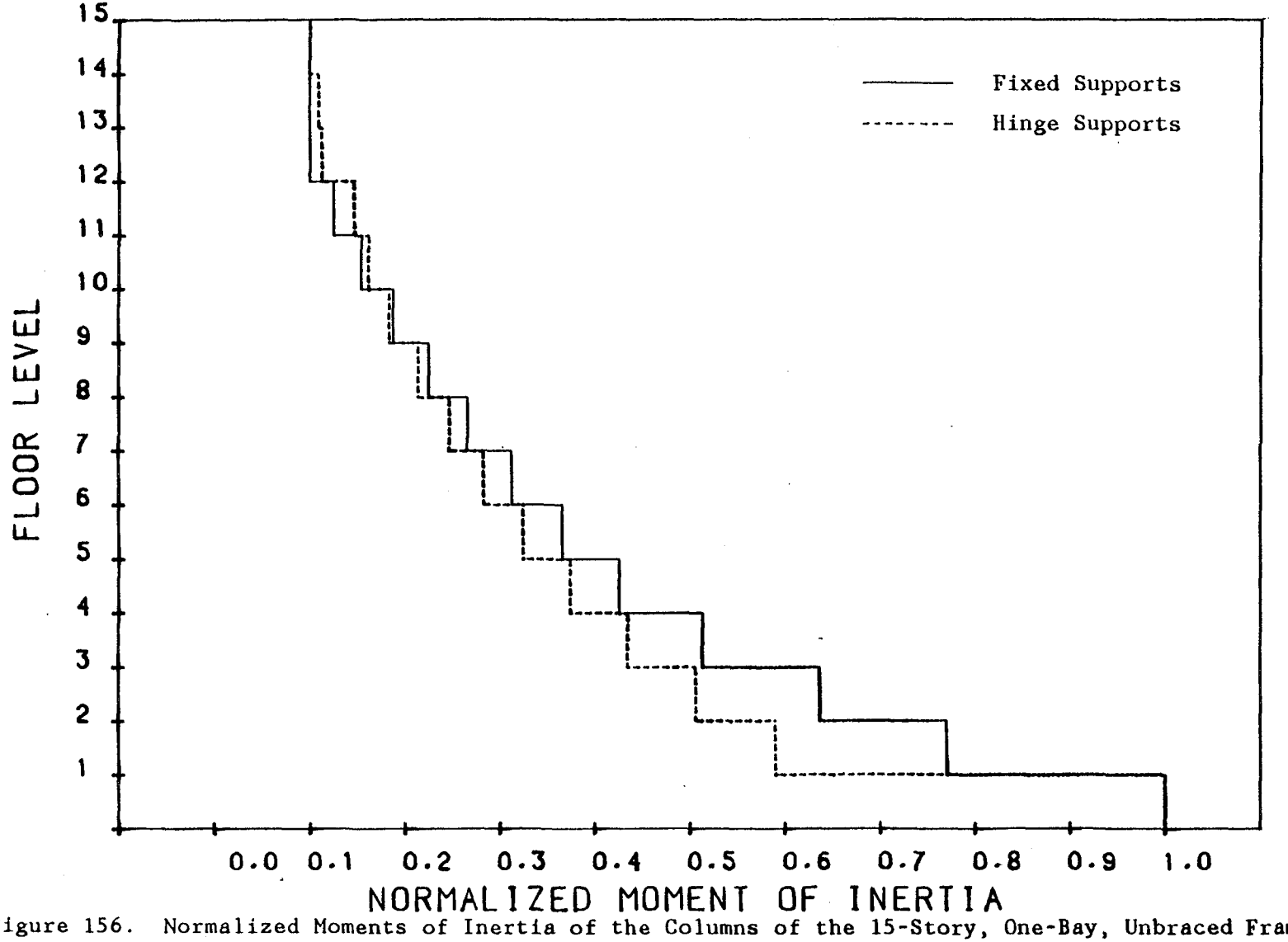

Figure 156. Normalized Moments of Inertia of the Columns of the 15-Story, One-Bay, Unbraced Frame for the Study of the Influence of Different Supports on the First-Floor-Rigidity.

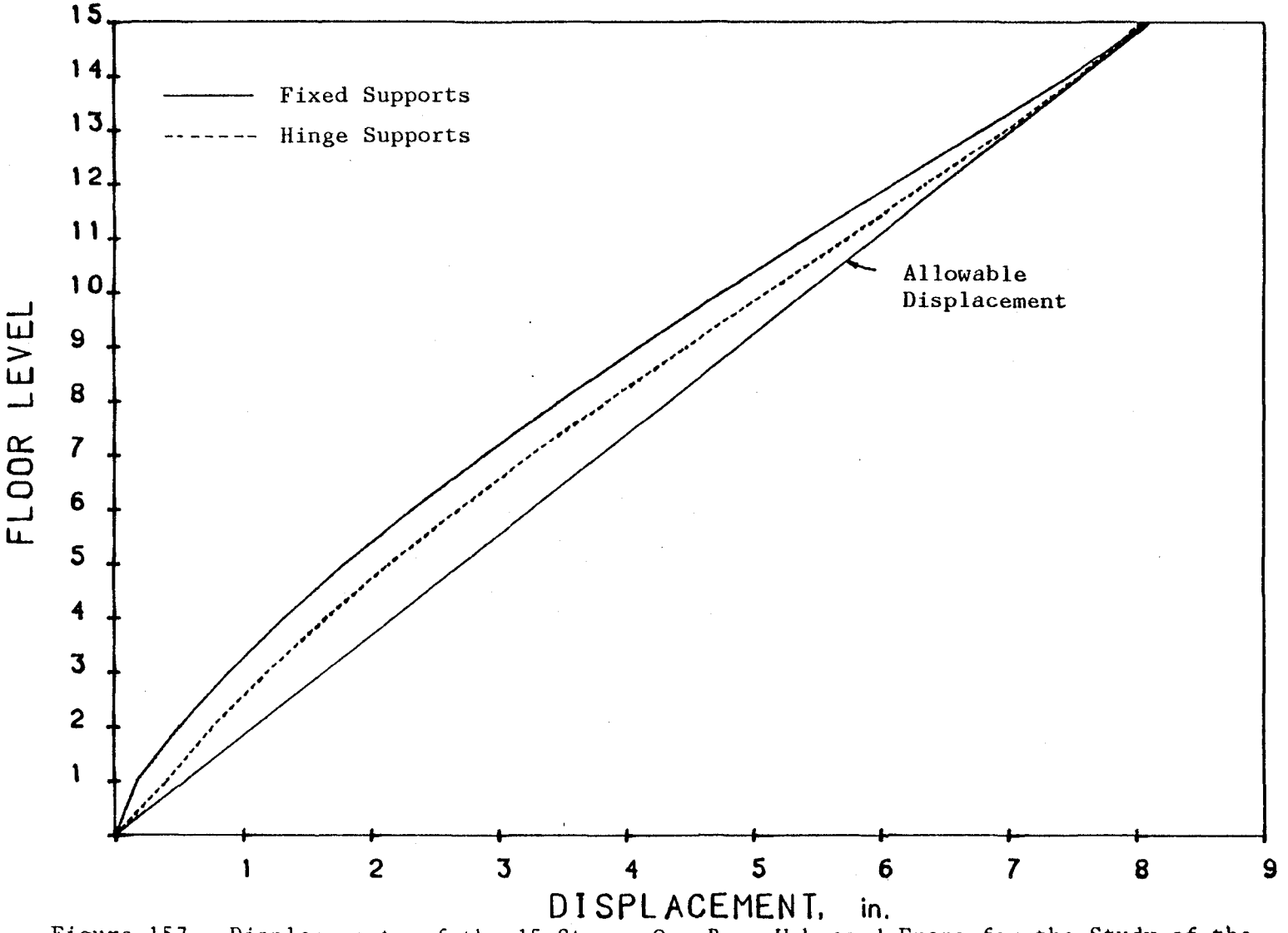

Figure 157. Displacements of the 15-Story, One-Bay, Unbraced Frame for the Study of the Influence of Different Supports on the First-Floor-Rigidity. (1 in. = 2.54 cm).

L. DETERMINATION OF DYNAMIC STORY DRIFT

As we mentioned in Section G of this chapter, when story drift limitations are imposed in the design, a more conservative design can be obtained than that is based on the displacement constraints. In static design, the story drift can be determined by using the static displacement without difficulty. However, in order to obtain a conservative dynamic design, a suitable superposition technique should be used to determine the dynamic story drifts.

By using the data obtained from the numerical example presented in Section J.2.b, which is designed on the basis of the ATC-3-06 design spectrum associated with displacement constraints, two methods were used to compute the dynamic story drifts. One is based on the total dynamic displacements, those are obtained by using the root-mean-square superposition of all the specified modal responses, and the story drift can be expressed as

$$\Delta_x = r_x - r_{x-1} \tag{6.1}$$

in which $r_x=(\sum_{i=1}^{m} \delta_{x,i}^2)^{1/2}$, $\delta_{x,i}$ is the response of mode i on floor level x, and m is total number of modes. The other is obtained by using the root-mean-square superposition of modal drifts, that is

$$\Delta_x = (\sum_{i=1}^{m} (\delta_{x,i} - \delta_{x-1,i})^2)^{1/2} \tag{6.2}$$

The modal responses, $\delta_{x,i}$ in Eqs. (6.1) and (6.2) are obtained by using the spectral analysis, and can be expressed as

$$\{\phi\}_i = \{\phi\}_i \left(\frac{L_{hi}}{m_i} S_{d,h} + \frac{L_{vi}}{m_i} S_{d,v} \right) \tag{6.3}$$

in which $\{\phi\}_i$ is eigenvector of mode i, $m_i = \{\phi\}_i^T [M] \{\phi\}_i$, $S_{d,h}$ is the spectral displacement corresponding to the horizontal ground motions, $S_{d,v}$ is the spectral displacement corresponding to the vertical ground motions, $L_{hi} = \{\phi\}_i^T [M] \{e\}_h$, $L_{vi} = \{\phi\}_i^T [M] \{e\}_v$, $\{e\}_h$ is a unit vector corresponding to horizontal direction, and $\{e\}_v$ is a unit vector corresponding to vertical direction.

The modal responses, $\delta_{x,i}$, total dynamic displacement, r_x, and the displacement based on the story drifts obtained from Eq. (6.2) are shown in Figure 158. From this figure, one can find that Eq. (6.2) provides larger drifts and displacements than Eq. (6.1). We can also find this result by comparing Eqs. (6.1) and (6.2) directly, that is

$$\left(\sum_{i=1}^{m} (\delta_{x,i} - \delta_{x-1,i})^2 \right)^{1/2} \geq \left(\sum_{i=1}^{m} \delta_{x,i}^2 \right)^{1/2} - \left(\sum_{i=1}^{m} \delta_{x-1,i}^2 \right)^{1/2}.$$

Therefore, a more conservative dynamic story drift should be based on Eq. (6.2). In the ATC-3-06 modal analysis provisions, Eq. (6.2) is used to calculate the story drifts.

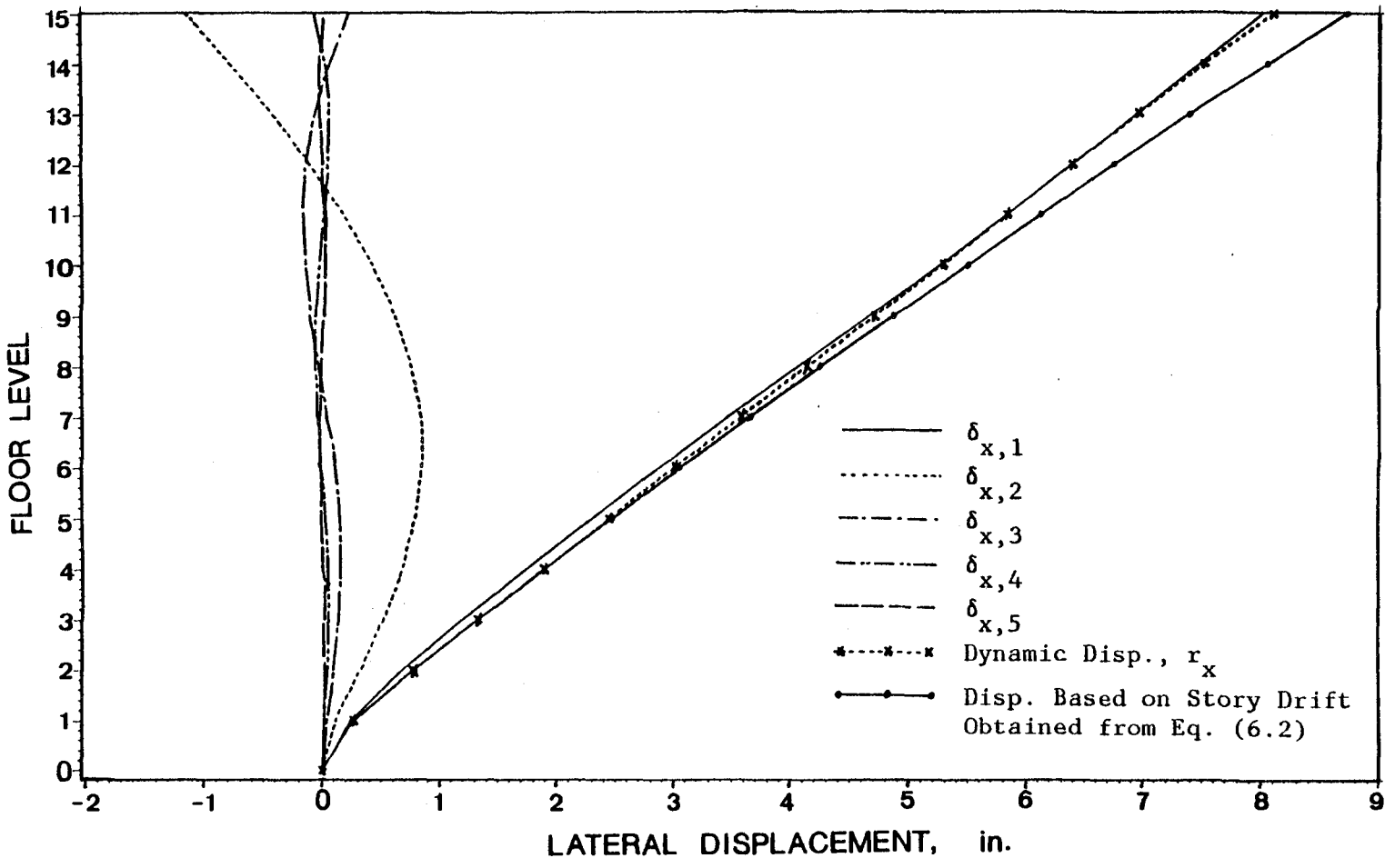

Figure 158. Comparison of the Dynamic Displacement with the Displacement Shape Based on the Dynamic Story Drifts. (1 in. = 2.54 cm)

VII. COMPLETE DESIGN OF A THREE-STORY THREE-BAY BUILDING

The computer program ODSEWS-2D-II was used to develop about 80 examples of minimum weight and minimum cost designs presented in Chapter VI. These optimum design results illustrate that the methodology and the computer program can be used for parametric studies and and code assessments, and they can also be used for prelimary design of selecting member sizes. In this Chapter, the computer program is used to help illustrate the completed design procedures that are based on the ATC-3-06 equivalent lateral force method. These include the initial design, selection of members, the structural analysis, the individual member check, and final design.

A. STRUCTURAL CONFIGURATION, DESIGN LOADINGS, AND CONSTRAINTS

Figure 159 is a plan view of a structure. There are three bays in the direction of analysis. Each bay is 30 feet (9.14 m) long. There are six bays in the orthogonal direction. Each bay is 20 feet (6.10 m) wide. The vertical configuation of the cross section plan A-A is shown in Figure 160. The structure is classified as being in Exposure Group I and being an ordinary moment frame with R=4.5 and C_d=4.0. It is located in an area having A_a=3, A_v=3, and a soil profile type S_3.

Table XIX shows the individual types of basic design loading and their magnitudes. The design loads at each floor level for one typical bay are summarized in Table XX based on loadings given in Table XIX.

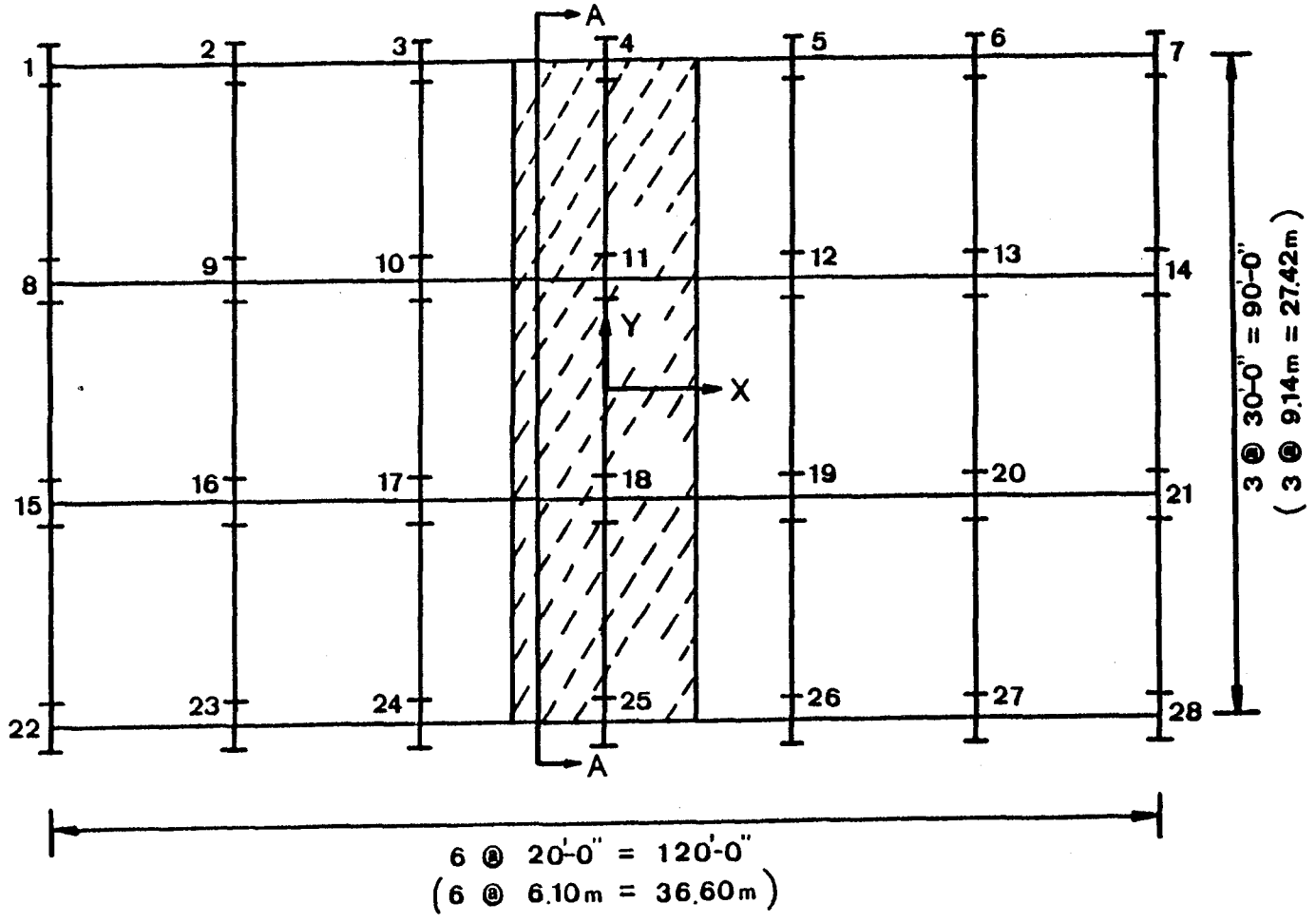

Figure 159. Plan View of the Three-Story, Three-Bay Building

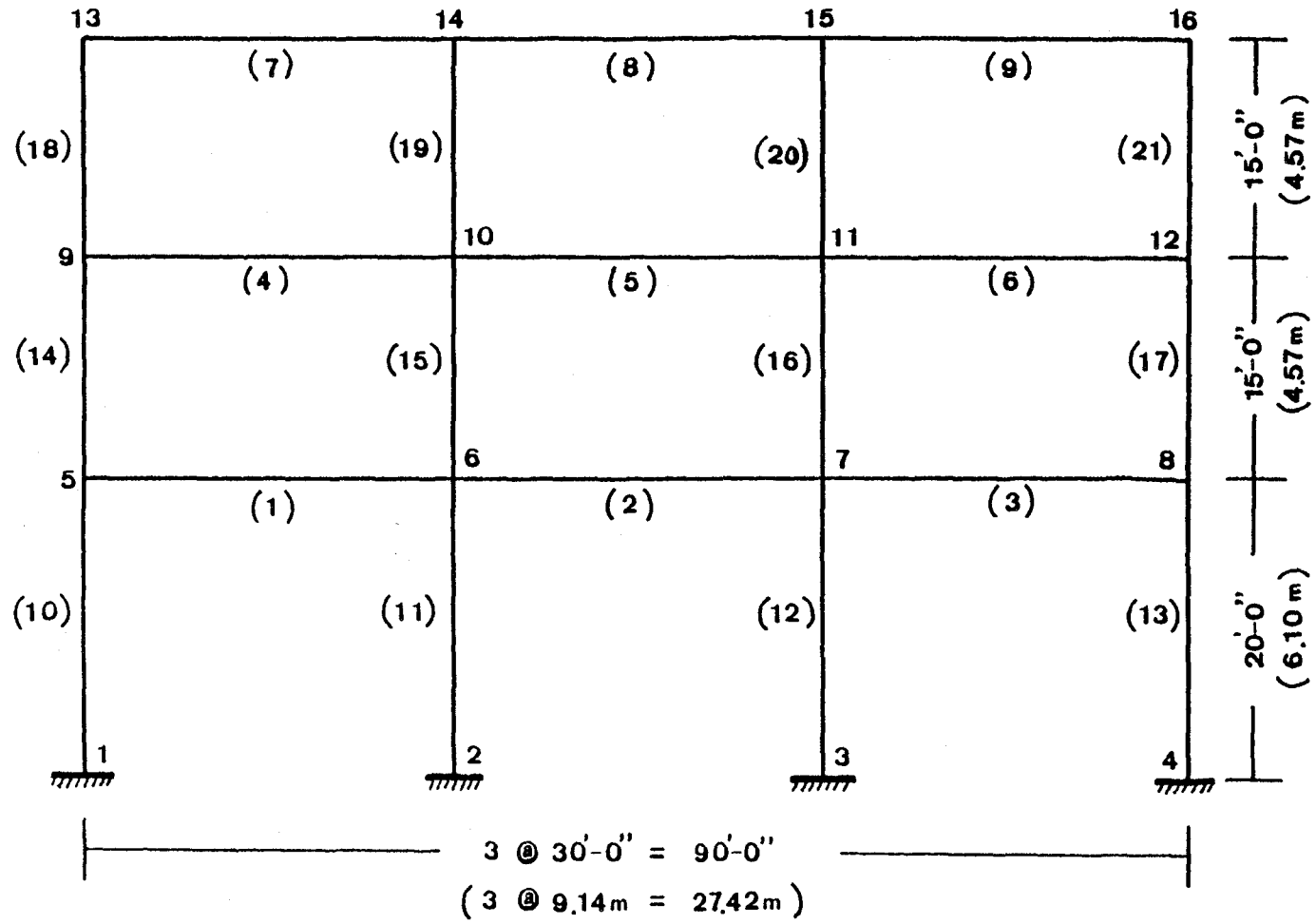

Figure 160. The Vertical Configuration of the Cross Section Plan A-A of the Three-Story, Three-Bay Building

TABLE XIX. THE BASIC DESIGN LOADINGS OF THE THREE-STORY, THREE-BAY STRUCTRAL DESIGN. (1 psf = 47.88 N/m^2)

Loading Type	Magnitude (psf)
Partitions (all floors)	20.00
Concrete Slab (all floors)	31.25
Floor Finish (all floors)	2.00
Ceiling (all floors)	8.00
Mechanical (all floors)	1.50
Insulation (roof)	2.00
Roofing	15.00
Live Load on Roof	30.00
Live Load on 1st and 2nd Floors	50.00
Snow Load	30.00

TABLE XX. DESIGN LOADS ON EACH FLOOR LEVEL FOR THE DESIGN OF THE THREE-STORY, THREE-BAY STRUCTURE. (1 lb/in. = 1.75 N/cm)

Floor Level	Dead Load lbs/in.	Live Load lbs/in.	Snow Load lbs/in.
1	104.58	83.33	
2	104.58	83.33	
3	96.25	50.00	50.00

All the structural members are designed on the basis of AISC wide flange sections and ASTM's designation of A36 steel. According to Section 3.7.1 of the ATC-3-06, it is necessary to provide the building and its components with sufficient strengths to resist the effect of the combined loads as indicated by Eq. (7.1) or, (7.2a) or (7.2b).

$$Q_c = 1.2Q_D + 1.0Q_L + 1.0Q_S \pm 1.0Q_E, \tag{7.1}$$

or

$$Q_c = 0.8Q_D \pm 1.0Q_E \tag{7.2a}$$

or for elements that are relatively brittle in the tensile mode of failure,

$$Q_c = 0.5Q_D \pm 1.0Q_E \tag{7.2b}$$

in which Q_c is the combination of the load effects, Q_D the effect of the dead load, Q_L the effect of the live load, Q_S the effect of the snow load, and Q_E the effect of the seismic forces.

The allowable story drift is $0.015h_{sx}/C_d$ according to the ATC-3-06 provisions, and the stress constraints are not considered in the initial design.

B. INITIAL DESIGN

By using the ODSEWS-2D-II computer program, the member sizes of the optimum weight design are obtained and given in Table XXI. Because stress constraints are not included in the design, the member

TABLE XXI. THE MOMENT OF INERTIA, SECTIONAL AREA AND SECTIONAL MODULUS OF THE INTIAL OPTIMUM DESIGN AND THE AISC SECTION SELECTED ON THE BASIS OF THE INITIAL DESIGN (1 in. = 2.54 cm)

Initial Optimum Design				Selected Sections			
Member No	I_x (in^4)	A (in^2)	S_x (in^3)	Designation	I_x (in^4)	A (in^2)	S_x (in^3)
1,3	251.26	7.36	25.16	W14x30	291.0	8.85	42.0
2	95.91	4.55	9.85	W12x26	103.0	4.71	17.1
4,6	149.24	5.68	15.20	W12x22	156.0	6.48	25.4
5	76.57	4.07	7.89	W12x14	88.6	4.16	14.9
7,9	117.89	5.04	12.07	W10x22	118.0	6.49	23.2
8	25.53	2.35	2.66	W 6x15	29.1	4.43	9.7
10,13	303.37	8.09	30.13	W10x54	303.0	15.80	54.6
11,12	227.63	7.01	22.88	W10x45	248.0	13.30	49.1
14,17	254.42	7.41	25.46	W10x45	248.0	13.30	49.1
15,16	155.33	5.79	15.80	W10x30	170.0	8.84	32.4
18,21	210.81	6.75	21.25	W10x39	209.0	11.50	42.1
19,20	100.63	4.66	10.33	W10x22	118.0	6.49	23.2

sizes are too small and have a maximum combined stress of 897.6 ksi (618.8 kN/cm^2) on member 8. This is much greater than the yielding stress of 36 ksi (24.8 kN/cm^2). Since the initial design is only a guide for the user who selects the sections of the members, it is not necessary for him to redesign the structure by considering the stress constraints.

C. SELECTION OF MEMBERS FROM THE AISC MANUAL

The structural members are first selected from the AISC Manual on the basis of the moment of inertia, the sectional area, and the sectional modulus of each member which were obtained from the initial design. These data are listed in Table XXI of the initial design results and the selected results. The selected section sizes are actually too small, because the stress constraints have not been considered. A more reasonable selection could be based on the member forces resulting from the initial design stage.

Now members are selected according to the member forces. For ordinary moment resistant frames, ATC-3-06 Chapter 10 specifies that the structural members should be selected and constructed according to Part 1 of the AISC Specification for a frame that is subjected to a combination of dead and live loads. When the frame is subjected to seismic forces acting alone or to a combination of load effects, as mentioned in Section A, the structural members must be designed and constructed in accordance with Part 1 of the AISC Specification and modified with the capacity reduction factor, allowable stresses, Euler

stress, shear strength, and P-Δ effects. For simplicity, structural members are selected according to the member forces that are due to the effect of gravity loads only.

For girders, the selection is based on the maximum bending moment of a member which has fully lateral support from concrete slab. For example, member 1 has a maximum bending moment of 2158.35 in.-kips (243.85 kN-m), and its required sectional modulus as based on a allowable bending stress of 24 ksi (16.55 kN/cm^2) is 89.93 in^3 (1473.7 cm^3). The W18x55 section is then selected from Part 2 of the AISC Manual.

The selection of columns is based on the interactive formulas given in Part 3 of the AISC Manual to include the effect due to the simultaneous action of the axial force and bending moment. Figure 161 shows the member forces of the tenth member, which is the exterior column on the first story. The bending factor, B_x, and the effective length factor, K, are assumed to be 0.2 and 1.2 respectively. The equivalent axial force, P_{equ}, is computed as 237.87 kips (1058.05 kN) according to the following formula

$$P_{equ} = P + M_x B_x \tag{7.3}$$

in which P is the axial force, and M_x the maximum bending moment. The W14x82 section is then selected from Part 3 of the AISC Manual. The allowable axial load, P_{all}, for this section is 261 kips (1160.93 kN). The selected member sections and their sectional properties are shown in Table XXII.

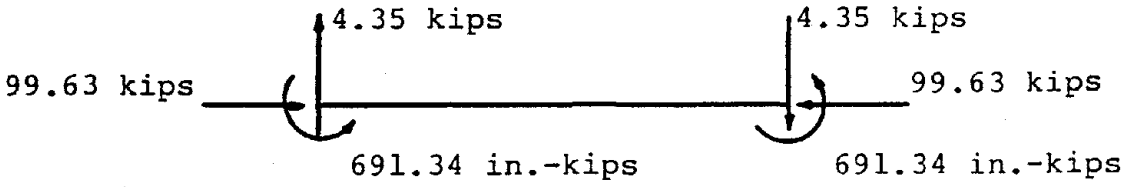

(a) Internal Forces of Member 10 Occasioned By Gravity Load

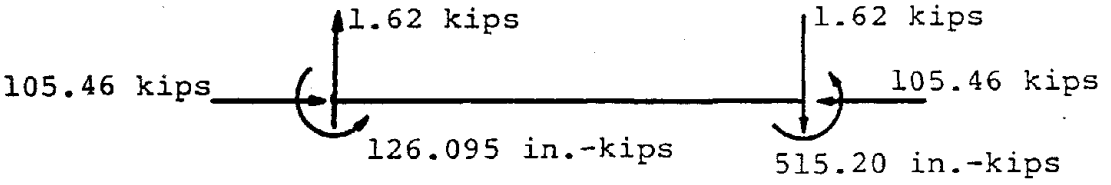

(b) Internal Forces of Member 10 Occasioned By the Combined Load Effects on the Basis of Eq. (7.1)

Figure 161. Internal Forces of Member 10 at Initial Design (1 in. = 2.54 cm, 1 kip = 4.448 kN)

TABLE XXII. THE MOMENT OF INERTIA, SECTIONAL AREA, AND SECTIONAL MODULUS OF THE SELECTED MEMBERS BASED ON THE MEMBER FORCES OF THE INITIAL DESIGN. (1 in. = 2.54 cm)

Member No	Designation	I_x (in^4)	A (in^2)	S_x (in^3)
1,3	W18x55	890.	16.2	98.3
2	W18x50	800.	14.7	88.9
4,6	W18x50	800.	14.7	88.9
5	W18x50	800.	14.7	88.9
7,9	W18x55	890.	16.2	98.3
8	W18x50	800.	14.7	88.9
10,13	W14x82	882.	24.1	123.0
11,12	W12x65	533.	19.1	87.9
14,17	W14x82	882.	24.1	123.0
15,16	W12x53	425.	15.6	70.6
18,21	W14x82	882.	24.1	123.0
19,20	W12x40	310.	11.8	51.9

D. ANALYSIS OF A SYSTEM

Before one can check the individual members, an analysis has to be made of the structure. To do this, the following three steps must be taken: 1) analyze the structure in the direction of the applied seismic forces, 2) analyze the structure in the direction perpendicular to the applied seismic forces to determine the orthogonal effects, and 3) compute the shear forces occasioned by the torsional moments in the vertical components.

The ODSEWS-2D-II computer program is used in the analysis as soon as the sections of the members have been determined. The analyzed results, which are based on the sections listed in Table XXII, are shown in Table XXIII.

According to Section 3.7.2 of the ATC-3-06, the building and its components must be designed for 100% of the effects of the seismic forces in the principal direction and 30% of the effects of the seismic forces in the orthogonal direction. But to determine the 30% in the orthogonal direction, one has to analyze the structure in the x direction as shown in Figure 159. The sections of the beams for this direction are arbitrarily chosen. For simplicity, they are selected according to the combined effects of the dead load, the live load, and the snow load. A W10x45 section is selected for the beams. At this stage, the building is first analyzed for the interior bay based on 30% of the seismic forces of the bay, and then the exterior bay is analyzed for the seismic forces in the amount of 50% of those used for the interior bay. The seismic forces in this direction are shown in Table XXIV. Table XXV contains a list of the bending moments of the

TABLE XXIII. THE ANALYZED RESULTS BASED ON THE SELECTED MEMBERS OF TABLE XXII. (1 in. = 2.54 cm, 1 kip = 4.448 kN)

Floor Level	Drift (in.)	Stability Coefficient	Seismic Forces (kips)	Story Shear (kips)
1	1.238	0.0344	2.437	13.286
2	0.947	0.0120	4.572	10.849
3	0.634	0.0047	6.278	6.278
Overturning Moment (ft-kips)			391.730	
Fundamental Period (sec)			1.595	
Eccentricity (feet)			1.105	

TABLE XXIV. SEISMIC FORCES IN THE ORTHOGONAL DIRECTION FOR THE COMPUTATION OF ORTHOGONAL EFFECTS. (1 kip = 4.448 kN)

Floor Level	Seismic Forces (kips)
1	5.519
2	8.902
3	12.213

TABLE XXV. THE MAXIMUM BENDING MOMENTS IN THE COLUMNS OF THE TYPICAL BAY OCCASIONED BY THE ORTHOGONAL EFFECTS. (1 in. = 2.54 cm, 1 kip = 4.448 kN)

	Floor Level	Moment at End i (in.-kips)	Moment at End j (in.-kips)
Interior Columns	1	186.52	191.24.
	2	159.33	169.02
	3	105.66	130.96
Exterior Columns	1	88.93	90.61
	2	81.83	73.14
	3	60.80	90.15

columns, at different floor levels, that have larger orthogonal effects.

According to Section 4.4 of the ATC-3-06, the torsional moments occasioned by the seismic forces contribute shear forces to the vertical components. There are two types of torsional moments: M_t, which results from the eccentricity between the mass center and resistance center for that story, and M_{ta}, the accidental torsional moment, which is computed as the story shear times a distance equal to 5% the dimension of the building in the story under consideration perpendicular to the direction of the applied seismic forces. The shears contributed to the vertical members by the torsional moments are proportional to the contribution of the members to the torsional stiffness of the story about its center of resistance. The shear distribution of any vertical member may be determined in accordance with the following formulas and Figure 162:

$$V_{xt} = \frac{M_r \, y \, k_x}{J_r} \tag{7.4}$$

$$V_{yt} = \frac{M_r \, x \, k_y}{J_r} \tag{7.5}$$

$$J_r = \Sigma \left(k_x y^2 + k_y x^2 \right) \tag{7.6}$$

$$x_r = \frac{\Sigma \, k_y x}{\Sigma \, k_y} \tag{7.7}$$

$$y_r = \frac{\Sigma \, k_x y}{\Sigma \, k_x} \tag{7.8}$$

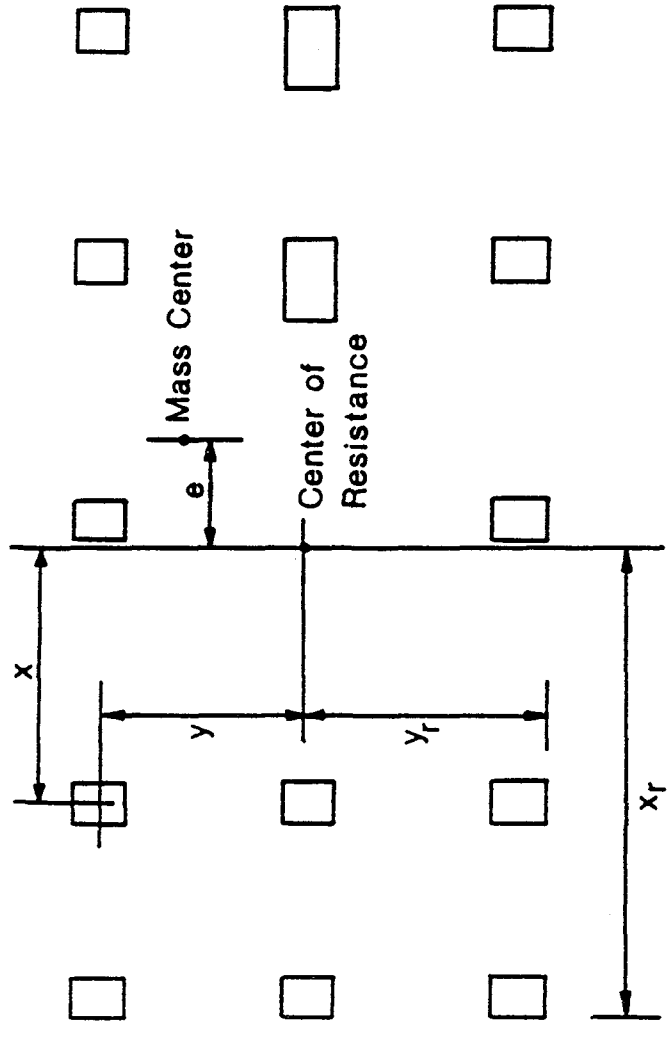

Figure 162. Torsional Distribution Diagram

$$k = \frac{12EI}{\ell} \tag{7.9}$$

in which V_{xt} is the shear induced by the torsional moment in the x direction, V_{yt} the shear induced by the torsional moment in the y direction, M_r the torsional moment of the resistance, which is the sum of M_t and M_{ta}, y the distance in the y dircetion from the center of the resistance to the vertical member, x the distance in the x dircetion from the center of the resistance to the vertical member, k_x the stiffness of the vertical component about the x axis, k_y the stiffness of the vertical component about the y axis, J_r the polar moment of inertia, x_r the distance in the x direction measured from the geometric center to the mass center, y_r the distance in the y direction measured from the geometric center to the mass center, E the modulus of elasticity, I the moment of inertia, and ℓ the length of the vertical member.

In computing the shear contributions for this example, the torsional moment, M_t, is neglected; however, the accidental torsional moment is considered. M_t is neglected for the following two reasons: 1) the mass center is the same as the geometric center, and 2) the relative displacements induced by the vibration of the building between any two floor levels are very small and the induced torsional moments are relatively smaller than the accidental torsional moments. The accidental torsional moments should be determined in accordance with the following formula:

$$(M_{ta})_x = V_x e \tag{7.10}$$

in which $(M_{ta})_x$ is the accidental torsional moment at level x, V_x is the story shear at level x, e is equal to 0.05D, and D is the dimension of the building in the orthogonal direction.

For this example of a six bay frame, where D is equal to 120 feet (36.58 m), we have

e = 0.05 x 120 = 6 feet (1.83 m), and

$(M_{ta})_1$ = (13.286)(6)(6) = 478.296 ft-kips (648.45 kN-m)

$(M_{ta})_2$ = (10.849)(6)(6) = 390.564 ft-kips (529.51 kN-m)

$(M_{ta})_3$ = (6.278)(6)(6) = 226.008 ft-kips (306.41 kN-m)

The shears occasioned by the torsional effects are then computed. These are listed in Table XXVI.

E. INDIVIDUAL MEMBER CHECK

As previously mentioned, the building and its components should be designed to satisfy Part 1 of the AISC Specification when it is subjected to a combination of dead load and live loads. When seismic loads are included, ATC-3-06 modifies Part 1 of the AISC Specification as follows: 1) the allowable stresses specified in AISC Sections 1.5.1, 1.5.2, 1.5.3, and 1.5.4 are multiplied by 1.7; 2) the Euler stress, F'_e, in AISC Section 1.6.1 is modified as $F'_e = (\pi^2 E)/(K\ell/r_e)^2$; 3) the allowable shear force, V_u, is changed to $V_u \leq 0.68F_y td$; and 4) the combined stresses considered in AISC Specification Sections 1.6.1 and

TABLE XXVI. THE CONTRIBUTION OF SHEARS DUE TO THE TORSIONAL EFFECTS

(1 kip = 4.448 kN)

Floor Level	Column Line No (Refer to Figure 159)	V_{xe} (kips)	V_{ye} (kips)
1	1,2,3,4,5,6,7, 22,23,24,25,26,27,28	0.5871	
	8,9,10,11,12,13,14, 15,16,17,18,19,20,21	0.1183	
	1,7,22,28		0.1314
	8,14,15,21		0.1545
	2,6,23,27		0.0876
	9,13,16,20		0.1029
	3,5,24,26		0.0438
	10,12,17,19		0.0514
	4,11,18,25		0.
2	1,2,3,4,5,6,7, 22,23,24,25,26,27,28	0.4877	
	8,9,10,11,12,13,14, 15,16,17,18,19,20,21	0.0783	
	1,7,22,28		0.1091
	8,14,15,21		0.0706
	2,6,23,27		0.0727
	9,13,16,20		0.0471
	3,5,24,26		0.0364

TABLE XXVI. THE CONTRIBUTION OF SHEARS DUE TO THE TORSIONAL EFFECTS (continued) (1 kip = 4.448 kN)

Floor Level	Column Line No. (Refer to Figure 159)	V_{xe} (kips)	V_{ye} (kips)
2	10,12,17,19		0.0235
	4,11,18,25		0.
3	1,2,3,4,5,6,7, 22,23,24,25,26,27,28	0.2962	
	8,9,10,11,12,13,14, 15,16,17,18,19,20,21	0.0347	
	1,7,22,28		0.0663
	8,14,15,21		0.0198
	2,6,23,27		0.0442
	9,13,16,20		0.0132
	3,5,24,26		0.0221
	10,12,17,19		0.0066
	4,11,18,25		0.

2.4 are modified by using K equal to 1.0 and C_m determined as it is for braced frames.

The selected structural members must satisfy the AISC and ATC-3-06 requirements. Each member is first checked by considering the effects of gravity loads only. Then the combined effects of the gravity loads and seismic forces are accounted for. Members 1 and 11 are used as examples to show the procedure for making a member check.

Figure 163 shows the internal forces of member 1, which is a girder on the first floor in the exterior bay. The maximum moment, M_{max}, is 2122.2 in.-kips (239.76 kN-m) when the gravity load only is considered. On the assumption that the girders are embedded in a concrete slab, the member is fully supported laterally. Thus,

$$\frac{M_{max}}{0.66F_y} = \frac{2122.2}{24} = 88.43 \text{ in}^3 \ (1449.1 \text{ cm}^3) \qquad \text{(o.k.)}$$

For W18x55 section, the sectional modulus, S_x, is 98.3 in^3 (1610.85 cm^3). The selected section provides enough capacity to resist the bending moment:

$$\frac{b_f}{2t_f} = 6.0 < \frac{65}{\sqrt{F_y}} = 10.83 \qquad \text{(o.k.)}$$

$$\frac{d}{t_w} = 46.4 < \frac{640}{\sqrt{F_y}} = 106.67 \qquad \text{(o.k.)}$$

The allowable live load deflection is determined as

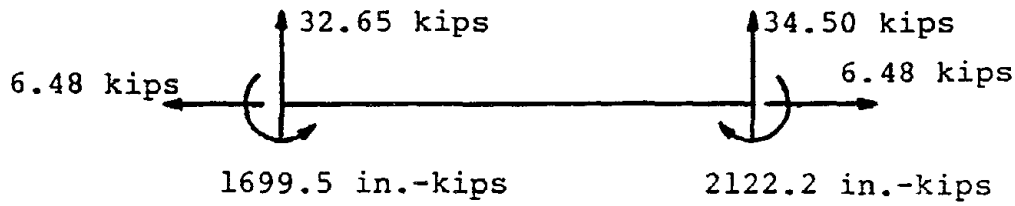

(a) Internal Forces of Member 1 Occasioned by Gravity Loads

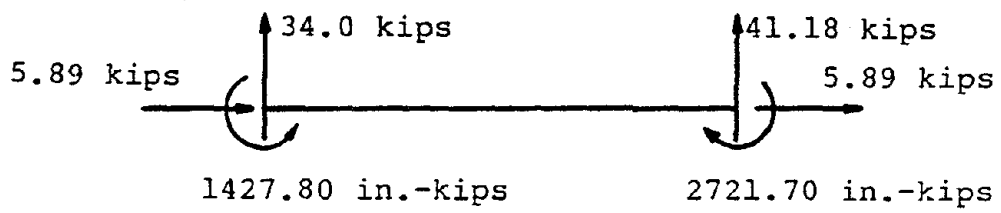

(b) Internal Forces of Member 1 Occasioned by Combined Load Effects on the Basis of Eq. (7.1)

Figure 163. Internal Forces of Member 1 at Redesign Stage (1 in. = 2.54 cm, 1 kip = 4.448 kN)

$$\delta = \frac{\ell}{360} = \frac{30 \times 12}{360} = 1.\ \text{in.}\ (2.54\ \text{cm}).$$

Therefore, the required moment of inertia is

$$I_{req'd} = \frac{5w\ell^3}{384E\delta} = 628.45\ \text{in}^4\ (26158.06\ \text{cm}^4)$$
$$< I_x = 890\ \text{in}^4\ (37044.60\ \text{cm}^4) \qquad \text{(o.k.)}$$

According to AISC Specification Section 1.5.1.2, the allowable shear force is

$$V_{all} = 0.4F_y dt_w = 101.7\ \text{kips}\ (452.36\ \text{kN})$$
$$> 35\ \text{kips}\ (155.68\ \text{kN}). \qquad \text{(o.k)}$$

For the case affected by the combination of load,

$$M_{max} = 2721.7\ \text{in.-kips}\ (307.5\ \text{kN-m})$$

$$\frac{M_{max}}{1.7(0.66F_y)} = \frac{2721.7}{40.4} = 67.37\ \text{in}^3\ (1104.00\ \text{cm}^3)$$
$$< 98.3\ \text{in}^3\ (1610.85\ \text{cm}^3) \qquad \text{(o.k.)}$$

$$V_{all} = 0.68F_y dt_w = 172.89\ \text{kips}\ (769.01\ \text{kN})$$
$$> 41.18\ \text{kips}\ (183.17\ \text{kN}). \qquad \text{(o.k.)}$$

The maximum positive moment is not checked, because it is only 1571.4 in.-kips (177.54 kN-m), which will not govern the design. The

combined stresses are also neglected, because the axial forces are in a tensional direction. Both requirements may need to be checked for other members.

The member forces of the interior column on the first story are shown in Figure 164. The member is first checked for the effect of the gravity load action only. For this, the axial stress is

$$f_a = \frac{P}{A} = \frac{209.33}{19.1} = 10.96 \text{ ksi } (7.56 \text{ kN/cm}^2),$$

and bending stress is

$$f_b = \frac{M}{S_x} = \frac{38.53}{87.9} = 0.438 \text{ ksi } (0.30 \text{ kN/cm}^2).$$

The bending coefficient, C_b, is

$$C_b = 1.75 + 1.05 \left(\frac{17.07}{38.53}\right) + 0.3 \left(\frac{17.07}{38.53}\right)^2 = 2.274,$$

and the maximum unbraced length is

$$\sqrt{\left(\frac{102000C_b}{F_y}\right)} r_T = 263.28 \text{ in. } (6.69 \text{ m})$$

$$\frac{20000C_b}{(d/A_f)F_y} = 756.51 \text{ in. } (19.22 \text{ m}) > 240 \text{ in. } (6.10\text{m})$$

Therefore, the allowable bending stress is

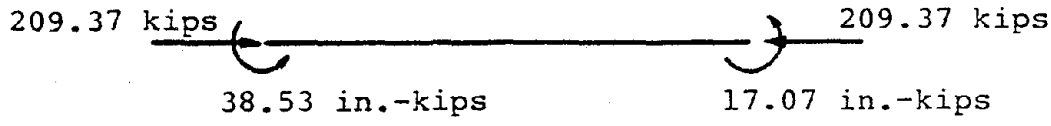

(a) Internal Forces of Member 11 Due to Gravity Loads

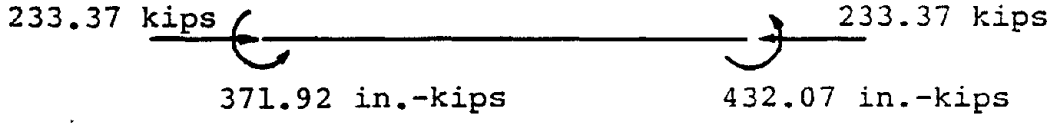

(b) Internal Forces of Member 11 Due to Combined Load Effects on the Basis of Eq. (7.1)

Figure 164. Internal Forces of Member 11 After Redesign (1 in. = 2.54 cm, 1 kip = 4.448 kN)

$$F_b = 0.6F_y = 22 \text{ ksi } (15.17 \text{ kN/cm}^2).$$

By using the alignment charts, the effective length factors are found to be $K_x = 1.31$ and $K_y = 1.29$. Then one calculates $K_y\ell/r_y$ as follows:

$$\frac{K_y\ell}{r_y} = \frac{1.29 \times 20 \times 12}{3.02} = 102.52.$$

From Table 3 in Appendix A of the AISC Specification,

$$F_a = 12.66 \text{ ksi } (8.729 \text{ kN/cm}^2).$$

In the plane of bending,

$$\frac{K_x\ell}{r_x} = \frac{1.31 \times 20 \times 12}{5.28} = 59.45.$$

From Table 3 in Appendix A of the AISC Specification,

$$F_e' = 42.19 \text{ ksi } (2.909 \text{ kN/cm}^2).$$

According to AISC Specification Section 1.6.1,

$$\frac{f_a}{F_a} + \frac{C_m f_b}{(1-f_a/F_e')F_b} = 0.889 < 1.0 \qquad \text{(o.k)}$$

$$\frac{f_a}{0.6F_y} + \frac{f_b}{F_b} = 0.518 < 1.0 \qquad \text{(o.k)}$$

The W12x65 section is acceptable for the gravity load actions. To check for the combined effects of the gravity loads and seismic forces, the orthogonal effects and the torsional effects are also considered. For this member, the orthogonal effects produce bending moments of

M_{y1} = 186.52 in.-kips (21.07 kN-m)
M_{y2} = 191.44 in.-kips (21.63 kN-m).

The shears occasioned by the torsional moments are

V_{xe} = 0.1183 kips (0.526 kN)
V_{ye} = 0.1029 kips (0.458 kN).

Thus, the bending moments are increased to

M_{x1} = 371.92 + 0.1029 x 10 x 12 = 384.27 in.-kips (43.41 kN-m)
M_{x2} = 432.07 + 0.1029 x 10 x 12 = 444.42 in.-kips (50.21 kN-m)
M_{y1} = 186.52 + 0.1183 x 10 x 12 = 200.72 in.-kips (22.68 kN-m)
M_{y2} = 191.24 + 0.1183 x 10 x 12 = 205.44 in.-kips (23.21 kN-m).

For the bending coefficient,

C_b = 2.88 > 2.3, use C_b=2.3.

The maximum unbraced length determined from the AISC Specification

is larger than the member length. Therefore, the allowable bending stresses in both axes are

$$F_{bx} = 1.7(0.6F_y) = 37.4 \text{ ksi } (25.79 \text{ kN/cm}^2)$$
$$F_{by} = 1.7(0.75F_y) = 45.9 \text{ ksi } (31.65 \text{ kN/cm}^2).$$

For both bending planes,

$$\frac{K_x \ell}{r_x} = \frac{(1.0)(20)(12)}{5.28} = 45.45$$

$$\frac{K_y \ell}{r_y} = \frac{(1.0)(20)(12)}{3.02} = 79.47.$$

The allowable axial stress is

$$F_a = 1.7 \times 15.41 = 26.20 \text{ ksi } (18.06 \text{ kN/cm}^2).$$

To check the combined load effects, the formulas in AISC Specification Section 1.6.1 are used.

$$f_a = \frac{P}{A} = \frac{233.37}{19.1} = 12.22 \text{ ksi } (8.43 \text{ kN/cm}^2)$$

$$\frac{f_a}{F_a} = 0.466 > 0.15$$

$$C_{mx} = 0.6 - 0.4\left(\frac{384.27}{444.42}\right) = 0.254 < 0.4, \text{ use } C_{mx} = 0.4$$

$$C_{my} = 0.6 - 0.4\left(\frac{200.72}{205.44}\right) = 0.209 < 0.4, \text{ use } C_{my}=0.4$$

$$F'_{ex} = \frac{\pi^2 E}{(K_x \ell/r_x)^2} = 138.56 \text{ ksi } (95.54 \text{ kN/cm2})$$

$$F'_{ey} = \frac{\pi^2 E}{(K_y \ell/r_y)^2} = 45.32 \text{ ksi } (31.25 \text{ kN/cm2})$$

$$\frac{f_a}{F_a} + \frac{C_{mx} f_{bx}}{(1-f_a/F'_{ex})F_{bx}} + \frac{C_{my} f_{by}}{(1-f_a/F'_{ey})F_{by}} = 0.596 < 1.0 \qquad \text{(o.k.)}$$

$$\frac{f_a}{F_a} + \frac{f_{bx}}{F_{bx}} + \frac{f_{by}}{F_{by}} = 0.622 < 1.0 \qquad \text{(o.k)}$$

Therefore, the W12x56 section is acceptable.

By following a similar procedure, all the sections selected in Section B will be acceptable. The building is therefore designed to have a total structural weight of 27,840 lbs (123.83 kN). Figure 165 shows the final design of this plane structure.

If the selected sections do not satisfy the AISC and ATC-3-06 requirements, it is necessary to reselect the section and repeat the procedures of Section D and this section.

F. REMARKS

In this chapter, the ODSEWS-2D-II has been used to illustrate the design procedures. Because this computer program is used to design a plane structure, several assumptions had to be made to determine the orthogonal effects and the torsional effects. The output solution of

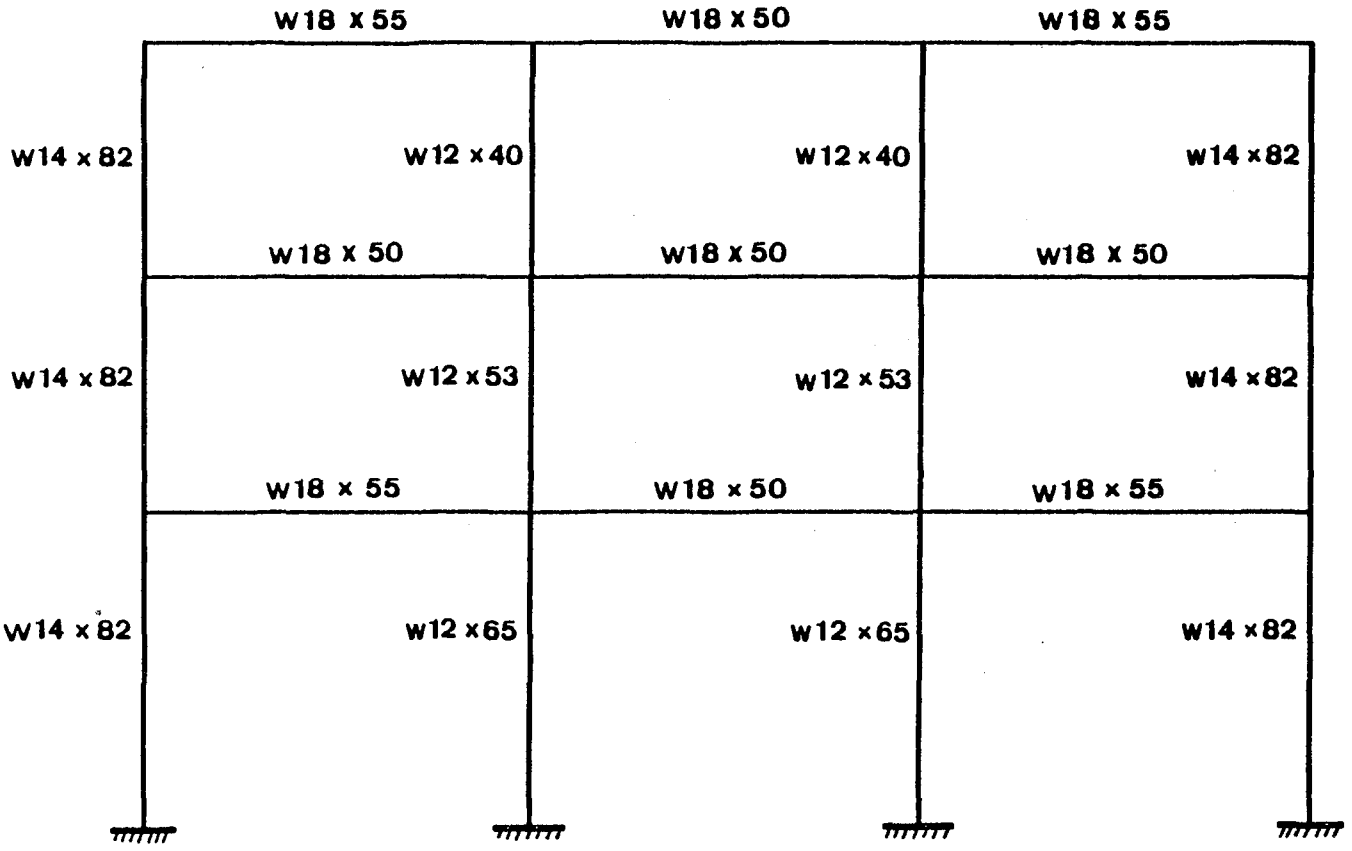

Figure 165. Final Design of the Three-Story, Three-Bay Building

the member stresses is due to the axial force combined with bending about the major axis. If an assumed stress constraint is imposed, the result will be over designed in the initial design. Since the initial design provides only a guide for selecting member sections, it may be desirable to select the members on the basis of the member forces.

VIII. REVIEW AND CONCLUSIONS

A. REVIEW

Studies of the parameters of ATC-3-06 provisions, comparisons of various code provisions, the effect of various constraints, the influence of different support conditions, the effects of vertical ground movements, the effect of second-order forces, and the effect of various bracing systems have been presented in this report.

It has been shown that the optimum design program, ODSEWS-2D-II, which was developed for multiple purposes, can be effectively used to design and analyze structures of trusses, unbraced frames, and braced frames. Its objective function can be either structural weight or cost. The technique of resizing individual members of a system is based on the optimal criterion and the constraint gradients.

The design loadings can be static loads, dynamic loads, or a combination of both. For the design of a seismic resistant structure, the design loadings include equivalent seismic forces determined according to the ATC-3-06 equivalent lateral force method or modal analysis method, the Uniform Building Code, and Chinese Seismic Design Code. For wind structural design, the power law is also available in the computer program. For dynamic loadings, several design spectra were coded in the subroutines CURVE1, CURVE2, CURVE3, and CURVE4. This was done by using least square curve fitted functions. For the determination of spectral acceleration one can use various design spectra. This can be easily accomplished by calling the subroutines, but seismic information as earthquake records and forcing functions can also be used.

The ODSEWS-2D-II program can be run on an AMDAHL 470V/7, 480V/8 or an IBM 4341 OS/VS1 system of the University of Missouri-Rolla. Detailed descriptions of the subroutines, input data, capacities, and modifications of the program's capacity are organized and given in a separate volume of the series report.[74]

B. CONCLUSIONS

The important conclusions derived from the investigation are summarized below.

(1) The presentation of optimality criterion technique combined with constraint gradients can be used to various structural systems.

(2) The upper bound of the fundamental period, $1.2T_a$, which is specified in the ATC-3-06 equivalent lateral force method, controls the design of almost all the design examples given in this report. Sophisticated mechanics may need not be used to find the natural period of a structure if the equivalent lateral force method is applicable.

Based on this observation, it is apparent that the seismic design coefficient, C_s, can be easily found for all map areas associated with any soil profile type without checking whether or not the fundamental period exceeds $1.2T_a$.

(3) In the ATC-3-06 provisions, the stability coefficient, θ, is determined to be inversely proportional to the story shears. On the basis of optimal solutions, it has been shown that almost all the stability coefficients are much smaller than the upper bound 0.1. According to the ATC-3-06, the P-Δ effect can be neglected in the

design. The lower values of A_a and A_v, the structure is less stiff. Consequently, the higher value of stability coefficient is found.

(4) For the ATC-3-06 provisions of the equivalent lateral force method and the modal analysis method, no matter whether the vertical configuration of structure is regular or irregular, the modal analysis method requires less optimal structural weight than the equivalent lateral force method. However, the stiffness distribution of a system resulting from using the both methods is almost identical which indicates that modal analysis technique is not necessarily required for irregular structures.

(5) Soil-structure interaction reduces the base shear and moment. Therefore, the design lateral forces are reduced, and a lighter optimal weight is obtained.

(6) In minimum cost design of the given unit costs of various items, the cost is mainly governed by the base charge, which includes the member costs and the extra size costs. According to the design example, the minimum cost design requires more weight than the minimum weight design. The distribution of the moments of inertia of the girders and columns show that the minimum cost design requires more uniform distribution than the minimum weight design.

(7) The design based on the Uniform Building Code has the lightest weight among the seismic resistant design provisions investigated because of the higher values of allowable story drifts that are required in the code. The allowable story drifts are not specified in the Chinese Code; if the allowable story drifts are used as specified

in the ATC-3-06 Provisions, the optimum weight of the design based on the Chinese Code is the heaviest.

The shear envelope associated with UBC increases abruptly at the top story; that is mainly due to the requirement of 0.07TV to account for the higher modes of a structure having long period. The influence of higher modes on structural responses is neglected in Chinese Code; it is therefore the shear envelope resulting from the code that is smoothly increased from the top to the first story.

(8) The constraint in story drifts is more important than the constraint in lateral displacements. The displacement constraint requires lighter structural design than the drift constraint; however several stories may violate the allowable story drifts and consequently a serious structural damage may result. The imposing of the constraint in story drifts always yields less lateral displacements than the allowable displacements based on the values of the allowable story drift.

(9) The moments of inertia of girders and columns are considerably reduced when the bracings are used in a structure. The eccentric K bracing system of model (d) requires the heaviest weight among all five bracing models because the lateral forces are not effectively resisted by bracings and relative larger sizes of girders are obtained. However, the bracings can provide better resistance to the gravity loads and the moments of inertia of columns are the smallest among all bracing systems. The K-braced system requires the lightest weight among all five bracing systems.

(10) The moments of inertia of girders of the double-bracing system provides better resistance to the lateral forces and, thus, its girders are considerably smaller than those of other bracing systems. The sizes of all the girders are governed by the lower bound of the relative size.

(11) The bracings of almost all bracing systems are relatively small at the top story. The distribution of areas of the bracings are increased gradually from top to the second story and then decreased abruptly at the first story. For the single-bracing system, the areas of the bracings are constant from the second story to the 12th story and are governed by the upper bound of the cross-sectional areas. For the eccentric K bracing system, the bracings from first to the top story are all governed by the upper bound of the cross-sectional area.

(12) Because the design of the bracing systems is governed by the lower bound of the fundamental period, $1.2T_a$, for the map area associated with A_a=7, A_v=7 and soil type 3, the design of other map areas are apparently controlled by $1.2T_a$.

(13) The wind forces determined according to the UBC provisions are almost equal to those determined based on the power law. Because UBC provides larger wind loads at the lower stories of a structure, it requires a heavier weight for the final design.

(14) The inclusion of vertical combined with horizontal ground motions in the design will require a heavier structural design than a design resulting from horizontal ground motions only. The consideration of the second-order P-Δ effect can even yield a heavier design

with an increment in weight around 3%~4%.

(15) The distribution of the moments of inertia of girders are always abruptly decreased from the second to the first floor for fixed supports. When a structure has hinge supports, the moment of inertia of the girder at the first floor is the largest and suddenly decresed at the second floor. The girders are then decreased almost linearly from the second floor to the top.

(16) For columns of 15-story, one-bay frame with fixed supports, the distribution of the moments of inertia is relatively small at the top floor. It is gradually increased from the 14th floor to the second, increasing abruptly at the first floor.

(17) For the 15-story, two-bay unbraced frame with fixed supports, the distribution of the exterior columns is similar to that of one-bay frame. However, for interior columns, the moment of inertia is the smallest still at the top floor, but it is increased from the top to the third floor and then decreased to the first floor.

(18) For structures with irregular vertical configuration, the distribution of the moments of inertia of columns and girders are different from those of the structures having regular vertical configuration. The example of 15-story setback structure requires an abruptly inreased moments of inertia of girders and columns on the 9th story, because the number of members is reduced at that floor.

(19) In dynamic design, because the eigenvector of the second mode changes sign on the upper stories, the effects on structural responses due to second mode can significantly affect the resizing of member sizes for long period buildings or high-rise buildings. For

this type of buildings, the strain energy combined with kinetic energy of higher modes may be either positive or negative on the upper stories. A modification of the energy distribution is developed in ODSEWS-2D-II.

(20) The dynamic story drift should be determined by combining the modal drifts based on the root-mean-square method. It provides a more conservative value than that is determined on the basis of total dynamic displacements.

(21) The individual member check of the 3-story 3-bay unbraced frame shows that the effect of accidental torsions specified in ATC-3-06 may be insignificant. The increased moments at the columns due to the effects of accidental torsions are too small to influence the design results.

(22) The ODSEWS-2D-II computer program can be used for the design and analysis of various systems. The design loading can be static loads, wind forces, interacting ground motions, seismic forces recommended in various code provisions, and any combination of these. The program can also be used for comparative studies of various code provisions, the effect of various seismic input and interacting ground motion, and the stiffness distribution of different typical structural systems. The program has options of design and analysis. It is apparent that using the program can accelerate the design process and consequently increases profit of a project.

BIBLIOGRAPHY

1. American Society of Civil Engineers, "Wind Forces on Structures," Transactions, ASCE, Vol. 91, 1968, 1124-1198.
2. American National Standards Institute, "American National Standard Building Code Requirements for Minimum Design Loads in Buildings and Other Structures," ANSI A58.1-1972.
3. Amendments to ATC-3-06, National Bureau of Standards, 1982.
4. Applied Technology Council, Tentative Provisions for the Development of Seismic Regulations for Buildings, ATC-3-06, National Bureau of Standards, Washington D. C., 1978.
5. Arora, J.S. and Haug, E.J., Jr., "Efficient Optimal Design of Structures by Generalized Steepest Descent Programming," International Journal for Numerical Methods in Engineering, Vol. 10, 1976, 747-766.
6. Balling, R.J., Pister, K.S., and Ciampi, V., "Optimum Seismic-Resistant Design of Planar Steel Frame," Earthquake Engineering and Structural Dynamics, Vol. 11, 1983.
7. Berg, Glen V., "Seismic Design Codes and Procedures," EERI, 1982.
8. Blodgett, O.W., "Design of Welded Structures," The James F. Lincoln Arc Welding Foundation, Cleveland Ohio, 1966.
9. Blume, J.A., "The Spectral Matrix Method of Damage Prediction," J. A. Blume and Assoc., Report No. NVO-99-33, 1968.
10. Blume, J.A., Sharpe, R.L., and Dalal, J., "Recommendation for Shape of Earthquake Response Spectra," Report prepared for the Directorate of Licensing, United States Atomic Energy Commission, Feb. 1973.

11. Bresler, B., Lin, T.Y., and Scalzi, J.B., "Design of Steel Structures," New York, John Wiley and Sons, 1968.

12. Brown, D.M. and Ang, A.H., "Structural Optimization by Nonlinear Programming," Journal of the Structural Division, ASCE, Vol. 92, ST 6, 1966, 319-340.

13. Cassis, J.H. and Schmit, L.A., Jr., "On Implementation of the Extended Interior Penalty Function," International Journal for Numerical Methods in Engineering, Vol. 10, 1976, 3-23.

14. Cheng, F.Y. and Botkin, M.E., "Nonlinear Optimum Design of Dynamic Damped Frames," Journal of the Structural Division, ASCE, Vol. 102, ST.3, 1976, 609-628.

15. Cheng, F.Y. and Botkin, M.E., "P-Δ Effect on Optimum Design of Dynamic Tall Buildings," Proceedings of the ASCE-IABSE Joint Regional Conference on Tall Buildings, Bangkok, Thailand, 621-632, January 1974.

16. Cheng, F.Y. and Srifuengfung, D., "Optimum Design for Simultaneous Multicomponent Static and Dynamic Inputs," Energy Technology Conference and Exhibition, American Society of Mechanical Engineers, September 1977, Proceedings of Structural Optimization Methods published by ASME and Air Force Flight Dynamics Laboratory, Wright-Patterson Air Force Base, Ohio.

17. Cheng, F.Y. and Srifuengfung, D., "Optimum Design of Seismic Structures Based on Energy Distribution," Annual Convention of the American Society of Civil Engineers, Pittsburgh, 1978, ASCE Monograph No. 3142, 1978, 107-133.

18. Cheng, F.Y., Srifuengfung, D., and Sheng, L.H., ODSEWS -- Optimum Design of Static, Earthquake, and Wind Steel Structures, Rept. NTIS, PB81-232738, National Science Foundation, January 1981.

19. Cheng, F.Y. and Oster, K.B., "Ductility Studies of Parametrically Excited Systems," Proceedings of the Sixth World Conference on Earthquake Engineering, New Delhi, India, January, 1977.

20. Cheng, F.Y. and Oster, K.B., "Dynamic Instability and Ultimate Capacity of Inelastic Systems Parametrically Excited by Earthquakes--Part II," Technical Report of the National Science Foundation, National Technical Information Service, U.S. Department of Commerce, PB261097/AS, 1976.

21. Cheng, F.Y., Venkayya, V.B., Khachaturian, N., et al., Computer Methods of Optimum Structural Design, 5th Annual Short Course Notes, Vols 1 and 2, University of Missouri-Rolla, MO, 1976.

22. Chinese Seismic Code Provisions for Industrial and Civil Structures (in Chinese), TJ 11-78, 1979, Beijing, China.

23. Clough, R. W. and Penzien, J., "Dynamics of Structures," New York, McGraw- Hill, 1975.

24. Culver, C.G., "Survey Results for Fire Loads and Live Loads in Office Buildings," NBS Building Science Series Report 85, Center for Building Technology, National Bureau of Standards, Washington D. C., 1976.

25. Czarnecki, R.M., "Earthquake Damage to Tall Buildings," Dept. of Civil Engineering Research Report R73-8, MIT, Cambridge, Mass., January 1973.

26. Davenport, A.G., "Gust Loading Factors," Journal of the Structural Division, ASCE, Vol. 93, ST 3, 1967.

27. Feng, T.T., Arora, J.S., and Haug, E.J., Jr., "Optimal Structural Design under Dynamic Loads," International Journal for Numerical Methods in Engineering, Vol. 11, 1977, 39-52.

28. Gellatly, R.A., Berke, L., and Gibson, W., "The Use of Optimality Criteria in Automated Structural Design," Presented at the Third WPAFB Conference on Matrix Methods in Structural Mechanics, October 1971.

29. Harris, J.T., Fenves, S.J., and Wright, R.N., "NBS Technical Note 1100," 1979.

30. Hart, G.C. , "Uncertainty Analysis, Loads and Safety," Prentice-Hall, 1982.

31. Housner, G.W., " Behavior of Structures During Earthquakes," Journal of Engineering Mechanics Division, ASCE, Vol. 85, EM4, Oct. 1959.

32. Housner, G.W., "Design Spectrum," Chapter 5, Earthquake Engineering, R.L. Wiegel, ed., Prentice-Hall, 1970.

33. Housner, G. W., "Strong Ground Motion," Chapter 4, Earthquake Engineering, R.L. Wiegel, ed., Prentice-Hall, 1970.

34. Housner, G.W., "Engineering Estimation of Ground Shaking and Maximum Earthquake Magnitude," 4th World Conference on Earthquake Engineering, 1969.

35. Kato, B., Nakamura, Y., and Ankura, H., "Optimum Earthquake Design of Shear Buildings," Journal of the Engineering Mechanics Division, ASCE, Vol. 98, EM. 4, 1972, 891-909.

36. Kavlie, D. and Moe, J., "Automated Design of Frame Structures," Journal of the Structural Division, ASCE, Vol. 97, ST. 1, 1971, 33-62.

37. Khot, N.S., Venkayya, V.B., Johnson, C.D., and Tischler, V.A., "Application of Optimality Criterion to Fiber Reinforced Composites," AFFDL-TR-73-6.

38. Liu, S.C. and Neghabat, F., "A Cost Optimization Model for Seismic Design of Structures," Bell Technology Journal, Vol. 51, 1972, 2209-2225.

39. Manual of Steel Construction, 8th Edition, American Institute of Steel Construction, 1980.

40. Moses, F., "Optimum Structural Design using Linear Programming," Journal of the Structural Division, ASCE, Vol.90, ST.6, 1964, 89-104.

41. Newmark, N.M. and Hall, W.J., "Earthquake Spectra and Design," EERI, 1982.

42. Newmark, N.M. and Hall, W.J., "Seismic Design Criteria for Nuclear Reactor Facilities," Proc., 4th WCEE, Santiago, Chile, 1969.

43. Peurifoy, R.L., "Estimating Construction Costs," McGraw-Hill, 1975.

44. Pierson, B.L., "A Survey of Optimal Structural Design under Dynamic Constraints," International Journal for Numerical Methods in Engineering, Vol. 4, 1972, 491-499.

45. Pope, G.G. and Schmit, L.A., "Structural Design Applications of Mathematical Programming Techniques," AGARDograph 149, Technical Editing and Reproduction Ltd., Harford House, London, England, Feb. 1971.

46. Prendergast, J.D. and Choi, C.D., "Three-dimensional Seismic Structural Analysis of Letterman Hospital," Technical Report M-175, 1976, Department of Army, Champaign, Ill.

47. Rao, S.S., "Structural Optimization Under Shock and Vibration Environment," The Shock and Vibration Digest, Vol. 11, No. 2, Feb., 1979.

48. Ray, D., Pister, K.S., and Polak, E., "Sensitivity Analysis for Hysteretic Dynamic Systems: Theory and Applications," EERC Report 76-12, University of California, Berkeley, 1976.

49. Schmit, L.A. and Farshi, B., "Some Approximation Concepts for Structural Synthesis," AIAA Journal, Vol. 12, 5, 1974, 692-699.

50. Seed, H.B., Ugas, C., and Lysmer, J., "Site Dependent Spectra for Earthquake-Resistant Design," Bulletin of the Seismological Society of America, Vol. 66, No. 1, Feb., 1976, 221-244.

51. She, S.H., "Response Spectrum of Vertical Earthquake Component," Journal of Harbin Architectural and Civil Engineering Institute, No. 2, 1982. (in Chinese)

52. Solnes, J. and Holst, O.L., "Optimization of Framed Structures under Earthquake Loads," Fifth World Conference on Earthquake Engineering, Rome, June 1973.

53. Sveinsson, B.I., Mayes, R.L., and McNiven, H.D., "Evaluation of Seismic Design Provisions for Masonry in the United States," Report EERC 81/10, August, 1981.

54. Taylor, J.E., "Minimum-Mass Bar for Axial Vibration at Specified Natural Frequency," AIAA Journal, Vol. 5, 10, 1967, 1911-1913.

55. Thom, H.C.S., "New Distribution of Extreme Winds in the United States," Journal of the Structural Division, ASCE, Vol. 91, ST 3, 1968.

56. Tso, W.K. and Dempsey, K.M., "Seismic Torsional Provisions for Dynamic Eccentricity," Earthquake Engineering and Structural Dynamics, Vol. 8., 1980, 275-289.

57. Uniform Building Code, International Conference of Building Officials, 1984 Edition.

58. Veletsos, A.S. and Damodaran Nair, V.V., " Seismic Interaction of Structures on Hysteretic Foundations," Journal of the Structural Division, ASCE, ST1, Jan., 1975, 109-129.

59. Veletsos, A.S. and Meek, J.W., "Dynamic Behavior of Building-Foundation Systems," Bulletin of the Seismological Society of America, Vol. 3, 1975, 259-274.

60. Venkayya, V.B., Khot, N.S., and Reddy, V.S., "Energy Distribution in an Optimum Structural Design," AFFDL-TR-68-156, 1968.

61. Venkayya, V.B., Khot, N.S., and Berke, L., "Application of Optimality Criteria Approaches to Automated Design of Large Practical Structures," Preprint of Paper Presented at the AGARD Second Symposium on Structural Optimization, Milan, Italy, April, 1973.

62. Venkayya, V.B., "Design of Optimum Structures," International Journal of Computers and Structures, Vol. 1, 1971, 265-309.

63. Venkayya, V.B. and Cheng, F.Y., "Resizing of Frames Sujected to Ground Motion," Proceedings of the International Symposium on Earthquake Structural Engineering, University of Missouri-Rolla, August, 1976.

64. Vitiello, E., "Optimum Design with Equivalent Seismic Loads," Fifth World Conference on Earthquake Engineering, Rome, June, 1973.

65. Walker, N.D., "Automated Design of Earthquake Resistant Multi-story Steel Building Frames," Report EERC 77-12, University of California, Berkeley, 1977.

66. Walker, N.D. and Pister, K.G., "Study of a Method of Feasible Directions for Optimal Elastic Design of Framed Structures Subjected to Earthquake Loading," Report EERC 75-39, University of California, Berkeley, 1975.

67. Yang, J.N., "Application of Optimal Control Theory to Civil Engineering Structures," Journal of the Engineering Mechanics Division, ASCE, EM.6, December, 1975.

68. Zagajeski, S.W. and Bertero, V.V., "Optimum Inelastic Design of Seismic-Resistant Reinforced Concrete Frame Structures," EERC Report 80/03, University of California, Berkeley, January, 1980.

69. Zarghamee, M.S., "Optimum Frequencies of Structures," AIAA Journal, Vol. 6, 4, 1968, 749-750.

70. Watabe, Makoto, "Summary of Current Seismic Code Requirements in the World," Proceedings of Seismic Risk and Its Use in Code Formulation, Edited by H. C. Shah and H. Shibata, 1983.

71. International Association for Earthquake Engineering, "Earthquake Resistant Regulations - A World List 1984," Association for Science Documents Information, Japan, 1984.

72. Building Seismic Safety Council, "Recommended Provisions for the Development of Seismic Regulations for New Buildings," Vols. I and II, 1984.

73. Whitman, R. V., "Damage Probability Matrices for Prototype Buildings," Research Report R73-57, MIT, 1973.

74. Cheng, F.Y. and Juang, D.S., "Assessment of ATC-03 for Steel Structures Based on Optimization Algorithm," Proceedings of the 8th World Conference on Earthquake Engineering, San Francisco, July, 1984, Vol. 5, pp. 435-442.

75. Cheng, F.Y., "Optimum Design of 2-D and 3-D Structures Subjected to Multicomponent Seismic Excitations," Proceedings of the AIT-CCNNA (U.S.-Taiwan) Joint Seminar on Research for Multiple Hazards Mitigation, Taiwan, January, 1984, pp. 182-202.

76. Cheng, F.Y. and Truman, K.Z., "Optimum Design of Reinforced Concrete and Steel 3-D Static and Seismic Building Systems with Assessment of ATC-03," Report Series 85-10 for the National Science Foundation, 1985.

77. Newmark, N.M. Consulting Engineering Services, " A Study of Vertical and Horizontal Earthquake Spectra," Directorate of Licensing United States Atomic Energy Commission, 1973.

78. Building Seismic Safety Council, "Amendments to ATC-3-06 Tentative Provisions for the Department of Seismic Regulations for Buildings for Use in Trial Designs," NBSIR 82-2626, BSSC 82-2, 1982 Foundation, 1985.

79. Cheng, F.Y. and Juang, D.S., "ODSEWS-2D-II - User's Manual for Optimum Design of 2-Dimensional Steel Structures for Static, Earthquake, and Wind Forces--Version II," National Science Foundation Report, 1985.

80. Schmit, L.A. and Miura, M., "Approximation Concepts for Efficient Structural Synthesis," NASA CR-2552, 1976.

81. Kan, M.R., Willmert, K.D. and Thornton, W.A., "A New Optimality Criterion Method for Large Scale Structures," AIAA/ASME 19th Structures, Structural Dynamics, and Materials Conference, Bethesda, Md., April 1978, pp. 47-58.

82. Dobbs M.W. and Nelson, R.B., "Application of Optimality Criteria to Automated Structural Design," AIAA Journal, Vol. 14, No. 10, 1976, pp. 1436-1443.

83. Rizzi, Paulo, "Optimization of Multiconstrained Structures Based on Optimality Criteria," AIAA/ASME/SAE 17th Structures, Structural Dynamics, and Materials Conference, King of Prussia, PA, May 1976, pp. 448-462.

84. Newmark, N. M. and Riddell, R., "Inelastic Spectra for Seismic Design," Proc. of 7th World Conference on Earthquake Engineering, Istanbul, Turkey, 1980, Vol. 4, pp. 129-136.

APPENDICES

APPENDIX A. CROSS SECTIONAL PROPERTIES OF THE AISC WF SECTIONS

In this research work, the girders and columns of a framework are assumed to be wide flange sections. The wide flange sections can be either selected from the AISC Manual[39] or designed for built-up wide flange sections. In this appendix, the formulas used for computing the sectional properties of the AISC WF sections are described.

In the AISC Manual, the sectional properties of WF steel sections are given. The interested sectional properties in this research are cross-sectional area, A, sectional modulus, S_x, and moment of inertia, I_x. Unfortunately, the direct relationships are not available for these three values. For programming convenience, the approximate relations for most economical WF sections were developed on the basis of curve fitting with selected algebraic expressions.[12] These relations are given as follows:

a. for $0 \leq I_x \leq 9000$ in^4,

$$S_x = \sqrt{60.6\ I_x + 84100} - 290,$$

and

$$A = 0.465\ \sqrt{I_x}\ ;$$

b. for 9000 in^4 $\leq I_x \leq$ 20300 in^4,

$$S_x = \frac{I_x - 8056.3}{1.876},$$

and

$$A = \frac{I_x + 2300}{256} .$$

APPENDIX B. CROSS-SECTIONAL PROPERTIES OF THE BUILT-UP SECTIONS

The AISC WF sections given in Appendix A may not adequate for the design of tall and heavy frameworks. The built-up sections are provided in the computer program to complement this inadequacy.

The cross-sectional area, A, the moment of inertia, I_x, the sectional modulus, S_x, and the shear flow, v, are respectively given as follows:

$$A = d^2 \left(\frac{t_w}{d} + 2 \frac{t_f}{d} \left(\frac{b}{d} - \frac{t_w}{d} \right) \right)$$

$$I_x = d^4 \left(\frac{b}{2d} \left(\frac{t_f}{d}\right)\left(1 - \frac{t_f}{d}\right)^2 + \frac{1}{12} \frac{t_w}{d} \left(1 - \frac{2t_f}{d}\right)^3 \right)$$

$$S_x = d^3 \left(\frac{b}{d} \left(\frac{t_f}{d}\right)\left(1 - \frac{t_f}{d}\right)^2 + \frac{1}{6} \frac{t_w}{d} \left(1 - \frac{2t_f}{d}\right)^3 \right)$$

and

$$v = \frac{d^2 \left(\frac{b}{2d} \left(\frac{t_f}{d}\right)\left(1 - \frac{t_f}{d}\right)^2 + \frac{1}{12} \frac{t_w}{d} \left(1 - \frac{2t_f}{d}\right)^3 \right) \frac{t_w}{d}}{\left(\frac{b}{2d} \left(\frac{t_f}{d}\right)\left(1 - \frac{t_f}{d}\right) + \frac{1}{8} \frac{t_w}{d} \left(1 - \frac{2t_f}{d}\right)^2 \right)}$$

in which b is the flange width, d the depth of the cross section, t_f the flange thichness, and t_w the web thickness.